INFORMATION TO USERS

This manuscript has been reproduced from the microfilm master. UMI films the text directly from the original or copy submitted. Thus, some thesis and dissertation copies are in typewriter face, while others may be from any type of computer printer.

The quality of this reproduction is dependent upon the quality of the copy submitted. Broken or indistinct print, colored or poor quality illustrations and photographs, print bleedthrough, substandard margins, and improper alignment can adversely affect reproduction.

In the unlikely event that the author did not send UMI a complete manuscript and there are missing pages, these will be noted. Also, if unauthorized copyright material had to be removed, a note will indicate the deletion.

Oversize materials (e.g., maps, drawings, charts) are reproduced by sectioning the original, beginning at the upper left-hand corner and continuing from left to right in equal sections with small overlaps. Each original is also photographed in one exposure and is included in reduced form at the back of the book.

Photographs included in the original manuscript have been reproduced xerographically in this copy. Higher quality 6" x 9" black and white photographic prints are available for any photographs or illustrations appearing in this copy for an additional charge. Contact UMI directly to order.

UMI

A Bell & Howell Information Company
300 North Zeeb Road, Ann Arbor MI 48106-1346 USA
313/761-4700 800/521-0600

INFORMATION TO USERS

This manuscript has been reproduced from the microfilm master. UMI films the text directly from the original or copy submitted. Thus, some thesis and dissertation copies are in typewriter face, while others may be from any type of computer printer.

The quality of this reproduction is dependent upon the quality of the copy submitted. Broken or indistinct print, colored or poor quality illustrations and photographs, print bleedthrough, substandard margins, and improper alignment can adversely affect reproduction.

In the unlikely event that the author did not send UMI a complete manuscript and there are missing pages, these will be noted. Also, if unauthorized copyright material had to be removed, a note will indicate the deletion.

Oversize materials (e.g., maps, drawings, charts) are reproduced by sectioning the original, beginning at the upper left-hand corner and continuing from left to right in equal sections with small overlaps. Each original is also photographed in one exposure and is included in reduced form at the back of the book.

Photographs included in the original manuscript have been reproduced xerographically in this copy. Higher quality 6" x 9" black and white photographic prints are available for any photographs or illustrations appearing in this copy for an additional charge. Contact UMI directly to order.

UMI

A Bell & Howell Information Company
300 North Zeeb Road, Ann Arbor MI 48106-1346 USA
313/761-4700 800/521-0600

THE COORDINATION CHEMISTRY OF TRIPODAL PHOSPHINE CHALCOGENIDE LIGANDS WITH PLATINUM GROUP METALS

by

Sherrie Fang Wang
B.Sc., Nankai University, 1985

A Dissertation Submitted in Partial Fulfilment of the
Requirements for the Degree of

DOCTOR OF PHILOSOPHY

in the Department of Chemistry

We accept this dissertation as conforming to
the required standard

Dr. K.R. Dixon, Supervisor (Department of Chemistry)

Dr. T.M. Fyles (Department of Chemistry)

Dr. D.J. Berg (Department of Chemistry)

Dr. A. Watton, Outside Member (Department of Physics)

Dr. R.G. Cavell, External Examiner (University of Alberta)

Abstract

Supervisor: Professor K.R. Dixon

This work set out to develop synthetic routes to transition metal complexes containing the ligands of general type $[PPh_2(X)][PPh_2(Y)][PPh_2(Z)]CH$ and $[PPh_2(X)][PPh_2(Y)][PPh_2(Z)]C^-$, where X,Y, Z = various combinations of O, S, Se and electron pairs. The aim would then be to fully characterise the complexes by various spectroscopic methods to determine the modes of coordination of the ligands and rationalise any dynamic processes which may be occurring in solution. Finally the complexes would be investigated in terms of chemical reactivity, especially with regards to potential catalytic activity.

The synthesis and characterisation of a series of rhodium, iridium, platinum, and palladium complexes containing the phosphine chalcogenide ligands, $[CH(P(S)Ph_2)_3]$/ $[C(P(S)Ph_2)_3]^-$ and $[CH(PPh_2)(P(S)Ph_2)_2]$/ $[C(PPh_2)(P(S)Ph_2)_2]^-$, are described. The crystal structures of seven of these complexes plus that of the ligand, $[CH(PPh_2)(P(S)Ph_2)_2]$, have been determined. These structures include $[Pd(\eta^3\text{-}C_4H_7)\{CH(PPh_2)(P(S)Ph_2)_2\text{-}P,S\}]BF_4 \cdot 2H_2O$, $[Pd(\eta^3\text{-}C_4H_7)\{CH(P(S)Ph_2)_3\text{-}S,S,S\}]BF_4$, $[Rh(cod)\{C(P(S)Ph_2)_3\text{-}S,S\}]$, $[Ir(CO)_2\{C(P(S)Ph_2)_3\text{-}S,S\}]$, $[Rh(cod)\{C(PPh_2)(P(S)Ph_2)_2\text{-}P,S\}] \cdot CH_2Cl_2$, $[RhI_2(^tBuNC)_2\{C(PPh_2)(P(S)Ph_2)_2\text{-}P,S\}]$, and $[Ir(cod)\{CH(PPh_2)(P(S)Ph_2)_2\text{-}P,S\}]BF_4 \cdot CH_2Cl_2$, which are all discussed in detail. The $[CH(P(S)Ph_2)_3]$ ligand coordinates in an η^3 mode to metal centres. The anionic ligand $[C(P(S)Ph_2)_3]^-$ coordinates to metals in an η^2 mode using two of its sulphur atoms, leaving a $-P(S)Ph_2$ group dangling. The ligand, $[CH(PPh_2)(P(S)Ph_2)_2]$, can either coordinate in an η^2 *P,S* mode, using a phosphorus and a sulphur atom, or in an η^3 *P,S,S* mode using a phosphorus and two sulphur atoms. The anionic ligand, $[C(PPh_2)(P(S)Ph_2)_2]^-$, acts as a

four electron donor, using one phosphorus and one sulphur atom, to metal centres.

The reaction of [Ir(cod){C(P(S)Ph_2)$_3$-*S,S*}] with CO to give [Ir(CO)$_2${C(P(S)Ph_2)$_3$-*S,S*}] is described. The reaction of [Rh(cod){C(PPh_2)(P(S)Ph_2)$_2$-*P,S*}] with ^{t}BuNC to give [Rh(^{t}BuNC)$_2${C(PPh_2)(P(S)Ph_2)$_2$-*P,S*}] is discussed. The subsequent oxidative additions of I_2 and benzyl bromide, to give isomeric mixtures of [RhI$_2$(^{t}BuNC)$_2$ {C(PPh_2)(P(S)Ph_2)$_2$-*P,S*}] and [RhBr(Bz)(^{t}BuNC)$_2$ {C(PPh_2)(P(S)Ph_2)$_2$-*P,S*}] respectively, are also presented.

The fluxional behaviours of [Pd(η^3-C_4H_7){CH(PPh_2)(P(S)Ph_2)$_2$-*P,S*}]BF_4, [Pd(η^3-C_4H_7){C(P(S)Ph_2)$_3$-*S,S*}], [Pt(MeOcod){C(P(S)Ph_2)$_3$-*S,S*}], and [Rh(cod){C(P(S)Ph_2)$_3$}] are discussed in detail. The two -Ph_2P=S groups in the above complexes undergo a rapid intramolecular site exchange at ambient temperature in solution. Line shape analysis of variable temperature $^{31}P\{^1H\}$ NMR data gives the following $\Delta G^{\circ *}$ for this dynamic exchange of coordinated and noncoordinated sulphur at 298 K.

[Pd(η^3-C_4H_7){CH(PPh_2)(P(S)Ph_2)$_2$-*P,S*}]BF_4	48 kJ/mol
[Pd(η^3-C_4H_7){C(P(S)Ph_2)$_3$-*S,S*}]	38 kJ/mol
[Pt(MeOcod){C(P(S)Ph_2)$_3$-*S,S*}]	48 kJ/mol
[Rh(cod){C(P(S)Ph_2)$_3$-*S,S*}]	46 kJ/mol

Dr. K.R. Dixon

Dr. T. M. Fyles

Dr. D. J. Berg

Dr. A. Watton

Dr. R. G. Cavell

Table of Contents

List of Tables

List of Figures

List of Schemes

List of Abbreviations

^{n}Bu	normal butyl
^{t}Bu	tertiary butyl
^{t}BuNC	tertiary butylisocynaide
Cod	1,5-cycloctadiene
Cp	cyclopentadienyl
Cp*	pentamethylcyclopentadienyl
DMSO	dimethylsulphoxide
Et	ethyl
IR	infrared
L	ligand
μ	bridging
M	metal
Me	methyl
MeoCod	η^3-8-methoxycycloocta-4-ene-1-yl
NMR	nuclear magnetic resonance
DNMR	dynamic nuclear magnetic resonance
NOE	Nuclear Overhauser Enhancement
Ph	phenyl
pz	pyrazolyl
THF	tetrahydrofuran
X	halogen

Acknowledgements

I would like to thank my supervisor, professor K.R. Dixon for his guidance and assistance during my Ph.D. studies. I would also like to thank Dr. N.J. Meanwell for advice and many helpful discussions throughout this project. I am extremely grateful to Dr. T.M. Fyles and Dr. D.E. Berry for their invaluable help in writing the final version of the thesis. Many thanks are also extended to Dr. J. Browning for determining all the crystal structures presented in this thesis. I would also like to thank Mrs. Greenwood for her help in learning the operation of the NMR spectrometer.

Dedication

To my parents and Neil for their love and belief in me. To my children, Michael and Jason, for giving me the time to finish this book.

Chapter 1

General Introduction

Tertiary phosphines, PR_3 (R = alkyl or aryl), are an extremely important class of monodentate ligands in the coordination chemistry of the transition metals. They are well known for their ability to stabilise metal complexes in both low and high oxidation states; a property which arises from the fact that they are both good σ-donors and π-acceptors. There are also numerous examples of tertiary phosphine complexes being used as homogeneous catalysts. Notable amongst these is Wilkinson's catalyst, $[RhCl(PPh_3)_3]$, which catalyses the homogeneous reduction of alkenes, alkynes, and other unsaturated substances, at 25 °C and 1 atmosphere pressure [1], and the propylene hydroformylation catalyst, $[RhH(CO)_2(PPh_3)_2]$ [2]. Homogeneous catalysts are generally more desirable than heterogeneous catalysts for several reasons [3]:

(i) They have very well defined stoichiometries which are easily reproducible.

(ii) Their selectivity can be "tuned" by changing the nature of their ligands (steric and electronic effects). Indeed, in recent years catalysts have been produced which are regioselective, stereoselective, or even enantioselective.

(iii) They often give higher rates of reaction than heterogeneous catalysts and usually require milder conditions of temperature and pressure.

Over the past twenty-five years there has been a growing interest in the use of polydentate phosphine ligands to make new transition metal complexes [4,5]. In comparison to monodentate phosphines, these polydentate phosphines confer a number of advantages in terms of the resulting complexes. These advantages include an increase in

nucleophilicity or basicity at the metal centre [4] and a greater control of the coordination number and stereochemistry of the complex [4]. Also both intra- and intermolecular exchange reactions tend to be slower and more controlled [4]. Finally, and very importantly, a greater degree of structural and bonding information can be obtained from phosphorus-phosphorus and metal-phosphorus coupling constants in the NMR spectra [6].

The focus of this thesis is the preparation of transition metal complexes of a class of polydentate phosphine ligands which can coordinate in a mono-, bi-, or even tridentate fashion. The ligands can also coordinate either as neutral molecules or uninegative anions.

Uninegative tridentate ligands in coordination chemistry are somewhat rare. They are of considerable interest because they are formally analogous to the η^5-cyclopentadienyl ligand, $C_5H_5^-$, which can be regarded as a 6-electron donor which occupies three coordination sites around the metal centre. There is a very extensive transition metal chemistry [7] of the cyclopentadienyl system; indeed these derivatives and substituted relatives are considered to be the most important of all carbocyclic π complexes. Although these cyclopentadienyl ligands are coordinated usually in a η^5 fashion, complexes with the ligand bonded as η^3 and η^1 are also well documented, as well as polynuclear complexes with the ligand bridging two metals as shown in **Figure 1.1**.

Figure 1.1 The Cyclopentadienide Ligand and its Various Modes of Coordination

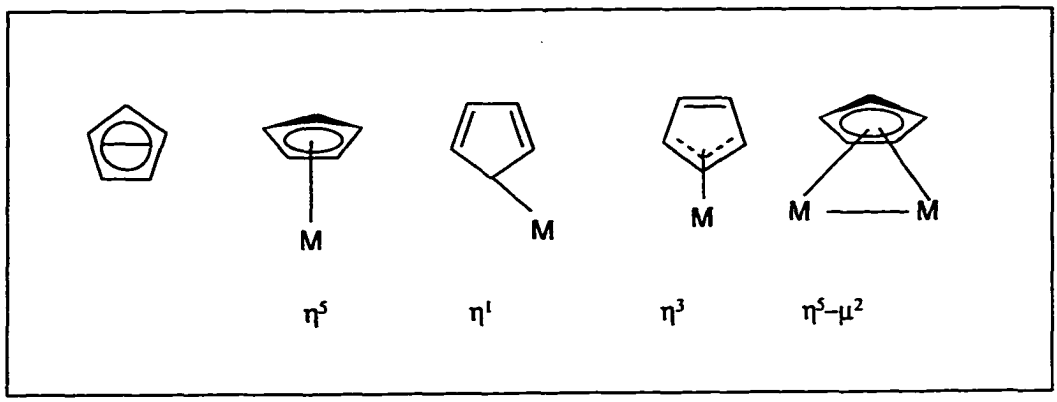

A large number of complexes with different substituted cyclopentadienide ligands, $[C_5R_5]^-$ (R = various alkyl or aryl groups), have also been synthesised. Most notable among these are the complexes containing the pentamethylcyclopentadienide ligand, $[C_5Me_5]^-$, which is usually denoted as Cp* [8]. The electron donating nature of the methyl groups in turn increases the electron donating capability of the ligand and a number of compounds with metals in unusually high oxidation states have been characterised. For example, the iridium(V) tetrahydride [9], $[(C_5Me_5)IrH_4]$, for which there is no C_5H_5 analogue.

One of the main reasons for the intensive studies of cyclopentadienyl compounds is their potential in the field of homogeneous catalysis. During a typical catalytic cycle the catalyst will have to undergo at least one, and probably more, of the following changes [10]:

(i) A change in the oxidation state of the metal as in oxidative addition or reductive elimination .

(ii) A change in the coordination number of the metal as in ligand coordination and ligand dissociation.

(iii) A change in stereochemistry.

(iv) A change in ligation.

Under typical reaction conditions it is not uncommon for the homogeneous catalyst to decompose irreversibly into the metal. In order to prevent this undesirable process a ligand must be present in the complex capable of binding the metal strongly enough to prevent decomposition occurring during the catalytic cycle [7]. The pentamethylcyclopentedienyl ligand has shown itself to be one of the most stable carbocyclic ligands. The ligand is able to remain coordinated to the metal under conditions that the cyclopentadienyl ring is known to be cleaved from the metal by a variety of reagents, including hydrogen [7].

There has been much interest over the last thirty years of developing inorganic analogues of the cyclopentadienyl ligands with hopes of both emulating the success of these ligands and maybe improving upon their properties. The following is an up to date summary of the handful of ligands which have been prepared and studied.

1.1 Tris(pyrazolyl)borate ion, $[RB(pz)_3]^-$

The pyrazole molecule, $C_3H_4N_2$, is thermally and hydrolytically very stable. It is a well known ligand in coordination chemistry and coordinates to metals and metalloids through the 2-N site [11]. Upon deprotonation, pyrazole becomes the pyrazolide ion. The ion can

coordinate through both nitrogen atoms. Typically it acts as a bridging ligand between two metal centres as shown in **Figure 1.2**.

Figure 1.2 Pyrazole and the Pyrazolide Ion as a Bridging Ligand

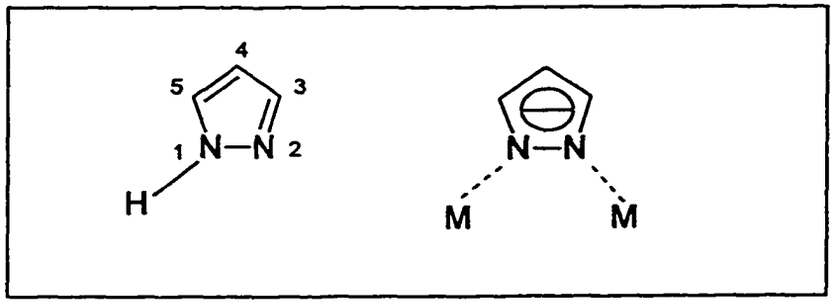

A class of polydentate ligands derived from pyrazoles are the geminally poly(1-pyrazolyl) substituted compounds. One important example is the neutral tris(pyrazolyl)methane $HC(pz)_3$, where pz is used to denote the pyrazolate anion [12]. However the most notable examples are the poly(1-pyrazolyl)borates, $[R_nB(pz)_{4-n}]^-$ where n = 0,1,2, or 3. When n = 1 and R = H, the resulting ion is the tris(pyrazolyl)borate ion, $[HB(pz)_3]^-$ [12], which was the first known example of an inorganic uninegative tridentate ligand and whose synthesis was reported by Trofimenko in 1966 [13]. This ion is shown on the left of **Figure 1.3**. It reacts readily with many inorganic and organometallic compounds yielding numerous derivatives, as exemplified by the molybdenum complexes, $[RB(pz)_3Mo(CO)_2X]$ (X = NO,Cl, N_2Ar, C_7H_7, allyl) [14] which are analogous to the "half-sandwiches" based on the cyclopentadienide ligand. The ligand binds to the metal centre in a tridentate mode, as shown on the right of **Figure 1.3**.

Figure 1.3 The tris(pyrazolyl)borate Ion and a Molybdenum Complex

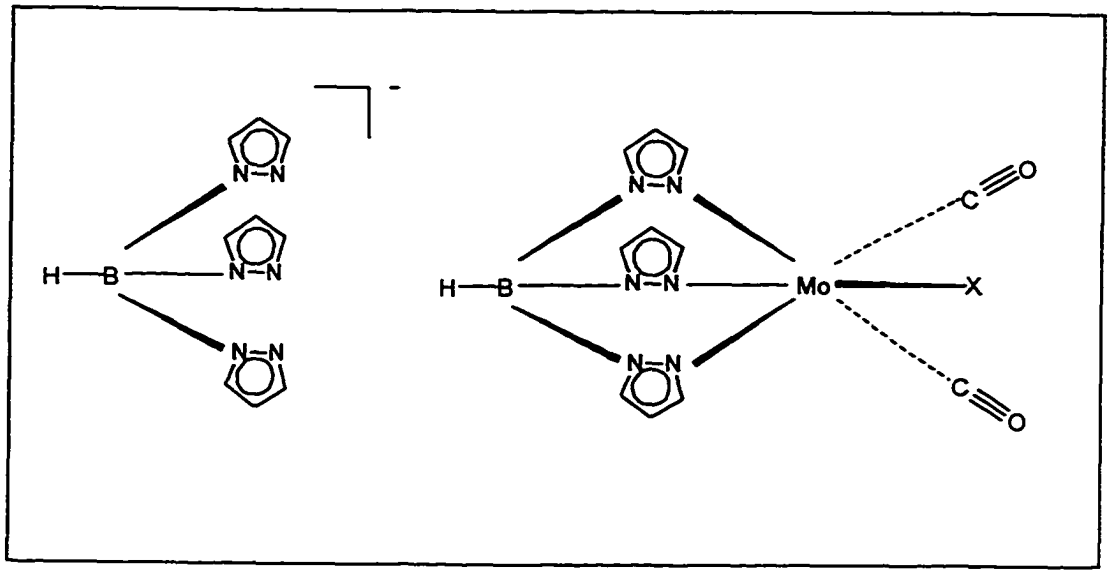

The preparation of these and other complexes are illustrated in **Scheme 1.1** [14]. Most of the derivatives correspond to their C_5H_5 counterparts, although some of these half-sandwich complexes are obtainable only in the $[RB(pz)_3]^-$ system. Generally, the tris(pyrazolyl)borate complexes are thermally and chemically more stable than the corresponding C_5H_5 compounds, properties which are believed to arise from a combination of steric and electronic factors. The stability of tris(pyrazolyl)borate complexes can also significantly be increased by using an alkyl-substituted pyrazole in the 3 position [14]. The pyrazole most often used for this purpose is 3,5-dimethylpyrazole. For example, $[HB(3,5\text{-}(CH_3)_2pz)_3Mo(NO)_2Cl]$ is indefinitely stable to storage whereas $[C_5H_5Mo(NO)_2Cl]$ is not and there is no known C_5H_5 analogue of $[HB(3,5\text{-}(CH_3)_2pz)_3MoCl_2NO]$ [14].

Scheme 1.1 Tris(pyrazolyl)borate Complexes of Molybdenum

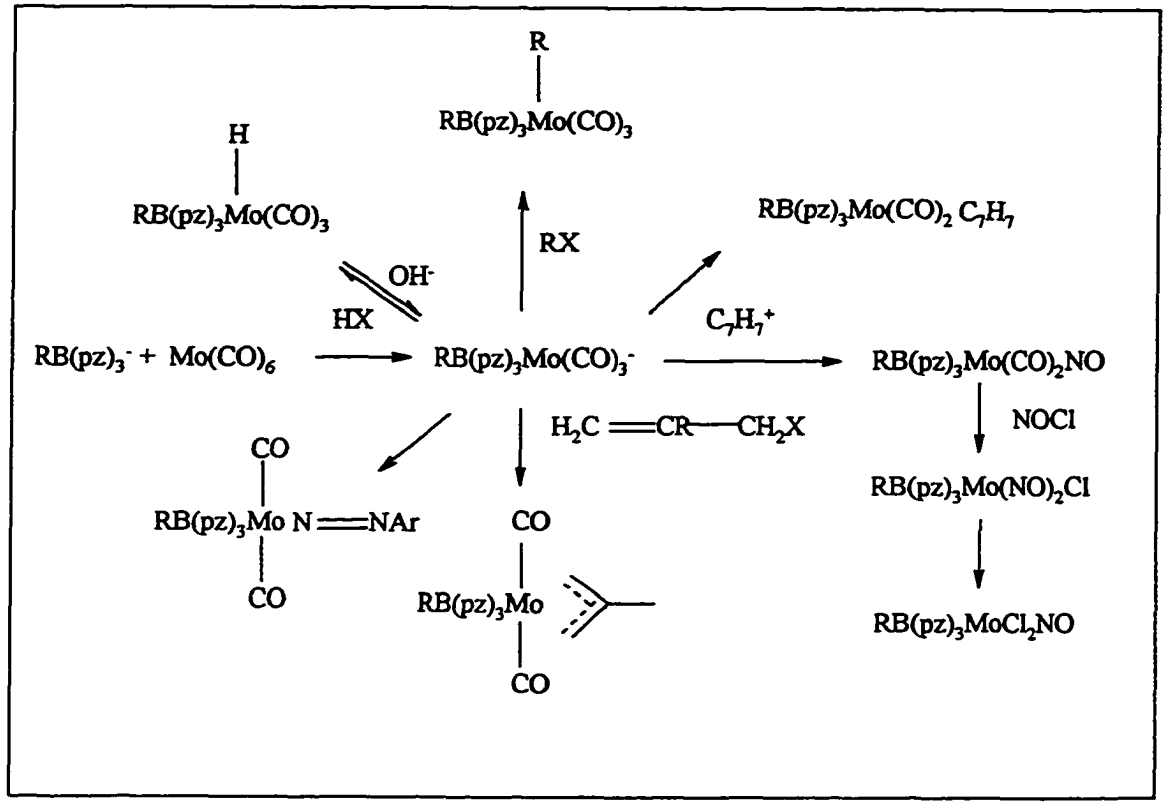

In the years since the discovery of the tris(pyrazolyl)borates an enormous amount of their coordination chemistry has been reported and several comprehensive reviews have been published [15, 16, 17]. The vast majority of these complexes have been with either $[HB(pz)_3]^-$ or $[HB(pz^*)_3]^-$. In a recent review [17] Trofimenko noted that care should be taken when drawing the analogy between tris(pyrazolyl)borate complexes and η^5-cyclopentadienyl compounds. In many cases the tris(pyrazolyl)borate ligand coordinates in a bidentate fashion to the metal centre, leaving the third pyrazolyl noncoordinated, or "dangling". The term *scorpionate ligand* has been coined to describe

the nature of this bonding in that it resembles the features of a scorpion which grabs its prey with two identical claws (two pyrazolide fragments) and then can also sting with the sharp point of its curling tail (the third pyrazolide fragment) [17] . This scorpion-like behaviour is, of course, not possible for the cyclopentadienyl ligand. There are now a number of examples of complexes where the ligand is initially bidentate but becomes tridentate when the metal complex is reacted in such a way to favour an increase in coordination number of the metal. For example the rhodium(I) square planar complex, $[HB(pz^*)_3Rh(CNR)_2]$, is protonated with tetrafluoroboric acid to produce the six-coordinate rhodium(III) complex cation, $[HB(pz^*)_3RhH(CNR)_2]^+$ as its tetrafluoroborate salt, as shown in the **Scheme 1.2** below [18]

Scheme 1.2 Protonation of $[HB(Pz^*)_3Rh(CN^tBu)_2]$

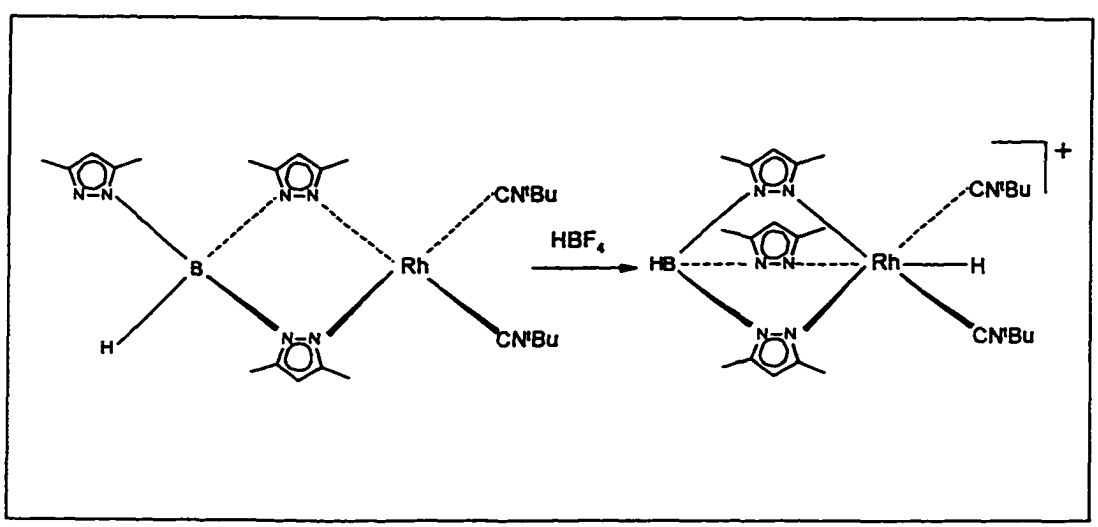

The observed product was somewhat surprising in that the metal, rather than the free pyrazolyl, was protonated. The rhodium complex, $[\{HB(pz^*)_3\}Rh(CO)(\eta^2\text{-alkene})]$

(where pz* = 3,5-dimethylpyrazole) [19], has been found to thermally activate C-H bonds in benzene under mild conditions to produce the hydrido complex, [{HB(pz*)$_3$}Rh(H)(Ph)(CO)]. Again, the [HB(pz*)$_3$]$^-$ ligand is bidentate in the square planar [{HB(pz*)$_3$}Rh(CO)(η^2-alkene)] but tridentate in the octahedral [{HB(pz*)$_3$}Rh(H)(Ph)(CO)], illustrating the versatility of the ligand in meeting the coordination requirements of the metal centre [20]. In a related study the fluxional behaviours of bis(pyrazolyl)methane allylpalladium complex and a [HB(pz*)$_3$]$^-$ complex have been studied [21]. The proposed mechanism of the exchange of coordinated and non-coordinated N atoms in these bidentate complexes, illustrated in **Scheme 1.3**, involves the cleavage of a Pd-N bond and isomerisation of the T-shaped intermediate, and finally the reformation of the Pd-N bond.

Scheme 1.3 The Proposed Mechanism of Exchange of Coordinated and Non-Coordinated N-atoms in $[Pd(\eta^3\text{-}C_3H_7)\{CH_2(pz)_2\}]$ (A = B = H)

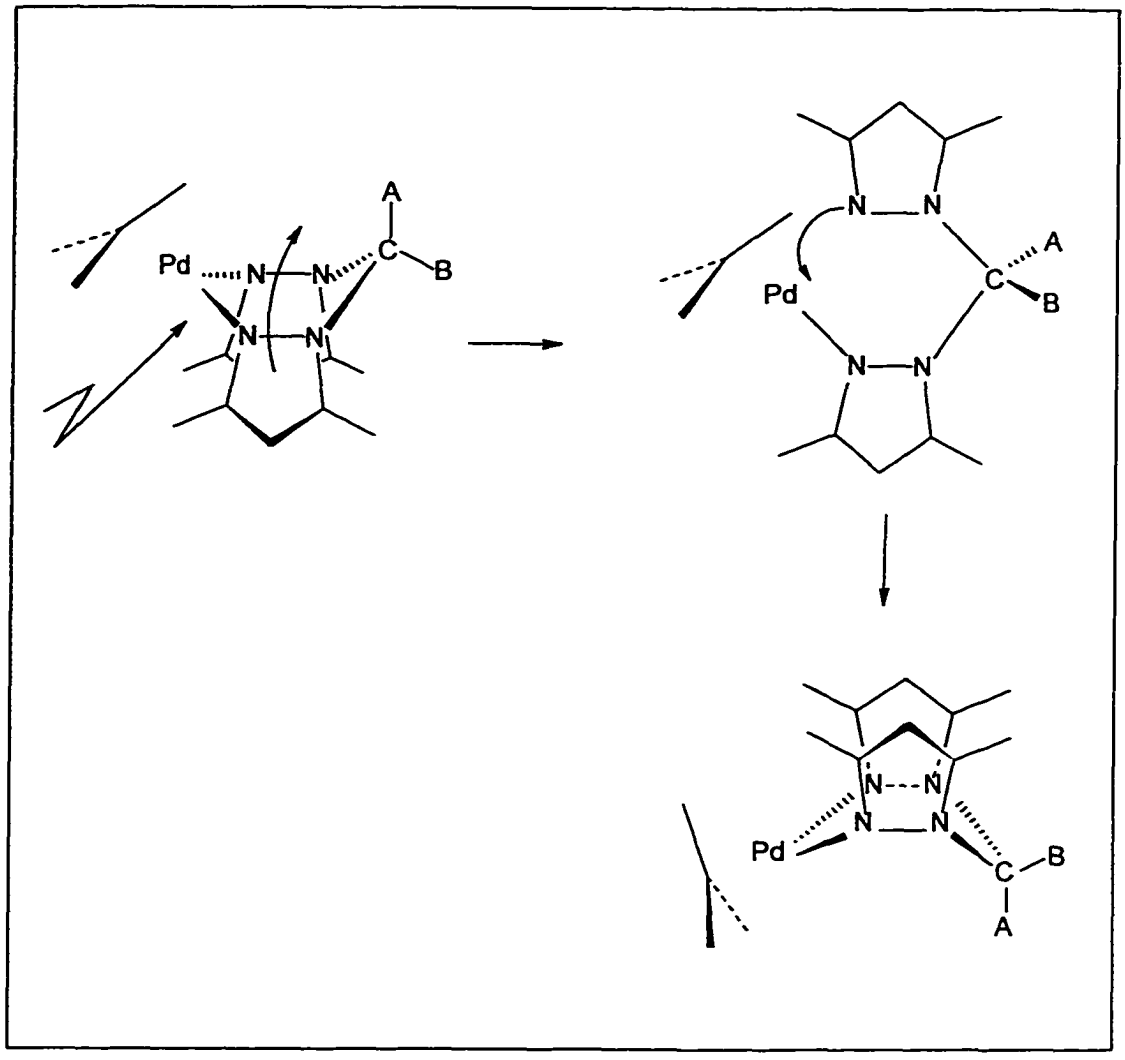

1.2 $[\eta^5\text{-}C_5H_5M(R_2PO)_3]^-$

Since 1987 Kläui et al have reported the syntheses of a new class of uninegative tridentate ligands, $[\eta^5\text{-}C_5R_5M(R'_2PO)_3]^-$ (M = Co, Rh; R= H, CH_3; R′ = alkyl, aryl or *O*-alkyl) [22]. This type of ion is shown in **Figure 1.4**.

Figure 1.4 The $[(C_5R_5)M(R'_2PO)_3]^-$ Ligand System (M = Co, Rh; R = H, CH_3; R′ = alkyl or aryl groups)

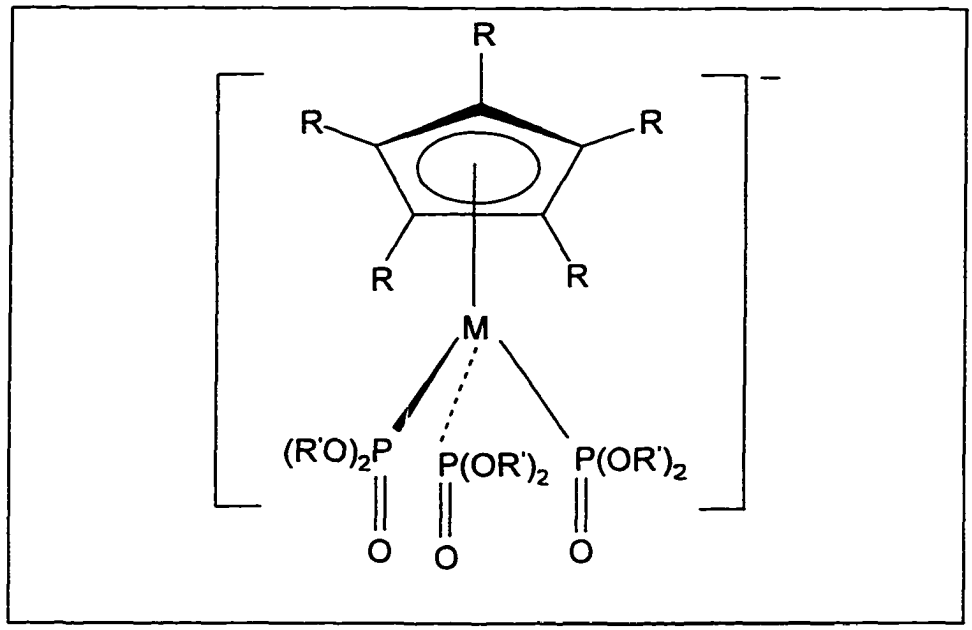

The ligating oxygen atoms are classified as hard bases being both σ-donors and good π-donors. Being σ-donors it would be expected that the ligands would stabilise metal complexes in middle to high oxidation states. This expectation is borne out by the preparation of titanium (II, III, or IV), vanadium (II, III, or IV), molybdenum(V), and tungsten(VI) complexes [23, 24]. However some low oxidation state complexes, such as the tungsten(I) compound, $[L_2W_2(CO)_4]$ (L = $[(C_5H_5)Co\{P(O)Et_2\}_3]^-$) [12], have also been prepared. In this case the π-donor feature of the ligand is seen as being very important, causing increased π backbonding from the metal to the carbonyl ligands. Kläui has also begun to explore the possibilities of replacing one or more of the oxygen donor atoms with other atoms capable of coordination. To this end he has synthesised the

related ruthenium based ligand, $[\{(C_6Me_6)\}RuCl(P(O)(OMe)_2)_2]^-$ [25] which is capable of bonding in an *O,O,Cl*-mode, as exemplified by the complexes $[(C_6Me_6)RuCl[P(O)(OMe)_2]_2MH(CO)_3]$ (M = W or Mo) [26]. Clearly the possibility of "tuning" the ligand to satisfy the bonding requirements of the metal is of great interest.

Numerous other complexes formed by this ligand have been reported. Unfortunately no platinum complexes could be prepared and Crabtree et al also failed to make iridium complexes [27]. Recently Klaüi et al have reported the synthesis of π-allylpalladium complexes with ligands of this type [28]. Interestingly they are the first examples of 18-electron π-allylpalladium compounds that are stabilised by a tripodal oxygen donor ligand. However, the X-ray structure of $[\{(C_5H_5)Co(P(OMe)_2O)_3\}Pd(C_3H_5)]\cdot H_2O$ shows two of the three oxygen donor atoms of the ligand coordinated strongly to the palladium while the third forms a hydrogen bond to a water molecule [28].

1.3 $[Ir(\eta^5\text{-}C_5Me_5)(pz)_3]^-$ and $[Ru(\eta^6\text{-}p\text{-cymene})(pz)_3]^-$

These are ligands which can be both compared to the tris(pyrazolyl)borates and the Kläui ligands, $[\eta^5\text{-}C_5R_5M(R'_2PO)_3]^-$ [29]. They are generally used for reactions in their neutral protonated forms, deprotonating readily in the presence of a base. The structures of the neutral precursors are shown below in **Figure 1.5**

Figure 1.5 The Neutral Precursors to $[Ir(\eta^5\text{-}C_5Me_5)(pz)_3]^-$ and $[Ru(\eta^6\text{-}p\text{-cymene})(pz)_3]^-$

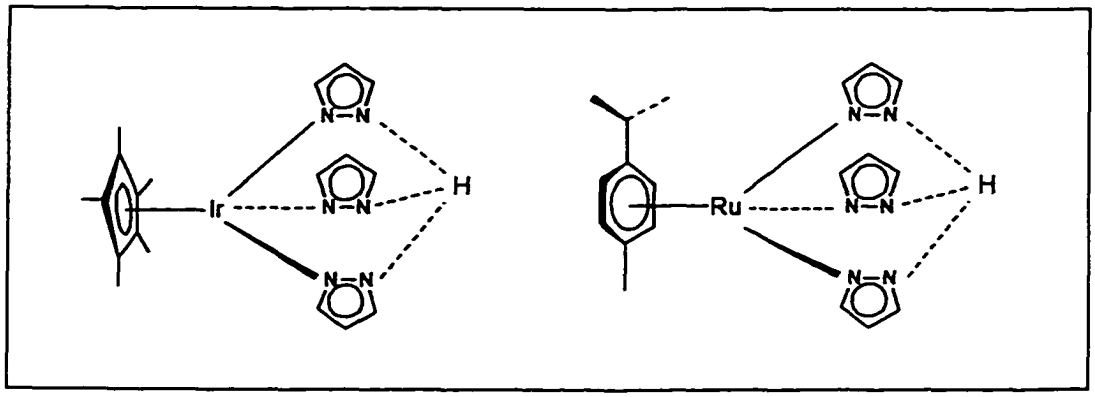

Spectroscopic evidence suggests there is a dynamic hydrogen bonding between the three pyrazolates [29].

Since reporting their syntheses in 1986 [29] Oro et al have prepared numerous complexes. For example, reactions of the ligand with the group 11 halide triphenylphosphine complexes, $[MCl(PPh_3)]_x$ ($x = 4$, M = Cu, Ag: $x = 1$, M = Au), in the presence of potassium hydroxide, yields the heterodinuclear complexes, $[Ir(\eta^5\text{-}C_5Me_5)(pz)_3M(PPh_3)]$, in which only two of the three pyrazolates bond to the group 11 metal, as shown in **Figure 1.6** [30]

Figure 1.6 The Bonding Arrangement in $[Ir(\eta^5\text{-}C_5Me_5)(pz)_3MPPh_3]$ (M = Cu, Ag, or Au)

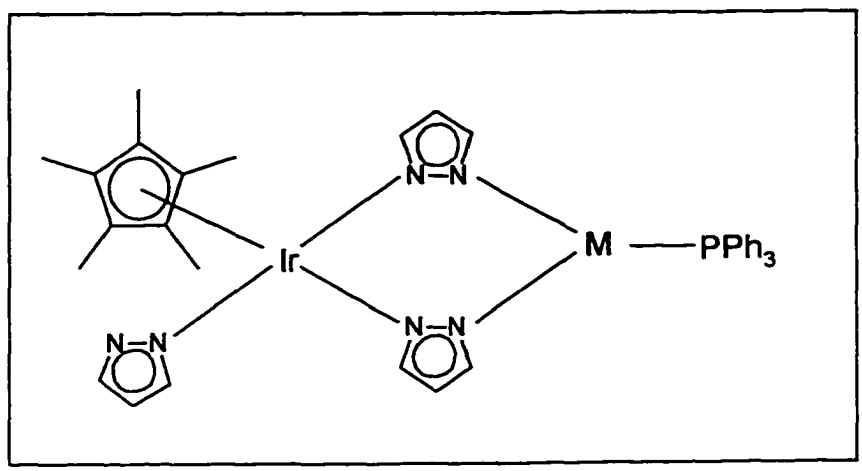

Interestingly, at ambient temperature in solution, ^1H NMR shows that there is a fast exchange between the coordinated and noncoordinated pyrazolates. On cooling the IrCu complex to 213 K the process is slowed down enough for two distinct pyrazolate signals to be observed in a 2:1 ratio [30]. Numerous heterodinuclear complexes have also been synthesised. In these complexes the ligand is either bidentate or tridentate, the mode of coordination generally depending upon the bonding requirements of the other metal centre. For example, the ligand is bidentate in $[Ir(\eta^5\text{-}C_5Me_5)(pz)(\mu\text{-}pz)_2Rh(CO)_2]$ [30], which contains a 16-electron rhodium(I), but tridentate in $[Ir(\eta^5\text{-}C_5Me_5)(\mu\text{-}pz)_3Rh(OOH)(dppe)][BF_4]$, which contains an 18-electron rhodium(III) [31].

Similar reactions and dynamic behaviours are observed in the ruthenium ligand as in the case of $[Ru(\eta^6\text{-}p\text{-cymene})(pz)_3M(PPh_3)]$ [32, 33].

1.4 Tris(diphenylphosphino)methane $(Ph_2P)_3CH$

Tris(diphenylphosphino)methane, $(Ph_2P)_3CH$, was originally prepared by Issleib and Abicht [34] in 1970. The ligand can be synthesised from bis(diphenylphosphino)methane (dppm) as shown in **Scheme 1.4** [34].

Scheme 1.4 The Preparation of $[(PPh_2)_3CH]$

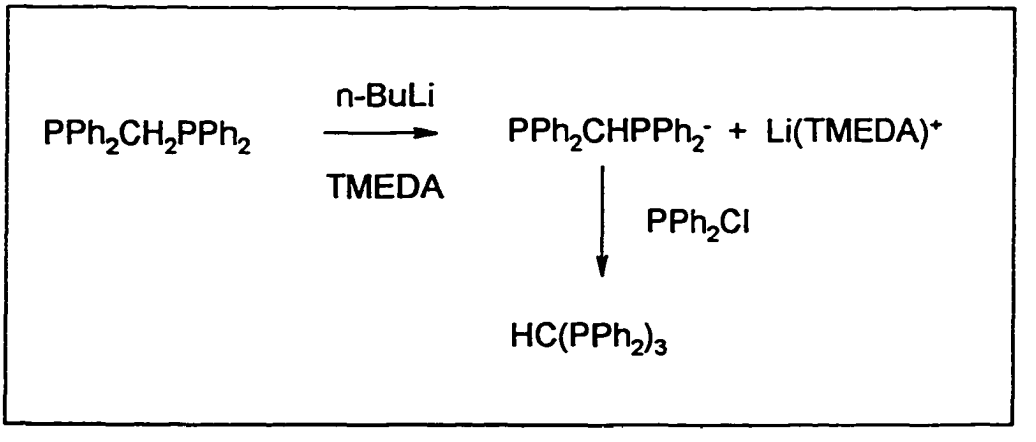

Since its synthesis the ligand has been used to make numerous complexes with many transition metals [35]. As in the case of its bidentate precursor, bis(diphenylphosphino)methane, the small bite angle in the ligand favours bridging modes of coordination rather than chelating modes. Indeed early research into its coordination chemistry showed that most of its compounds are polynuclear with each of the three phosphorous atoms coordinated to a different metal centre. For example, reaction of $(PPh_2)_3CH$ with AgO_2CR (R = Me, Et, *i*-Pr, C_6H_5), yields the trinuclear complexes $[\{(Ph_2P)_3CH\}Ag_3(O_2CR)_3]$, shown in **Figure 1.7** [36].

Figure 1.7 The Structure of [{$(PPh_2)_3CH$}$Ag_3(O_2CR)_3$]

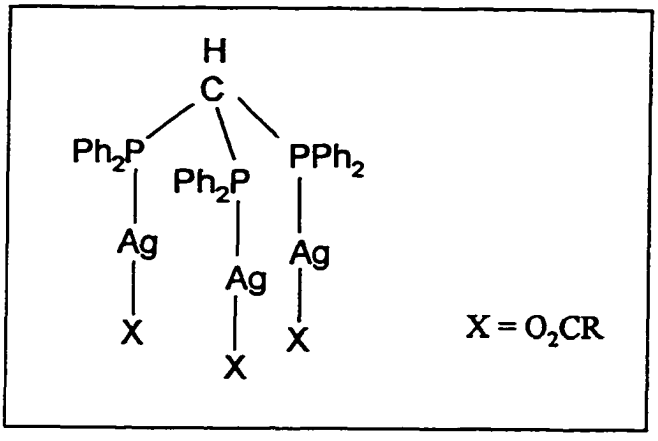

Osborn has synthesised a number of metal clusters with the ligand capping one face of a triangular array of metal atoms. For example, reaction of $Co_4(CO)_{12}$ with $HC(PPh_2)_3$ results in the substitution of three carbonyl ligands and the formation of $[Co_4(CO)_9\{(Ph_2P)_3CH\}]$ which is believed to have a tetrahedral metal framework with the tripod ligand capping one face of a triangular arrangement of cobalt atoms [37]. In a similar reaction the tripod ligand reacts with $Ru_3(CO)_{12}$ in tetrahydrofuran at room temperature. At least eight products were obtained of which one was the simple substitution product, $[\{(Ph_2P)_3CH\}Ru(CO)_9]$. Analysis of the cluster by ^{31}P NMR shows all three phosphorus atoms are equivalent, confirming that the tripod ligand symmetrically caps a triangular face of three ruthenium atoms [38].

The ligand has also been successfully used in template syntheses. A notable example is the reaction of $[CH(PPh_2)_3]$ with $[Ni(CO)_4]$ to give $[Ni_3(CO)_6\{(PPh_2)_3CH\}]$. The tripod ligand is seen as helping in the construction of the complex and effectively acts as a template [39]. A synthesis of a tetranuclear iridium cluster has been reported by Smith et

al [40]. The reaction is between the mononuclear $[IrCl(CO)_2(CH_3C_6H_4NH_2\text{-}p]$ and $CH(PPh_2)_3$ in the presence of Zn and CO and produces $[Ir_4(CO)_9\{CH(PPh_2)_3\}]$, in which the ligand is bonded in an η^3-μ^3 mode, along with a trinuclear cluster [40].

The first example of a complex in which all phosphorus atoms of the tridentate ligand are coordinated to only one metal centre was reported in 1984 by Goodrich and Selegue [41]. Ultraviolet radiation of [Fe(*p*-xylene)(Cp)][PF_6] and tris(diphenylphosphino)methane gave [Fe{$(PPh_2)_3CH$}(Cp)][PF_6]. A crystal structure analysis conclusively proved that the ligand was coordinating in an η^3 fashion to the iron atom, as shown in **Figure 1.8**.

Figure 1.8 The Crystal Structure of [Fe{$(PPh_2)_3CH$}(Cp)][PF_6]

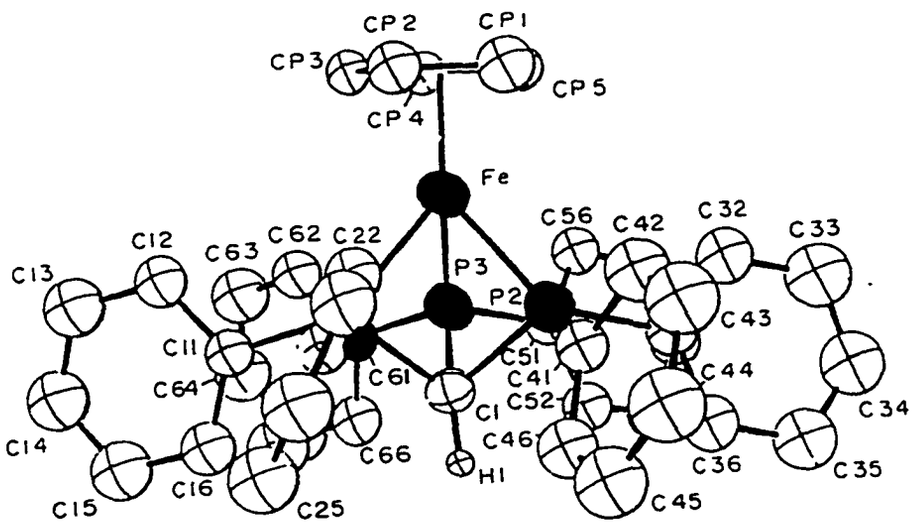

Since 1984 a number of other examples have been reported. The rhodium and iridium complexes, [{$(PPh_2)_3CH$}M(Cod)][BF_4], can be made according to the pathway shown in **Scheme 1.5** [42].

Scheme 1.5 The Synthesis of $[\{(PPh_2)_3CH\}M(Cod)]BF_4$

$$[M(Cod)_2]BF_4 + HC(PPh_2)_3 \longrightarrow [\{(PPh_2)_3CH\}M(Cod)]BF_4$$

(M = Rh, Ir)

Detailed NMR studies of the complexes show them to be 4-coordinate, presumably of square planar geometry, in solution with the tris(diphenylphosphino)methane acting as a bidentate ligand with only two phosphorus atoms coordinated to the metal centre [42], the third phosphorus atom dangling, as shown in **Figure 1.9**.

Figure 1.9 The Structure of $[\{(PPh_2)_3CH\}M(Cod)]^+$

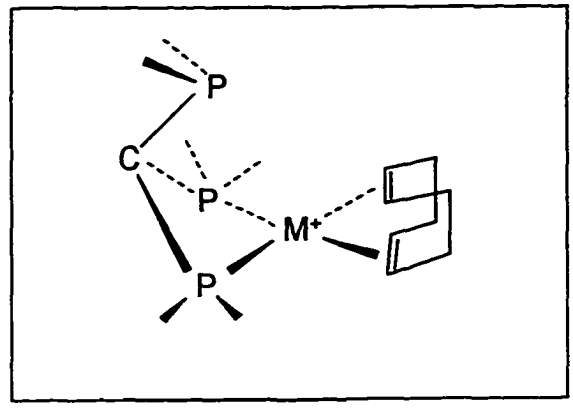

Detailed variable temperature ^{31}P NMR studies showed both complexes to be fluxional in solution. At room temperature the coordinated and uncoordinated phosphorus atoms are rapidly exchanging positions. The mechanism is proposed to be an intramolecular exchange process involving an associative pathway and the formation of a five-coordinate

intermediate, as illustrated in **Figure 1.10** [42].

Figure 1.10 The Proposed Mechanism for the Intramolecular Exchange Process in $[\{(PPh_2)_3CH\}M(Cod)]^+$

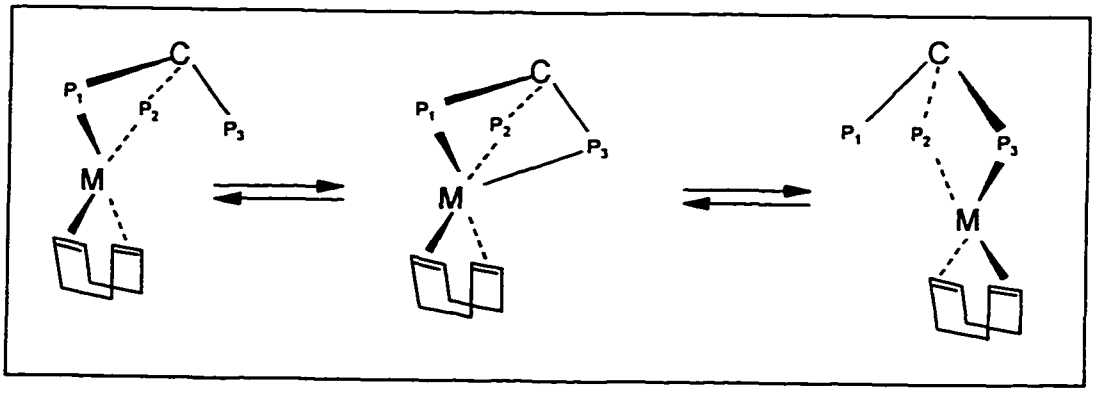

The mononuclear iron carbonyl, $[\{(PPh_2)_3CH\}Fe(CO)_3]$, has been synthesised [43]. It is one of several products produced by the reaction of $CH(PPh_2)_3$ and $Fe(CO)_5$. The complex has been characterised by both ^{31}P NMR and crystal structure analysis. Both in solution and the solid state only two phosphorus atoms of the tripod ligand are coordinated. Surprisingly an NMR study shows no exchange process occurring between the coordinated and non-coordinated phosphorus atoms in solution at room temperature [43]. In fact the dangling (or pendant) phosphorus atom has been utilised to synthesise heterobimetallic complexes. For example $[\{(PPh_2)_3CH\}Fe(CO)_3]$ reacts with one equivalent of $[Rh(CO)_2Cl]_2$ in tetrahydrofuran at 25°C to give $[(CO)_3FeRh\{(PPh_2)_3CH\}]^+[Rh(CO)_2Cl_2]^-$ [42]. The cation is essentially held together by

coordination of the dangling phosphorus atom to the rhodium and the formation of a Rh-Fe bond (Rh-Fe, 2.776(2) Å).

Another product of the reaction between the ligand and $Fe(CO)_5$ is $[\{(PPh_2)_3CH\}Fe(CO)_4]$, a complex in which only one of the phosphorus atoms of the ligand is coordinated [35]. The ligand is also monodentate in the molybdenum compound, $[\{(PPh_2)_3CH\}Mo(CO)_5]$ [35]. Beckett et al have reported the syntheses of the mononuclear chelated complexes of the general formula, $[M(\eta^2\text{-}(Ph_2P)_3CH)_2]^{n+}X_n$, (M = Rh, Ir, n = 1; M = Pd, Pt, n = 2; X = Cl^- or BF_4^-) [44]. In all of these complexes the geometry is essentially square planar with each ligand bonding in a bidentate mode to the metal centre. An X-ray structure determination of the $[Pt(\eta^2\text{-}(Ph_2P)_3CH)_2]^{2+}$ cation shows considerable distortion in the four-membered chelate ring as illustrated by the P-Pt-P bond angle of only 72.2°, as compared to a normal bond angle of 90° [44].

In summary then, numerous complexes of $[(PPh_2)_3CH]$ have been made and several different modes of coordination observed. These include the ligand acting as an $\eta^3\text{-}\mu_3$ bridging ligand, an $\eta^3\text{-}\mu_2$ bridging-chelating ligand, an η^2 or η^3 chelating ligand, and an η^1 monodentate ligand. These modes are summarised in **Figure 1.11**.

Figure 1.11 The Various Modes of Coordination Observed in Complexes of $[(PPh_2)_3CH]$

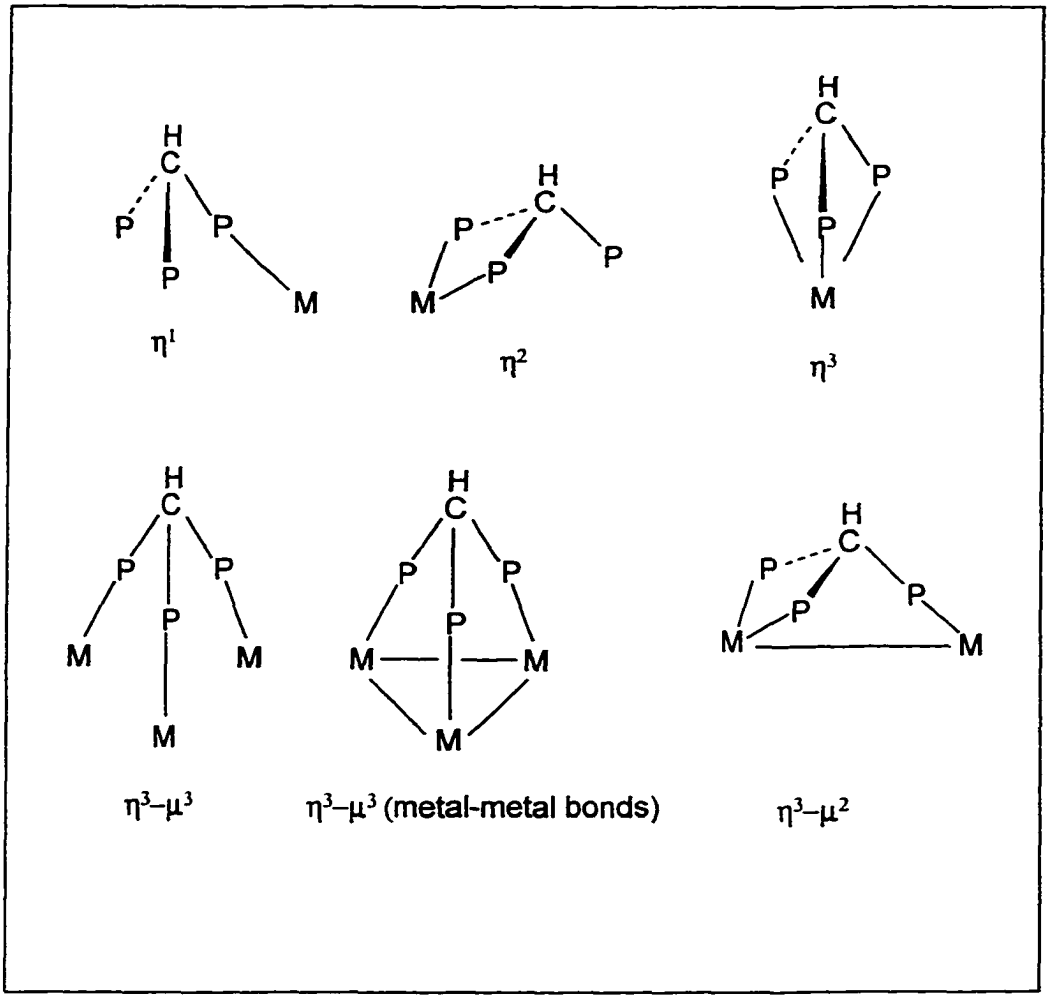

1.5 Chalcogenide Derivatives of Tris(diphenylphosphino)methane and Related Anions.

The phosphorus atoms of $(PPh_2)_3CH$ are quite susceptible to oxidation and the ligand is best stored under an inert atmosphere [34]. The group of Grim oxidised the ligand with various group 16 elements to obtain numerous derivatives [45]. For example, if

$(PPh_2)_3CH$ is carefully oxidised using controlled amounts of hydrogen peroxide at 0°C, $[Ph_2P(O)]_3CH$ can be isolated in good yield. When $(PPh_2)_3CH$ is heated with varying amounts of sulphur in toluene at 100°C, the sulphonated derivatives, $[PPh_2(S)][PPh_2]_2CH$, $[PPh_2(S)]_2[PPh_2]CH$, and $[PPh_2(S)]_3CH$ are produced. Similarly selenium can be used to produce $[PPh_2(Se)][PPh_2]_2CH$ and $[PPh_2(Se)]_2[PPh_2]CH$. The inability to synthesise $[PPh_2(Se)]_3CH$ was attributed to the extra steric requirements of the selenium atom as compared to the sulphur atom (the covalent radius of a selenium atom is 180 pm as compared to 102 pm for a sulphur atom) [45]. Numerous other ligands of the type $[PPh_2(X)][PPh_2(Y)][PPh_2(Z)]CH$ (where X,Y, and Z are various combinations of chalcogens and electron pairs) can be synthesised by further reactions of the ligands just described [45] . For example, $[PPh_2(S)][PPh_2(O)]_2CH$ and $[PPh_2(S)]_2[PPh_2(O)]CH$ were prepared by oxidation of $[PPh_2(S)][PPh_2]_2CH$ and $[PPh_2(S)]_2[PPh_2]CH$ with hydrogen peroxide at 0°C. Similarly, $[PPh_2(Se)][PPh_2(O)]_2CH$ and $[PPh_2(Se)]_2[PPh_2(O)]CH$ were prepared in the same manner by careful oxidation of $[PPh_2(Se)][PPh_2]_2CH$ and $[PPh_2(Se)]_2[PPh_2]CH$ respectively, although in this case the products could not be isolated in pure form and were characterised by NMR [45].

Studies of the ligands by variable temperature ^{31}P NMR have shown that there is a large barrier to rotation about the phosphorus methane carbon bond both in $[PPh_2(S)]_2[PPh_2]CH$ and $[PPh_2(S)]_3CH$ [46]. The activation energies for the rotation were estimated to be 29 and 49 kJ/mol respectively. At room temperature the $^{31}P\{^1H\}$ NMR spectrum of $[PPh_2(S)]_3CH$ shows only a singlet at 41.9 ppm. At -75°C a doublet (38.6 ppm) and a triplet (46.8 ppm) are observed which correspond to an AX_2 pattern. The

inequality of the phosphorus atoms is supported by the crystal structure of the ligand which essentially shows two equivalent phosphorus sulphur bonds pointing in a roughly antiparallel fashion to the C-H bond on the methine carbon [46]. The remaining phosphorus sulphur bond is essentially parallel to the methine C-H bond. Similar barriers to rotation were observed in $[PPh_2(O)]_2[PPh_2]CH$, and $[PPh_2(O)]_3CH$. Here the energies of activation for rotation around the P-C bonds were smaller (38.7 and 39.6 kJ/mol respectively). The greater ease of rotation would be expected when based on the smaller size of the chalcogen atom [45]. The crystal structure is shown on the left in **Figure 1.12.**

Figure 1.12 The Crystal Structure of $[(Ph_2P(S))_3CH]$ and the Representation of the Solid State Structure of the Molecule [46]

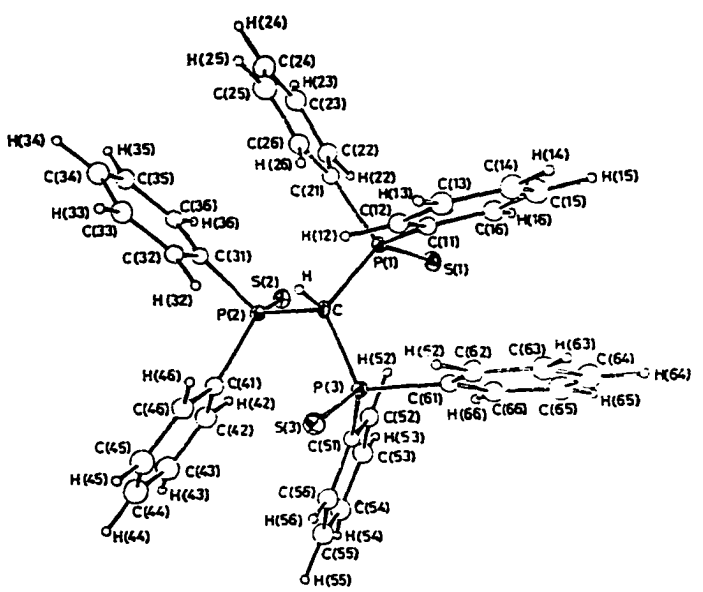

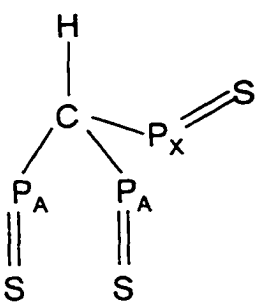

Grim also explored the possibility of deprotonating these ligands at the methine carbon in the hope of producing uninegative ligands which are potentially tridentate [46]. As previously mentioned the only other example of a tridentate uninegative ligand is the tris(pyrazolyl)borate ion and its analogues. The deprotonation at the methine carbon does not seem unreasonable in the light of the fact that the related ligands, $[Ph_2P(X)CH_2P(Y)Ph_2]$ (X = S or electron pair, Y = S or electron pair) can be deprotonated at the methylene carbon by reaction with n-butyllithium in tetrahydrofuran at 24°C to give the uninegative ions, $[Ph_2P(X)CH_2P(Y)Ph_2]^-$, as their lithium salts [36]. However numerous attempts to deprotonate $[PPh_2(S)]_3CH$ using a wide variety of bases proved initially unsuccessful [47]. Fortunately it was found that complexes containing the anionic ligand could be prepared by direct reaction of the neutral ligand with various metal complexes. For example, the reaction of $[PPh_2(S)]_3CH$ with mercuric halides in ethanol solution produced compounds of the formula $[(Ph_2P(S))_3C)HgX$, where X = Cl, Br, or I [48]. It was believed that as the ligand coordinates to the metal the mercury makes the methine hydrogen more acidic and aids in its transfer to the solvent. Analogous cadmium compounds were also synthesised although the presence of a mild base, such as triethylamine, was required [48]. It should be noted that no reaction occurred between triethylamine and $[PPh_2(S)]_3CH$ in the absence of the cadmium salt, emphasising the crucial role that the metal plays in the deprotonation of the ligand. The ^{31}P NMR spectra of the mercury complexes each consisted of a singlet with mercury-199 satellites, illustrating the equivalence of the phosphorus nuclei. A crystal structure determination was performed on a mercury complex of the related ligand, $[Me_2P(S)]_2[Ph_2P(S)]C^-$. In

$\{[Me_2P(S)]_2[Ph_2P(S)]C\}HgCl$ the mercury atom is in an essentially distorted tetrahedral environment with the ligand coordinated in a tridentate mode [48]. Two platinum complexes, $[PtCl(PEt_3)\{C(P(S)Ph_2)_3\}]$ and $[Pt(PEt_3)_2\{C(P(S)Ph_2)_3\}][BF_4]$, were reported by our group in 1986 [49]. These again were prepared by the reaction of the neutral ligand with $[Pt_2Cl_4(PEt_3)_2]$ and $[Pt_2Cl_2(PEt_3)_2][BF_4]_2$ respectively. Both complexes are square planar around the platinum(II) centre with the ligand bonding in a bidentate mode, as shown in **Figure 1.13**.

Figure 1.13 Bonding Modes in $[PtCl(PEt_3)\{C(P(S)Ph_2)_3\}]$ and $[Pt(PEt_3)_2\{C(P(S)Ph_2)_3\}]BF_4$

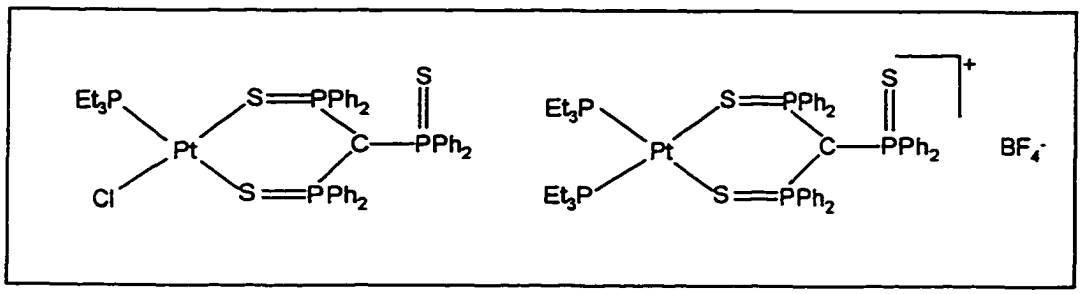

At room temperature the ^{31}P NMR spectrum of $[PtCl(PEt_3)\{C(P(S)Ph_2)_3\}]$ corresponds to the static structure shown in **Figure 1.13**, and there is no evidence for intramolecular exchange between the coordinated sulphur atoms and the noncoordinated sulphur [49]. However, at 130°C in DMSO the ^{31}P NMR spectrum indicates fast exchange between the noncoordinated sulphur and the coordinated sulphur which is *trans* to the triethylphosphine ligand. The coordinated sulphur which is *trans* to the chloro ligand does

not undergo exchange but is seen rather as acting as a pivot to anchor the ligand to the metal. Although a mechanism was not proposed an analysis of the variable temperature spectra yielded a large negative entropy of activation, ΔS^{o*}, which suggests an associative mechanism with a 5-coordinate activated complex with all three sulphur atoms coordinated. The labialising of the bond *trans* to the triethylphosphine ligand was rationalised by the *trans* effect which is greater for the phosphine than it is for the chloro ligand. Interestingly the other complex, $[Pt(PEt_3)_2\{C(P(S)Ph_2)_3\}][BF_4]$, was shown by ^{31}P NMR to undergo rapid exchange between all three sulphur atoms even at room temperature. This observation is not surprising in view of the fact that both sulphur atoms are *trans* to the labialising triethylphosphines.

In 1982 Grim et al reported the synthesis of the tetra-n-butylammonium salt of the anion $[PPh_2(S)]_3C^-$ by the reaction of $[PPh_2(S)]_3CH$ with lithium methoxide in methanol followed by metathesis with tetra-n-butylammoniuum iodide [50]. The salt was reported to be a high melting, fairly air stable crystalline solid. The high stability of the anion was in large part attributed to the large degree of mesomeric stabilisation as depicted in **Figure 1.14**.

In 1986 Grim et al reported the syntheses of the anions $[\{Ph_2P(O)\}_n\{Ph_2P(S)_{3-n}C]^-$ (n = 1,2, or 3) from their neutral precursors by proton abstraction using lithium methoxide [45]. The lithium salts of the anions were all reported to be air-stable, high melting, crystalline solids. The preparation of the anion made the future syntheses of complexes of the ligand potentially easier. The synthesis of the chalcogenide derivatives of $CH(PPh_2)_3$ also offered an opportunity to adjust the hardness or softness of the ligand

Figure 1.14 Mesomeric Stabilisation of the $[(P(S)Ph_2)_3C]^-$ Anion

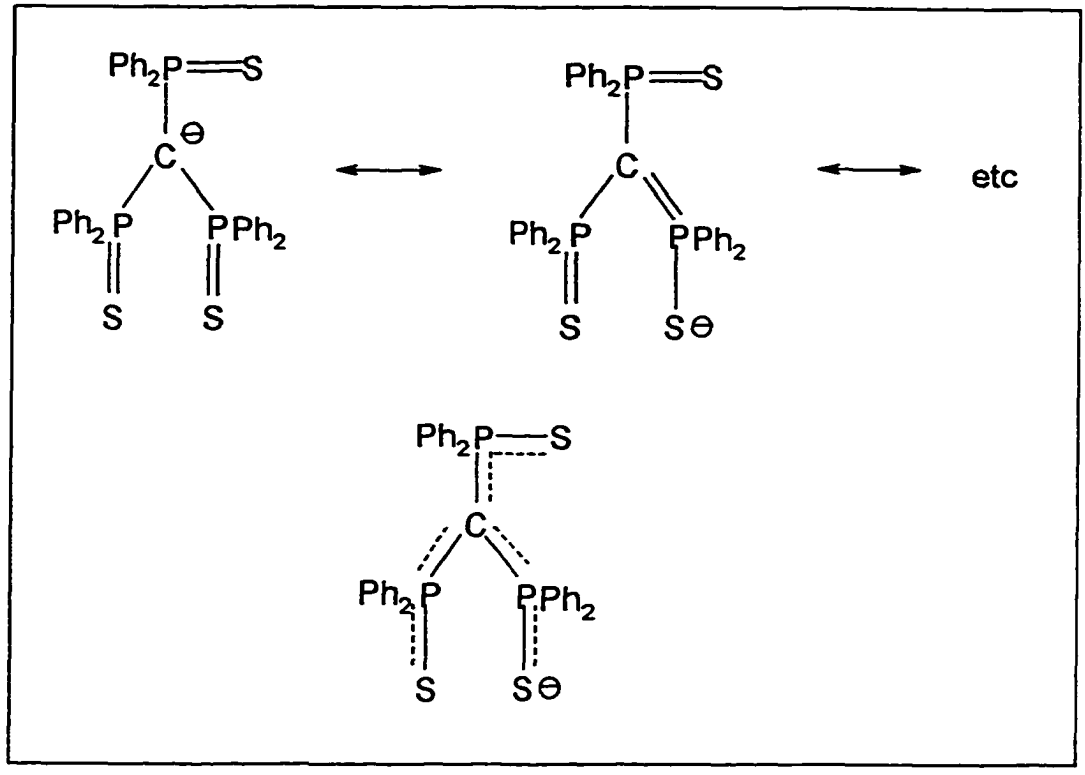

to suit the corresponding hardness or softness of the metal. In the anion $[PPh_2(S)]_3C^-$ the sulphurs are soft donors and would be expected to form stable complexes with soft metal acceptors and indeed complexes with the soft metal ions, Hg^{2+} [48], Ag^+ [51], and Au^+ [52], have been prepared. Interestingly the ligand was found to coordinate in a tridentate fashion in $[\{(Ph_2P(S))_3C\}HgX]$ [48] and $[\{(Ph_2P(S))_3C\}AgP(n\text{-}Bu)_3]$ [51], but only bidentate in $[\{(Ph_2P(S)_3C\}Au(n\text{-}BuPPh_2)]\cdot CH_3CN$ [52]. In a 1996 paper Gimeno et al described the synthesis and characterisation of $[\{(Ph_2P(S))_3C\}Ag(PPh_3)]$ in which the ligand coordinates in a tridentate mode [53]. In 1991 Grim et al reported the synthesis of $[Ir\{(Ph_2P(S))_3C\}(Cod)]$ by the reaction of the lithium salt of the anion with

$[(Cod)Ir(\mu\text{-}Cl)]_2$ [54]. The crystal structure was reported and showed a square planar complex with the ligand coordinated in a bidentate fashion. During the course of our own studies we also synthesised and characterised the same compound by a different route [55] and this will be discussed later in this thesis. In contrast, reaction of $[PPh_2(S)]_3C^-$ with some harder metals, such as Fe(II), have not led to the isolation of stable products [56]. In summary then the different observed modes of coordination for the $[PPh_2(S)]_3C^-$ ligand are η^2 (*S,S*), η^3 (*S,S,S*), and η^1 (*C*), and are shown in **Scheme 1.6**.

Scheme 1.6 The Various Modes of Coordination Observed in Complexes of $[(Ph_2P(S))_3C]^-$

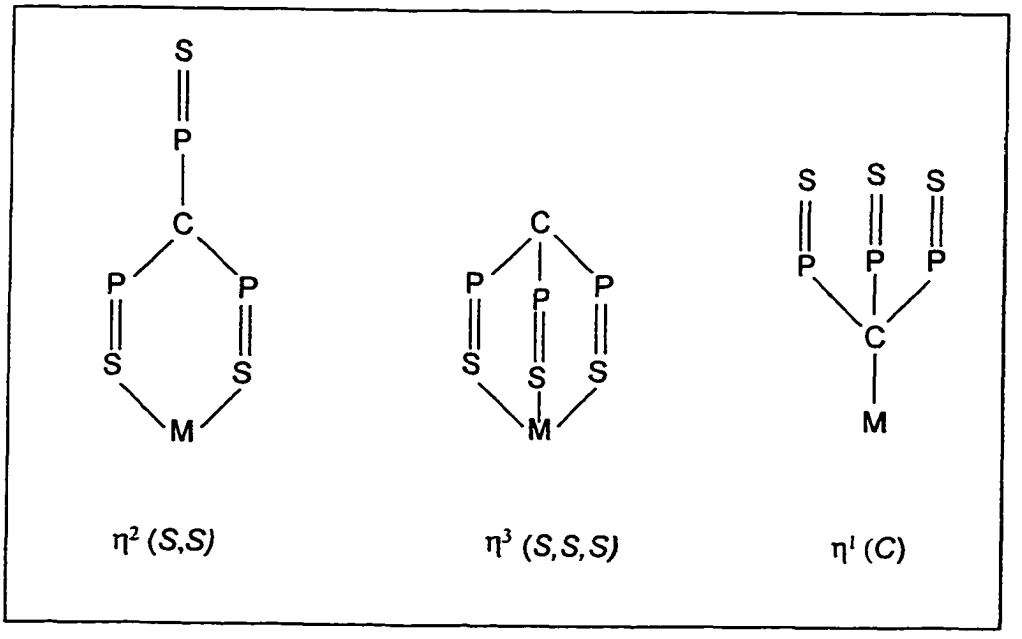

It was thought that the use of derivatives with oxygen atoms, harder donors than sulphur atoms, such as $[PPh_2(O)]_3CH$, might lead to the isolation of stable derivatives

when reacted with hard acceptors. In fact recent research has shown that this type of ligand forms stable complexes with both hard and soft metal centres. Reger et al have reported the synthesis of the homoleptic $[\{(\eta^2\text{-}Ph_2P(O))_3C\}_2Sn]$ in which the ligands are both coordinated in a bidentate, rather than a tridentate, fashion [57]. The X-ray crystal structure showed essentially trigonal planar geometry around the methine carbon in each ligand, much as expected for an sp^2 hybridised carbon. Another factor in favouring two coordination was seen as the high steric crowding between the six phenyl groups that three coordination of the ligand would require. However in the gold(I) complex, $[Au\{(Ph_2P(O))_3C\}(PPh_3)]$, the ligand, as shown by the crystal structure, is monodentate and is coordinated to the gold by the methanide carbon [58]. In a recent development Crabtree et al have prepared a number of rhodium and iridium complexes containing the tris(triphenyloxophosphoranyl)methanide ligand, $[PPh_2(O)]_3C^-$ [27]. Surprisingly, this ligand was not only found to form complexes with Ir(I) and Ir(III), but also with the much rarer Ir(V) and also to coordinate both in bidentate and tridentate modes. For example the iridium(I) complex, $[\{Ph_2P(O)\}_3CIr(C_2H_4)_2]$, reacted readily with sterically small silanes, $R_2R'SiH$, at 25°C, to give double oxidative addition products, $[\{Ph_2P(O)\}_3CIrH_2(SiR_3)_2]$ [59]. The ligand is bidentate in the former complex but tridentate in the latter. The reaction is shown in **Scheme 1.7**.

Scheme 1.7 The Reaction of $[Ir\{C(Ph_2P(O)_3\}(C_2H_4)_2]$ with Silanes

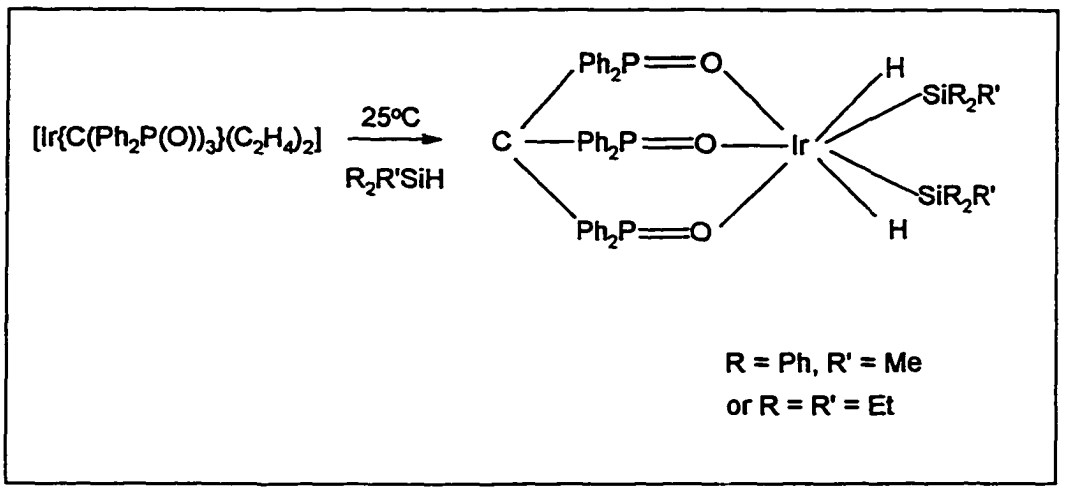

Interestingly the complexes $[\{Ph_2P(O)\}_3ClIr(ol)_2]$ (ol = C_2H_4, or cyclooctene) were also found to catalyse the hydrosilylation and dehydrogenative silylation of ethene with triphenylsilane or diphenylmethylsilane in dichloromethane. A unique feature of this catalysis is that no other olefinic substrate other than ethylene could be hydrosilylated [27].

1.6 Bisphosphine Chalcogenide Ligands

Even though bisphosphine chalcogenide ligands are bidentate rather than tridentate, they deserve some description here because of their close relationship to the trisphosphine chalcogenide ligands described in this thesis. Indeed the trisphosphine chalcogenide ligands can be seen as a natural extension of the bisphosphine chalcogenide ligands. Much work [60] had been performed in the laboratory of K.R. Dixon on these ligands for almost

ten years prior to the current work being started. Many of the ligands studied by Dixon's group can be represented by the general formula $[R'_2P(X)CHRP(Y)R''_2]^n$ (n = 0 or 1; R = H, CH_3, electron pair; R′ = alkyl, aryl; R′′= alkyl, aryl; X = S, electron pair; Y = S, Se). Numerous complexes were prepared, including those of palladium, platinum, rhodium, iridium, and ruthenium. In some cases the mode of coordination of a particular ligand varied from complex to complex. For example, the anionic disulphide ligand, $[Ph_2P(S)CHP(S)Ph_2]^-$, as its lithium salt, was found to cleave the chloro-bridged dimers, $[M(Cod)(\mu\text{-}Cl)]_2$ (M = Rh or Ir), to give the neutral complexes, $[M(Cod)\{Ph_2P(S)CHP(S)Ph_2\text{-}S,S\}]$, which contain six-membered chelate rings formed by *S,S* coordination [61]. In a similar reaction the platinum dimer, $[Pt_2Cl_2(\mu\text{-}Cl)_2(PEt_3)_2]$ reacts with $[Li][Ph_2P(S)CHP(S)Ph_2]$ to give $[PtCl(PEt_3)\{Ph_2P(S)CHP(S)Ph_2\text{-}C,S\}]$, in which the metal binds to the methine carbon and one sulphur atom of the ligand to produce a four-membered chelate ring [62]. The molecule is also fluxional in solution, with rapid exchange occurring between the coordinated and dangling sulphur atoms. The strong Pt-C bond is seen as acting as a fixed pivot for the exchange of the sulphur atoms. The lability of the platinum sulphur bond is again interpreted in terms of the strong *trans* effect of the triethylphoshine. This theory is further supported by the fact that the geometric isomer of the complex, in which the coordinated sulphur is now *trans* to chlorine rather than the phosphine, is static at the same temperature, 25 °C [62]. These complexes are depicted in **Figure 1.15**.

Figure 1.15 Structures of [M(Cod){PPh_2CHPPh_2-*S,S*}] and [PtCl(PEt_3){PPh_2CHPPh_2-*C,S*}]

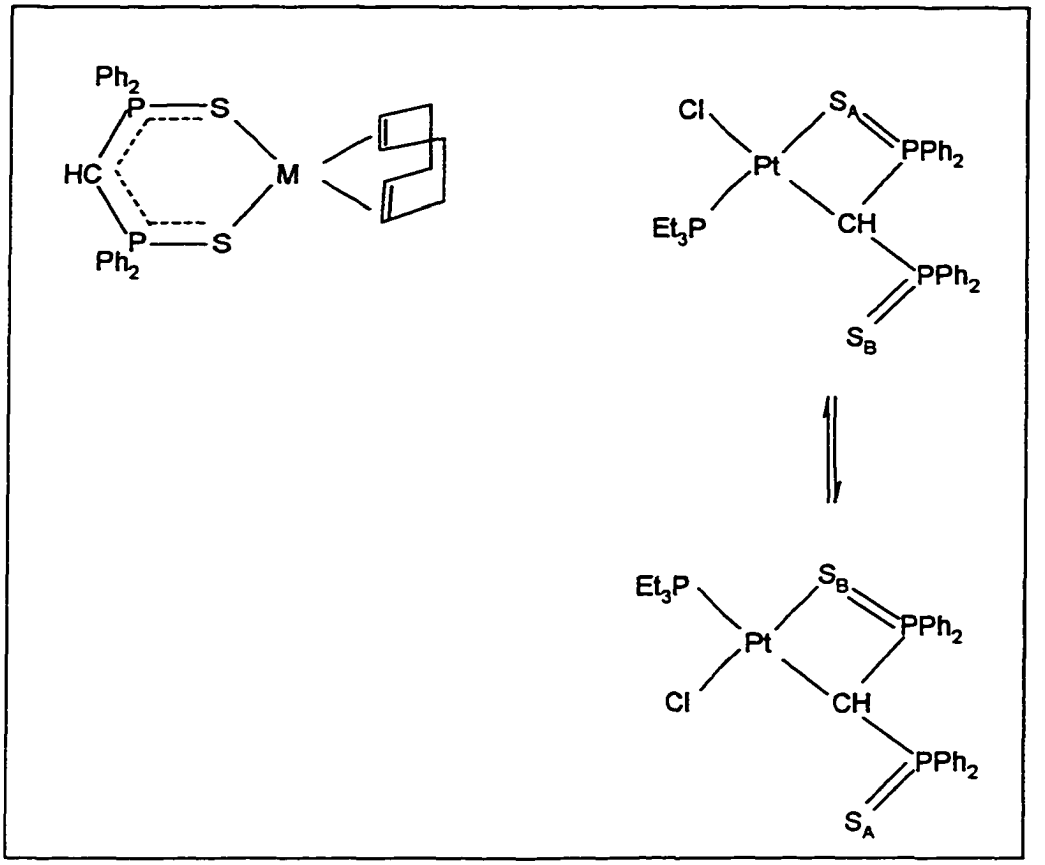

A number of complexes containing bisphosphine monochalcogenide ligands were also synthesised [63]. These included [$Ph_2PCH_2P(S)Ph_2$] and its anion, [$Ph_2PCHP(S)Ph_2$]$^-$. Generally chelating *P,S*-coordination was observed [63]. One notable exception is the ruthenium benzene complex, [$RuCl_2(\eta^6$-benzene){$Ph_2PCH_2P(S)Ph_2$-*P*}] where the ligand is monodentate, bonded to the metal via the phosphorus atom [64]. Abstraction of one equivalent of chloride with silver tetrafluoroborate induces the dangling sulphur atom to

coordinate at the ruthenium at the vacant site and yield the *P,S*-coordinated complex, [RuCl(η^6-benzene){$Ph_2PCH_2P(S)Ph_2$}-*P,S*]BF_4 as shown in **Scheme 1.8**.

Scheme 1.8 The Reaction of [RuCl(η^6-C_6H_6){$Ph_2PCH_2P(S)Ph_2$}-*P,S*] with $AgBF_4$

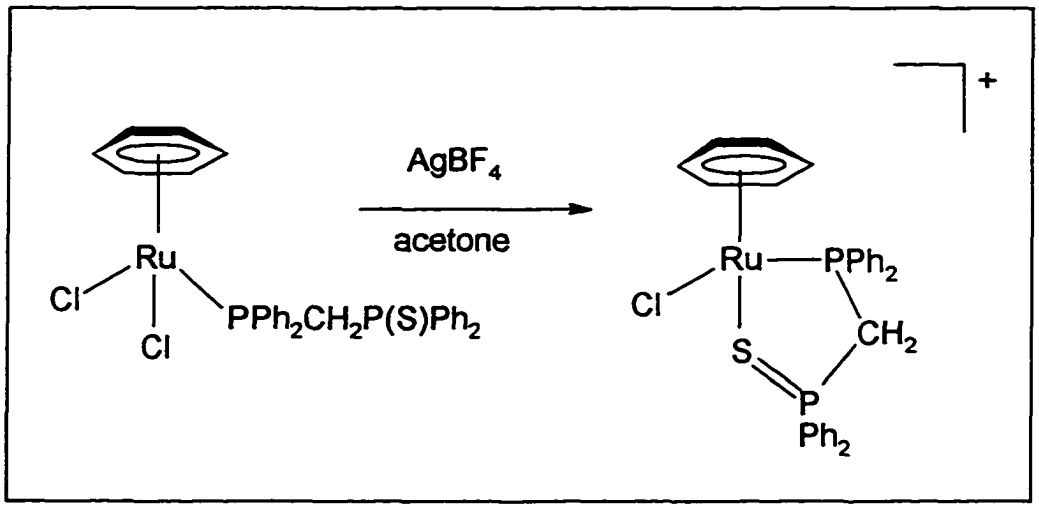

1.7 Goals and Objectives

At the time that this PhD work was begun in 1988 only a small number of metal complexes had been made with the [PPh_2(X)][PPh_2(Y)][PPh_2(Z)]CH and [PPh_2(X)][PPh_2(Y)][PPh_2(Z)]C^- ligand systems. This thesis will describe the synthesis and characterisation of new complexes containing some of the above tridentate ligands just described. Clearly it is beyond the scope of this project to research the coordination chemistry of all the different permutations of ligand some of which are very difficult to prepare. Rather it will focus on the preparation of complexes of palladium, platinum,

rhodium, and iridium with the ligands $[(PPh_2)(PPh_2(S))_2CH]$ and $[(PPh_2(S))_3CH]$ and their anionic derivatives. Based on the observations made in the chemistry of the chalcogenide derivatives of bis(diphenylphosphino)methane there should be significant differences in the coordination chemistry of the two ligand systems. On the one hand $[(PPh_2(S))_3CH]$ and $[(PPh_2(S))_3C]^-$ are both potentially tridentate, *S,S,S*-donor ligands whereas $[(PPh_2)(PPh_2(S))_2CH]$ and $[(PPh_2)(PPh_2(S))_2C]^-$ are both potentially tridentate, *P,S,S*-donor ligands. However, depending on the coordination requirements of the metal centre we may also expect to observe bidentate and even mondentate coordination. The modes of coordination of the ligands will therefore be thoroughly investigated in the solid state by X-ray diffraction studies, and in the solution state by NMR. Also the effect of substituting a strong M-P bond with a weaker, more labile, M-S bond will be studied. Based on related systems we expect to observe dynamic intramolecular exchange processes which can be effectively probed using ^{31}P NMR. These dynamic intramolecular exchange processes are of great interest because the potential site switching among the coordinated groups and the noncoordinated groups of the chelate ligands may provide some better understanding of catalysis. Also of interest will be the effect of removing the methine proton from the neutral ligand and the resulting changes, if any, in the coordinating properties of the ligand. In addition the reactivity of the complexes will be researched and compared to other related ligand systems, especially where catalytic activity has been observed. Characterisation of the complexes will be primarily by multinuclear NMR spectroscopy and microanalysis. In addition a number of crystal structures will be presented and discussed in detail.

Chapter Two will be concerned with the preparation of palladium allyl complexes of $[(PPh_2(S))_3CH]$, $[(PPh_2(S))_3C]^-$, $[(PPh_2)(PPh_2(S))_2CH]$, and $[(PPh_2)(PPh_2(S))_2C]^-$. In particular detailed studies of the fluxional behaviours of some of these complexes will be described, as well as descriptions of the crystal structures of $[Pd(\eta^3\text{-}C_4H_7)(CH(PPh_2)(P(S)Ph_2)_2\text{-}P,S)]BF_4 \cdot 2H_2O$ and $[Pd(\eta^3\text{-}C_4H_7)(CH(P(S)Ph_2)_3\text{-}S,S,S)]BF_4$. Chapter Three will discuss the preparation and characterisation of a number of iridium, rhodium, and platinum complexes of $[CH(P(S)Ph_2)_3]$ and $[C(P(S)Ph_2)_3]^-$. Variable temperature ^{31}P NMR will be used to probe the nature of the fluxional processes exhibited in $[Pt(MeoCod)\{C(P(S)Ph_2)_3\}]$ and $[Rh(Cod)\{C(P(S)Ph_2)_3\}]$. In addition the crystal structures of $[Rh(Cod)\{C(P(S)Ph_2)_3\text{-}S,S\}]$ and $[Ir(Cod)\{C(P(S)Ph_2)_3\text{-}S,S\}]$ will be described. In Chapter Three the preparation and characterisation of rhodium, iridium, and platinum complexes of the anion $[C(PPh_2)(P(S)Ph_2)_2]^-$ is presented. Also reactions of $[M(Cod)\{C(PPh_2)(P(S)Ph_2)_2\text{-}P,S\}]$ (M = Ir or Rh) will be explored in terms of ligand substitution and oxidative addition. The crystal structures of $[Rh(Cod)\{C(PPh_2)(P(S)Ph_2)_2\text{-}P,S\}]$ and $[RhI_2(^t\text{-}BuNC)_2\{C(PPh_2)(P(S)Ph_2)_2\text{-}P,S\}]$ are also described. Finally, Chapter Five will present the coordination chemistry of the neutral ligand, $[CH(PPh_2)(P(S)Ph_2)_2]$. In particular the preparation of complexes of palladium, platinum, rhodium, and iridium will be discussed. The crystal structures of the ligand and the iridium complex, $[Ir(Cod)\{CH(PPh_2)(P(S)Ph_2)_2\text{-}P,S,S\}]BF_4 \cdot CH_2Cl_2$, will also be described.

Chapter Two

Coordination Chemistry of Palladium π-allyl Complexes with $[CH(P(S)Ph_2)_3]$/ $[C(P(S)Ph_2)_3]^-$ and $[CH(PPh_2)(P(S)Ph_2)_2]$/ $[C(PPh_2)(P(S)Ph_2)_2]^-$

2.1 Synthesis and Characterization

The palladium complexes of $CH(PPh_2)(P(S)Ph_2)_2$ and $CH(P(S)Ph_2)_3$ have been synthesised in 57% and 65% yields respectively by reaction of the free ligands with $[Pd(\eta^3\text{-}C_4H_7)(\mu\text{-}Cl)]_2$ in the presence of $NaBF_4$, as shown in **Scheme 2.1**.

Scheme 2.1 Reactions of $CH(PPh_2)(P(S)Ph_2)_2$ and $CH(P(S)Ph_2)_3$ with $[Pd(\eta^3\text{-}C_4H_7)(\mu\text{-}Cl)]_2$

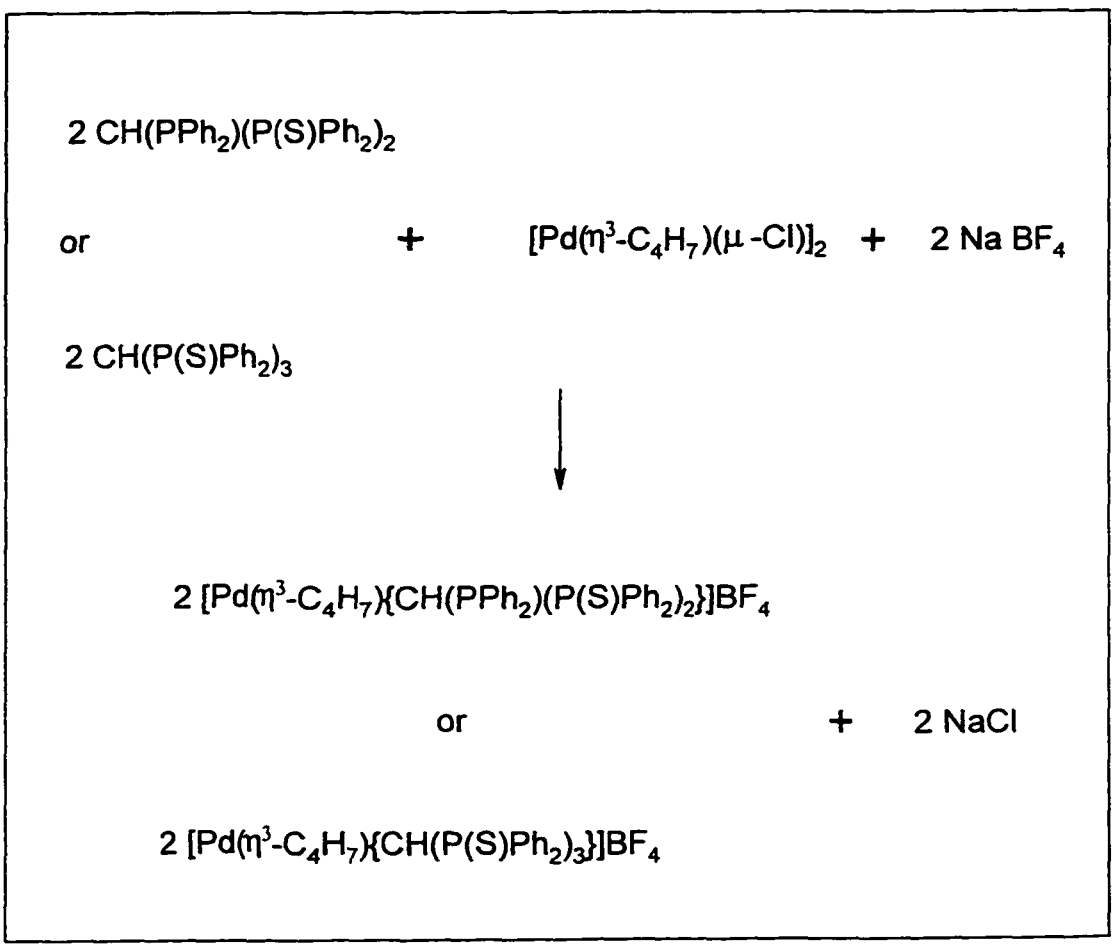

Both compounds are air stable, yellow crystalline materials. They have been fully characterized by microanalysis and ^{31}P $\{^1H\}$ NMR as well as by X-ray diffraction .

The complexes of $[C(PPh_2)(P(S)Ph_2)_2]^-$ and $[C(P(S)Ph_2)_3]^-$ have been synthesised in 64% and 53% yields by the reaction of the free ligands with $[Pd(\eta^3\text{-}C_4H_7)(\mu\text{-}Cl)]_2$, in the presence of a weak base, diethylamine, in the molar ratio of 2:1, as shown in **Scheme 2.2**.

Scheme 2.2 Reactions of $CH(PPh_2)(P(S)Ph_2)_2$ and $CH(P(S)Ph_2)_3$ with $[Pd(\eta^3\text{-}C_4H_7)(\mu\text{-}Cl)]_2$ in the Presence of Diethylamine.

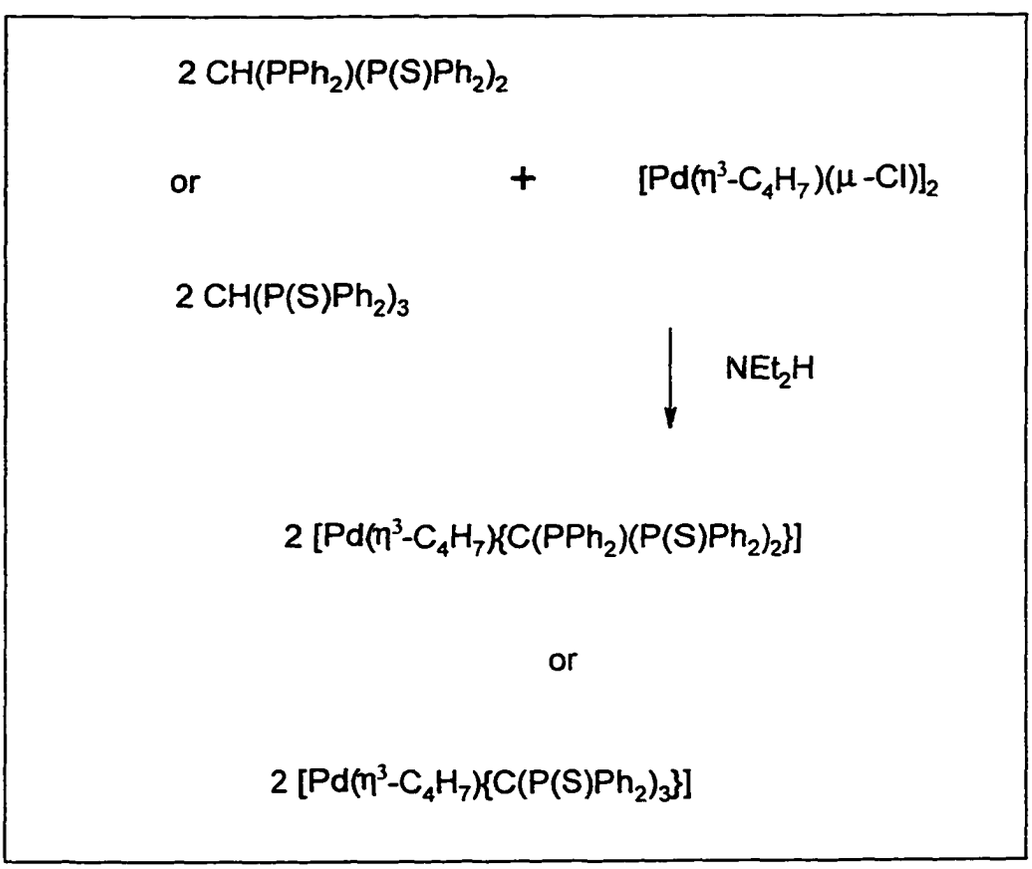

Both of the above two complexes are air-stable, crystalline compounds. $[Pd(\eta^3\text{-}C_4H_7)\{C(PPh_2)(P(S)Ph_2)_2\}]$ is bright-yellow and $[Pd(\eta^3\text{-}C_4H_7)\{C(P(S)Ph_2)_3\}]\cdot CH_2Cl_2$ is an orange material. They are fully characterized by microanalysis and $^{31}P\ \{^1H\}$NMR. The dissociation of the methine proton occurs only after the addition of the weak base, diethylamine. This observation confirms that the ligand coordinates to the metal before it deprotonates.

There were no reactions observed when the Pt analogue, $[Pt(\eta^3\text{-}C_4H_7)(\mu\text{-}Cl)]_2$, was combined with the ligands under the same conditions. This may either be that palladium is a more labile metal than platinum, or that the tripodal ligands may not be strong enough nucleophilic ligands for the platinum metal centre, or a combination of both factors.

Nuclear magnetic resonance parameters for the complexes $[Pd(\eta^3\text{-}C_4H_7)\{C(PPh_2)(P(S)Ph_2)_2\}]$, $[Pd(\eta^3\text{-}C_4H_7)\{CH(PPh_2)(P(S)Ph_2)_2\}]BF_4$, $[Pd(\eta^3\text{-}C_4H_7)\{C(P(S)Ph_2)_3\}]$ and $[Pd(\eta^3\text{-}C_4H_7)\{CH(P(S)Ph_2)_3\}]BF_4$ are collected in **Tables 2.1** and **2.2**. The ^1H spectra , shown in **Figure 2.1**, serve mainly to confirm the presence of the methine proton in the protonated complexes. The resonances appear as quartets with two bond P-H couplings of about 9 to 11 Hz at 6.1 to 6.2 ppm, and this interpretation is also confirmed by multiplicity sorting (DEPT) experiments at ambient temperature and by the presence of a typical BF_4^- band at 1009 cm^{-1} in the infrared spectrum of both protonated complexes. For both ^1H NMR spectra, the resonances of multiplets around 7 to 8 ppm are assigned to the aromatic protons of the phenyl groups. The resonances of singlets around 4.2 to 4.3 ppm are assigned to H_{syn} and 3.2 to 3.5 ppm

are assigned to H_{anti} of the allyl group. As well, the singlets appearing around 2.0 to 2.3 ppm are assigned to CH_3 of the allyl group. The three small peaks appearing next to the allyl protons on the ^1H NMR spectrum of $[Pd(\eta^3\text{-}C_4H_7)\{CH(P(S)Ph_2)_3\}]BF_4$, shown in **Figure 2.1(A)**, are due to the presence of the deprotonated complex of $[Pd(\eta^3\text{-}C_4H_7)\{C(P(S)Ph_2)_3\}]$. The resonances at 5.3 ppm on both spectra and 0.8 to 1.6 ppm on the spectrum of $[Pd(\eta^3\text{-}C_4H_7)\{CH(PPh_2)(P(S)Ph_2)_2\}]BF_4$, shown in **Figure 2.1(B)** are assigned to the solvents. The signal of methine carbon of $[Pd(\eta^3\text{-}C_4H_7)\{C(P(S)Ph_2)_3\}]$ was not observed on its $^{13}C\{^1H\}$ NMR spectrum due to the lack of NOE effect.

Table 2.1. Selected Nuclear Magnetic Resonance Parameters for Complexes (A) $[Pd(\eta^3\text{-}C_4H_7)\{CH(PPh_2)(P(S)Ph_2)_2\}]BF_4$; (B)$[Pd(\eta^3\text{-}C_4H_7)\{C(PPh_2)(P(S)Ph_2)_2\}]$

Complex	**A**	**B**
Notes	a,c	b,c
δH of C(1)	6.08	N/A
J(P-H)	8.5	N/A
$\delta(P_A)$	52.3	62.2
$\delta(P_B)$	52.3	43.8
$\delta(P_C)$	48.6	35.1
$J(P_A\text{-}P_B)$	N/A	48.2
$J(P_A\text{-}P_C)$	39.4	121.9
$J(P_B\text{-}P_C)$	39.4	17.8

Notes: a. CD_2Cl_2 solution.

b. Dichloromethane solution with an external C_6D_6 lock.

c. The labelling scheme is presented on the page 44.

Figure 2.1 ^{1}H NMR Spectra of (A) $[Pd(\eta^3\text{-}C_4H_7)\{CH(P(S)Ph_2)_3\}]BF_4$ in CD_2Cl_2; (B) $[Pd(\eta^3\text{-}C_4H_7)\{CH(PPh_2)(P(S)Ph_2)_2\}]BF_4$ in CD_2Cl_2 at 250 MHz and Ambient Temperature.

(A) $[Pd(\eta^3\text{-}C_4H_7)\{CH(P(S)Ph_2)_3\}]BF_4$

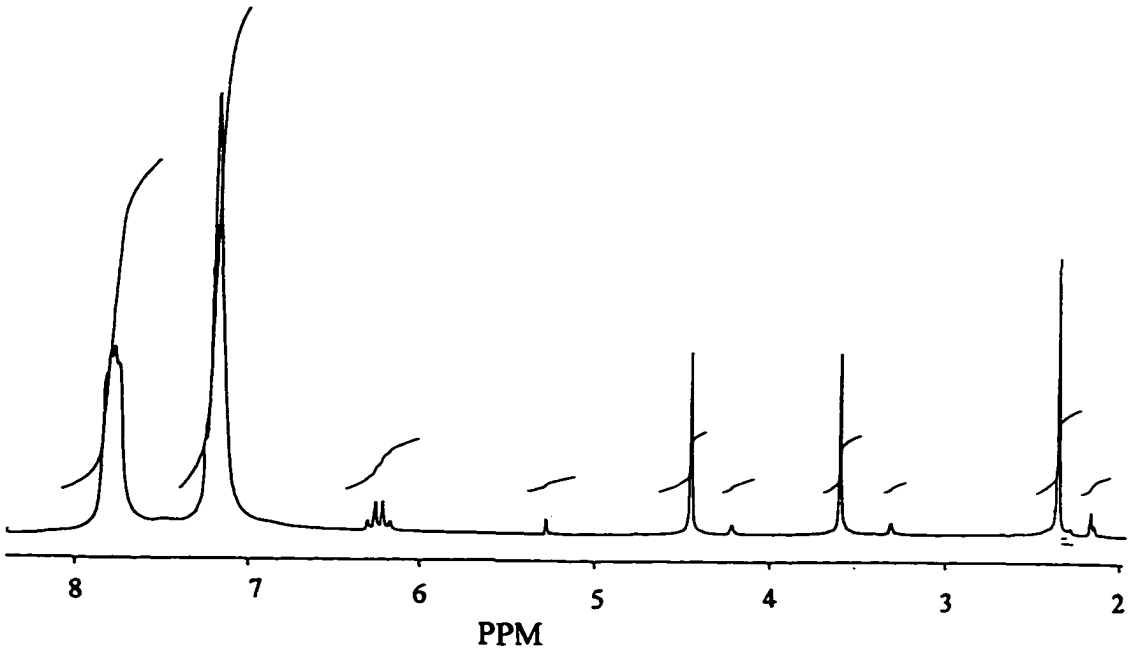

(B) $[Pd(\eta^3\text{-}C_4H_7)\{CH(PPh_2)(P(S)Ph_2)_2\}]BF_4$

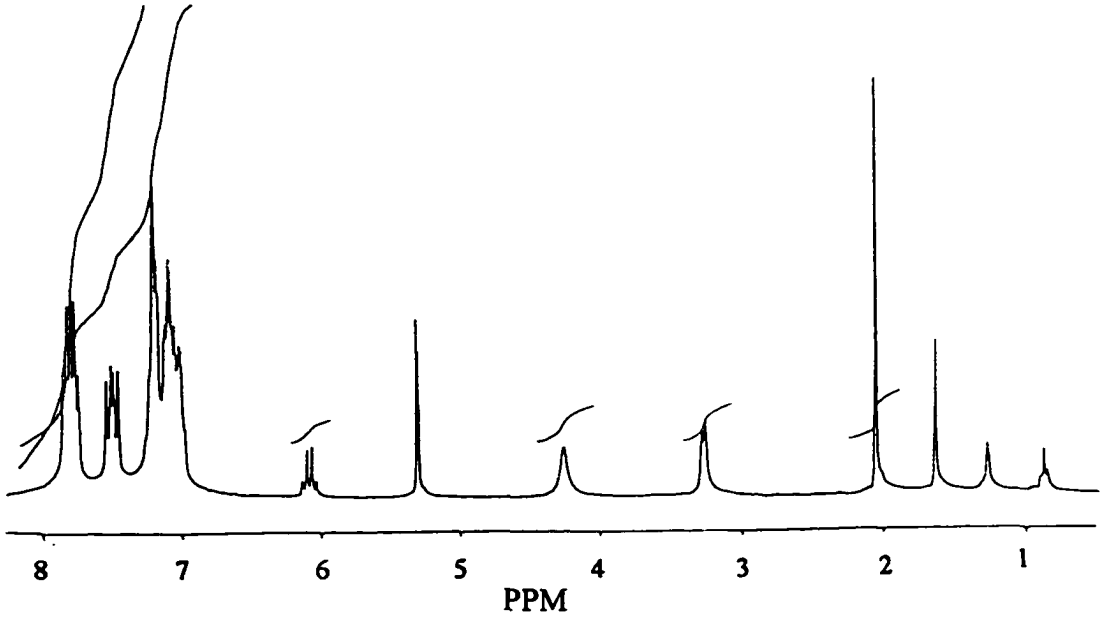

Table 2.2 Selected Nuclear Magnetic Resonance Parameters for Complexes $[Pd(\eta^3\text{-}C_4H_7)\{CH(P(S)Ph_2)_3\}]BF_4$ and $[Pd(\eta^3\text{-}C_4H_7)\{C(P(S)Ph_2)_3\}]$

Complex	$[Pd(\eta^3\text{-}C_4H_7)\{CH(P(S)Ph_2)_3\}]BF_4$	$[Pd(\eta^3\text{-}C_4H_7)\{C(P(S)Ph_2)_3\}]$
Notes	a,b	c
δP	41.9 [a]	41.3
$\delta(C_A)$	36.4 [b]	nr[d]
$J(P\text{-}C_A)$	30.6 [b]	N/A[e]
$\delta(H_A)$	6.2 [a]	N/A[e]
$J(P\text{-}H_A)$	10.9 [a]	N/A[e]

Notes: a. CD_2Cl_2 solution.

b. $CDCl_3$ solution.

c. Dichloromethane solution with an external C_6D_6 lock.

d. Not observed

e. Not applicable

The $^{31}P\{^1H\}$ NMR of $[Pd(\eta^3\text{-}C_4H_7)\{C(PPh_2)(P(S)Ph_2)_2\}]$ showed three resonances, each a doublet of doublets, as expected for η^2-P,S coordination. This is a simple first order pattern with three signals for the $[C(PPh_2)(P(S)Ph_2)_2]^-$ ligand. The labelling scheme for the various phosphorus atoms are as follows (phenyl groups have been omitted for clarity):

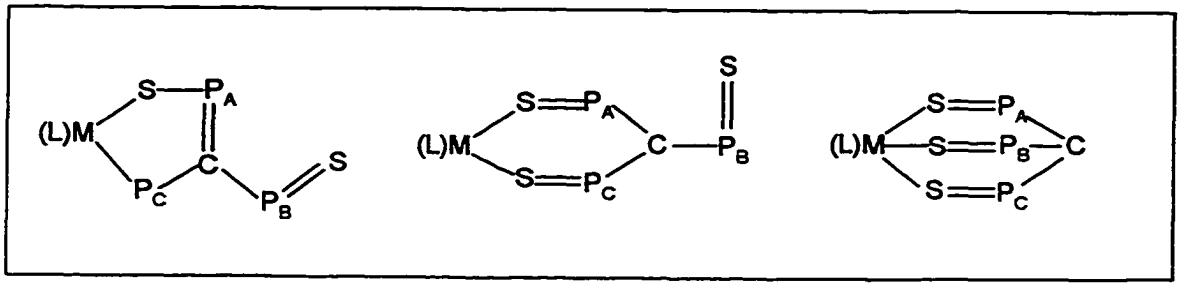

The δP_B value of 43.8 ppm is similar to those for the $Ph_2P{=}S$ groups of the free ligands, $CH(PPh_2)(P(S)Ph_2)_2$ (43.5 ppm), and $CH(P(S)Ph_2)_3$ (41.9 ppm) and also corresponds closely to the non-coordinated $Ph_2P{=}S$ groups of related complexes of our research, reported in Chapter Four of this thesis, such as $[Rh(Cod)\{C(PPh_2)(P(S)Ph_2)_2\}]$ (42.3 ppm), and $[Ir(cod)\{C(PPh_2)(P(S)Ph_2)_2\}]$ (41.7 ppm) [65]. It is then an indication of a "dangling" $Ph_2S{=}P$ resonance.

The δP_A and $^2J(P_A\text{-}P_C)$ (62.8 ppm, 122 Hz) are comparable to the values of the complexes in our other related studies discussed in detail in Chapter Four, such as $[Rh(Cod)\{C(PPh_2)(P(S)Ph_2)_2\}]$ (56.0 ppm, 114 Hz) , $[Ir(Cod)\{C(PPh_2)(P(S)Ph_2)_2\}]$ (65.6 ppm, 112 Hz), $[Rh(^tBuNC)_2\{C(PPh_2)(P(S)Ph_2)_2\}]$ (63.7 ppm, 132 Hz) , $[PtCl(PEt_3)\{C(PPh_2)(P(S)Ph_2)_2\}]$ (isomer ii, 62.8 ppm, 110 Hz) and $[Pt(MeoCod)\{C(PPh_2)(P(S)Ph_2)_2\}]$ (isomer ii, 67.2 ppm, 143 Hz) [65]. The increase in the value of δP_A, as compared with the free ligand $CH(PPh_2)(P(S)Ph_2)_2$ [46], is largely due to the deshielding commonly observed during the formation of the 5-membered chelate ring [66]. As we can see here, changing metals doesn't significantly alter the observed

coordination shifts. This is in agreement with what Hilts observed in the complexes Rh, Ir, Pd and Pt complexes of the related ligand, $CH_2(PPh_2)(P(S)Ph_2)$ [63].

The δP_C (35.1 ppm) and $J(P_B\text{-}P_C)$ (18 Hz) values are comparable to those of $[Rh(Cod)\{C(PPh_2)(P(S)Ph_2)_2\}]$ (39.5 ppm, 20 Hz) , $[Ir(Cod)\{C(PPh_2)(P(S)Ph_2)_2\}]$ (36.3 ppm, 15 Hz) and $[Pt(MeoCod)\{C(PPh_2)(P(S)Ph_2)_2\}]$ (isomer ii, 35.7 ppm, 20 Hz) [65], since changing metals doesn't significantly affect the coordination shifts [66]. The δP_C value shows a sizable increase compared with the δP_C of -10 ppm in the free ligand, $CH(PPh_2)(P(S)Ph_2)_2$. This substantial deshielding is due to the coordination and formation of the 5-membered chelate ring [66]. However, the deshielding in the palladium complex is less than that found in $[Rh(^tBuNC)_2\{C(PPh_2)(P(S)Ph_2)_2\}]$ where the two ^tBuNC ligands result in a further downfield shift of 50.8 ppm [65].

In contrast, the ^{31}P NMR spectrum of the protonated complex $[Pd(\eta^3\text{-}C_4H_7)\{CH(PPh_2)(P(S)Ph_2)_2\}]BF_4$ consists of only two resonances; a triplet at 48.6 ppm and a doublet at 52.3 ppm with a coupling of 39 Hz. The doublet shift of δ_A and δ_B at 52.3 ppm is similar to $[Ir(Cod)\{CH(PPh_2)(P(S)Ph_2)_2\}]BF_4$ (52.8 ppm) [67], $[Rh(Cod)\{CH(PPh_2)(P(S)Ph_2)_2\}]BF_4$ (51.5 ppm) and $[PdCl(PEt_3)\{CH(PPh_2)(P(S)Ph_2)_2\}]BF_4$ (52.8 ppm) [67]. When compared with the coordinated $Ph_2P{=}S$ of δ_B at 62.8 ppm and the non-coordinated $Ph_2P{=}S$ of δ_A at 43.8 ppm in the protonated complex, $[Pd(\eta^3\text{-}C_4H_7)\{CH(PPh_2)(P(S)Ph_2)_2\}]BF_4$, the value of 52.3 ppm of the doublet in the deprotonated complex is an intermediate between coordinated and non-coordinated $Ph_2P{=}S$ groups, which suggests an interchange between the coordinated $Ph_2P{=}S$ of and the non-coordinated $Ph_2P{=}S$ groups in the deprotonated

complex. The triplet of δP_C at 48.6 ppm is similar to $[Rh(Cod)\{CH(PPh_2)(P(S)Ph_2)_2\}]BF_4$ (46.7 ppm) [67], but markedly different from $[Ir(Cod)\{CH(PPh_2)(P(S)Ph_2)_2\}]BF_4$ (37.3 ppm) [67]. This perhaps is due to its closer resemblance in geometry to the rhodium complex where the ligand most likely coordinates to the metal centre via an η^2-P, S mode while in the iridium complex the ligand coordinates to the metal centre in an η^3-P, S, S mode. The fact that the $^{31}P\{^1H\}$ NMR spectrum of the complex displays a doublet and a triplet gives two possibilities in the determination of the coordination mode; a tripodal η^3-P,S,S 5-coordination or a bidentate η^2-P,S 4-coordination with dynamic exchange between the two Ph_2P=S groups. The low temperature $^{31}P\{^1H\}$ NMR study shows the latter is the case and the detailed study will be discussed later in this chapter. **Figure 2.2** shows the $^{31}P\{^1H\}$ NMR spectra of $[Pd(\eta^3\text{-}C_4H_7)\{C(PPh_2)(P(S)Ph_2)_2\}]$ and $[Pd(\eta^3\text{-}C_4H_7)\{CH(PPh_2)(P(S)Ph_2)_2\}]BF_4$.

Both $^{31}P\{^1H\}$ NMR spectra of $[Pd(\eta^3\text{-}C_4H_7)\{C(P(S)Ph_2)_3\}]$ and $[Pd(\eta^3\text{-}C_4H_7)\{CH(P(S)Ph_2)_3\}]BF_4$ showed singlets at +41.3 ppm and +41.9 ppm respectively, which are closer to the chemical shift of +39.8 ppm in the fluxional $[Rh(Cod)\{C(P(S)Ph_2)_3\}]$ [68]. This suggests either an η^2-S,S 4-coordination, with a dynamic intramolecular exchange process between all three Ph_2P=S groups, or an η^3-S,S,S 5-coordination. To distinguish between the two possible coordination modes, and to study any possible fluxional behaviour, variable low temperature $^{31}P\{^1H\}$ NMR experiments have been carried out. The low temperature $^{31}P\{^1H\}$ NMR of $[Pd(\eta^3\text{-}C_4H_7)\{C(P(S)Ph_2)_3\}]$ showed a doublet and a triplet, which suggests a η^2-S,S 4-coordination with a dynamic intra-molecular exchange process occurring at ambient

Figure 2.2 $^{31}P\{^{1}H\}$ NMR Spectra of (A) $[Pd(\eta^3\text{-}C_4H_7)\{C(PPh_2)(P(S)Ph_2)\}]$ in CH_2Cl_2/C_6D_6; (B) $[Pd(\eta^3\text{-}C_4H_7)\{CH(PPh_2)(P(S)Ph_2)_2\}]BF_4$ in CD_2Cl_2 at 101.3 MHz and Ambient Temperature.

(A) $[Pd(\eta^3\text{-}C_4H_7)\{C(PPh_2)(P(S)Ph_2)\}]$

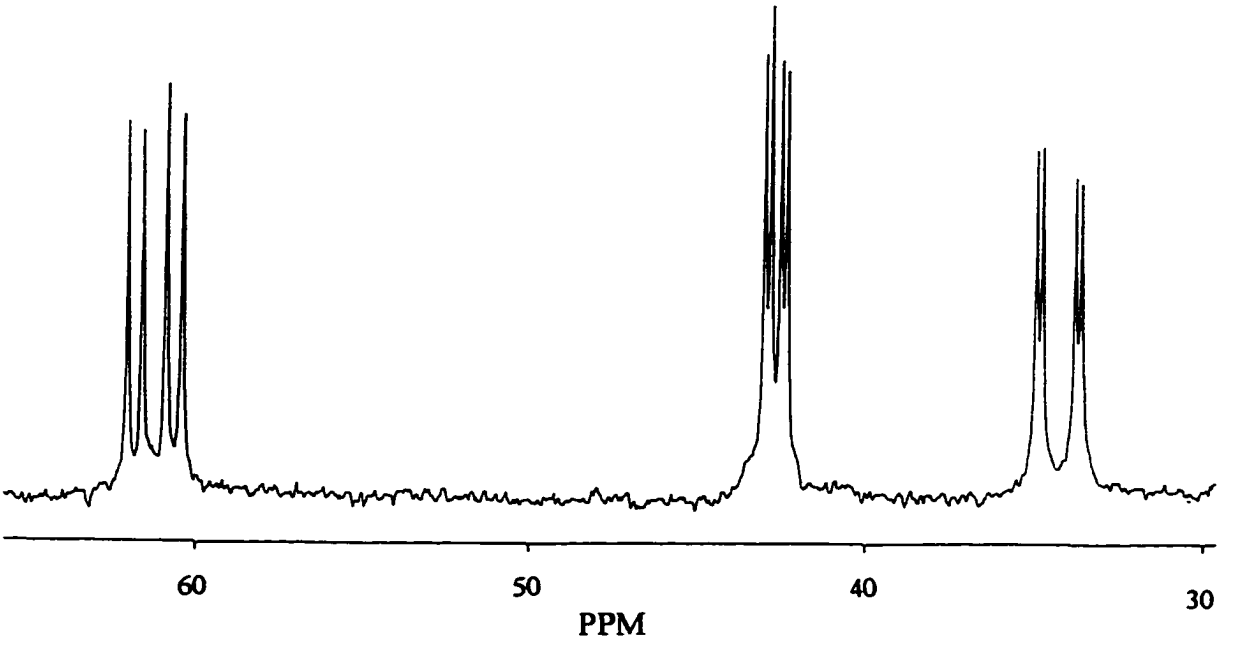

(B) $[Pd(\eta^3\text{-}C_4H_7)\{CH(PPh_2)(P(S)Ph_2)_2\}]$

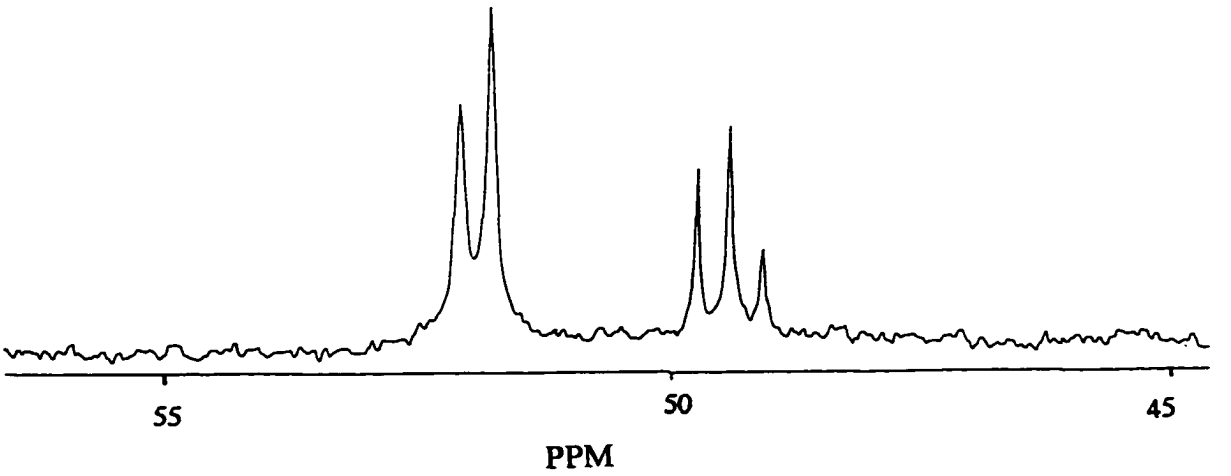

temperature. However, the low temperature $^{31}P\{^1H\}$ NMR of $[Pd(\eta^3\text{-}C_4H_7)\{CH(P(S)Ph_2)_3\}]BF_4$, recorded down to -90°C, gave no indication of any slowing of such a process, and prompted us to examine the complex by X-ray diffraction, which shows a 5-coordinate structure with η^3-S,S,S coordination in the solid-state. The ^1H NMR of $[Pd(\eta^3\text{-}C_4H_7)\{CH(P(S)Ph_2)_3\}]BF_4$ shows a quartet at 6.2 ppm, assigned to a methine proton, coupled through the methine carbon to three equivalent phosphorus nuclei. The coupling constant, $^2J(P\text{-}H)$, is 10.9 Hz.

2.2 Dynamic NMR of $[Pd(\eta^3\text{-}C_4H_7)\{CH(PPh_2)(P(S)Ph_2)_2\}]BF_4$

The ^{31}P NMR spectrum of $[Pd(\eta^3\text{-}C_4H_7)\{C(PPh_2)(P(S)Ph_2)_2\}]$, illustrated in **Figure 2.2A**, supports a rigid 4-coordinate structure with η^2-P,S coordination at ambient temperature. In contrast, the ambient temperature $^{31}P\{^1H\}$ NMR spectrum of $[Pd(\eta^3\text{-}C_4H_7)\{CH(PPh_2)(P(S)Ph_2)_2\}]BF_4$, illustrated in **Figure 2.2B**, shows equivalency between the coordinated $P_A(S)Ph_2$ group and the non-coordinated $P_B(S)Ph_2$ group. The doublet at +52.0 ppm is assigned to the exchanging P_A and P_B. The triplet at +49.0 ppm is assigned to P_C. The coupling constant, $J(P_A\text{-}P_C)$ or $J(P_B\text{-}P_C)$, is 39.2 Hz. As the temperature is reduced, the doublet at +52.0 ppm begins to broaden at first and at -35°C resolves into two doublets at +52.8 ppm and +49.5 ppm. The triplet at +49.0 ppm does not split into a doublet of doublets until -60°C. The spectra over the temperature range from ambient to -50°C are shown in **Figure 2.3**.

Figure 2.3 $^{31}P\{^{1}H\}$ NMR Spectra of $[Pd(\eta^3\text{-}C_4H_7)\{CH(PPh_2)(P(S)Ph_2)_2\}]BF_4$ in CD_2Cl_2 from -50°C to Ambient Temperature at 101.3 MHz.

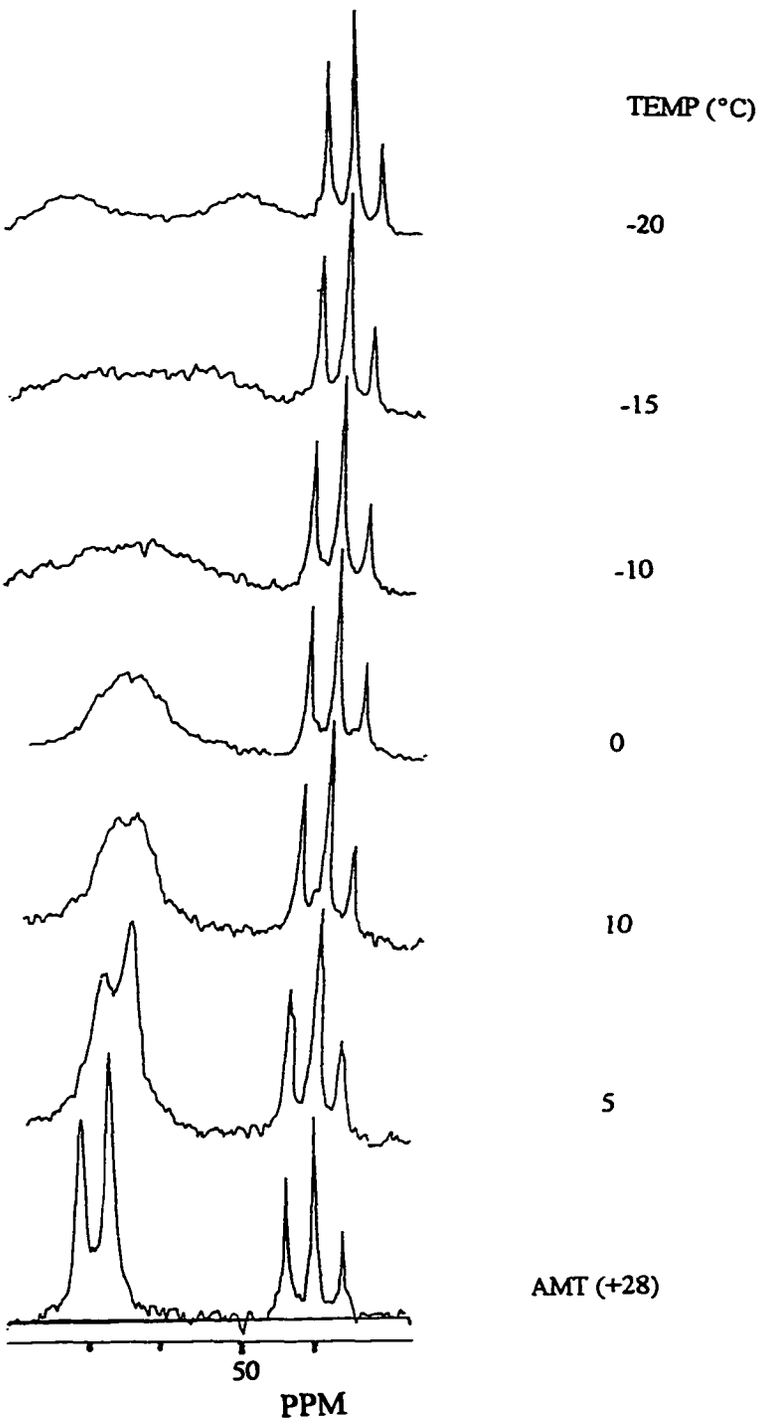

Figure 2.3 continued.. $^{31}P\{^{1}H\}$ NMR Spectra of $[Pd(\eta^3\text{-}C_4H_7)\{CH(PPh_2)(P(S)Ph_2)_2\}]BF_4$ in CD_2Cl_2 from -50°C to Ambient Temperature at 101.3 MHz.

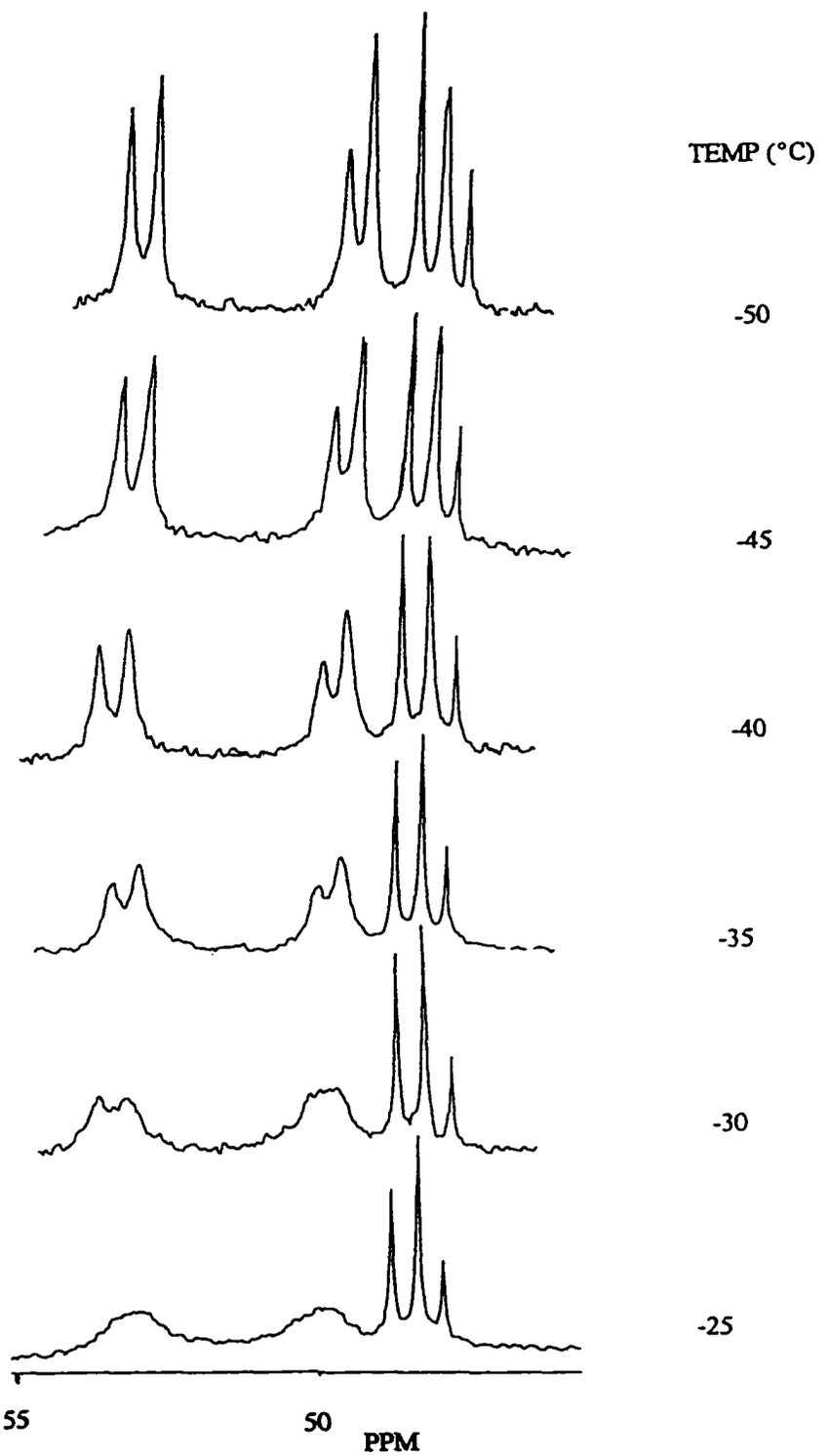

Scheme 2.3 Dynamic Exchange Between Coordinated and Noncoordinated Phosphorus Atoms in $[Pd(\eta^3\text{-}C_4H_7)\{CH(PPh_2)(P(S)Ph_2)_2\}]BF_4$ (phenyl groups have been omitted for clarity).

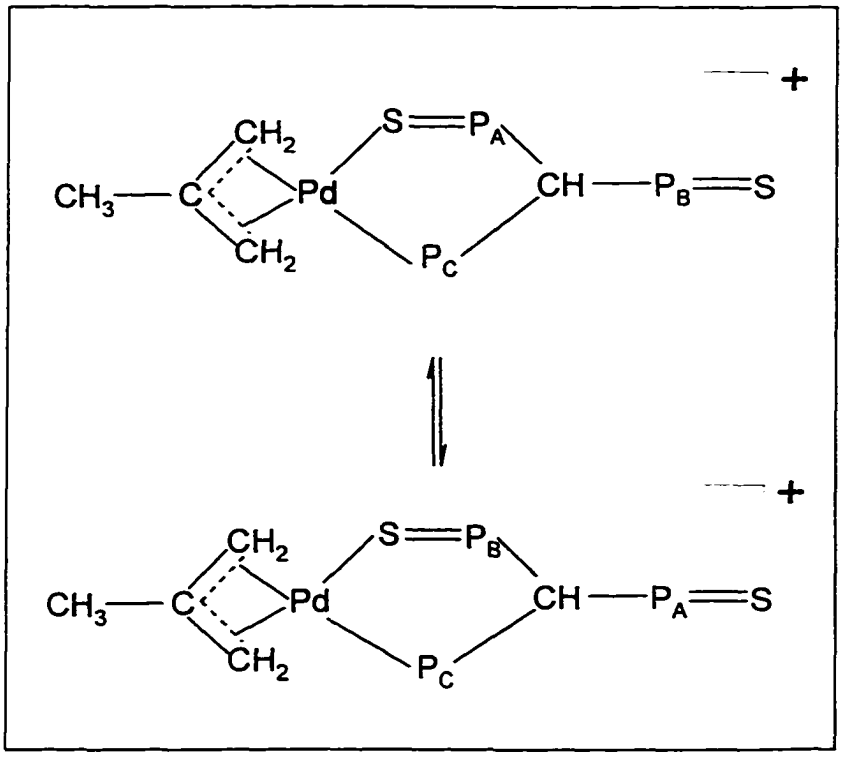

Table 2.3 Rate Constants $k_r(s^{-1})$ for Phosphorus Interchange $P_A \rightleftharpoons P_B$ in $[Pd(\eta^3\text{-}C_4H_7)\{CH(PPh_2)(P(S)Ph_2)_2\}]BF_4$.

temp(K)	303	283	278	273	263	258	253	248	243	238	233	228	223
k_r (s^{-1})	$3x10^4$	$1.5x10^4$	4000	3000	1250	850	225	200	130	65	40	20	15

The spectra shown in **Figure 2.3** are consistent with the observation that $[Pd(\eta^3\text{-}C_4H_7)\{CH(PPh_2)(P(S)Ph_2\}]BF_4$, in solution at ambient temperature, may undergo a dynamic process in which the $S{=}P_APh_2$ and $S{=}P_BPh_2$ groups rapidly exchange positions, as shown in **Scheme 2.3**. This process can be frozen out at -50°C resolving P_A at +52.8 ppm and P_B at +49.5 ppm with $J(P_A\text{-}P_C)$ = 42.6 Hz and $J(P_B\text{-}P_C)$ = 34.8 Hz. The rate constants (k_r) have been derived from line-shape fitting with the DNMR3 program of Kleier and Binsch [69] (performed by Dr. D. Berry), and the results are shown in **Table 2.3**. From this data, an Eyring [70,71] plot of ln (k_r/T) against 1/T gives a good straight line (R = 0.997). The comparison with the standard transition state theory equation

$$\ln (k_r/T) = -\Delta H^{\circ\ddagger}/RT + \Delta S^{\circ\ddagger}/R + \ln (k/h) \qquad \text{equation (1)}$$

enables $\Delta H^{\circ\ddagger}$, $\Delta S^{\circ\ddagger}$ and therefore $\Delta G^{\circ\ddagger}$, to be calculated, which are shown in **Table 2.4**. **Table 2.4** also includes an Arrhenius activation energy, E_a, which is derived from the slope of an Arrhenius [72] plot (ln k_r against 1/T) using

$$\ln k_r = -E_a/RT + \ln A \qquad \text{equation (2)}$$

The value of $\Delta S^{\ddagger}$ for the interchange between coordinated and non-coordinated $Ph_2P{=}S$ groups in $[Pd(\eta^3\text{-}C_4H_7)\{CH(PPh_2)(P(S)Ph_2)_2\}]BF_4$ is a relative large, positive value (24.5 J/K), which suggests a dissociative mechanism. The tetrahedral geometry of the methine carbon should also lead to a lower activation energy for the formation of the intermediate,

as compared to the trigonal planar geometry around the methine carbon in the deprotonated complex, $[Pd(\eta^3\text{-}C_4H_7)\{C(PPh_2)(P(S)Ph_2)_2\}]$, which shows a rigid η^2-P,S coordination mode of the ligand towards the Pd centre. This is in accordance with the dissociative mechanisms proposed for palladium allyl complexes with monodentate ligands [73-79] such as amines [73,74,75], CO [76] and also with macrocycles [77,78], polyenes [79], and chelate N-donor ligands [80-83], where three-coordinate Pd activated complexes were formed. The suggested mechanism for $[Pd(\eta^3\text{-}C_4H_7)\{CH(PPh_2)(P(S)Ph_2)_2\}]BF_4$ is shown in **Scheme 2.4**. The suggested mechanism based on the value of $\Delta S°'$, however, didn't account for any solvent effects on the entropy change. Therefore the values must be used cautiously.

Table 2.4. Rate Plots and Thermodynamic Parameters for Phosphorus Interchange $P_A \rightleftharpoons P_B$ in $[Pd(\eta^3\text{-}C_4H_7)\{CH(PPh_2)(P(S)Ph_2)_2\}]BF_4$.

ln k_r/T vs 1/T	slope -6640
	intercept 26.71
ln k_r vs 1/T	slope -6890
	intercept 33.20
$\Delta H°'$, kJ mol^{-1}	55 (±3)
$\Delta S°'$, JK^{-1}	24 (±4)
$\Delta G°'$, kJ mol^{-1}	48 (±2)
E_a, kJ mol^{-1}	57 (±3)

Scheme 2.4 Suggested Mechanism for the Interchange $P_A \rightleftharpoons P_B$ in $[Pd(\eta^3\text{-}C_4H_7)\{CH(PPh_2)(P(S)Ph_2)_2\}]BF_4$ (phenyl groups are omitted for clarity).

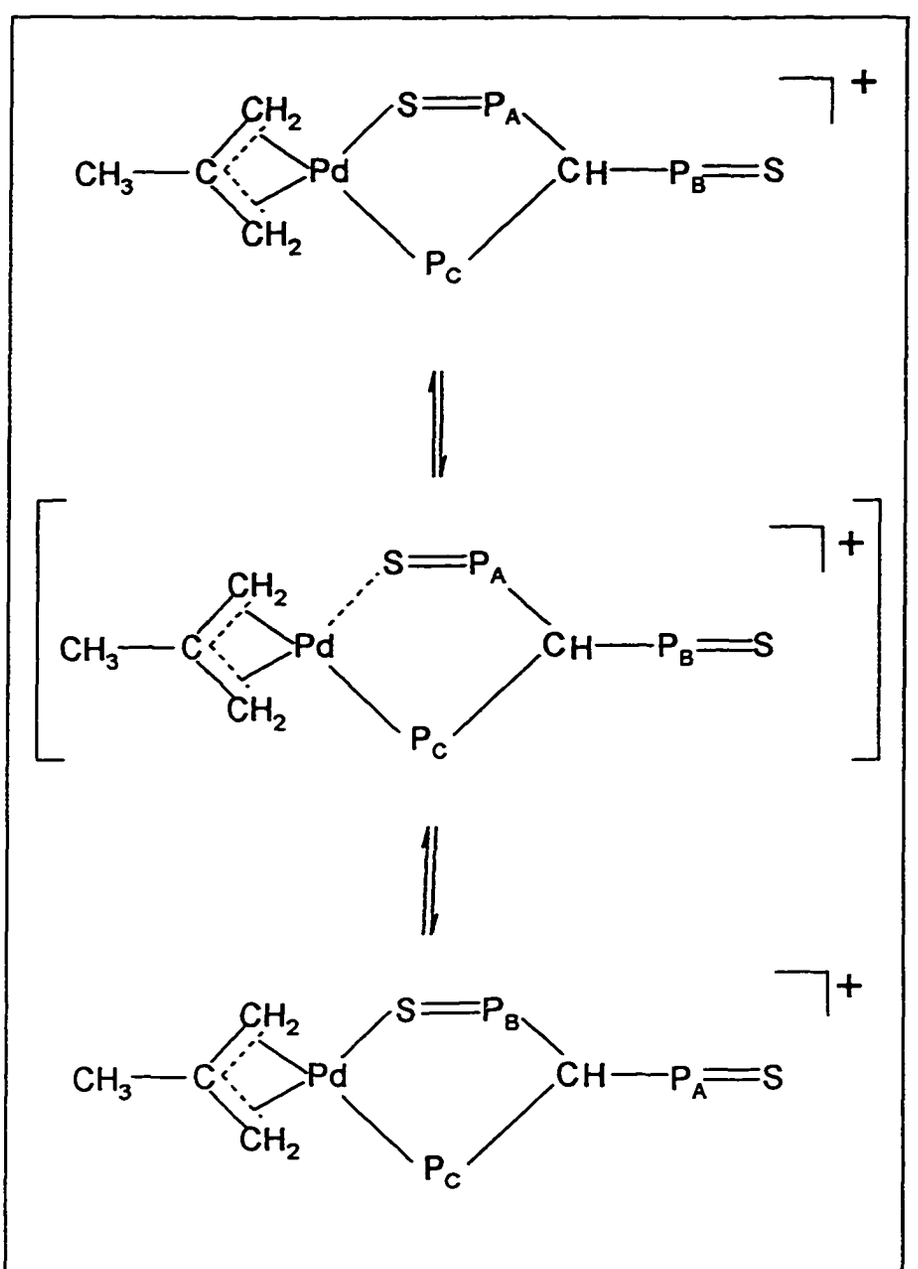

2.3 Dynamic NMR of $[Pd(\eta^3\text{-}C_4H_7)\{C(P(S)Ph_2)_3\}]$

The $^{31}P\{^1H\}$ NMR spectra of $[Pd(\eta^3\text{-}C_4H_7)\{C(P(S)Ph_2)_3\}]$ and $[Pd(\eta^3\text{-}C_4H_7)\{CH(P(S)Ph_2)_3\}]BF_4$ each show a singlet, the former at +40.4 ppm, and the latter at +40.9 ppm, at ambient temperature. However, as the temperature is reduced, the singlet of $[Pd(\eta^3\text{-}C_4H_7)\{C(P(S)Ph_2)_3\}]$, at +40.4 ppm, begins broadening around -50 °C and resolves into two "singlets" at -70 °C with shifts of +42.4 ppm and +40.5 ppm. The signal at +40.5 ppm is broadened significantly at -80 °C. This signal would be expected to split further into two peaks at lower temperatures since P_A, P_B and P_C would be different from one another but this was not achieved because of the closeness of the temperature to the freezing point of the solvent, deuterated dichloromethane. The spectra over the temperature range from ambient to -90 °C of $[Pd(\eta^3\text{-}C_4H_7)\{C(P(S)Ph_2)_3\}]$ are shown in **Figure 2.4**. The spectra shown in **Figure 2.4** are consistent with a process that at ambient temperature in solution $[Pd(\eta^3\text{-}C_4H_7)\{C(P(S)Ph_2)_3\}]$ undergoes a dynamic process in which the coordinated $P_A(S)Ph_2$ exchanges rapidly with the non-coordinated $P_B(S)Ph_2$ group, as shown in **Scheme 2.5**.

This process can be frozen at -70 °C, resolving P_A at +42.4 ppm and P_B at +40.5 ppm. The line-shape simulations derived from the DNMR3 program of Kleier and Binsch [69] were performed under the assumption of an exchange process based on an η^2 structure with two different chemical shifts in a 2:1 ratio at the slow exchange limit and with complete mutual exchange at the fast exchange limit. The results of the analysis are shown in **Figure 2.5** and **Table 2.5**.

Scheme 2.5 Dynamic Exchange Between Coordinated and Noncoordinated Phosphorus Atoms in $[Pd(\eta^3\text{-}C_4H_7)\{C(P(S)Ph_2)_3\}]$ (phenyl groups have been omitted for clarity).

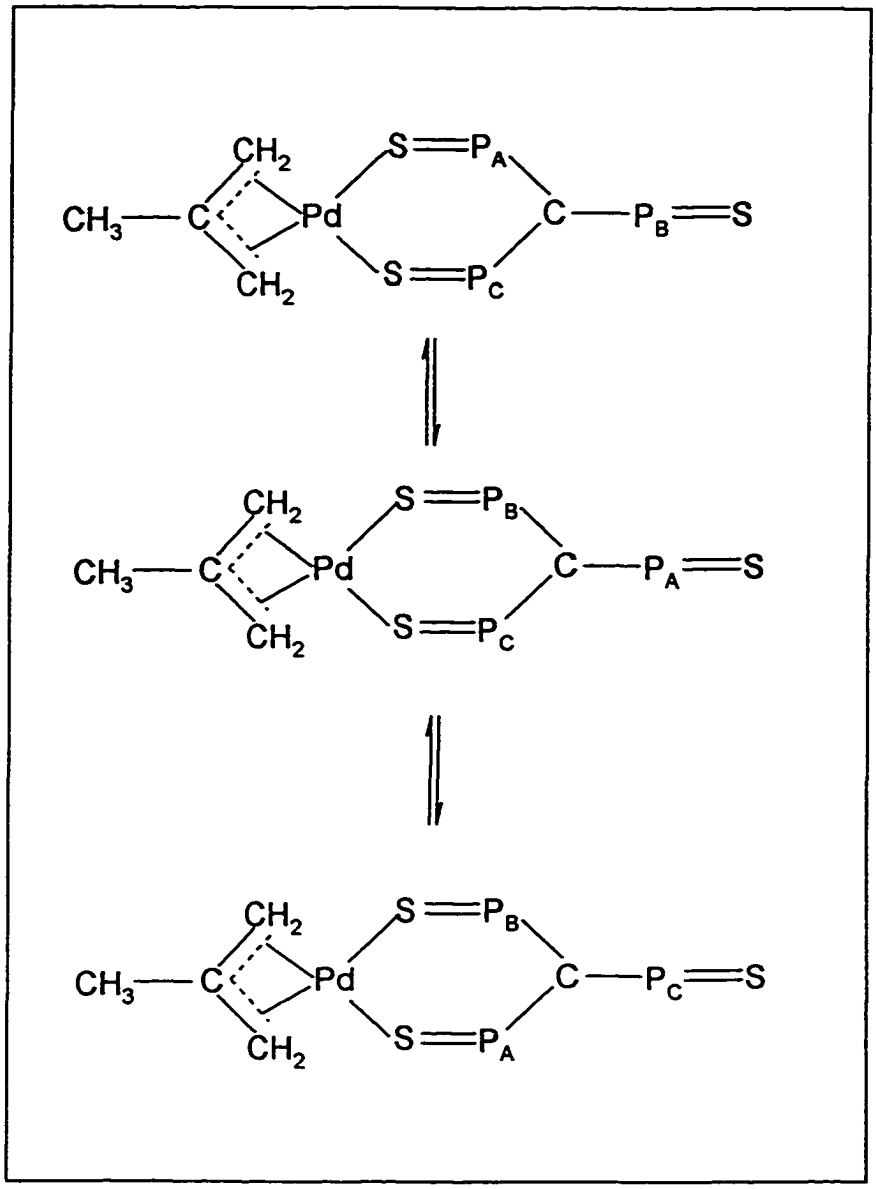

Figure 2.4 $^{31}P\{^1H\}$ NMR Spectra of $[Pd(\eta^3\text{-}C_4H_7)\{C(P(S)Ph_2)_3\}]$ in CD_2Cl_2 from Ambient Temperature to -90 °C at 101.3 MHz.

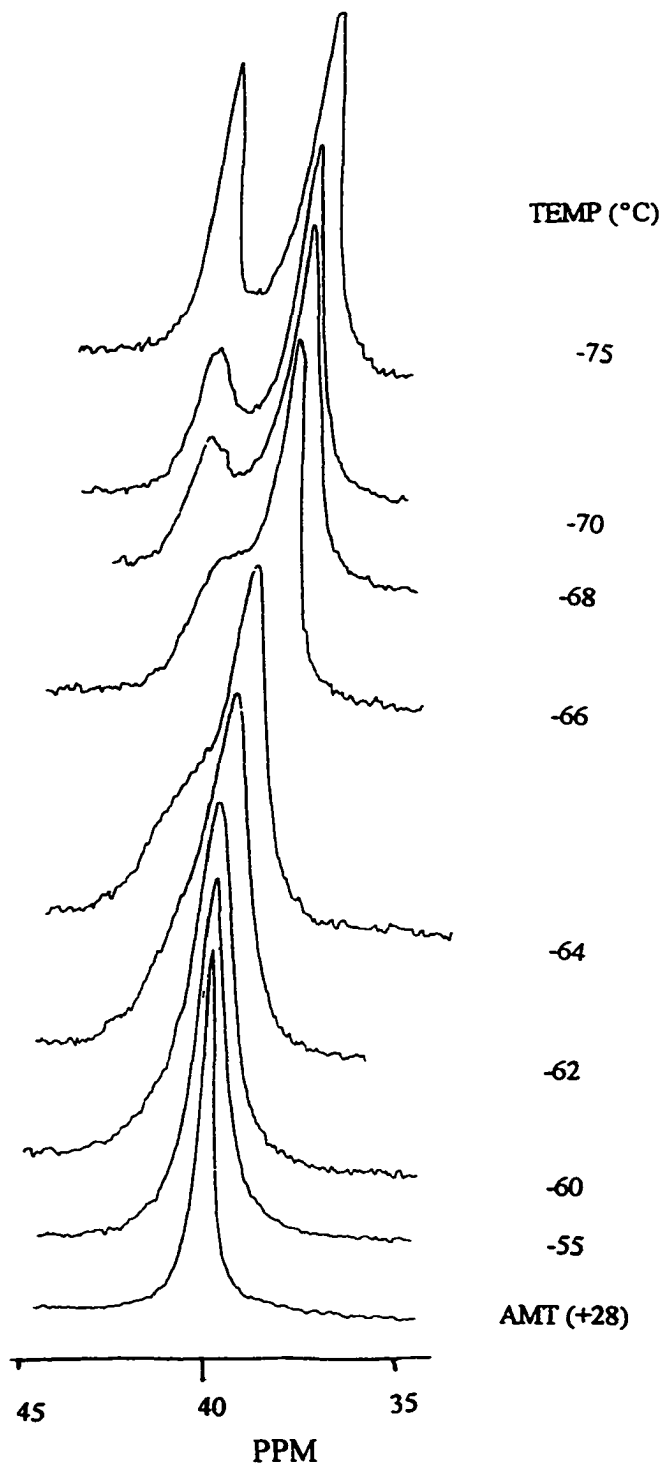

Figure 2.5 Calculated Line Shapes for the ^{31}P NMR Spectra of $[Pd(\eta^3\text{-}C_4H_7)\{C(P(S)Ph_2)_3\}]$

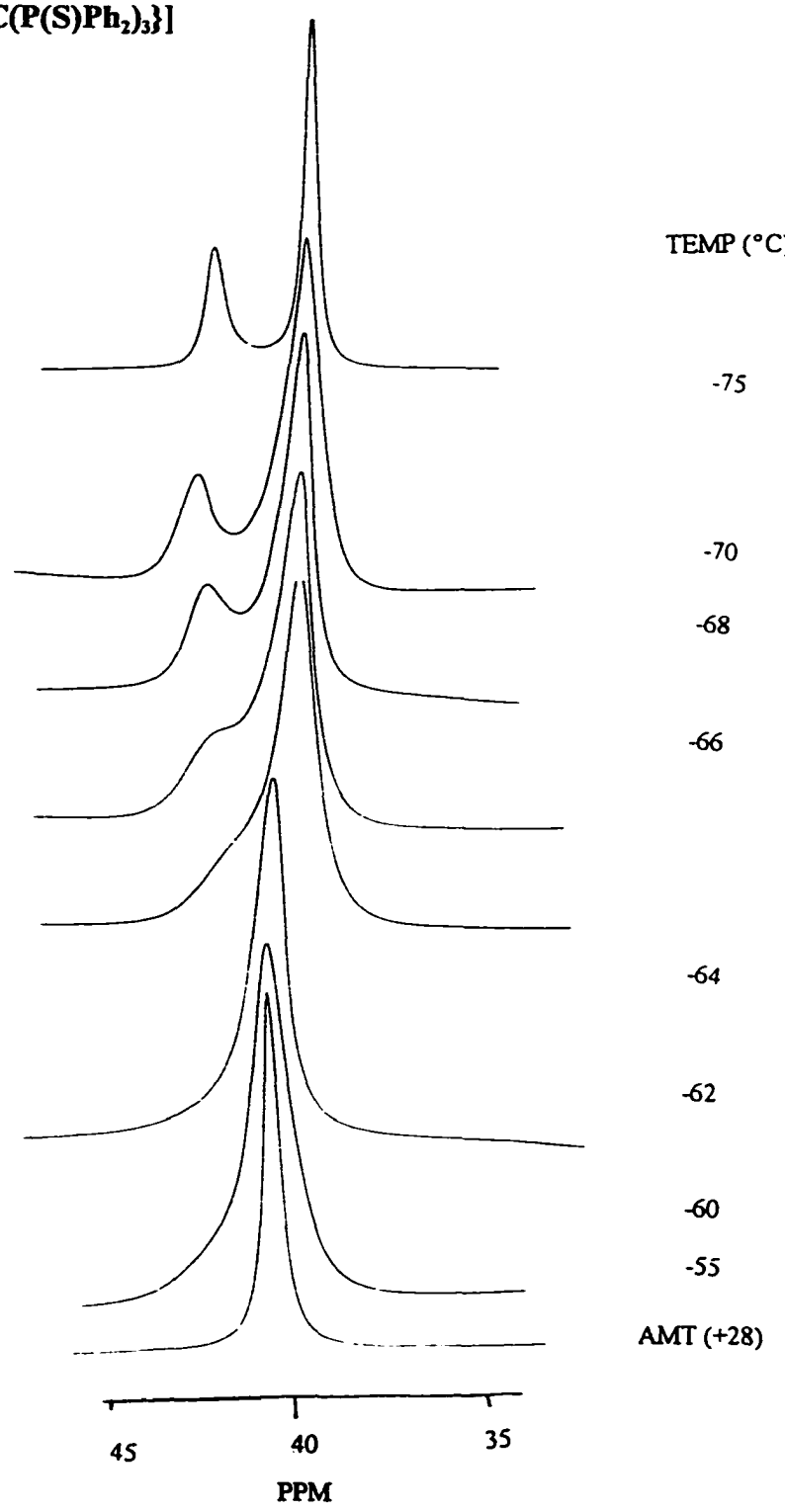

Table 2.5 Rate Constants $k_r(s^{-1})$ for Phosphorus Interchange $P_A \rightleftharpoons P_B$ in $[Pd(\eta^3\text{-}C_4H_7)\{C(P(S)Ph_2)_3\}]$.

temp (K)	218	213	211	209	207	205	203	198
$k_r(s^{-1})$	1000	400	300	240	190	130	100	50

From this rate data an Eyring plot [70,71], shown in **Figure 2.6**, of ln (k_r/T) against 1/T gives a good straight line (R = -0.988). The comparison with the standard transition state theory equation (1) enables $\Delta H°'$, $\Delta S°'$ and therefore $\Delta G°'$ to be calculated. These values are shown in **Table 2.6**. **Table 2.6** also includes an Arrhenius activation energy equation, E_a, which is derived from the slope of an Arrhenius [72] plot (ln k_r against 1/T) using equation (2).

In contrast, the low temperature VT ^{31}P NMR of $[Pd(\eta^3\text{-}C_4H_7)\{CH(P(S)Ph_2)_3\}]BF_4$ down to -90°C does not show any splitting of the singlet at +40.9 ppm. In other words, exchange between P_A and P_B is faster than 10^3 s assuming the linewidth is no less than 1 ppm. The value of $\Delta S'$ for the interchange between coordinated and non-coordinated Ph_2P=S groups in $[Pd(\eta^3\text{-}C_4H_7)\{C(P(S)Ph_2)_2\}]$ is a relative large, positive value (35.8 J/K), which suggests a dissociative mechanism, as observed in palladium allyl complexes with monodentate ligands [73-79] such as amines [73-75], CO [76] and also with macrocycles [77,78], polyenes [79], and chelate N-donor ligands [80-83], where tricoordinate Pd activated complexes were proposed. There is also evidence to support an associative mechanism. The observation that a tripodal mode of coordination of the ligand is adopted in the solid-state of

$[Pd(\eta^3\text{-}C_4H_7)\{CH(P(S)Ph_2)_3\}]BF_4$, discussed in detail later in this Chapter suggests a 5-coordinate, 18-electron intermediate is likely for the exchange process in $[Pd(\eta^3\text{-}C_4H_7)\{C(P(S)Ph_2)_3\}]$. We therefore propose an associative mechanism, observed by Crociani [84] and Hansson [85] in other palladium allyl complexes, for the deprotonated complex, $[Pd(\eta^3\text{-}C_4H_7)\{C(P(S)Ph_2)_3\}]$, shown in **Scheme 2.6**.

Scheme 2.6 Suggested Mechanism for the Exchange $P_A \rightleftharpoons P_B \rightleftharpoons P_C$ in $[Pd(\eta^3\text{-}C_4H_7)\{C(P(S)Ph_2)_3\}]$ (phenyl groups are omitted for clarity).

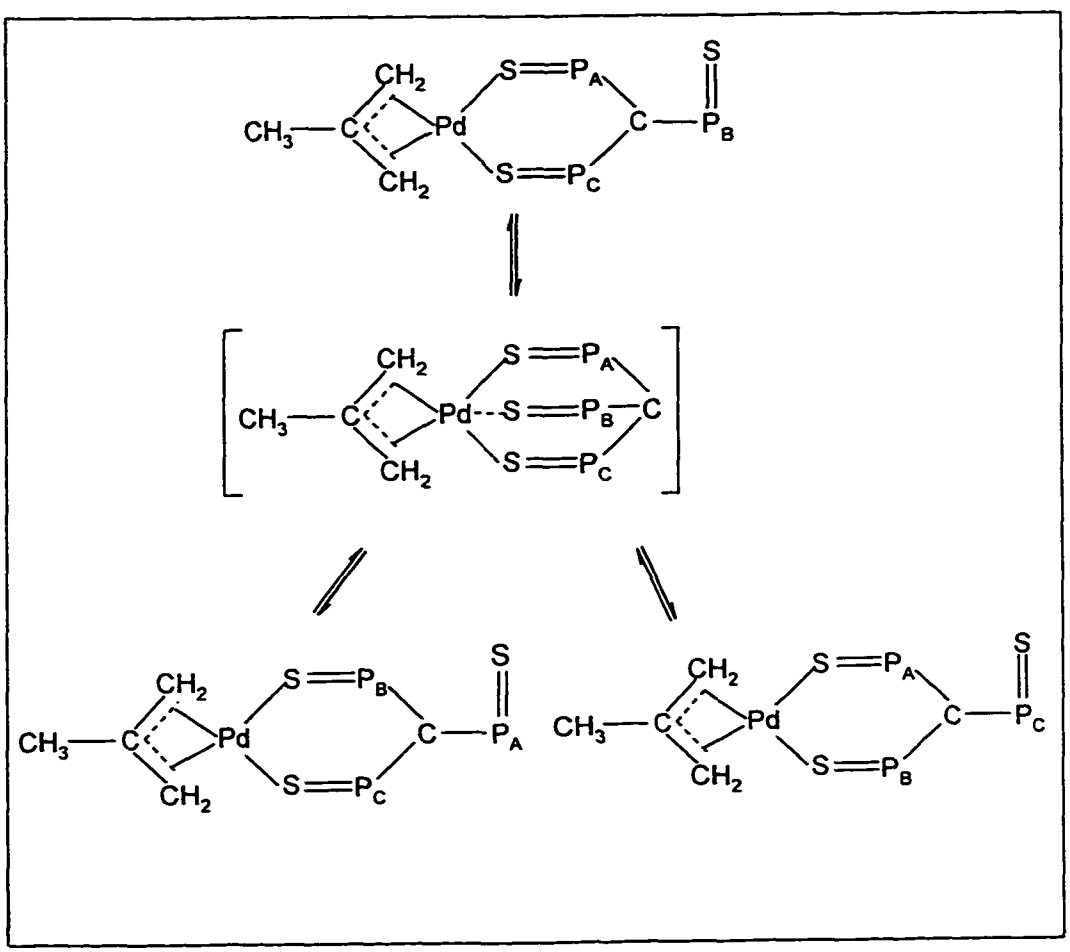

Table 2.6. Rate Plots and Thermodynamic Parameters for Phosphorus Interchange $P_A \rightleftharpoons P_B$ in $[Pd(\eta^3\text{-}C_4H_7)\{C(P(S)Ph_2)_3\}]$.

$\ln k_r/T$ vs 1/T	slope -5838
	intercept 28.06
$\ln k_r$ vs 1/T	slope -6036
	intercept 34.35
$\Delta H^{\circ\ddagger}$, kJ mol^{-1}	49 (±4)
$\Delta S^{\circ\ddagger}$, JK^{-1}	36 (±4)
$\Delta G^{\circ\ddagger}$, kJ mol^{-1}	38 (±3)
E_a, kJ mol^{-1}	50 (±4)

Figure 2.6 The Eyring Plot of the Rate Data for Intra-molecular Phosphorus Interchange $P_A \rightleftharpoons P_B$ in $[Pd(\eta^3\text{-}C_4H_7)\{C(P(S)Ph_2)_3\}]$.

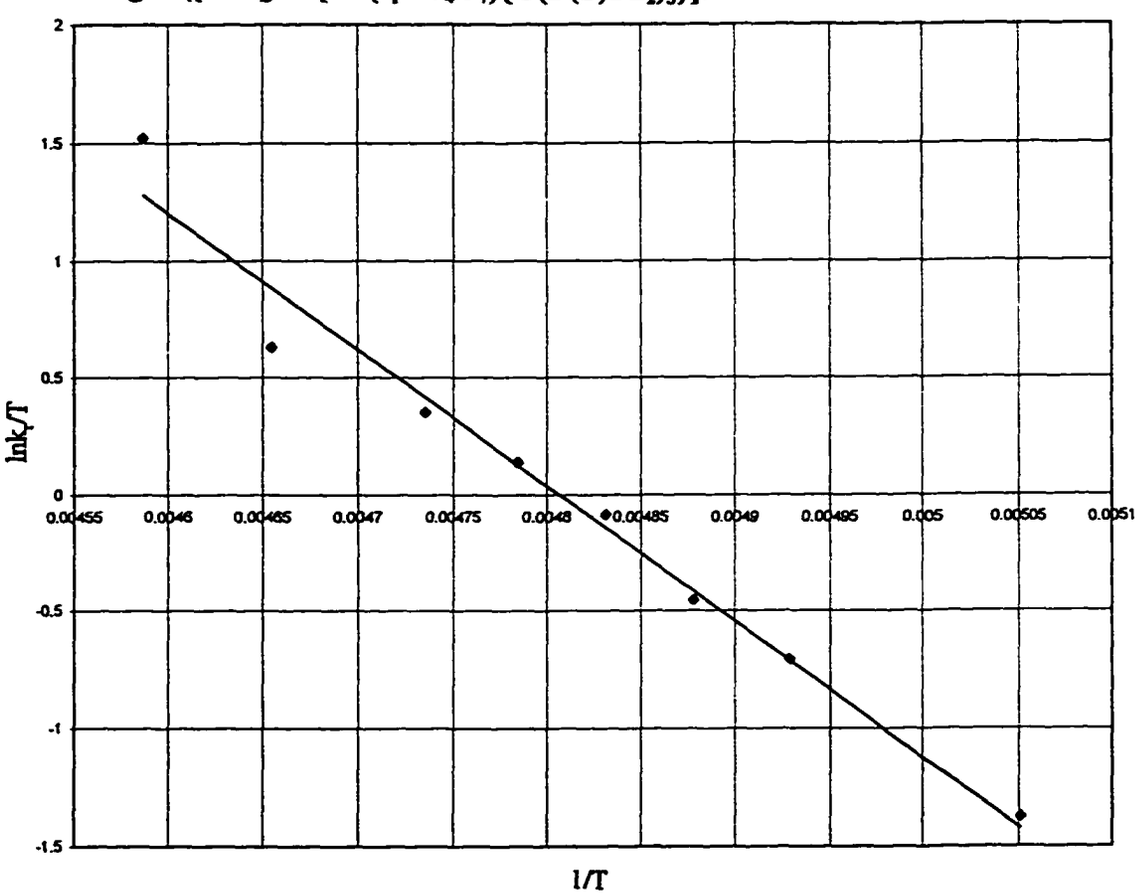

2.4 Solid-state Structure of $[Pd(\eta^3\text{-}C_4H_7)\{CH(PPh_2)(P(S)Ph_2)_2\}]BF_2.2H_2O$

$[Pd(\eta^3\text{-}C_4H_7)\{CH(PPh_2)(P(S)Ph_2)_2\}]BF_4.2H_2O$ was prepared as described in the experimental part of Chapter Seven and crystals suitable for study by X-ray diffraction were grown by recrystallisation from diethyl ether and hexanes. All the atoms except the water molecules and the hydrogen atom attached to the central carbon of the ligand were treated anisotropically, the atoms of the water molecules and H_1 are refined isotropically. The hydrogen atom (H_1) was located and refined in normal fashion. The crystallographic techniques employed are described in detail in Chapter Seven and Appendix. The crystallographic data for $[Pd(\eta^3\text{-}C_4H_7)\{CH(PPh_2)(P(S)Ph_2)_2\}]BF_4.2H_2O$ are listed in **Table 2.7**.

The structure of a single cation of $[Pd(\eta^3\text{-}C_4H_7)\{CH(PPh_2)(P(S)Ph_2)_2\}]BF_4.2H_2O$ is shown as an ORTEP[86] diagram in **Figure 2.7**, along with the atomic labelling scheme. Unit cell and other parameters related to the crystal structure determinations are in **Table 2.7**, fractional atomic coordinates and temperature parameters are in **Appendix Table I**, anisotropic temperature parameters in **Appendix Table II**, selected bond lengths and bond angles in **Tables 2.8** and **2.9** respectively. The parameters for hydrogen bond lengths and bond angles are listed in **Appendix Table III** and **Tables 2.10**.

Table 2.7 Crystallographic Data for $[Pd(\eta^3\text{-}C_4H_7)\{CH(PPh_2)(P(S)Ph_2)_2\}]BF_4.2H_2O$ and $[Pd(\eta^3\text{-}C_4H_7)\{CH(P(S)Ph_2)_3\}]BF_4$

Complex	$[Pd(\eta^3\text{-}C_4H_7)\{CH(PPh_2)(P(S)Ph_2)_2\}]$ $BF_4.2H_2O$	$[Pd(\eta^3\text{-}C_4H_7)\{CH(P(S)Ph_2)_3\}]$ BF_4
Formula	$C_{41}H_{42}BF_4O_2P_3S_2Pd$	$C_{41}H_{38}BF_4PdP_3S_3$
FW	917	913
Space group	$P2_1/C$ (No. 14)	R3 (No. 146)
a, Å	13.403(3)	16.375(1)
b, Å	12.625(2)	16.375(1)
c, Å	30.416(6)	16.371(1)
α, deg	90.0	101.312(6)
β, deg	117.52(1)	101.281(7)
γ, deg	90.0	101.312(6)
V, Å^3	4564	4094
Z	4	3
Diffractometer	Picker 4-circle	Nonius
Radiation (λ, Å)	Mo Kα(0.71069)	Cu Kα(1.542)
μ, cm^{-1}	6.79	1.542
Transform factor range	0.785-0.865	
Temperature, K	295	295
No. of obs. reflcns (I>3.06(I))	8605/3806	3426
Parameters refined	481	364
R	0.0848	0.0779
R_w	0.1243	0.0975

The structure shows an approximately square planar metal centre with $CH(PPh_2)(P(S)Ph_2)_2$ coordinated in a bidentate fashion through one phosphorus and one sulphur atom, with the second sulphur atom non-coordinated ("dangling") but held close to the palladium atom. The π-methylallyl group is coordinated in an η^3 fashion to the palladium centre. This can be confirmed by the observation that all three allyl carbons have virtually identical bond distances to the palladium atom (2.19 Å, 2.19 Å, and 2.21 Å). There are relatively small distortions of the square plane. The maximum deviation of the plane defined by P(3) - S(1) - C(71) - C(72) is 0.038 Å, and the distance between Pd(1) and that plane is only 0.096 Å. Angles at the metal centre are close to 90° with the angle of P(3) - Pd(1) - S(1) being 95.2°. The Pd - S bond, 2.33 Å, and the Pd - P bond, 2.30 Å, are in the same range as observed previously in the related iridium complex, reported in Chapter Five of this thesis, $[Ir(Cod)\{CH(PPh_2)(P(S)Ph_2)_2\}]BF_4$ [67]. In $[Ir(Cod)\{CH(PPh_2)(P(S)Ph_2)_2\}]BF_4$ the Ir - S and Ir - P bond lengths are 2.44 Å and 2.31 Å respectively. Within the phosphorus sulphide chelating ring, the most important structural observation is the approximately tetrahedral arrangement of phosphorus atoms around C(1) and the location of H(1). The P - C(1) - P angles are 102° to 117°, which is closer to tetrahedral geometry (109° 28') than planar (120°). This is another confirmation of the existence of the proton attached to the central carbon of the ligand. As expected, the P - S bonds to the coordinated sulphur, 1.99 Å, are slightly longer than that to the non-coordinated sulphur, 1.94 Å. The average P-S bond length is 1.97 Å, slightly longer than that in the free ligand (1.95 Å) [67] indicating a slight lengthening of the P-S bond upon coordination to the metal. This is consistent with previous observations in related

Figure 2.7 ORTEP Plot for a Single Cation of

$[Pd(\eta^3\text{-}C_4H_7)\{CH(PPh_2)(P(S)Ph_2)_2\}]BF_4.2H_2O$

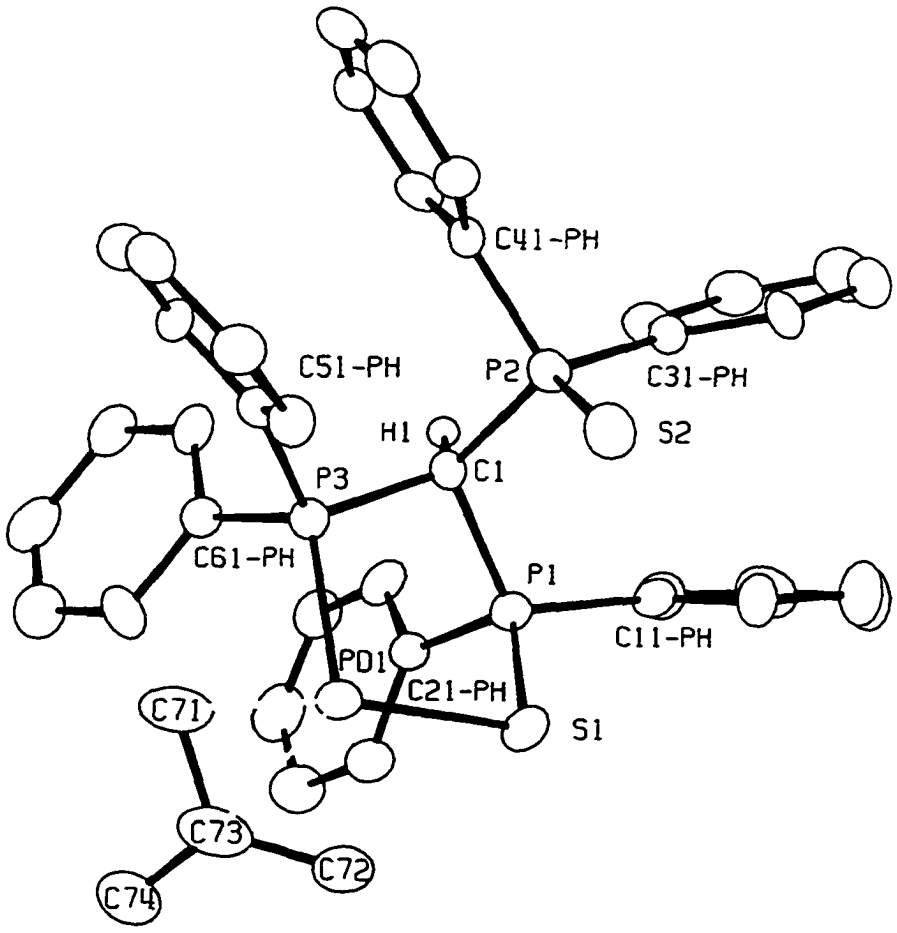

complexes [67,87]. These P-S bond lengths may be compared with $[Ir(Cod)\{CH(PPh_2)(P(S)Ph_2)_2\}]BF_4$ [67], the only other reported protonated $CH(PPh_2)(P(S)Ph_2)_2$ complex, at 2.00 Å and 1.98 Å. The lengthening of the P-S bond upon coordination is probably due to the lower electronic density available at the sulphur atom after its coordination to the metal centre. The C-PPh_2 bond length, 1.92 Å, is slightly longer than the C-$P(S)Ph_2$ bonds (1.89 Å and 1.85 Å) in the palladium complex, as

expected for a phosphorus (III) [66]. This may be compared to the free ligand discussed in detail in Chapter Five, $CH(P(S)Ph_2)_2PPh_2$ [67]; 1.90 Å for the C-PPh_2 bond, and 1.86 Å, 1.87 Å for the C-$P(S)Ph_2$ bonds. The much shorter Pd-P bond length of 2.30 Å is relatively short when one considers the sum of the covalent radii of palladium and phosphorus is 2.47 Å [88]. This is suggestive of a very strong bond between the palladium and the phosphorus of the coordinated Ph_2P group. On the other hand, the 'normal' Pd-S bond length of 2.33 Å is slightly longer than the sum of the covalent radii of palladium and sulphur (2.32 Å [89]). This observation then is suggestive of a rather weak Pd-S bond between the palladium and the coordinated Ph_2P=S group. This perhaps explains why in solution the fluxional exchange occurred via rupture of the Pd-S bond.

Table 2.8 Selected Bond Lengths (Å) for

$[Pd(\eta^3\text{-}C_4H_7)\{CH(PPh_2)(P(S)Ph_2)_2\}]BF_4.2H_2O$

Atoms	Distance	Atoms	Distance
Pd(1) - S(1)	2.332(5)	P(1) - C(11)	1.822(19)
Pd(1) - P(3)	2.296(3)	P(1) - C(21)	1.823(15)
Pd(1) - C(71)	2.191(27)	P(2) - C(1)	1.835(15)
Pd(1) - C(72)	2.206(15)	P(2) - C(31)	1.807(19)
Pd(1) - C(73)	2.185(26)	P(2) - C(41)	1.797(12)
S(1) - P(1)	1.991(5)	P(3) - C(1)	1.917(18)
S(2) - P(2)	1.945(5)	P(3) - C(51)	1.823(14)
P(1) - C(1)	1.886(12)	P(3) - C(61)	1.820(14)

Estimated standard deviations are given in parentheses

Table 2.9 Selected Bond Angles(°) for $[Pd(\eta^3\text{-}C_4H_7)\{CH(PPh_2)(P(S)Ph_2)_2\}]BF_4.2H_2O$

Atoms	Angle	Atoms	Angle
S(1) - Pd(1) - P(3)	95.2(2)	C(11) - P(1) - C(21)	108.0(8)
S(1) - Pd(1) - C(71)	163.8(4)	S(2) - P(2) - C(1)	113.1(5)
S(1) - Pd(1) - C(72)	95.5(6)	S(2) - P(2) - C(31)	113.5(5)
S(1) - Pd(1) - C(73)	129.5(6)	S(2) - P(2) - C(41)	114.2(5)
P(3) - Pd(1) - C(71)	99.5(4)	C(1) - P(2) - C(31)	107.9(7)
P(3) - Pd(1) - C(72)	168.3(6)	C(1) - P(2) - C(41)	104.2(6)
P(3) - Pd(1) - C(73)	132.9(6)	C(31) - P(2) - C(41)	103.0(7)
C(71) - Pd(1) - C(72)	69.3(7)	Pd(1) - P(3) - C(1)	110.3(4)
C(71) - Pd(1) - C(72)	39.1(8)	Pd(1) - P(3) - C(51)	111.4(5)
C(72) - Pd(1) - C(73)	38.7(8)	Pd(1) - P(3) - C(61)	116.2(5)
Pd(1) - S(1) - P(1)	99.4(2)	C(1) - P(3) - C(51)	112.0(7)
S(1) - P(1) - C(1)	112.7(5)	C(51) - P(3) - C(61)	104.9(6)
S(1) - P(1) - C(11)	107.1(4)	P(1) - C(1) - P(2)	116.6(7)
S(1) - P(1) - C(21)	113.0(6)	P(1) - C(1) - P(3)	102.1(7)
C(1) - P(1) - C(11)	113.6(7)	P(2) - C(1) - P(3)	115.1(7)
C(1) - P(1) - C(21)	102.3(6)		

Estimated standard deviations are given in parentheses

Table 2.10 Interatomic Distances (Å) and Bond Angles (°) Involving Hydrogen Atoms for $[Pd(\eta^3\text{-}C_4H_7)\{CH(PPh_2)(P(S)Ph_2)_2\}]BF_4.2H_2O$

Atoms	Distance	Atoms	Angle
H(1) - C(1)	1.073(62)	P(1) - C(1) - H(1)	102.8
		P(2) - C(1) - H(1)	93.8
		P(3) - C(1) - H(1)	126.9

Estimated standard deviations are in parentheses

2.5 Solid-state Structure of $[Pd(\eta^3\text{-}C_4H_7)\{CH(P(S)Ph_2)_3\}]BF_4$

The crystal of $[Pd(\eta^3\text{-}C_4H_7)\{CH(P(S)Ph_2)_3\}]BF_4$ was prepared by vapour diffusion of hexanes into solutions of the complex in dichloromethane. The metal atoms, all phosphorus and sulphur atoms, the central carbons of the $CH(P(S)Ph_2)_3$ and $CH(PPh_2)(P(S)Ph_2)_2$ ligands, and all the carbons of the methylallyl groups were treated anisotropically; the remaining carbon atoms, i.e. phenyl carbons, tetrafluoroborate anion, isotropically. No hydrogen atoms, including methine hydrogen, H(1), were located. The crystallographic techniques employed are described in detail in Chapter Seven and the Appendix The crystallographic data for $[Pd(\eta^3\text{-}C_4H_7)\{CH(P(S)Ph_2)_3\}]BF_4$ are listed in **Table 2.7**.

The structure of one molecule of a single cation of $[Pd(\eta^3\text{-}C_4H_7)\{CH(P(S)Ph_2)_3\}]BF_4$ is

shown as an ORTEP [86] diagram in **Figure 2.8** along with the atomic labelling scheme. Unit cell and other parameters related to the crystal structure determination are in **Table 2.7**, whereas fractional atomic coordinates and temperature parameters are listed in **Appendix Table IV**. Anisotropic temperature parameters are located in **Appendix Table V**. Selected bond distances and bond angles are found in **Tables 2.11** and **2.12** respectively.

Figure 2.8 ORTEP Plot for a Single Cation of $[Pd(\eta^3\text{-}C_4H_7)\{CH(P(S)Ph_2)_3\}]BF_4$

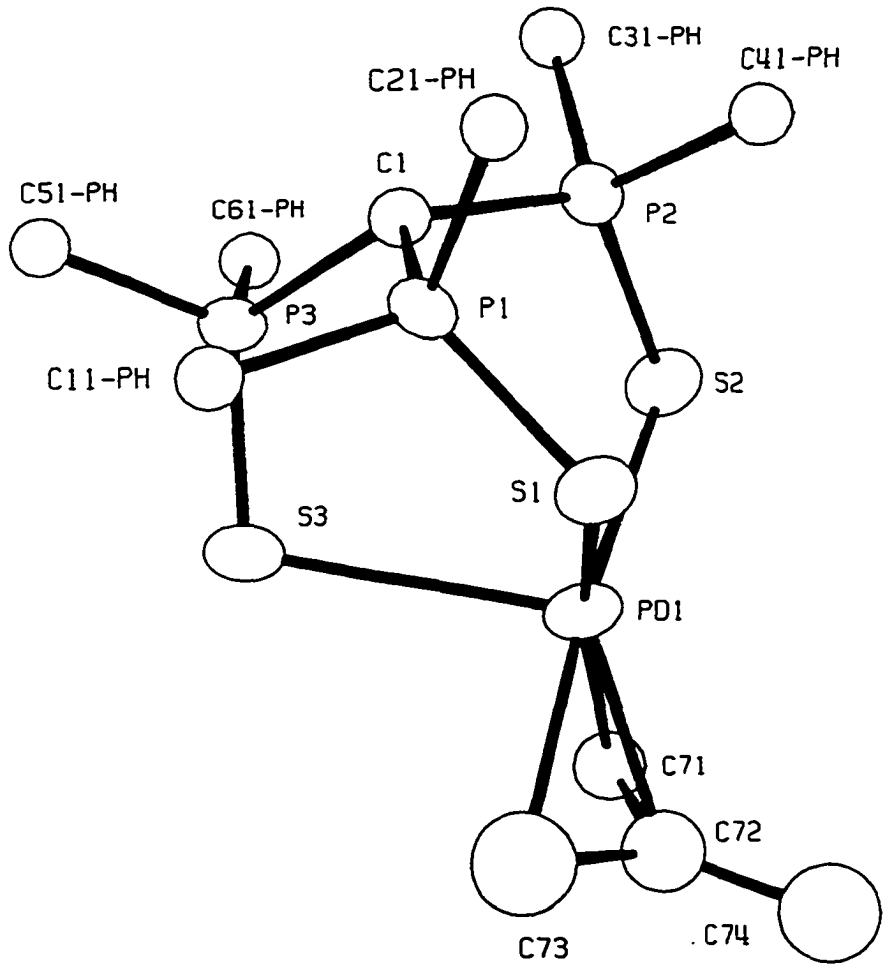

The asymmetric unit contains one molecule and a third of a second molecule. The second molecule was located at a special position associated with the space group. The structure of the first molecule shows irregular five-coordination geometry about the metal centre with the $HC(P(S)Ph_2)_3$ ligand coordinated in a tridentate fashion through three sulphur atoms. The three S-Pd-S angles range from 92° to 99°, and are slightly larger than the angles observed in the related iridium complex $[Ir(Cod)\{CH(PPh_2)(P(S)Ph_2)_2$- *P,S,S*$\}]BF_4 \cdot CH_2Cl_2$ [67], the angles in which range from 81° to 92°. The π-methylallyl group is coordinated in an η^3 fashion to the palladium centre. This can be demonstrated by the observation that all three allyl carbons have virtually identical bond distances to the palladium atom (2.15 Å, 2.16 Å,2.16 Å). The Pd-S bond lengths (2.39, 2.49, and 2.84 Å) observed in the complex are all longer than the sum of the covalent radii of palladium and sulphur (2.32 Å [89]). This suggests that these bonds are relatively weak. In solution there are three possibilities which would agree with the singlet (down to -90°C) observed in the ^{31}P NMR spectrum. The complex could be 4-coordinate undergoing fast exchange between the coordinated and non-coordinated sulphurs involving a 5-coordinate intermediate. Also possible is a rigid 5-coordinate complex if chemical shift separation among the phosphorus atoms is less than 10 ppm. The fact that rather weak bonding between the Pd-S bonds suggests that all three $Ph_2P{=}S$ groups undergo facile exchange in solution, which cannot be frozen on the NMR time scale, even at temperatures approaching -90°. These bond distances between the palladium centre and the coordinated sulphurs (2.39 Å, 2.49 Å, and 2.84 Å) are longer than those found in $[Pd(\eta^3\text{-}C_4H_7)\{CH(PPh_2)(P(S)Ph_2)_2\}]BF_4 \cdot 2H_2O$ (both 2.33 Å); the only other

protonated tripodal palladium complex which has had a complete X-ray study performed. This observation suggests that the Pd-S bonding in a tridentate bonding mode with a tripodal ligand is weaker than in the bidentate complex, $[Pd(\eta^3\text{-}C_4H_7)\{CH(PPh_2)(P(S)Ph_2)_2\}]BF_4 \cdot 2H_2O$ simply because the steric crowding by six phenyl groups is larger. Therefore the longer metal to sulphur bonds help alleviate this problem. That perhaps is why a facile exchange of all three $S=PPh_2$ is possible in solution, observed as one singlet in $^{31}P\{^1H\}$ NMR at -90°C. The P-S bond distances range from 1.96 Å to 2.01 Å and are longer than in the free ligand, $CH(P(S)Ph_2)_3$, 1.94 Å[87]. This observation is consistent with the related complexes, $[Ir(Cod)\{CH(PPh_2)(P(S)Ph_2)_2\text{-}P,S,S\}]BF_4$ [68] and $[Pd(\eta^3\text{-}C_4H_7)\{CH(PPh_2)(P(S)Ph_2)_2\}]BF_4$ of this Chapter, where the P-S bond lengthens upon coordination of the ligand to the metal centre. The other important structural observation is the approximately tetrahedral arrangement of phosphorus atoms around the methine carbon, C(1). The P-C(1)-P angles range from 112° to 114° which is closer to tetrahedral geometry (109° 28') than trigonal planar (120°). This confirms the presence of the proton attached to the methine carbon of the tripodal ligand.

Table 2.11 Selected Bond Lengths (Å) for $[Pd(\eta^3\text{-}C_4H_7)\{CH(P(S)Ph_2)_3\}]BF_4$

Atoms	Distance	Atoms	Distance
S(1)-Pd(1)	2.391(7)	P(1)-S(1)	1.971(9)
S(2)-Pd(1)	2.487(7)	P(2)-S(2)	1.980(8)
S(3)-Pd(1)	2.844(7)	P(3)-S(3)	1.948(8)
C(71)-Pd(1)	2.153(23)	C(1)-P(1)	1.849(19)
C(72)-Pd(1)	2.162(28)	C(1)-P(2)	1.847(20)
C(73)-Pd(1)	2.161(31)	C(1)-P(3)	1.927(20)

Estimated standard deviations are given in parentheses

Table 2.12 Selected Bond Angles (°) for $[Pd(\eta^3\text{-}C_4H_7)\{CH(P(S)Ph_2)_3\}]BF_4$

Atoms	Bond Angle	Atoms	Bond Angle
S(2)-Pd(1)-S(1)	99.6(2)	C(1)-P(1)-S(1)	113.3(7)
S(3)-Pd(1)-S(1)	95.2(2)	C(1)-P(2)-S(2)	114.9(7)
S(3)-Pd(1)-S(2)	92.5(2)	C(1)-P(3)-S(3)	112.9(7)
P(1)-S(1)-Pd(1)	108.2(3)	P(2)-C(1)-P(1)	113.9(11)
P(2)-S(2)-Pd(1)	104.9(3)	P(3)-C(1)-P(1)	111.5(10)
P(3)-S(3)-Pd(1)	103.7(3)	P(3)-C(1)-P(2)	113.1(10)

Estimated standard deviations are given in parentheses

The structure of a third of the second molecule (cation) $[Pd(\eta^3\text{-}C_4H_7)\{CH(P(S)Ph_2)_3\}]BF_4$ is shown as an ORTEP diagram in **Figure 2.9**, along with the atomic labelling scheme. Unit cell and other parameters related to the crystal structure determination are in **Table 2.7**, whereas fractional atomic coordinates and temperature parameters are listed in **Appendix Table IV**. Anisotropic temperature parameters are located in **Appendix Table V**. Selected bond lengths and bond angles are found in **Tables 2.13**.

The structure of the second molecule shows a totally symmetric five-coordination geometry about the metal centre with the $HC(P(S)Ph_2)_3$ ligand coordinated in a tridentate fashion through three sulphur atoms and the π-methylallyl group coordinated in an η^3 fashion. The bond distance between the palladium centre and the coordinated sulphurs is 2.55Å, slightly longer than two of the Pd-S bonds found in the other molecule but shorter than the third. Similar observations apply to the P-S bonds of 1.97Å, and P-C (methine) bond of 1.90 Å, while the bond distances in the symmetric molecule tend to be somewhere among those found in the irregular five-coordinate complex. Similar comparisons can be made with the bond angles.

Figure 2.9 ORTEP Plot for a Third Molecule of a Single Cation of $[Pd(\eta^3\text{-}C_4H_7)\{CH(P(S)Ph_2)_3\}]BF_4$

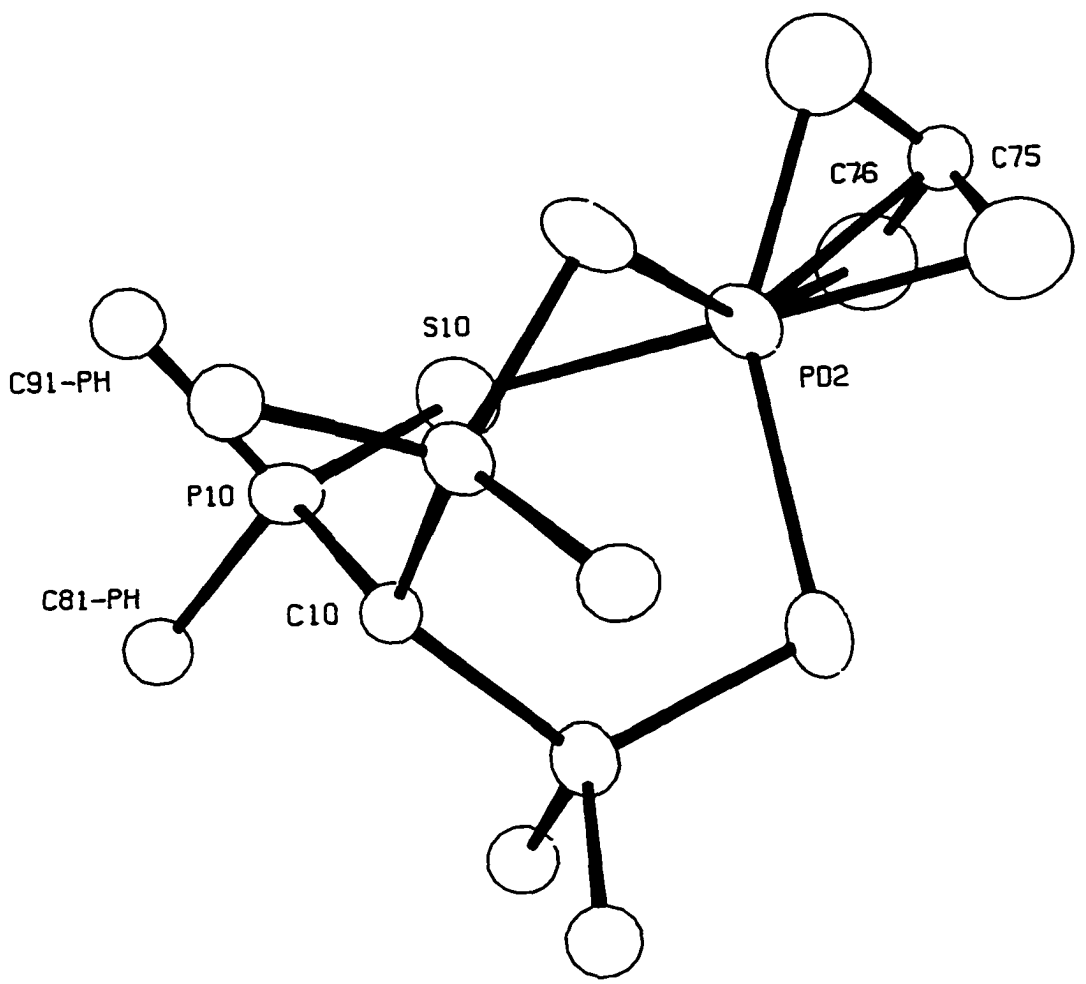

Table 2.13 Selected Bond Distances (Å) and Bond Angles (°) for a Third of a Molecule of $[Pd(\eta^3\text{-}C_4H_7)\{CH(P(S)Ph_2)_3\}]BF_4$

Atoms	Angle	Atoms	Distance
C(75)-Pd(2)-S(10)	121.4 (1)	S(10)-Pd(2)	2.554(7)
C(76)-Pd(2)-S(10)	92.6 (8)	C(75)-Pd(2)	2.152(33)
C(76)-Pd(2)-S(75)	35.9(9)	C(76)-Pd(2)	2.176(41)
P(10)-S(10)-Pd(2)	107.2 (3)	P(10)-S(10)	1.967(8)
S(10)-Pd(2)-S(10)	95.3(2)	C(10)-P(10)	1.873(10)
C(10)-P(10)-S(10)	113.5(9)		

Estimated standard deviations are in parentheses

2.6 Conclusion

The new palladium complexes, $[Pd(\eta^3\text{-}C_4H_7)\{C(PPh_2)(P(S)Ph_2)_2\}]$, $[Pd(\eta^3\text{-}C_4H_7)\{CH(PPh_2)(P(S)Ph_2)_2\}]BF_4$, $[Pd(\eta^3\text{-}C_4H_7)\{C(P(S)Ph_2)_3\}]$ and $[Pd(\eta^3\text{-}C_4H_7)\{CH(P(S)Ph_2)_3\}]BF_4$ have been synthesised. In all the complexes except $[Pd(\eta^3\text{-}C_4H_7)\{CH(P(S)Ph_2)_3\}]BF_4$ the palladium centres are 4-coordinate with essentially square planar geometry with the phosphine chalcogenide ligands coordinated in a bidentate fashion to the metal. For the complexes containing $CH(PPh_2)(P(S)Ph_2)_2$ and $[C(PPh_2)(P(S)Ph_2)_2]^-$ the coordination is via a phosphorus and a sulphur atom whereas for $[C(P(S)Ph_2)_3]^-$ coordination is by two sulphur atoms. In

$[Pd(\eta^3\text{-}C_4H_7)\{CH(P(S)Ph_2)_3\}]BF_4$, as shown by the solid state crystal structure, the palladium is 5-coordinate with the $CH(P(S)Ph_2)_3$ ligand coordinated in a tridentate fashion, via all three sulphurs, to the metal centre. Comprehensive studies by ^{31}P NMR spectroscopy have shown that two of the complexes, $[Pd(\eta^3\text{-}C_4H_7)\{CH(PPh_2)(P(S)Ph_2)_2\}]BF_4$ and $[Pd(\eta^3\text{-}C_4H_7)\{C(P(S)Ph_2)_3\}]$, undergo dynamic intramolecular exchange between the coordinated and non-coordinated $P(S)Ph_2$ groups. In contrast, $[Pd(\eta^3\text{-}C_4H_7)\{C(PPh_2)(P(S)Ph_2)_2\}]$ is rigid in this respect. In all four complexes the 2-methylallyl group is coordinated in an η^3 mode to the palladium atom, occupying two coordination sites. The fluxionality of the 2-methylallyl ligand and ligand exchange processes in palladium 2-methylallyl complexes have been thoroughly investigated [32-38] prior to this work.

The interesting comparisons between the four compounds, in terms of fluxionality and coordination modes, can give us some insight into the factors that influence them. In the case of $[Pd(\eta^3\text{-}C_4H_7)\{CH(PPh_2)(P(S)Ph_2)_2\}]BF_4$ and $[Pd(\eta^3\text{-}C_4H_7)\{C(PPh_2)(P(S)Ph_2)_2\}]$ we have found that both are 4-coordinate, but $[Pd(\eta^3\text{-}C_4H_7)\{CH(PPh_2)(P(S)Ph_2)_2\}]BF_4$ shows fluxional behaviour at ambient temperature whereas $[Pd(\eta^3\text{-}C_4H_7)\{C(PPh_2)(P(S)Ph_2)_2\}]$ is rigid. This is most likely explained by the differing geometries around the methine carbons of the ligands. A lower activation energy would be required to undergo an exchange between the coordinated and dangling $Ph_2P{=}S$ groups for the tetrahedral geometry in the protonated complex than that for the trigonal planar geometry in the deprotonated complex at the methine carbons of the $HC(PPh_2)(P(S)Ph_2)_2$ and $[C(PPh_2)(P(S)Ph_2)_2]^-$ ligands. Although we have shown that

$[Pd(\eta^3\text{-}C_4H_7)\{CH(P(S)Ph_2)_3\}]BF_4$ is 5-coordinate with the $HC(P(S)Ph_2)_3$ ligand bonded in a tridentate fashion, this may only be true for the solid state. In solution there are three possibilities which would agree with the singlet (down to -90°C) observed in the ^{31}P NMR spectrum. The complex could be 4-coordinate undergoing fast exchange between the coordinated and non-coordinated sulphurs involving a 5-coordinate intermediate. Also possible is a rigid 5-coordinate complex. Based upon our studies of $[Pd(\eta^3\text{-}C_4H_7)\{C(PPh_2)(P(S)Ph_2)_2\}]$ and $[Pd(\eta^3\text{-}C_4H_7)\{CH(PPh_2)(P(S)Ph_2)_2\}]BF_4$ where the protonated complex is fluxional but the deprotonated complex is rigid at ambient temperature, as well as the fact that palladium (II) has a strong preference for 4-coordination it seems most likely that $[Pd(\eta^3\text{-}C_4H_7)\{CH(P(S)Ph_2)_3\}]BF_4$ is 4-coordinate in solution and is undergoing a fast exchange which cannot be frozen out at -90 °C. A dissociative mechanism is proposed for $[Pd(\eta^3\text{-}C_4H_7)\{CH(PPh_2)(P(S)Ph_2)_2\}]BF_4$, shown in **Scheme 2.4**. whilst an associative mechanism is proposed for $[Pd(\eta^3\text{-}C_4H_7)\{C(P(S)Ph_2)_3\}]$, shown in **Scheme 2.6**. The activation energy for the exchange between the coordinated and non-coordinated phosphorus atoms are were calculated to be 57 and 51 kJ/mol for $[Pd(\eta^3\text{-}C_4H_7)\{CH(PPh_2)(P(S)Ph_2)_2\}]BF_4$ and $[Pd(\eta^3\text{-}C_4H_7)\{CH(P(S)Ph_2)_3\}]BF_4$ respectively using DNMR3 [69] and subsequent Eyring [70,71] plots . Now we can compare the behaviour of the two ligands and their corresponding anions in palladium allyl complexes in terms of the order of decreasing activation energy for rotation around the P-C bond (i.e. the exchange between the coordinated and non-coordinated $Ph_2P{=}S$ groups) is:

$[C(PPh_2)(P(S)Ph_2)_2]^-$ > $CH(PPh_2)(P(S)Ph_2)_2$ > $[C(P(S)Ph_2)_3]^-$ > $CH(P(S)Ph_2)_3$

This study also provides some insight into the differences between the two tripodal ligands, $CH(PPh_2)(P(S)Ph_2)_2$ and $CH(P(S)Ph_2)_3$. It suggests that a tridentate mode of coordination is preferred in complexes containing $CH(P(S)Ph_2)_3$ whereas a bidentate coordination mode is preferred for complexes containing $CH(PPh_2)(P(S)Ph_2)_2$ or $[C(PPh_2)(P(S)Ph_2)_2]^-$. This might simply be explained by steric effects, caused by the phenyl groups, and because 5-membered bis-chelate rings, as formed by the $CH(PPh_2)(P(S)Ph_2)_2$ and $[C(PPh_2)(P(S)Ph_2)_2]^-$ ligands with the metal centre, would have some ring strain.

Chapter Three

Coordination Chemistry of $[CH(P(S)Ph_2)_3]$ and $[C(P(S)Ph_2)_3]^-$; Rhodium, Iridium, and Platinum Complexes

3.1 Synthesis and Characterization

Reactions of $[M(Cod)(\mu\text{-}Cl)]_2$ (M = Rh or Ir) with 2 mole equivalents of $[CH(P(S)Ph_2)_3]$, in the presence of a suitable counterion (BF_4^- or ClO_4^-), results in the cleavage of the chloro bridges and the formation of $[M(Cod)\{CH(P(S)Ph_2)_3\}]Z$ (M = Rh, Z = BF_4^-; M = Ir, Z = ClO_4^-). These compounds were fully characterised by microanalysis of C and H % and $^{31}P\{^1H\}$ NMR. The synthetic scheme is shown in **Scheme 3.1**.

Scheme 3.1 Synthesis of $[M(Cod)\{CH(P(S)Ph_2)_3\}]Z$

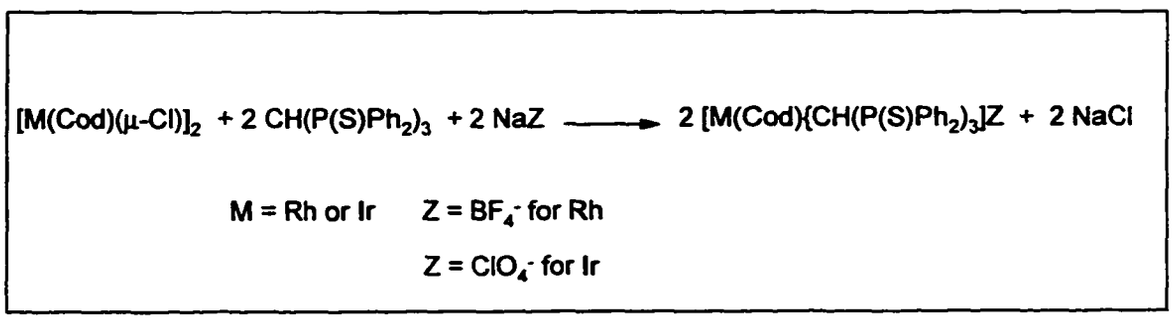

However, because of the high acidity of the methine proton of the coordinated ligand $[CH(P(S)Ph_2)_3]$, addition of a weak base, such as diethylamine, results in the formation of the neutral complexes $[M(Cod)\{C(P(S)Ph_2)_3\}]$ (M = Rh, Ir) as air-stable yellow crystals in 66 to 70% yields. The complexes were fully characterised by microanalysis of C and H % and $^{31}P\{^1H\}$ NMR and a solid state structure of $[Rh(Cod)\{C(P(S)Ph_2)_3\}]$ was obtained by an X-ray diffraction study of a single crystal. The synthetic scheme is shown in **Scheme 3.2**.

Scheme 3.2 Synthesis of {M(Cod){C(P(S)Ph$_2$)$_3$}]

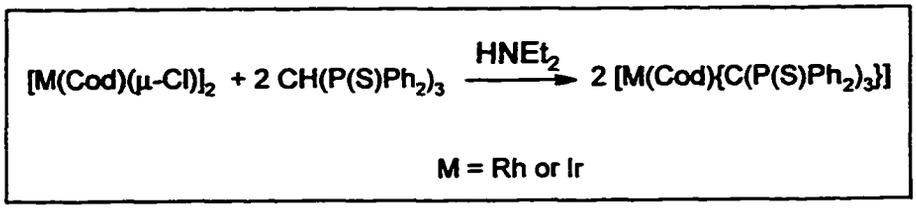

Further reaction of carbon monoxide with [Ir(Cod){C(P(S)Ph$_2$)$_3$}] produces pale yellow crystals of [Ir(CO)$_2${C(P(S)Ph$_2$)$_3$}] in 60% yield. This complex was again characterised by microanalysis and $^{31}P\{^1H\}$ NMR as well as by an X-ray diffraction study. Unfortunately the isolation of a rhodium analogue proved not to be possible.

Reaction of [Pt(MeoCod)(μ-Cl)]$_2$ with two equivalents of CH(P(S)Ph$_2$)$_3$ resulted in the formation of [Pt(MeoCod){C(P(S)Ph$_2$)$_3$}], isolated as a yellow powder in 90% yield as shown in **Scheme 3.3**. Repeated attempts at recrystallisation failed to produce a product suitable for microanalysis.

Scheme 3.3 Synthesis of [Pt(MeoCod){C(P(S)Ph$_2$)$_3$}]

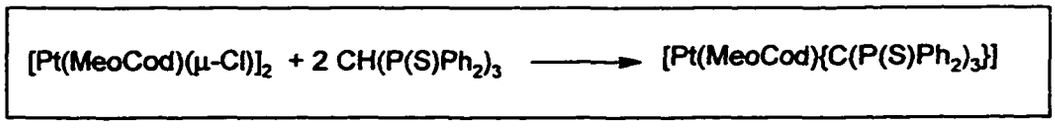

The trisphosphine sulphide ligands can coordinate in bidentate or tridentate fashion to a metal centre, as shown in **Scheme 3.4.**

Scheme 3.4 Possible Coordination Modes of $CH(P(S)Ph_2)_3$ in Metal Complexes. (Phenyl groups are omitted for clarity).

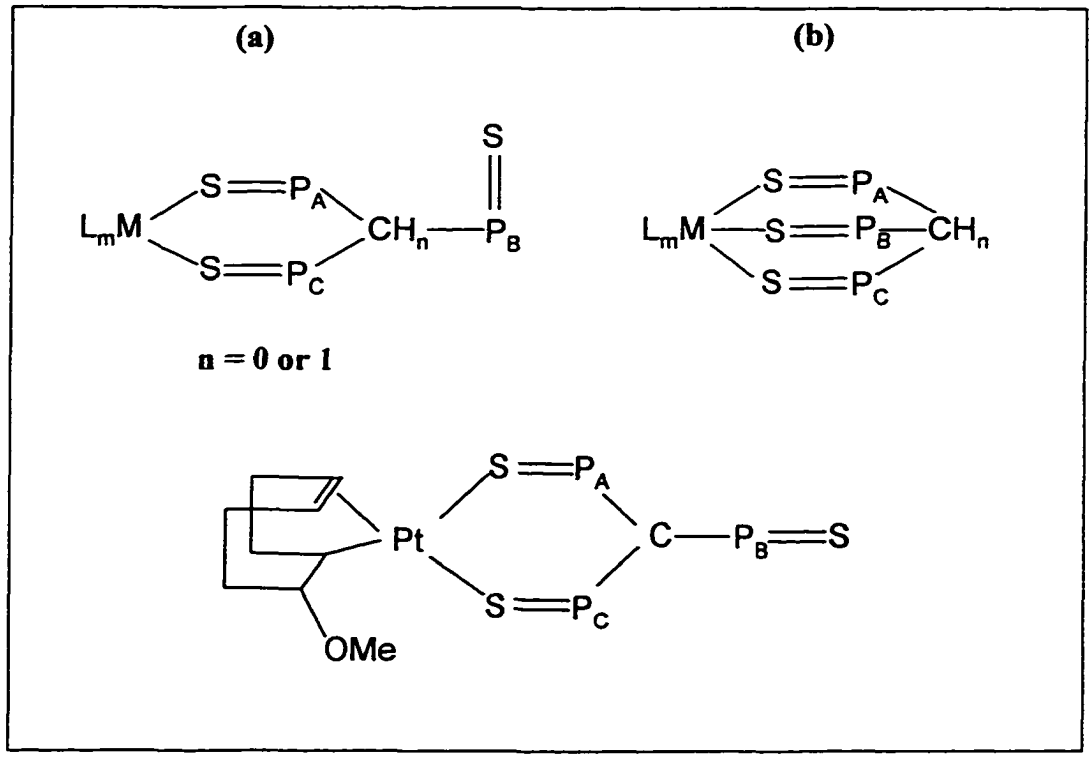

If the other ligands are symmetrical, as in the case of *Cod* or carbon monoxide, the actual coordination mode can be determined by ^{31}P NMR, which will show two resonances if mode (a) has occurred or one resonance if mode (b) is the case. If an unsymmetrical ligand, such as MeoCod, is coordinated to the metal centre, the $^{31}P\{^1H\}$ NMR spectrum will show three resonances. However, in either case, if a dynamic intra-molecular exchange was occurring at ambient temperature, the spectrum would be expected to show only a single line. Therefore a low temperature $^{31}P\{^1H\}$ NMR study would be required to actually determine the mode of coordination, and to study the fluxional behaviour of the ligands in general.

Table 3.1 ^{31}P {^{1}H} NMR Parameters for Deprotonated Complexes

Complex	Notes	δP
[Rh(Cod){C(P(S)Ph_2)$_3$}]	a,b	39.8
[Ir(Cod){C(P(S)Ph_2)$_3$}]	a	37.2
[Ir(CO)$_2${C(P(S)Ph_2)$_3$}]	c	37.7

Notes: a) CH_2Cl_2 solution with external C_6D_6 lock.

b) Variable temperature spectra in CD_2Cl_2 solution show two shifts, 43.0 and 38.0 ppm, in a 1:2 ratio at -54°C and a single shift, 40.1 ppm, at magnet ambient temperature (+26°C).

c) $CDCl_3$ solution.

The ^{31}P {^{1}H} NMR spectra essentially show single resonances with the exception of [Pt(MeoCod){C(P(S)Ph_2)$_3$}] which exhibited two resonances at room temperature. The shifts of the phosphorus nuclei in the protonated complexes are around +41 ppm, which differ little from that of the free ligand, CH(P(S)Ph_2)$_3$ that gives a peak at +41.9 ppm. In the deprotonated complexes the phosphorus shifts range from +39.8 ppm to +37.2 ppm that differ somewhat to that of the anionic ligand [C(P(S)Ph_2)$_3$]$^-$ which gives a peak at +45.2 ppm [45]. This illustrates the insensitivity of the phosphorus nuclei to the nature of

Table 3.2 ^{31}P {^{1}H} NMR and Selected ^{1}H NMR and ^{13}C NMR Parameters for Protonated Complexes in $CDCl_3$ Solution.

Complex	δP	$\delta(C_A)$	$J(P\text{-}C_A)$	δH_A	$J(P\text{-}H_A)$
$[Rh(Cod)\{CH(P(S)Ph_2)_3\}]BF_4$	41.4	35.3	29	6.18	11
$[Ir(Cod)\{CH(P(S)Ph_2)_3\}]ClO_4$	41.2	31.2	38	6.28	11

Table 3.3 ^{31}P {^{1}H} NMR Parameters for $[Pt(MeoCod)\{C(P(S)Ph_2)_3\}]$[a,b]

Complex	δP_A	δP_B	δP_C	$J(P_A\text{-}P_B)$	$J(P_B\text{-}P_C)$	$J(P_A\text{-}P_C)$
$[Pt(MeoCod)\{C(P(S)Ph_2)_3\}]$	41.0	41.0	36.0	23	26	12

Notes: a) $CDCl_3$ solution.

b) Variable temperature spectra in toluene-d_8 solution show three shifts, 37.4, 43.4 and 36.0 ppm, in a 1:1:1 ratio at -40°C; and two shifts, 41.0 and 36.0 ppm, at magnet ambient temperature (+26°C).

the metal, the charge on the complex, and the nature of the other ligands attached to the metal. In the case of each protonated complex the ^{1}H NMR was run to detect the presence of the methine proton which evidently appears as a quartet at around +6 ppm with typical two bond P-H couplings of about 11 Hz. The presence of a proton on the methine carbon

is also confirmed by multiplicity sorting experiments (DEPT) on the ^{13}C NMR. The ^{31}P NMR parameters for deprotonated complexes are collected in **Table 3.1**. In **Table 3.2** partial ^{31}P, ^{1}H and ^{13}C NMR data for the protonated complexes is presented. **Table 3.3** contains ^{31}P NMR data for [Pt(MeoCod){C(P(S)Ph_2)$_3$}], the labelling scheme is shown in **Scheme 3.4**.

The ^{31}P NMR spectrum of [Pt(MeoCod){C(P(S)Ph_2)$_3$}] at ambient temperature shows only two resonances; a broad signal at +41 ppm and a triplet at +36 ppm. Because of the unsymmetrical nature of the complex, unless a dynamic intramolecular exchange is involved, the ^{31}P NMR should give rise to three distinct resonances. A variable temperature ^{31}P NMR is therefore required and the results of such a study are discussed later on in this chapter. The broad singlet at +41 ppm is assigned to both P_A and P_B with exchange occurring between the coordinated P_A=S and "dangling" P_B=S groups at ambient temperature. The triplet at +36 ppm is assigned to P_C, which is *trans* to the double bond in MeoCod . The ^{31}P NMR parameters for Pt(MeoCod){C(P(S)Ph_2)$_3$}] are listed in **Table 3.3**.

3.2 Dynamic NMR of [Pt(MeoCod){C(P(S)Ph_2)$_3$}]

The ^{31}P NMR spectrum of [Pt(MeoCod){C(P(S)Ph_2)$_3$}] at ambient temperature shows an exchange between the coordinated P_A(S)Ph_2 group and the non-coordinated P_B(S)Ph_2 group, with a broad singlet at +41 ppm. When the temperature is reduced this singlet broadens initially and then, at -40°C, resolves into two signals; an apparent doublet at

+43.4 ppm and a triplet at +37.4 ppm. The triplet at +36 ppm remains much the same as it is at ambient temperature as described in the previous section. The spectra over the temperature range of ambient to -40 °C are shown in **Figure 3.1**. When the temperature was increased, the lineshapes of the two resonances began to broaden and eventually merge into one broad peak at +100 °C. The peak became sharper as the temperature reached +110 °C. The spectra over the temperature range of +110 °C to +28 °C are shown in **Figure 3.2**. The lineshape simulations were derived from lineshape fitting with the DNMR 3 computer program of Kleier and Binsch [69]. The simulations assume that there are two exchange processes occurring based on an η^2 structure as shown in **Scheme 3.4**.

The first exchange occurs between P_A and P_B and the second between all three phosphorus atoms. It also assumes that the three different chemical shifts are in a 1:1:1 ratio at the slow exchange limit and complete mutual exchange at the fast exchange limit. The rate constants for the exchange process, over a range of temperature, have been derived and are listed in **Table 3.4** and **Table 3.5**. From this data Eyring [70,71] plots of $\ln(k_r/T)$ versus 1/T has enabled the values of $\Delta H^{\circ\ddagger}$, $\Delta S^{\circ\ddagger}$, $\Delta G^{\circ\ddagger}$ to be estimated for both processes. As well, Arrhenius [72] plots of ln k versus 1/T have allowed E_a to be calculated. The results are shown in **Table 3.6**.

Figure 3.1 $^{31}P\{^{1}H\}$ NMR Spectra of [Pt(MeoCod){C(P(S)Ph$_2$)$_3$}] at 101.3 MHZ in $(CD_3)_2SO$ from -40 °C to +28 °C.

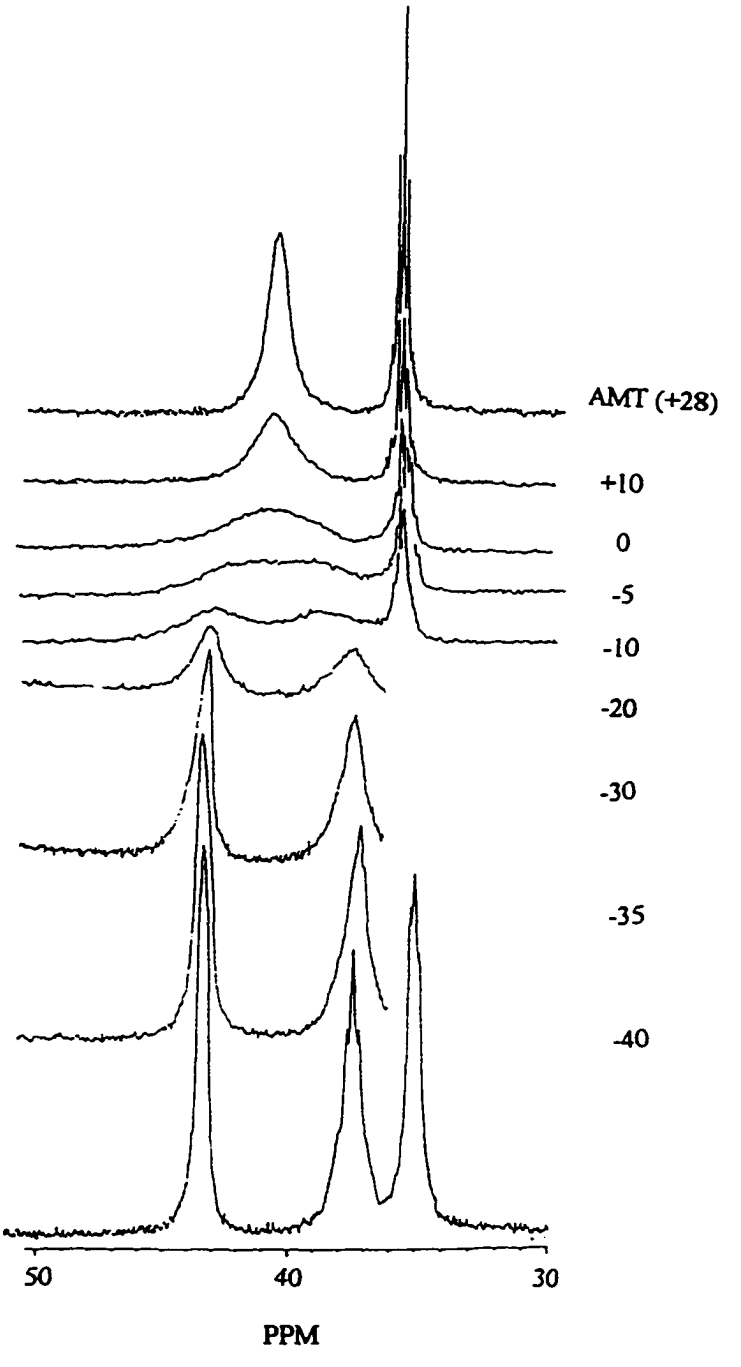

Figure 3.2 $^{31}P\{^{1}H\}$ NMR Spectra of [Pt(MeoCod){C(P(S)Ph$_2$)$_3$}] from +28°C to +110°C at 101.3 MHZ in CD_2Cl_2.

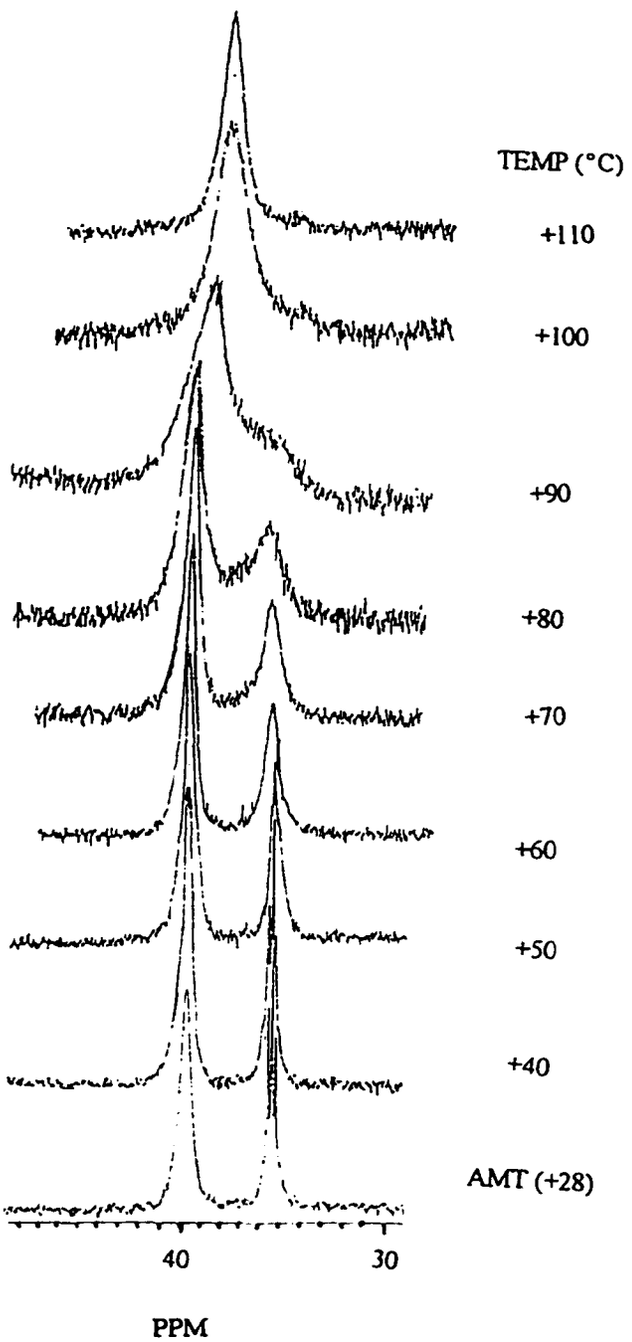

Table 3.4 Rate Constants, $k_r(s^{-1})$, for Phosphorus Interchange $P_A \leftrightarrows P_B$ in [Pt(MeoCod){C(P(S)Ph$_2$)$_3$}]

temp (K)	301	283	273	268	263	253	243	238	233
rate constant (k_r)	$2x10^4$	4,000	2,000	1,000	500	100	40	10	1

Table 3.5 Rate Constants, $k_r(s^{-1})$, for Phosphorus Interchange $P_A \leftrightarrows P_B \leftrightarrows P_C$ in [Pt(MeoCod){C(P(S)Ph$_2$)$_3$}]

temp (K)	313	353	363	373	383
rate constant (k_r)	$5x10^3$	$1x10^4$	$3x10^4$	$3x10^4$	$6x10^4$

There are two exchange processes involved. At ambient temperature, because of the stronger *trans*-influence of the σ-bond over the π-bond, only exchange between P_A and P_B occurs. At higher temperature, the energy provided by heat overcomes the transitional energy barrier required by the exchange between all three phosphorus atoms. This enables all three phosphorus atoms to appear to be equivalent. The large positive $\Delta S^{\circ\circ}$ (+98 J/K)

Table 3.6 Rate Plots and Thermodynamic Parameters for Phosphorus Interchange in [Pt(MeoCod){C(P(S)Ph$_2$)$_3$}]

(a) $P_A \rightleftharpoons P_B$

(b) $P_A \rightleftharpoons P_B \rightleftharpoons P_C$

	(a)	**(b)**
ln(k_r) vs 1/T	slope -9517	slope -4400
	intercept 42.1	intercept 22.3
ln(k_r/T) vs 1/T	slope -9260	slope -4058
	intercept 35.5	intercept 15.5
$\Delta H^{\circ *}$, kJ/mol	77 (±2)	34 (±4)
$\Delta S^{\circ *}$, J/K	98 (±3)	-69 (±4)
$\Delta G^{\circ *}$, kJ/mol	48 (±2)	54 (±3)
E_a, kJ/mol	79 (±3)	37 (±4)

value for the exchange between P_A and P_B suggests a dissociative pathway. An associative pathway is however suggested for the exchange between all the three phosphorus atoms due to its large negative value of $\Delta S^{\circ *}$ (-69 J/K) for the second exchange among all phosphorus atoms. We propose a dissociative pathway, shown in **Scheme 3.5**, for the first dynamic exchange of the non-coordinated P_A=S group with the coordinated P_B=S

Scheme 3.5 Suggested Mechanism for the Intramolecular Exchange of $P_A \approx P_B$ in [Pt(MeoCod){C(P(S)Ph$_2$)$_3$}] at Ambient Temperature (phenyl groups are omitted for clarity).

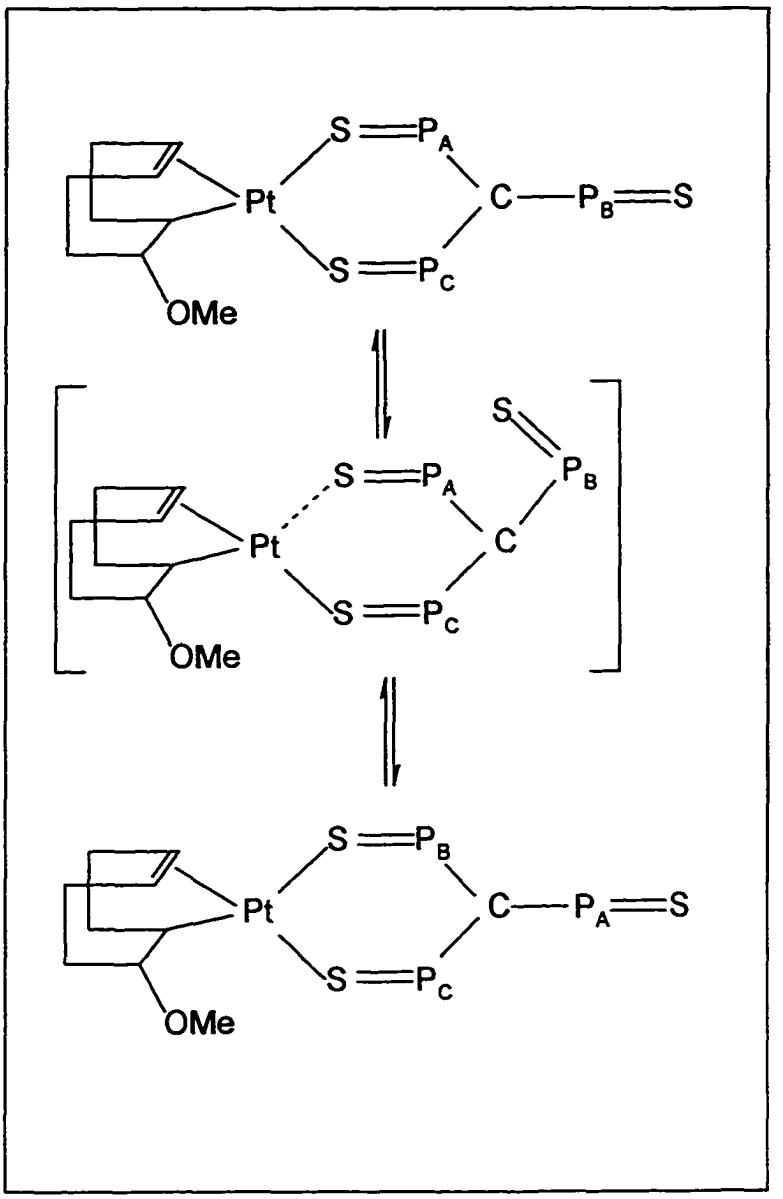

group, in which a three-coordinate activated complex forms with the rupture of the Pt-S bond *trans* to the σ-bond of the MeoCod ligand because of its stronger *trans*-influence over the π-bond of the MeoCod ligand. The non-coordinated P_B=S group then attaches

to the platinum metal centre as the coordinated P_A=S group leaves the metal. The value of ΔG^{o*} for this process is 48 kJ/mol. An associative pathway, shown in **Scheme 3.6**, is suggested for the exchange between all the three phosphorus atoms as evidenced by the large negative value of ΔS^{o*} (-69 J/K).

Scheme 3.6 Proposed Mechanism for $P_A \rightleftharpoons P_B \rightleftharpoons P_C$ Exchange in $[Pt(MeoCod)\{C(P(S)Ph_2)_3\}]$

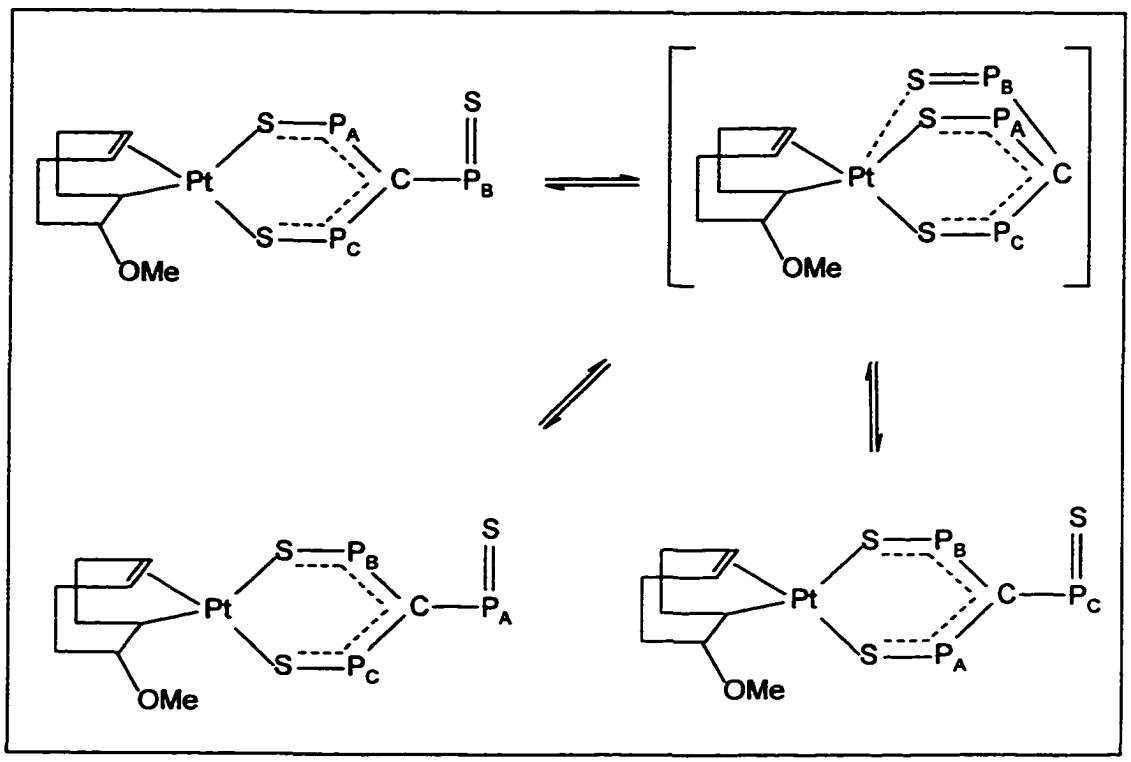

3.3 Dynamic NMR of [Rh(Cod)(P(S)Ph$_2$)$_3$}]

Both the ^{31}P NMR spectra of [Rh(Cod){CH(P(S)Ph$_2$)$_3$}]BF$_4$ and [Rh(Cod){C(P(S)Ph$_2$)$_3$}] exhibit a singlet at ambient temperature. Low temperature ^{31}P NMR studies of both have been performed. The ^{31}P NMR spectrum of [Rh(Cod){CH(P(S)Ph$_2$)$_3$}]BF$_4$ remains a sharp singlet from ambient temperature down to -100 °C, suggesting either a very fast exchange process or very small chemical shift differences, or both. In contrast, as the temperature is reduced, the ^{31}P NMR of [Rh(Cod){C(P(S)Ph$_2$)$_3$}], originally consisting of a singlet at 39.8 ppm at ambient temperature, begins broadening at -20 °C and resolves into two "singlets" at -54 °C, with shifts of 43 ppm and 38 ppm. The signal at 38 ppm is broadened significantly when the temperature is lowered further and would be expected to split into two peaks eventually because of the inequivalence of the two coordinated P(S)Ph$_2$ groups caused by the restricted rotation of the `dangling' P(S)Ph$_2$ group. This, however is not observed because of the closeness of the freezing point of the solvent, CD_2Cl_2. The spectra over the temperature range from ambient to -54 °C are shown in **Figure 3.3**.

The spectra shown in **Figure 3.3** are consistent with the suggestion that at ambient temperature in solution [Rh(Cod){C(P(S)Ph$_2$)$_3$}] undergoes a fluxional process in which the coordinated P(S)Ph$_2$ exchanges rapidly with the non-coordinated P(S)Ph$_2$ group, as shown in **Scheme 3.7**.

This process can be frozen out at -54 °C resolving P_A at +43 ppm and P_B/P_C at +38 ppm. The line shape simulations derived from the DNMR3 computer program of Kleier

and Binsch [69] were performed under the assumption of an exchange process based on an η^2 structure with two different chemical shifts in a 2:1 ratio at the slow exchange limit and with complete mutual exchange at fast exchange limit. The results of the analysis are shown in **Figure 3.4**, from calculated lineshapes, and **Table 3.7** for rate constants at different temperatures.

Scheme 3.7 Intramolecular Exchange of [Rh(Cod){C(P(S)Ph$_2$)$_3$}] at Ambient Temperature(phenyl groups are omitted for clarity).

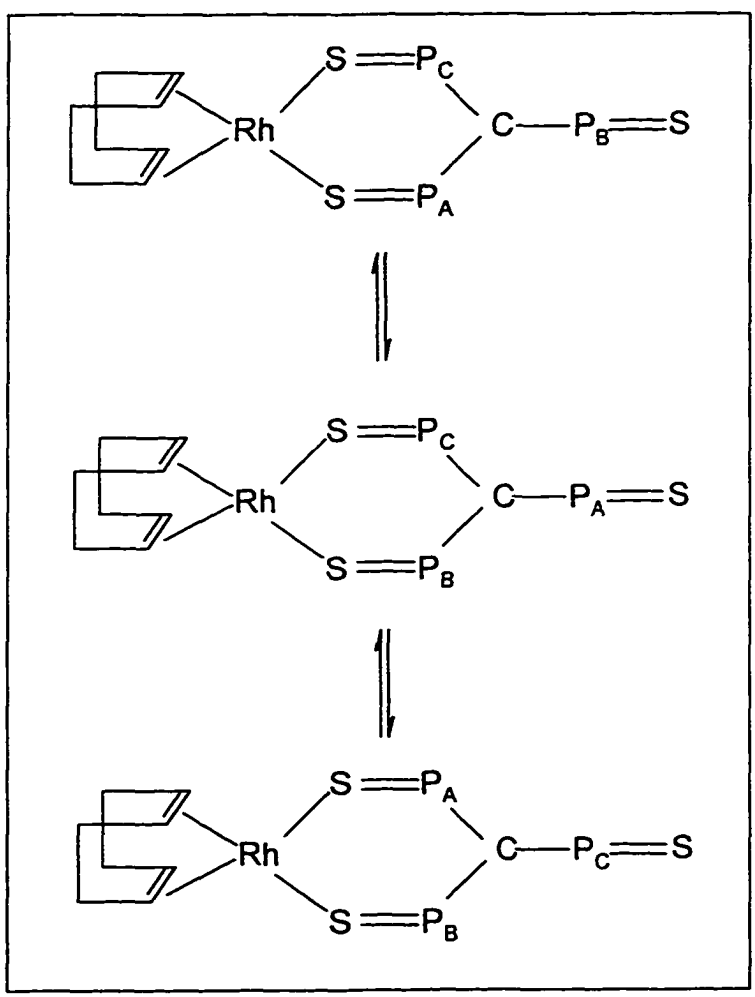

Figure 3.3 $^{31}P\{^{1}H\}$ NMR Spectra of [Rh(Cod){C(P(S)Ph$_2$)$_3$}] in CD_2Cl_2 from -54°C to AMT at 145.9 MHZ.

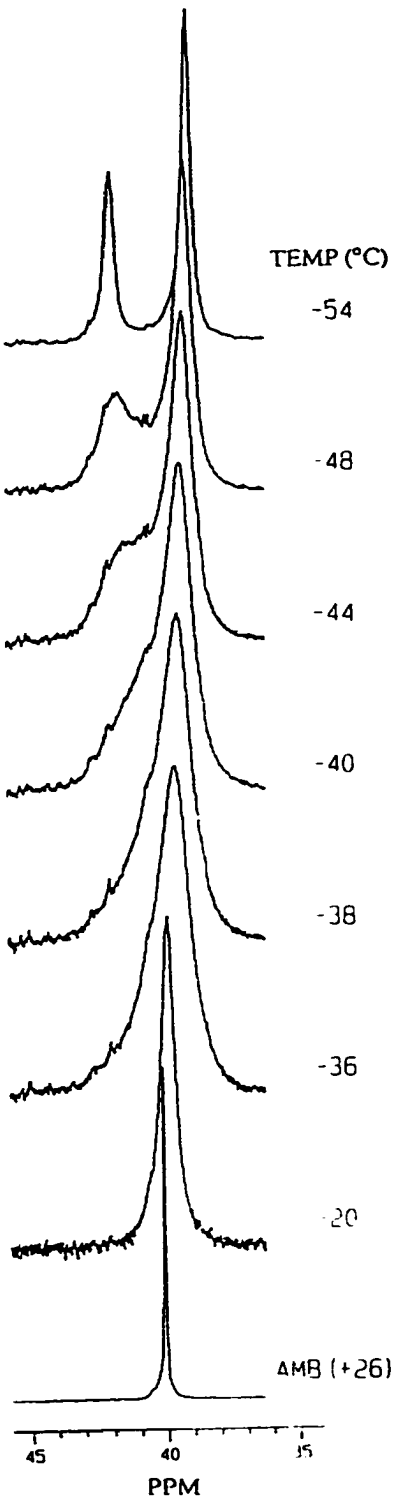

Figure 3.4 Calculated Lineshapes for [Rh(Cod){C(P(S)Ph$_2$)$_3$}].

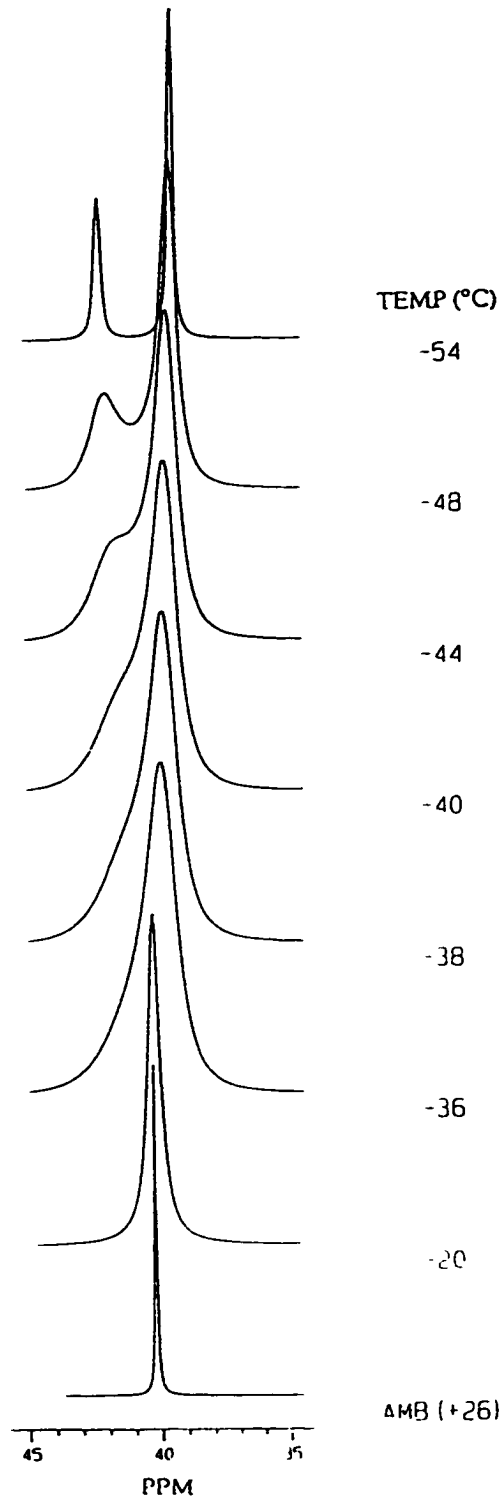

Table 3.7 Rate Constants $k_r(s^{-1})$ for Phosphorus Interchange $P_A \rightleftharpoons P_B$ in the Complex [Rh(Cod){C(P(S)Ph$_2$)$_3$}].

temp (K)	253	237	235	233	229	225	219
rate constant (k_r)	2,200	650	575	500	410	260	20

And from the data in **Table 3.7** an Eyring [70,71] plot, shown in **Figure 3.5**, of ln (k_r/T) against 1/T, shown in **Figure 3.5**, gives a good straight line (R = 0.989).

Figure 3.5 The Eyring Plot of the Rate Data for Intramolecular Phosphorus Interchange $P_A \rightleftharpoons P_B$ in [Rh(Cod){C(P(S)Ph$_2$)$_3$-*S*,*S*}]

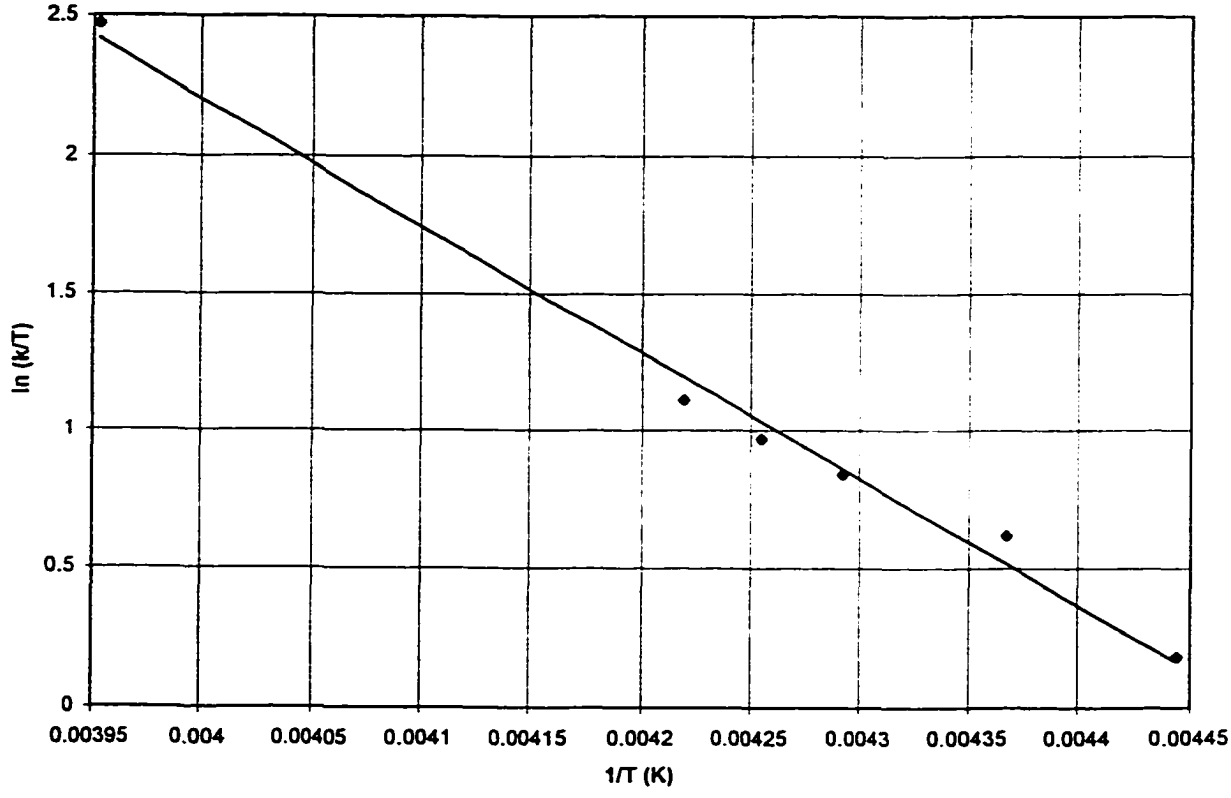

The comparison with the standard transition state theory equation (1) enables $\Delta H^{\circ *}$, $\Delta S^{\circ *}$ and hence $\Delta G^{\circ *}$ to be calculated. These values are shown in **Table 3.8**, which also includes a value for the Arrhenius [72] activation energy, E_a, which is derived from the slope of an Arrhenius plot of ln k_r against 1/T using equation (2)

Table 3.8 Rate Plots and Thermodynamic Parameters for Phosphorus Interchange in [Rh(Cod){C(P(S)Ph$_2$)$_3$}].

ln k_r/T vs 1/T	slope	-4588
	intercept	20.56
ln k_r vs 1/T	slope	-4852
	intercept	27.14
$\Delta H^{\circ *}$, kJ mol^{-1}	+38 (±2)	
$\Delta S^{\circ *}$, JK^{-1}	-27 (±3)	
$\Delta G^{\circ *}$, kJ mol^{-1}	+46 (±2)	
E_a, kJ mol^{-1}	+40 (±4)	

A negative value of $\Delta S^{\circ *}$ of -27 J/K is obtained. This suggests an associative pathway involving a 5-coordinate activated complex in the process of exchange between coordinated and non-coordinated Ph_2P=S groups. **Scheme 3.8** illustrates the proposed mechanism.

Scheme 3.8 Suggested Mechanism for the Intramolecular Exchange of [Rh(Cod){C(P(S)Ph$_2$)$_3$-*S*,*S*}] at Ambient Temperature (phenyl groups are omitted for clarity).

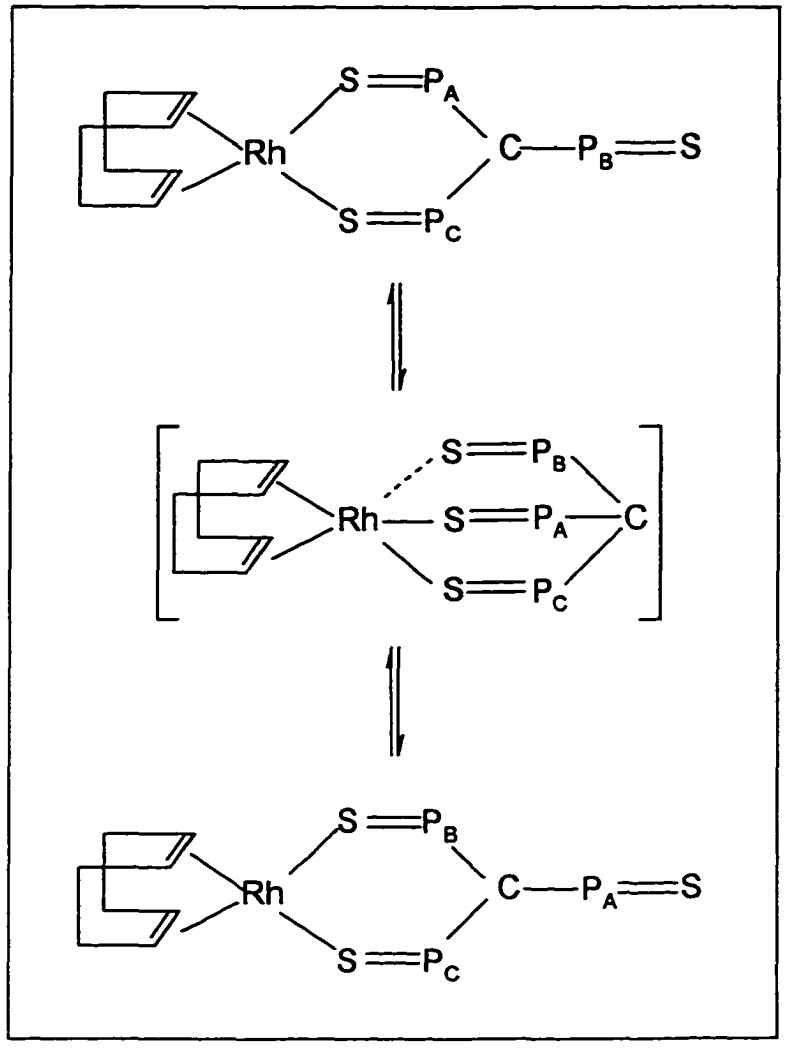

The fluxionality of the *Cod* ligand and ligand exchange in *Cod*-rhodium complexes have been thoroughly investigated [97-100]. We expect the fluxional behaviour of the *Cod* ligand to be similar to that observed by Heitner and Lippard [99,100].

3.4 Solid-state Structure of [Rh(Cod){η^2-C(P(S)Ph_2)$_3$-*S*,*S*}]

[Rh(Cod){C(P(S)Ph_2)$_3$}] was prepared as described in the experimental part of Chapter Seven and crystals suitable for study by X-ray diffraction were grown by recrystallisation from dichloromethane and hexanes. The crystallographic techniques employed are described in detail in Chapter Seven and Appendix. Selected crystallographic data are listed in **Table 3.9**. The metal atom, all phosphorus and sulphur atoms, the central carbons of the C(P(S)Ph_2)$_3$ ligands, and the carbon atoms of the Cod ligand were treated anisotropically; the remaining carbon atoms were refined isotropically. Hydrogen atoms were not located.

The structure of a single molecule of [Rh(Cod){C(P(S)Ph_2)$_3$}] is shown as an ORTEP diagram in **Figure 3.6**, along with the atomic labelling scheme. Unit cell and other parameters related to the crystal structure determinations are in **Table 3.9**. Selected fractional atomic coordinates and temperature parameters are in **Appendix Table VI**, anisotropic temperature parameters in **Appendix Table VII**. Selected interatomic distances and bond angles in **Tables 3.10** and **3.11** respectively.

Table 3.9 Selected Crystallographic Data for [Rh(Cod){C(P(S)Ph$_2$)$_3$}] and [Ir(CO)$_2${C(P(S)Ph$_2$)$_3$}]

	[Rh(Cod){C(P(S)Ph$_2$)$_3$}]	[Ir(CO)$_2${C(P(S)Ph$_2$)$_3$}]
formula	$C_{45}H_{42}P_3RhS_3$	$C_{39}H_{30}IrO_2P_3S_3$
fw	874.8	912.0
space group	Pbca(No. 61)	Pbca(no. 61)
a, Å	20.427(4)	22.140(6)
b, Å	16.931(2)	22.317(5)
c, Å	23.138(3)	14.792(3)
V, Å^3	8002	7309
Z	8	8
density calc/obs, g/cm^3	1.43/1.46	1.66/1.64
diffractometer	Picker 4-circle	Picker 4-circle
radiation (λ, Å)	Mo K_α (0.71069)	Mo K_α (0.71069)
μ, cm^{-1}	7.19	42.06
transm factor range	0.86-0.91	0.45-0.73
temperature, K	295	295
No. of obs reflcns (I>2σ(I))	3400	1994
R	0.067	0.068
R_w	0.067	0.068

$w = 1/(\sigma^2(F) + 0.001F^2)$; $\Delta = \| F_o| - | F_c \|$ $R = (\Sigma\Delta/\Sigma F_o)$; $R_w = (\Sigma w \Delta^2/\Sigma w F_o^2)^{1/2}$

Figure 3.6 ORTEP Plot for a Single Molecule of [Rh(Cod){C(P(S)Ph$_2$)$_3$}]

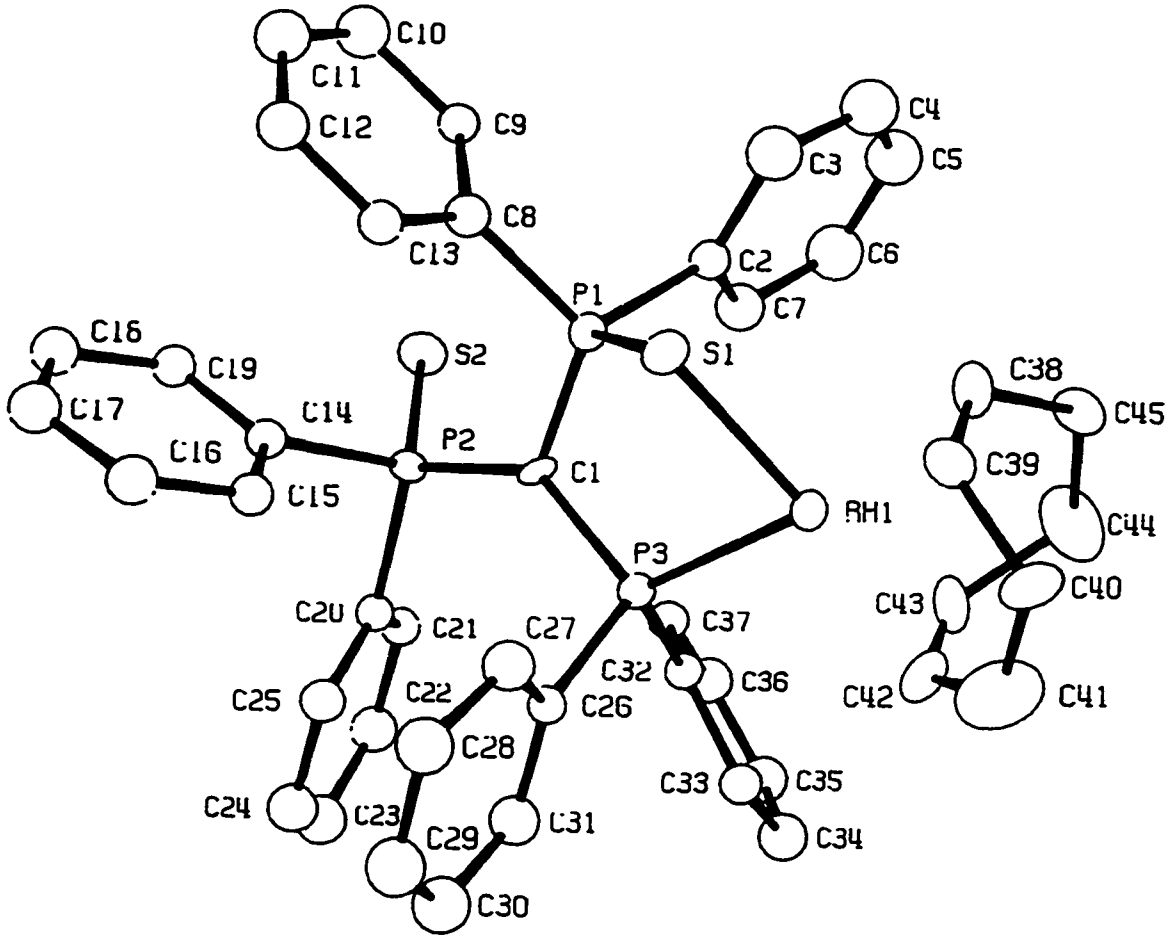

The structure shows an approximately square planar metal centre with $[C(P(S)Ph_2)_3]^-$ coordinated in bidentate fashion through two coordinated sulphur atoms, and the third sulphur atom non-coordinated, pointed away from the Rh(I) centre. The *Cod* ligand is coordinated via its two double bonds to the rhodium atom. There are relatively small distortions of the square plane with the rhodium atom lying only 0.04 Å out of the plane defined by S_1, S_2 and the centroids of the two double bonds in Cod. The angles at the rhodium centre are close to 90°, with S(1) - Rh - S(2) at 93.4°. This angle is comparable to those observed in [PtCl(PEt$_3$){C(P(S)Ph$_2$)$_3$}] (S - Pt - S, 94.9°) [101] and

Table 3.10 Selected Bond Angles (°) for [Rh(Cod){C(P(S)Ph$_2$)$_3$}].

Atoms	Distance	Atoms	Distance
S(1) - Rh(1)	2.356(3)	C(1) -P(1)	1.781(10)
S(2) - Rh(1)	2.337(3)	C(2) - P(1)	1.829(10)
C(38) - Rh(1)	2.163(10)	C(8) - P(1)	1.834(10)
C(39) - Rh(1)	2.178(11)	C(1) - P(2)	1.749(10)
C(42) - Rh(1)	2.133(11)	C(14) - P(2)	1.824(10)
C(43) - Rh(1)	2.137(11)	C(20) - P(2)	1.824(10)
P(1) - S(1)	2.027(4)	C(1) - P(3)	1.776(10)
P(2) - S(2)	2.039(4)	C(26) - P(3)	1.848(11)
P(3) - S(3)	1.968(4)	C(32) - P(3)	1.841(11)

Estimated standard deviations are given in parentheses

Table 3.11 Selected Bond Angles (°) for [Rh(Cod){C(P(S)Ph$_2$)$_3$}].

Atoms	Angle
S(2) - Rh(1) - S(1)	93.4(1)
C(38) - Rh(1) - S(1)	153.7(4)
C(38) - Rh(1) - S(2)	88.3(3)
C(39) - Rh(1) - S(1)	167.2(3)
C(39) - Rh(1) - S(2)	92.8(3)
C(39) - Rh(1) - C(38)	37.7(4)
C(42) - Rh(1) - S(1)	89.2(3)
C(42) - Rh(1) - S(2)	160.0(4)
C(42) - Rh(1) - C(38)	98.0(5)
C(42) - Rh(1) - C(39)	81.2(5)
C(43) - Rh(1) - S(1)	87.4(3)
C(43) - Rh(1) - S(2)	161.1(4)
C(43) - Rh(1) - C(38)	82.7(5)
C(43) - Rh(1) - C(39)	90.3(5)
C(43) - Rh(1) - C(42)	38.8(4)
P(1) - S(1) - Rh(1)	108.8(1)
P(2) - S(2) - Rh(1)	111.0(1)
C(1) - P(1) - S(1)	111.8(4)
C(2) - P(1) - S(1)	108.7(3)
C(2) - P(1) - C(1)	112.1(5)
C(8) - P(1) - S(1)	101.5(4)
C(8) - P(1) - C(1)	116.5(5)
C(8) - P(1) - C(2)	105.4(5)
C(1) - P(2) - S(2)	115.9(4)

Atoms	Angle
C(14) - P(2) - S(2)	102.6(4)
C(14) - P(2) - C(1)	110.6(5)
C(20) - P(2) - S(2)	111.7(3)
C(20) - P(2) -C(1)	111.8(3)
C(20) - P(2) - C(14)	103.1(5)
C(1) - P(3) - S(3)	116.8(3)
C(26) - P(3) - S(3)	109.8(4)
C(26) - P(3) - C(1)	108.6(5)
C(32) - P(3) - S(3)	110.0(4)
C(32) - P(3) - C(1)	106.9(5)
C(32) - P(3) - C(26)	103.9(5)
P(2) - C(1) - P(1)	114.2(5)
P(3) - C(1) - P(1)	122.8(6)
P(3) - C(1) - P(2)	122.1(6)

Estimated standard deviations are in parentheses

$[Rh(Cod)\{C(P(O)Ph_2)_2(P(S)Ph_2)\}]$ (S - Rh - O, 95.7°) [102]. The bond distances between the rhodium centre and the coordinated sulphur atoms are 2.36 Å and 2.34 Å, similar to Rh - S in $[Rh(Cod)\{C(P(O)Ph_2)_2(P(S)Ph_2)\}]$ (Rh - S, 2.31 Å) and the two coordinated sulphur atoms in $[Rh(Cod)\{SS(CH_3)C_2(CN)_2\}]$ (Rh - S, 2.30 Å) [103]. The Rh-S bond length of 2.35 Å is slightly shorter than the sum of the covalent radii for rhodium and sulphur, 2.38 Å. This is suggestive of a relatively strong coordination of sulphur atoms to the Rh centre. The strong Rh-S interaction causes the P=S to lengthen somewhat, as shown by the P-S bond distance in the complex. The P - S bond distances range from 2.03 Å, 2.04 Å for coordinated sulphur atoms, to 1.97 Å for the non-coordinated sulphur atom. These distances are comparable to those in $[N(n\text{-}Bu)_4][C\{P(S)Ph_2\}_3]$ (average 1.98 Å) [48], where the P - S bonds lengthen upon coordination of the ligand $[C\{P(S)Ph_2\}_3]^-$ to the rhodium centre, as demonstrated here, from 1.98 Å to 2.03 Å and 2.04 Å upon coordination. The methine carbon of the $[C\{P(S)Ph_2\}_3]^-$ ligand is essentially planar with an average P - C - P bond angle of 119.7° with P(3) 0.28 Å from the P(1) - C(1) - P(2) plane. This is confirmation of the deprotonated nature of the ligand. The P - C bonds, 1.75 Å and 1.78 Å, are similar in length to those in $[N(n\text{-}Bu)_4][C\{P(S)Ph_2\}_3]$ (average 1.76 Å) [48], shorter than in $HC\{P(S)Ph_2\}_3$ (average 1.88 Å) [87], but considerably longer than those in typical ylides (1.62 Å to 1.66 Å) [104, 105]. These comparisons are consistent with the idea that the lone pair on the sp^2 hybridised C(1) methine carbon atom is delocalised over the chelate portion of the ligand resulting in the partially double bonded structure of the coordinated anion, $[C\{P(S)Ph_2\}_3]^-$. The 6-membered chelate ring $[Rh\text{-}S_2\text{-}P_2\text{-}C_1\text{-}P_1\text{-}S_1]$ has a distorted boat configuration with sulphur and phosphorus at the

prows and the Rh-S bond forming one side of the boat. The angles at sulphur [Rh-S_1-P_1, Rh-S_2-P_2] of 108.8° and 111.0° are comparable to the M-S-P bond angles commonly found in monodentate tertiary phosphine sulphide complexes, such as *trans* - [$(Et_2PhPS)_2PdCl_2$] (107.6°) [106] and *trans*-[$(n\text{-}Bu_3PS)_2PdCl_2$] (112.0°) [107].

The Rh-Cod bonding is normal. The four Rh-C distances, average 2.17 Å, are slightly longer than those in [Rh(Cod){$C(P(O)Ph_2)_2(P(S)Ph_2)$}] (2.12 Å) [102], [Rh(Cod)(acac)] (2.10 Å) [108] and [Rh(Cod){$PhC(O)CHC(O)CF_3$}] (2.12 Å) [109]. The olefinic bonds, C 38-C 39, C 43-C 42, 1.40 Å and 1.42 Å respectively, are comparable to those in [Rh(Cod){$C(P(O)Ph_2)_2(P(S)Ph_2)$}] (1.39 Å) [102] and [Rh(Cod)(acac)] (1.41 Å) [108], but are longer than the 1.34 Å distance in the free *Cod* molecule [110]. This bond lengthening is expected when olefin bonds coordinate to a metal centre.

3.5 Solid-state Structure of [$Ir(CO)_2\{C(P(S)Ph_2)_3$-S,S}]

[$Ir(CO)_2\{C(P(S)Ph_2)_3\}$] was prepared as described in the experimental part of Chapter Seven and crystals suitable for study by X-ray diffraction were grown by recrystallisation from dichloromethane and hexanes. The metal atom, all phosphorus and sulphur atoms, the central carbons of the $C(P(S)Ph_2)_3$ ligands, and the carbon and oxygen atoms of the carbonyl ligands were treated anisotropically; the remaining carbon atoms were refined isotropically. Hydrogen atoms were not located. The crystallographic techniques employed have been described in detail in Chapter Seven and Appendix. The

final difference maps for $[Ir(CO)_2\{C(P(S)Ph_2)_3\}]$ showed small peaks (ca. 1.6 e $Å^{-3}$) near the iridium atoms but structure gave no indication that material had been overlooked.

The structure of a single molecule of $[Ir(CO)_2\{C(P(S)Ph_2)_3$- *S,S*$\}]$ is shown as an ORTEP diagram in **Figure 3.7**, along with the atomic labelling scheme. Unit cell and other parameters related to the crystal structure determination are listed in **Table 3.9**. Fractional atomic coordinates and temperature parameters are in **Appendix Table VIII** anisotropic temperature parameters in **Appendix Table IX**. Selected interatomic distances and bond angles are given in **Tables 3.12** and **3.13** respectively.

The structure shows an approximately square planar Ir(I) metal centre with $[C(P(S)Ph_2)_3]^-$ coordinated in a bidentate fashion through two coordinated sulphur atoms, with the third sulphur atom non-coordinated and pointing away from the metal centre. Two carbonyl ligands are also coordinated to the iridium. There are relatively small distortions of the square plane; the carbonyl carbons, C(2) and C(3), are +0.286 and -0.109 Å respectively from the plane defined by Ir-S(1)-S(2). The angles at the Ir(I) centre are close to 90°, with the largest angle of S(2)-Ir-S(1) at 93.4° and the smallest for C(3)-Ir(1)-S(1) at 86.7°. These angles compare to S(1)-Ir(1)-S(2) at 95.3° for $[Ir(Cod)\{C(P(S)Ph_2)_3\}]$ [53], published later after our own study. The bond distances between the iridium centre and the coordinated sulphurs are 2.35 Å and 2.37 Å, which are similar to those found in $[Ir(Cod)\{C(P(S)Ph_2)_3\}]$ [111], 2.38 Å and 2.33 Å but are similar to the sum of the covalent radii of iridium and sulphur (2.39 Å [112]).

Figure 3.6 ORTEP Plot for a Single Molecule of $[Ir(CO)_2\{C(P(S)Ph_2)_3\}]$.

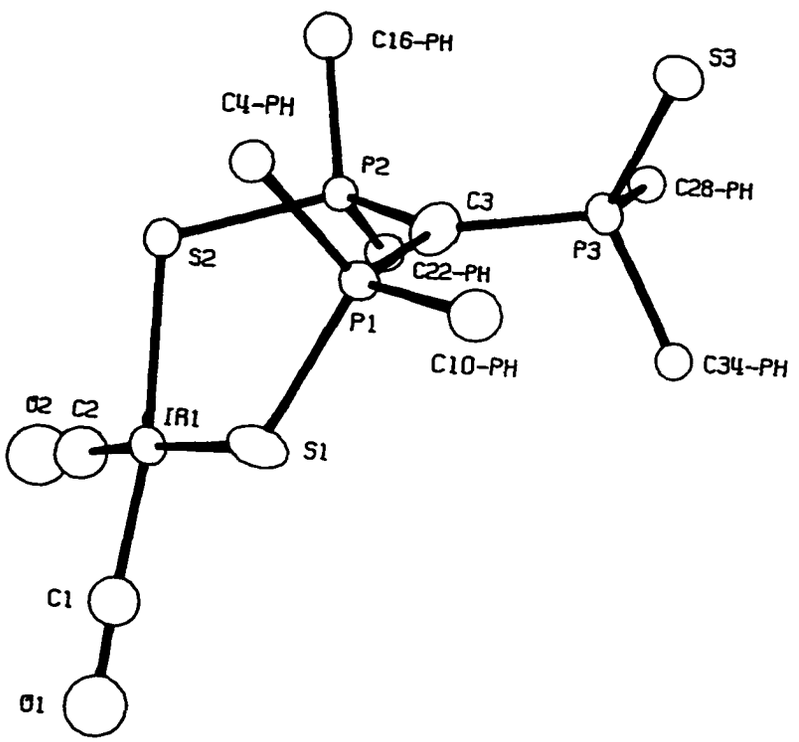

This is an indication of the relatively strong Ir-S bonds formed in this complex. This makes the P=S bonds somewhat longer. The coordinated $P(S)Ph_2$ groups have P-S bond lengths of 2.07 Å and 2.05 Å compared to the shorter non-coordinated P-S bond length of 1.97 Å, which is expected of phosphine chalcogenide bonds being longer upon coordination. The P-C bonds within the chelate ring, 1.76 Å and 1.73 Å are similar in length to those in $[Ir(Cod)\{C(P(S)Ph_2)_3\}]$ [111] and $[C(P(S)Ph_2)_3]^-$ (1.76) [48], but shorter than in $CH\{P(S)Ph_2\}_3$ (av. 1.88 Å) [31], as expected for the delocalisation in the anion. The $[C(P(S)Ph_2)_3]^-$ ligand remains planar at the central carbon with P(3) 0.073 Å from the plane P(1)-C(1)-P(2). The angles around C(1) are from 117° to 124°, giving a

Table 3.12 Selected Interatomic distances (Å) for $[Ir(CO)_2\{C(P(S)Ph_2)_3\text{-}S,S\}]$

Atoms	Distance	Atoms	Distance
S(1) - Ir(1)	2.348(8)	C(10) - P(1)	1.81(3)
S(2) - Ir(1)	2.370(7)	C(1) - P(2)	1.73(3)
C(3) - Ir(1)	1.81(3)	C(16) - P(2)	1.84(3)
C(2) - Ir(1)	1.77(4)	C(22) - P(2)	1.82(3)
P(1) - S(1)	2.066(11)	C(1) - P(3)	1.81(3)
P(2) - S(2)	2.048(10)	C(28) - P(3)	1.82(3)
P(3) - S(3)	1.969(10)	C(34) - P(3)	1.82(3)
C(1) - P(1)	1.76(3)	C(2) - O(2)	1.22(4)
C(4) - P(1)	1.82(3)	C(3) - O(1)	1.19(4)

Estimated standard deviations are in parentheses.

total of 361°. This data suggests that considerable delocalisation remains within the ligand and the deprotonation of the methine carbon in the ligand.

Table 3.12 Selected Bond Angles (°) for $[Ir(CO)_2\{C(P(S)Ph_2)_3\text{-}S,S\}]$

Atoms	Angles
S(2) - Ir(1) - S(1)	93.4(3)
C(3) - Ir(1) - S(1)	86.7(10)
C(3) - Ir(1) - S(2)	170.9(11)
C(2) - Ir(1) - S(1)	175.5(11)
C(2) - Ir(1) - S(2)	89.4(11)
C(2) - Ir(1) - C(3)	91.2(15)
P(1) - S(1) - Ir(1)	110.8(4)
P(2) - S(2) - Ir(1)	108.6(4)
C(1) - P(1) - S(1)	116.9(11)
C(4) - P(1) - S(1)	108.0(10)
C(4) - P(1) - C(1)	111.8(14)
C(10) - P(1) - S(1)	101.5(11)
C(10) - P(1) - C(1)	113.6(14)
C(10) - P(1) - C(4)	103.9(14)
C(1) - P(2) - S(2)	112.0(12)
C(16) - P(2) - S(2)	100.7(11)
C(16) - P(2) - C(1)	114.9(15)
C(22) - P(2) - S(2)	108.5(9)
C(22) - P(2) - C(1)	115.4(13)
C(22) - P(2) - C(16)	104.1(14)
C(1) - P(3) - S(3)	114.2(10)
C(28) - P(3) - S(3)	107.4(9)
C(28) - P(3) - C(1)	109.2(13)

Atoms	Angles
C(34) - P(3) - S(3)	112.6(9)
C(34) - P(3) - C(1)	108.7(13)
C(34) - P(3) - C(28)	104.2(12)
O(1) - C(3) - Ir(1)	178(3)
O(2) -C(2) - Ir(1)	178(3)
P(2) -C(1) - P(1)	117(2)
P(3) - C(1) - P(1)	119(2)
P(3) - C(1) - P(2)	124(2)

Estimated standard deviations are given in parentheses.

3.6 Conclusion

The new rhodium, iridium and platinum complexes, $[Rh(Cod)\{C(P(S)Ph_2)_3\}]$, $[Ir(Cod)\{C(P(S)Ph_2)_3\}]$, $[Ir(CO)_2\{C(P(S)Ph_2)_3\}]$ and $[Pt(MeoCod)\{C(P(S)Ph_2)_3\}]$ have been synthesised. A study of the coordination chemistry of Pt, Rh and Ir complexes of the deprotonated ligand, $[C(P(S)Ph_2)_3]^-$ has been carried out. The tripodal ligand $[C(P(S)Ph_2)_3]^-$ acts as a 4-electron donor via two sulphur atoms in the formation of metal complexes by adopting an η^2 structure as follows (phenyl groups are omitted for clarity.):

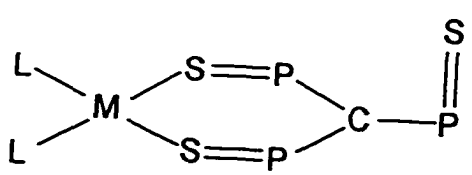

These structures have been confirmed by X-ray studies in the case of [Rh(Cod){C(P(S)Ph_2)$_3$-*S,S*}], [Ir(CO)$_2${-C(P(S)Ph_2)$_3$-*S,S*}] and more recent findings by Grim et al [53] in the case of [Ir(Cod){C(P(S)Ph_2)$_3$-*S,S*}]. The geometry around each metal centre is usually slightly distorted square planar.

The variable temperature ^{31}P NMR studies of [Rh(Cod){C(P(S)Ph_2)$_3$-*S,S*}] and [Pt(MeoCod){C(P(S)Ph_2)$_3$-*S,S*}] show intramolecular exchange between coordinated and uncoordinated Ph_2P=S groups. A dissociative pathway is suggested for the exchange in [Pt(MeoCod){C(P(S)Ph_2)$_3$-*S,S*}] at ambient temperature, as shown in **Scheme 3.5.** Associative pathways involving five-coordinate intermediates were proposed for the exchange processes occurring in [Pt(MeoCod){C(P(S)Ph_2)$_3$}] at higher temperatures, and the exchange in [Rh(Cod){C(P(S)Ph_2)$_3$}], as shown in **Schemes 3.6** and **3.8**.

Chapter Four

Coordination Chemistry of $[C(PPh_2)(P(S)Ph_2)_2]^-$; Rhodium, Iridium, and Platinum Complexes

4.1 Synthesis and Characterisation

Reactions of two mole equivalents of $[CH(PPh_2)(P(S)Ph_2)_2]$ with the chlorobridged complexes, $[M_2Cl_2(Cod)_2]$, M = Rh or Ir, $[Pt_2Cl_4(PEt_3)_2]$, and $[Pt_2Cl_2(MeoCod)_2]$, in the presence of a weak base, diethylamine, results in the cleavage of the chloro bridges and the formation of the neutral complexes, $[M(Cod)\{C(PPh_2)(P(S)Ph_2)_2\text{-}P,S\}]$ (M = Rh or Ir), $[PtCl(PEt_3)\{C(PPh_2)(P(S)Ph_2)_2\text{-}P,S\}]$, and $[Pt(MeoCod)\{C(PPh_2)(P(S)Ph_2)_2\text{-}P,S\}]$. Hydrogen chloride is eliminated and the resulting complexes of the anion $[C(PPh_2)(P(S)Ph_2)_2]^-$ were isolated as air-sensitive crystals in yields ranging from 60% to 80%. With the exception of the colourless appearance of $[Pt(MeoCod)\{C(PPh_2)(P(S)Ph_2)_2\text{-}P,S\}]$, the complexes are generally yellow or orange in colour. The synthesis schemes are shown in **Schemes 4.1, 4.2** and **4.3**, along with the labelling schemes. The complexes were fully characterized by $^{31}P\{^1H\}$ NMR and microanalysis of C and H%. In the case of $[Rh(Cod)\{C(PPh_2)(P(S)Ph_2)_2\text{-}P,S\}]$, a X-ray diffraction study was performed to determine its solid-state structure which shows a η^2 coordination of the ligand through phosphorus and sulphur atoms. The detail of this study will be discussed later in this Chapter.

Scheme 4.1 Synthesis of [M(Cod){C(PPh$_2$)(P(S)Ph$_2$)$_2$-*P*,*S*}] (M = Rh or Ir)

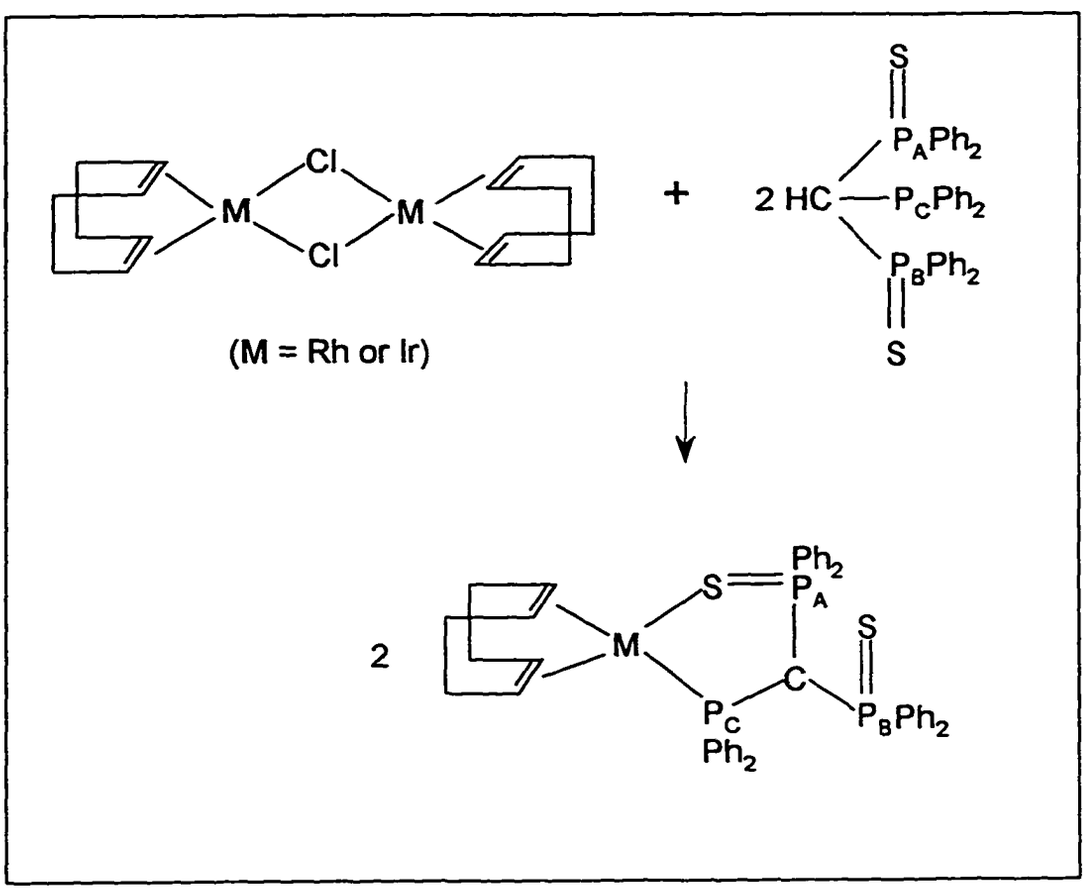

Scheme 4.2 Synthesis of [PtCl(PEt$_3$){C(PPh$_2$)(P(S)Ph$_2$)$_2$-*P*,*S*}]

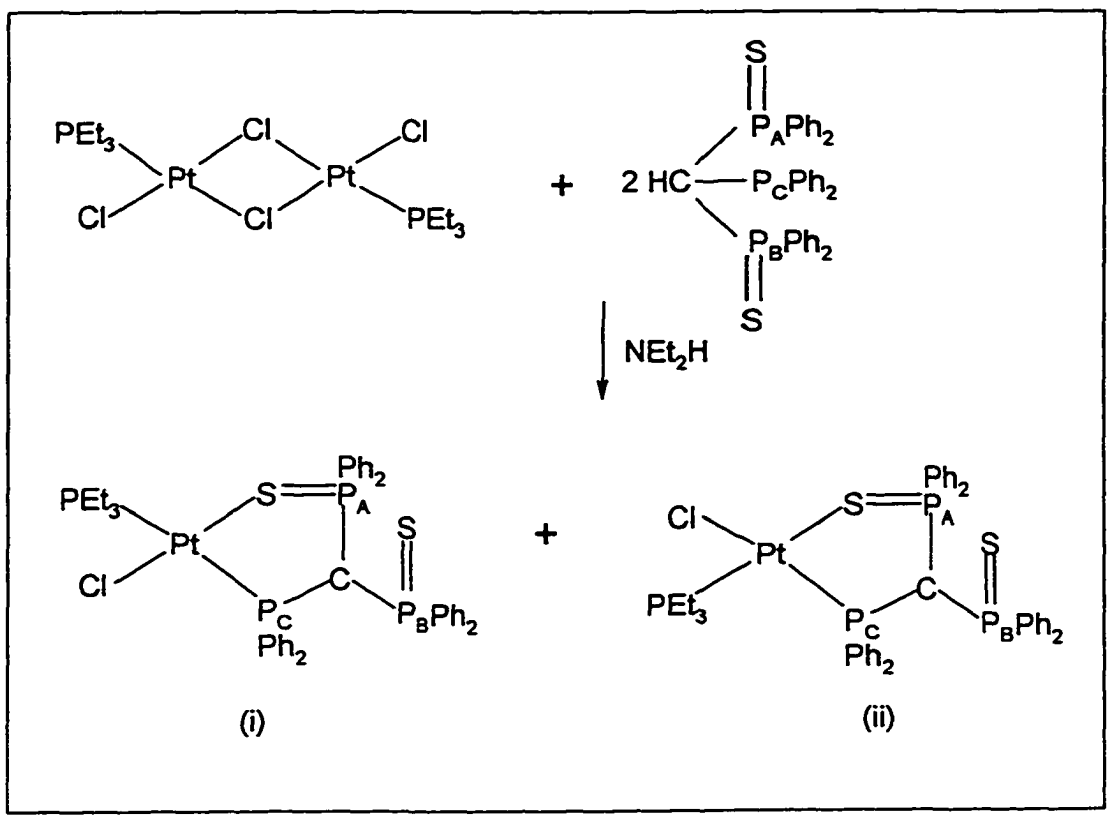

Scheme 4.3 Synthesis of [Pt(MeoCod){C(PPh$_2$)(P(S)Ph$_2$)$_2$-*P,S*}]

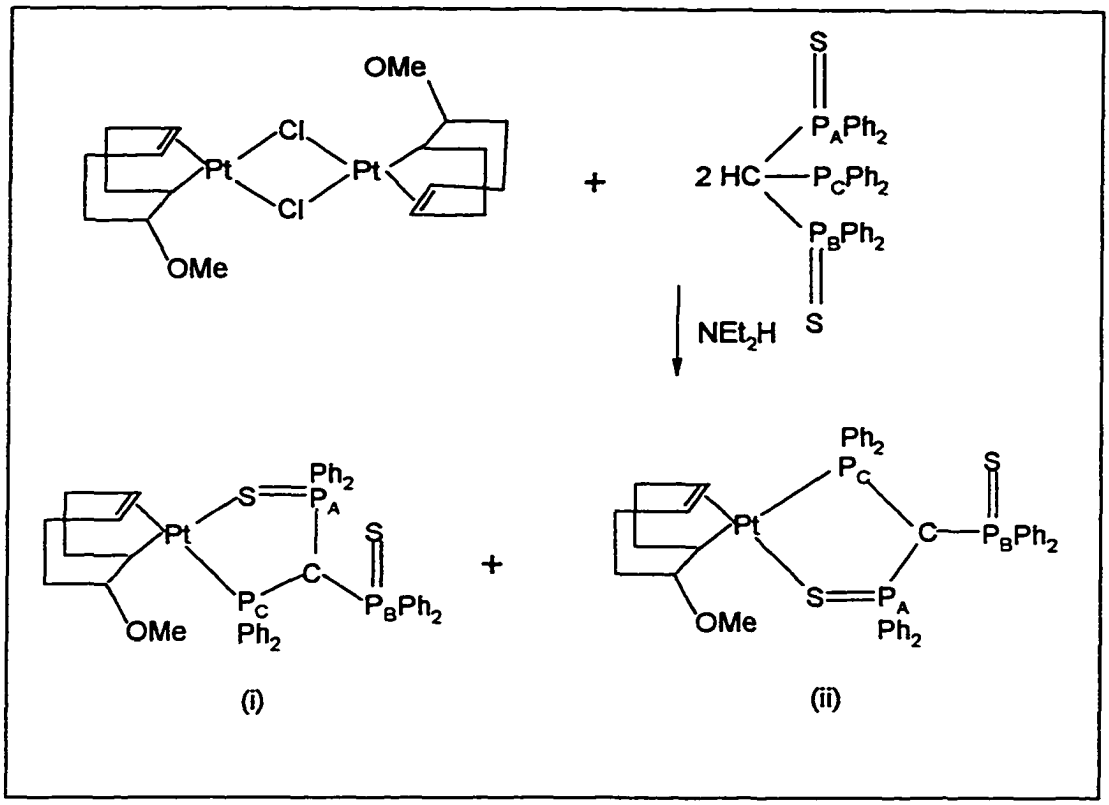

Based on the analysis of the ^{31}P NMR spectra and X-ray studies, all the product complexes contain the ligand bonded in a bidentate fashion with a *P,S* mode of coordination. With a symmetric ligand such as *Cod* as the other ligand, there is only one possible isomer. However, when the other ligand is asymmetric, or when there are two different monodentate ligands coordinated the reaction products can be mixtures of two isomers, as in the cases of [PtCl(PEt$_3$){C(PPh$_2$)(P(S)Ph$_2$)$_2$-*P,S*} where isomer(i) and (ii) occur in about a 10 : 1 ratio, and of [Pt(MeoCod){C(PPh$_2$)(P(S)Ph$_2$)$_2$-*P,S*}] where

isomer(i) and (ii) occur in about 3 : 2 ratio. Separation of those isomers was not possible because of decomposition during recrystallization. When no base is present, reactions often result in mixtures of complexes of the anion and of the neutral ligand, $CH(PPh_2)(P(S)Ph_2)_2$. However, in only a few cases, discussed in details in next Chapter, can such complexes of the neutral ligand be isolated. These are $[Ir(Cod)\{CH(PPh_2)(P(S)Ph_2)_2\text{-}P,S,S\}]BF_4$ and $[MCl(PEt_3)\{CH(PPh_2)(P(S)Ph_2)_2\text{-}P,S\}]BF_4$ (M = Pt, Pd). The fact that complexes of $CH_2(PPh_2)(P(S)Ph_2)$ [63] can be readily prepared by using a strong basic reagent, such as sodium hydride, for removal of the methine proton of the ligand [112, 113], whereas complexes of $CH(P(S)Ph_2)_3$ normally deprotonate during formation, suggest that $CH(PPh_2)(P(S)Ph_2)_2$ may be intermediate in behaviour between $CH_2(PPh_2)(P(S)Ph_2)$ and $CH(P(S)Ph_2)_3$. The other structural difference between complexes of $CH(PPh_2)(P(S)Ph_2)_2$ and $CH_2(PPh_2)(P(S)Ph_2)$ lies in the different coordination modes of the ligands towards the metal centres. As in the case of the complex $[PtCl(PEt_3)\{CH(PPh_2)(P(S)Ph_2)\text{-}C,S\}]$ [63], the $\{CH(PPh_2)(P(S)Ph_2)\}^-$ ligand coordinates through *C,S*. However, there is no evidence for such a coordination mode in any of the complexes of $[C(PPh_2)(P(S)Ph_2)_2]^-$ studied here. This is because the strongly ligating PPh_2 group disfavours formation of the *C,S* bonded mode, as in the case of the complexes of $[CH(PPh_2)(P(S)Ph_2)]^-$. Also steric crowding in the ligand will be substantial if the methine carbon of the ligand binds to the metal centre.

4.2 Reactions of [M(Cod){C(PPh$_2$)(P(S)Ph$_2$)$_2$-*P*,*S*}]

Further reactions of [M(Cod){C(PPh$_2$)(P(S)Ph$_2$)$_2$-*P*,*S*}] (M = Rh, Ir) were investigated. The oxidative additions of iodomethane, iodine, and benzyl bromide were studied. However, the results were inconclusive, either because of incomplete partial reactions, or because complicated mixtures of isomers were obtained. Naturally, oxidative addition reactions for this type of complex are of some interest. The site of reaction may not only be at the metal centre but also at the methine carbon of the phosphine chalcogenide ligand [114]. When an excess of tertiarybutylisocyanide was added to [M(Cod){C(PPh$_2$)(P(S)Ph$_2$)$_2$-*P*,*S*}], a substitution reaction occurred, producing [M(^{t}BuNC)$_2${C(PPh$_2$)(P(S)Ph$_2$)$_2$-*P*,*S*}], as illustrated in **Scheme 4.4**. The complexes were characterised by ^{31}P{^{1}H} NMR, microanalysis, and infrared, which showed a strong CN absorption at around 2100 cm^{-1} in each case. Unfortunately, the microanalysis data for the iridium complex were in poor agreement with the expected values. This may have been because the complex was difficult to crystallise and thus some solvent may have been present in the crystals.

Scheme 4.4 Reactions of [M(Cod){C(PPh$_2$)(P(S)Ph$_2$)$_2$-*P*,*S*}] with Tertiarybutylisocyanide

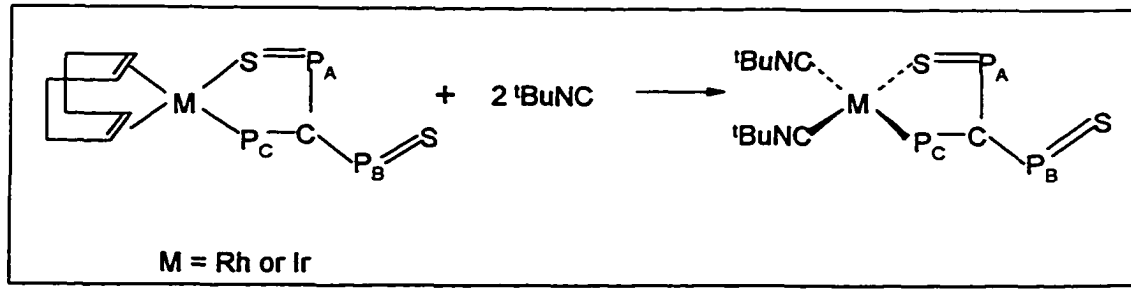

The oxidative additions of benzyl bromide and iodine to $[M(^tBuNC)_2\{C(PPh_2)(P(S)Ph_2)_2\text{-}P,S\}]$ were studied. The products were characterised by ^{31}P NMR and microanalysis. In the case of $[Rh(^tBuNC)_2\{C(PPh_2)(P(S)Ph_2)_2\text{-}P,S\}I_2]$ a solid state structure was determined by X-ray diffraction.

Oxidative addition of iodine or benzyl bromide to $[Rh(^tBuNC)_2\{C(PPh_2)(P(S)Ph_2)_2\text{-}P,S\}]$ gave more conclusive results than was the case with the iridium analogue. When iodine was added to $[M(^tBuNC)_2\{C(PPh_2)(P(S)Ph_2)_2\text{-}P,S\}]$ at -60 °C a kinetically preferred product was initially formed. Five minutes later the ^{31}P NMR showed at least three different isomers but overlap of their NMR signals prevented reliable assignments. Four hours later a stable mixture of two isomers was obtained. One of these two isomers has been determined to have the following structure by X-ray analysis:

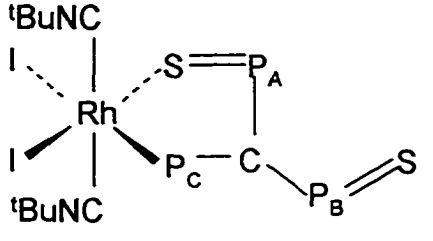

The other isomer, labelled as *isomer ii* in **Table 4.1**, is most likely a *cis*-isomer which has the structure of either isomer III or IV, shown in **Scheme 4.6** later in the conclusion part of this Chapter, since the $^1J(Rh\text{-}P_c)$ is very similar to the value in the above structure. This would not be expected with a change in the *trans* ligand from iodide to ^{t}BuNC.

The atom labelling schemes are collected in **Schemes 4.1, 4.2, 4.3, 4.4, 4.5,** and **4.6** where the compounds and their structures were labelled individually. The $^{31}P\{^{1}H\}$ nuclear magnetic resonance parameters for the complexes are listed in **Table 4.1** All the $^{31}P\{^{1}H\}$ spectra are simple first order patterns with three resonances for the phosphine chalcogenide ligand, $[C(PPh_2)(P(S)Ph_2)_2]^-$. The assignments of the ^{31}P parameters for all the complexes were based on that of $[Rh(Cod)\{C(PPh_2)(P(S)Ph_2)_2\text{-}P,S\}]$. However, the assignments of chemical shifts presents some problems. In this case, the highest field resonance at 39.5 ppm, a doublet (134 Hz) of doublets (115 Hz) of doublets (20 Hz), can be easily assigned to P_C because of its largest coupling constant (134 Hz) arising from $^{1}J(Rh\text{-}P_C)$. Assignments of the two remaining resonances, a doublet (115 Hz) of doublets (46 Hz) at 56.0 ppm and a doublet (46 Hz) of doublets (20 Hz) of doublets (11 Hz) at 42.3 ppm seemed to be initially straight forward. Assuming $^{2}J(Rh\text{-}P_A) > {}^{3}J(Rh\text{-}P_B)$, which is reasonable based on the relation between the coupling strength and bond distances, will, of course, place P_A at 42.3 and P_B at 56.0 ppm. Unfortunately, this assumption leads to a number of inconsistencies in other assignments and with literature comparisons [66]. One of these major inconsistencies is the chemical shift of P_B. Because P_B represents the non-coordinated P=S group, it should be relatively little affected by changes in the metal and associated ligands [66]. Examining **Table 4.1**, it is clear that a relatively constant chemical shift of around 40 ppm should be expected for P_A in the case of $[Rh(Cod)\{C(PPh_2)(P(S)Ph_2)_2\text{-}P,S\}]$ had the assumption of $^{2}J(Rh\text{-}P_A) > {}^{3}J(Rh\text{-}P_B)$ been used. We therefore prefer to assign the resonances around 40 ppm to P_B and the lower field resonances to P_A. In the case of $[Rh(Cod)\{C(PPh_2)(P(S)Ph_2)_2\text{-}P,S\}]$, P_A should thus

be 56.0 ppm and P_B should be 42.3 ppm. This assignment makes ^2J(Rh- P_A) > ^3J(Rh-P_B) which is not uncommon in heteronuclear coupling situations by any means. A number of other comparisons support this assignment even though some ambiguity must remain.

1. The $\delta(P_B)$ values are very similar to those for the P=S groups in the free ligand where they are "dangling". The examples are 40.4 ppm for $CH_2(PPh_2)(P(S)Ph_2)$ [112, 115], 43.5 ppm for $CH(PPh_2)(P(S)Ph_2)_2$, and 41.9 ppm for $CH(P(S)Ph_2)_3$ [45,115]. The $\delta(P_B)$ values around 40 ppm are also very close to those of the non-coordinated P=S groups found in [$PtCl(PEt_3)\{C(P(S)Ph_2)_3$-*S,S*}] which is 42.3 ppm [116], and [$Rh(Cod)\{C(P(S)Ph_2)_3\}$-*S,S*] which is also 42.3 ppm [117], but markedly different from the shift of coordinated P=S in [$Rh(Cod)\{CH(PPh_2)(P(S)Ph_2)_2$-*P,S*}] which is 54.2 ppm [113,115]. All these comparisons suggest that $\delta(P_B)$ of the non-coordinated P=S group of all the complexes discussed in this chapter should indeed be around 40 ppm.

2. The $\delta(P_A)$ and $^2J(P_A$-$P_C)$ values assigned to [$Rh(Cod)\{C(PPh_2)(P(S)Ph_2)_2$-*P,S*}] (56.0 ppm, 115 Hz) are comparable to those found in [$Rh(Cod)\{CH(PPh_2)(P(S)Ph_2)$-*P,S*}] (54.2 ppm, 121 Hz) which adopts a similar structure. [113,115]. Similar comparisons can also be made in regard to [$PtCl(PEt_3)\{C(PPh_2)(P(S)Ph_2)_2$-*P,S*}], where $\delta(P_A)$ and $^2J(P_A$-$P_C)$ values are 53.2 ppm and 76 Hz respectively for isomer (i) and 62.8 ppm and 110 Hz for isomer (ii), and [$PtCl(PEt_3)\{CH(PPh_2)(P(S)Ph_2)$-*P,S*}] where $\delta(P_A)$ and $^2J(P_A$-$P_C)$ for the *cis* isomer are 45.5 ppm and 81 Hz and 58.7 ppm and 117 Hz for the *trans* isomer [112, 115].

3. With reference to the relative magnitude of ^2J(M-P) and ^3J(M-P), we note that ^2J(Rh-P) was too small to resolve and ^3J(Rh-P) is 11 Hz in

[Rh(Cod){C(PPh_2)($P(S)Ph_2$)$_2$-*P,S*}] and related complexes [113,115]. Moreover, the J(Pt-P_A) values assigned to [PtCl(PEt_3){C(PPh_2)($P(S)Ph_2$)$_2$-*P,S*}] (27 and 78 Hz, **Table 4.1**) are comparable to the known values of ^2J(Pt-P) in the isomers of [PtCl(PEt_3){CH(PPh_2)($P(S)Ph_2$)-*P,S*}] (42 and 50 Hz) [112, 115] which are smaller than the J(Pt-P_B) values (225 and 197 Hz). This indicates that the two-bond coupling between platinum and phosphorus is ^2J(Pt-P_A), which therefore reinforces the assignments of P_A and P_B in **Table 4.1** as the correct ones, which assumes that ^2J(M-P) < ^3J(M-P)

The ^{31}P spectra for the platinum complexes are somewhat complicated by the ^{195}Pt sidebands due to its 33.8% abundance. The ^{31}P NMR data for the complexes are summarised in **Tables 4.2** and **4.3**. The simple first order ^{195}Pt spectra of those complexes provide great help in confirming the ^{31}P NMR assignments. The ^{195}Pt NMR spectrum of [PtCl(PEt_3){C(PPh_2)($P(S)Ph_2$)$_2$-*P,S*}] exhibits a total of sixteen lines corresponding to a doublet of doublets of doublets of doublets. The ^{195}Pt NMR spectrum of [Pt(MeoCod){C(PPh_2)($P(S)Ph_2$)$_2$-*P,S*}] shows a total of eight lines corresponding to a doublet of doublets of doublets. The ^{195}Pt NMR parameters are summarised in **Table 4.3**. The major assumption of the assignments of the ^{195}Pt parameters here is based on the *trans influence* which presumes that the smaller ^1J(Pt-P) couplings are *trans* to the Pt-P bond in [PtCl(PEt_3){C(PPh_2)($P(S)Ph_2$)$_2$-*P,S*}] and to the Pt- C_6 bond in [Pt(MeoCod){C(PPh_2)($P(S)Ph_2$)$_2$-*P,S*}] respectively.

Table 4.1 ^{31}P NMR Parameters for Rhodium and Iridium Complexes of $[C(P_CPh_2)(P_{A,B}(S)Ph)_2]^-$

Compound[a]	Isomer	$\delta(P_A)$	$\delta(P_B)$	$\delta(P_C)$	$J(P_A\text{-}P_B)$	$J(P_A\text{-}P_C)$	$J(P_B\text{-}P_C)$	$J(M\text{-}P_A)$	$J(M\text{-}P_B)$	$J(M\text{-}P_C)$
Rh(Cod)L		56	42.3	39.5	46	115	20	nr[b]	11	134
Ir(Cod)L		65.6	41.7	36.3	47	112	15			
Rh(^{t}BuNC)$_2$L		63.7	41.8	50.8	44	132	16		10	115
Ir(^{t}BuNC)$_2$L		64.5	44.6	48.0	37	110	11			
RhI$_2$(^{t}BuNC)$_2$L	i	67.1	39.6	52.2	33	87	11	nr	7	92
RhI$_2$(^{t}BuNC)$_2$L	ii	65.3	37.1	51.0	27	87	nr	nr	nr	91
RhBrBz(^{t}BuNC)$_2$L	i	60.5	39.6	51.7	29	103	nr	nr	nr	93
RhBrBz(^{t}BuNC)$_2$L	ii	65.1	41.0	52.3	32	92	nr	nr	nr	96

Chemical shifts (δ) are quoted in parts per million relative to 85% H_3PO_4. Coupling constants (J) are in Hz.

Notes: a. L represents the ligand, $[C(PPh_2)(P(S)Ph_2)_2]^-$

b. nr = not resolvable

Table 4.2 ^{31}P **NMR Parameters for** $[Pt(Cl)(P_DEt_3)\{C(P_CPh_2)(P_{A,B}(S)Ph_2)_2\}]$

Compound	δP_A	δP_B	δP_C	δP_D	$J(P_A\text{-}P_B)$	$J(P_A\text{-}P_C)$	$J(P_A\text{-}P_D)$	$J(P_B\text{-}P_C)$	$J(P_B\text{-}P_D)$	$J(P_C\text{-}P_D)$	$J(Pt\text{-}P_D)$
isomer (i)	53.2	40.3	24.5	8.3	26	76	6	nr[a]	nr	10	3218
isomer (ii)	62.8	43.2	34.6	15.3	43	110	43	nr	12	423	2396

Table 4.3 ^{195}Pt **NMR Parameters for Platinum Complexes of** $[C(P_CPh_2)(P_{A,B}(S)Ph_2)_2]$

Compound	$\delta(Pt)$	$J(Pt\text{-}P_A)$	$J(Pt\text{-}P_B)$	$J(Pt\text{-}P_C)$	$J(Pt\text{-}P_D)$
$[Pt(Cl)(P_DEt_3)\{C(P_CPh_2)(P_{A,B}(S)Ph_2)_2\}]$ isomer (i)	-9.1	27	225	3623	3221
$[Pt(Cl)(P_DEt_3)\{C(P_CPh_2)(P_{A,B}(S)Ph_2)_2\}]$ isomer (ii)	62.0	78	197	2200	2396
$[Pt(MeoCod)\{C(P_CPh_2)(P_{A,B}(S)Ph_2)_2\}]$ isomer (i)	208.6	56	245	3834	NA[b]

Chemical shifts (δ) are quoted in parts per million relative to 85% H_3PO_4. Coupling constants (J) are in Hz.

Notes: a. nr = not resolvable

b. NA = not available

4.3 Solid-State Structure of [Rh(Cod){C(PPh$_2$)(P(S)Ph$_2$)-*P*,*S*}]·CH$_2$Cl$_2$

[Rh(Cod){CH(PPh$_2$)(P(S)Ph$_2$)-*P*,*S*}]·CH$_2$Cl$_2$ was prepared as described in the experimental section aof Chapter Seven and crystals suitable for study by X-ray diffraction were grown by vapour diffusion of hexanes into solutions of the complex in dichloromethane. The crystallographic techniques employed are described in detail in Chapter Seven and Appendix. Selected crystallographic data are listed in **Table 4.4**. The metal atoms and all phosphorus, sulphur, and chlorine atoms were treated anisotropically, as was the central carbon atom, C(1), of the P,S ligand in [C(P$_C$Ph$_2$)(P$_{A,B}$(S)Ph$_2$)$_2$]$^-$ and the carbons of the Cod ligand, C(38-46). All other atoms were refined isotropically. Hydrogen atoms were not located and are not included in the refinements. The final difference maps had minima/maxima of -0.65/0.75 and -1.1/0.88 Å^{-3} respectively, with no indication that any material had been overlooked.

The structure of a single molecule of [Rh(Cod){CH(PPh$_2$)(P(S)Ph$_2$)-*P*,*S*}]·CH$_2$Cl$_2$ is shown as an ORTEP diagram in **Figure 4.1**, along with the atomic labelling scheme. The unit cell and other parameters related to the crystal structure determinations are given in **Table 4.4**. Fractional atomic coordinates and isotropic temperature parameters are in **Appendix Table X**, anisotropic temperature parameters in **Appendix Table XI**. The most important bond lengths and bond angles are collected in **Tables 4.5** and **4.6** respectively.

Table 4.4 Crystallographic Data for [Rh(Cod){C(PPh$_2$)(P(S)Ph$_2$)-*P,S*}]·CH$_2$Cl$_2$ (A) and [RhI$_2$(^{t}BuNC)$_2$ {C(PPh$_2$)(P(S)Ph$_2$)-*P,S*}] (B)

Complex	(A)	(B)
formula	$C_{46}H_{44}Cl_2P_3S_2Rh$	$C_{47}H_{48}I_2N_2P_3S_2Rh$
fw	927.7	1154.7
space group	$P2_1/c$(No 14)	$P42_1/c$(No114)
a, Å	12.294(3)	30.174(3)
b, Å	16.063(5)	30.174(3)
c, Å	21.384(5)	11.317(2)
α, deg	90	90
β, deg	91.60(3)	90
γ, deg	90	90
V, Å^3	4221	10304
Z	4	8
diffractometer	Picker 4-circle	Enraf-Nonius CAD4
radiation (λ, Å)	Mo Kα (0.71069)	Cu Kα (1.542)
μ, cm^{-1}	6.89	17.38
transm factor range	0.90 - 0.93	
temperature, K	295	295
no of observed reflections (I>3.0σ(I))	2915	1369
parameters refined	307	167
R	0.087	0.084
R_w	0.094	0.095

$w = 1/(\sigma^2(F) + 0.001F^2)$; $\Delta = \| F_o| - |F_c \|$. $R = (\Sigma\Delta/\Sigma F_o)$; $R_w = (\Sigma w\, \Delta^2/\Sigma w\, F_o^2)^{1/2}$

Figure 4.1 ORTEP Plot for a Single Molecule of

$[Rh(Cod)\{C(PPh_2)(P(S)Ph_2)_2$-*P*,*S*$\}]\cdot CH_2Cl_2$

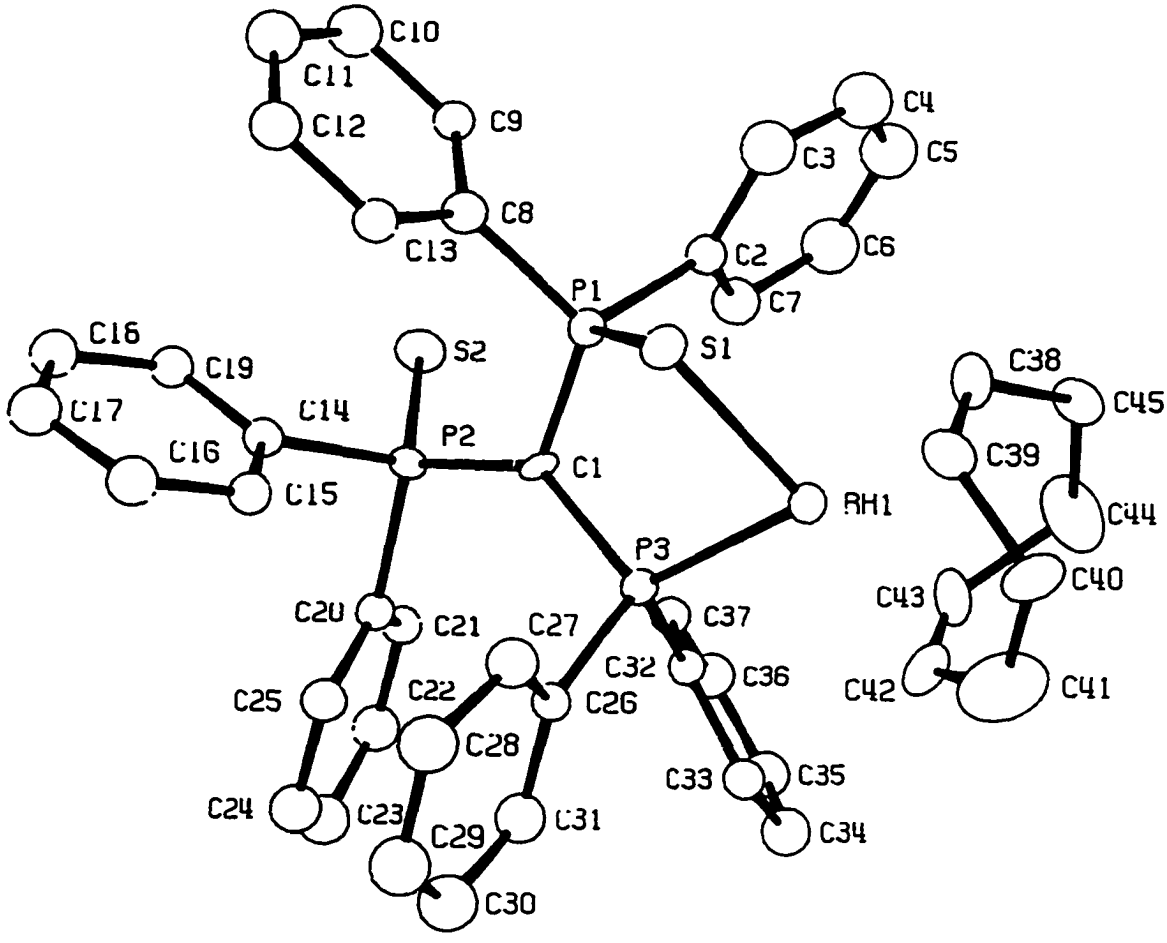

The structure shows an approximately square planar rhodium centre with $[C(PPh_2)(P(S)Ph_2)_2]^-$ coordinated in a bidentate fashion through phosphorus and one sulphur atom. The second sulphur atom is non-coordinated ("dangling") and lies over 6 Å away from the rhodium. The *Cod* ligand is coordinated via its two double bonds to the rhodium centre. There are relatively small distortions of the square plane. Angles at the metal centre are close to 90°, ranging from 87 to 95°, with S(1)-Rh(1)-P(3) at 88.3°. This angle is slightly smaller than those observed in $[Rh(Cod)\{C(P(S)Ph_2)_3\}]$ (S-Rh-S, 93.4°)

of Chapter Three [68] and [Rh(Cod){C(P(O)Ph_2)$_2$(P(S)Ph_2)}] (S-Rh-O, 95.7°) [102]. All ligating atoms with the metal centre are within 0.04 Å of the least squares plane. The bond distance between the rhodium centre and the coordinated sulphur is 2.36 Å, similar to the Rh-S bond length in [Rh(Cod){C(P(S)Ph_2)$_3$}], discussed in Chapter Three (Rh-S, 2.36 Å and 2.34 Å) [68]. The rhodium-phosphorus bond distance is 2.34 Å.

The P-S bonds lengthen upon coordination of the ligand, [C(PPh_2)(P(S)Ph_2)$_2$]$^-$ to the rhodium centre, as observed here, from 1.97 Å for the non-coordinated sulphur atom, to 2.03 Å for the coordinated sulphur atom, as expected.

The geometry at the methine carbon (C1) is closer to a distorted trigonal planar geometry than tetrahedral geometry. This strongly suggests the carbon atom is indeed deprotonated. The P-C-P bond angles are in the range 111° - 133°. The large value of P(2)-C(1)-P(3) (133°) is most likely due to steric crowding. The geometry around C(1) is almost planar with C(1) lying only 0.014 Å out of the P(1-3) plane. The Rh-Cod bonding is normal and comparable to extensive investigations previously reported [107,108].

Table 4.5 Selected Interatomic Bond Distances (Å) in

[Rh(Cod){C(PPh$_2$)(P(S)Ph$_2$)-*P*,*S*}]·CH$_2$Cl$_2$

Atoms	Distance
Rh(1)-C(*x*)	2.05
Rh(1)-C(*y*)	2.11
Rh(1)-S(1)	2.361(4)
Rh(1)-P(3)	2.336(4)
Rh(1)-C(38)	2.21(2)
Rh(1)-C(39)	2.23(2)
Rh(1)-C(42)	2.15(2)
Rh(1)-C(43)	2.16(2)
S(1)-P(1)	2.032(6)
S(2)-P(2)	1.971(6)
P(1)-C(1)	1.74(2)
P(1)-C(2)	1.80(2)
P(1)-C(8)	1.81(2)
P(2)-C(1)	1.76(1)
P(2)-C(14)	1.85(2)
P(2)-C(20)	1.85(2)
P(3)-C(1)	1.77(1)
P(3)-C(26)	1.84(2)
P(3)-C(32)	1.83(2)

C(*x*) and C(*y*) are the respective midpoints of the C(42)-C(43) and C(38)-C(39) double bonds. Estimated standard deviations are given in parentheses.

Table 4.6 Selected Bond Angles (°) in [Rh(Cod){C(PPh$_2$)(P(S)Ph$_2$)-*P,S*}]·CH$_2$Cl$_2$

Atoms	Angle
C(*x*)-Rh(1)-C(*y*)	87.1
C(*x*)-Rh(1)-P(3)	95.4
C(*y*)-Rh(1)-S(1)	89.1
S(1)-Rh(1)-P(3)	88.3(1)
Ph(1)-S(1)-P(1)	92.6(2)
S(1)-P(1)-C(1)	110.7(5)
Rh(1)-P(3)-C(1)	108.7(5)
P(1)-C(1)-P(2)	116.9(8)
P(1)-C(1)-P(3)	110.4(8)
P(2)-C(1)-P(3)	132.7(9)

C(*x*) and C(*y*) are the respective midpoints of the C(42)-C(43) and C(38)-C(39) double bonds. Estimated standard deviations are given in the parentheses.

4.4 Solid-State Structure of [RhI$_2$(^{t}BuNC)$_2${C(PPh$_2$)(P(S)Ph$_2$)$_2$}]

[RhI$_2$(^{t}BuNC)$_2${CH(PPh$_2$)(P(S)Ph$_2$)-*P,S*}]was prepared as described in the experimental section of Chapter Seven and crystals suitable for study by X-ray diffraction were grown by vapour diffusion of hexanes into solutions of the complex in dichloromethane. The crystallographic techniques employed are described in detail in

Chapter Seven and Appendix. Selected crystallographic data are listed in **Table 4.4**. The metal atoms, and all phosphorus, sulphur, and iodine atoms were treated anisotropically, as was the central carbon atom, C(1), of the ligand, $[C(P_CPh_2)(P_{A,B}(S)Ph_2)_2]^-$. The six phenyl groups were refined as rigid hexagons each with different group temperature factors, which are included in the refinement

The structure of a single molecule of $[RhI_2(^t\text{-BuNC})_2\{C(PPh_2)(P(S)Ph_2)_2\}]$ is shown as an ORTEP diagram in **Figure 4.2**, along with the atomic labelling scheme. The unit cell and all other parameters related to the crystal structure determination are listed in **Table 4.4**. Fractional atomic coordinates and isotropic temperature parameters are give in **Appendix Table XII**, anisotropic temperature parameters in **Appendix Table XIII**. The most significant bond lengths and bond angles are collected in **Table 4.7** and **4.8** respectively.

The structure shows approximately octahedral geometry at the metal centre with $[C(PPh_2)(P(S)Ph_2)_2]^-$ occupying two of the square planar sites in a bidentate fashion through one phosphorus and one sulphur atom. Two iodide ligands occupy the remaining square planar sites. Octahedral coordination is completed by two tert-butylisocyanide ligands in the axial positions. There is slight distortion from octahedral geometry. All atoms forming the equatorial square plane are within 0.03Å of the least squares plane. The inter bond angles inside the equatorial plane range from 87° to 93°. The interbond angles within the octahedron are all in the range 86° to 95°.

The comparison of bond angles and bond lengths of this complex with other known

Figure 4.2 ORTEP Plot for a Single Molecule of

$[RhI_2(^t\text{-BuNC})_2\{C(PPh_2)(P(S)Ph_2)_2\}]$

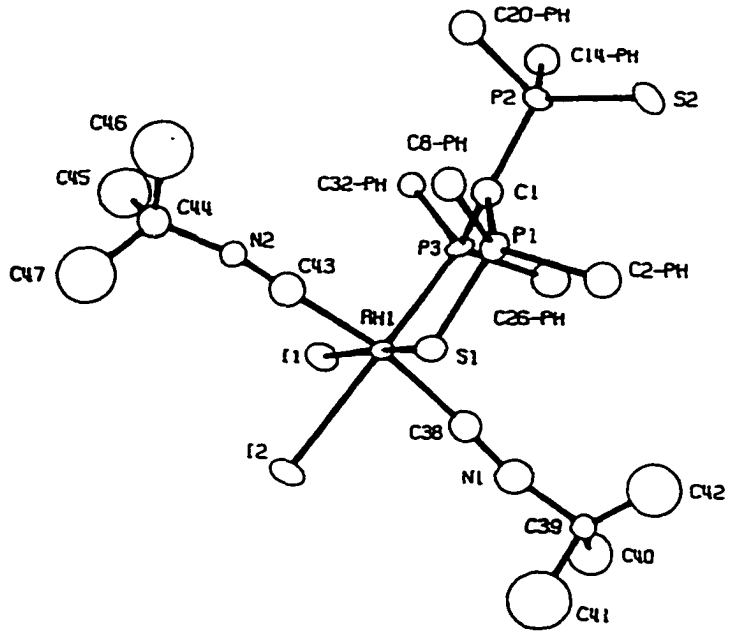

complexes of P,S ligand systems shows very similar values. The non-coordinated P=S bond length is 1.97 Å and the coordinated P=S bond length is 2.00 Å. This slight bond lengthening was also seen in $[Rh(Cod)\{C(P(S)Ph_2)_3\}]$ of Chapter Three [68] and $[Rh(Cod)\{C(PPh_2)(P(S)Ph_2)_2\}]$ [65] discussed earlier in this Chapter. The rhodium-sulphur bond length is 2.35Å, similar to Rh-S in $[Rh(Cod)\{C(P(S)Ph_2)_3\}]$ (Rh-S, 2.34 Å and 2.36 Å) [68] and $[Rh(Cod)\{C(PPh_2)(P(S)Ph_2)_2\}]$ (Rh-S, 2.36 Å) [61]. The rhodium-phosphorus bond length is 2.36Å, similar to Rh-P in $[Rh(Cod)\{C(PPh_2)(P(S)Ph_2)_2\}]$ (Rh-P, 2.34 Å) [65]. The P-Rh-S bond angle is 89.4°, comparable to those observed in $[Rh(Cod)\{C(P(S)Ph_2)_3\}]$, discussed in Chapter Three (S-Rh-S, 93.4°) [68] and $[Rh(Cod)\{C(PPh_2)(P(S)Ph_2)_2\}]$ (S-Rh-P, 88.3°) [65].

Table 4.7 Selected Interatomic Distances (Å) in $[RhI_2(^tBuNC)_2\{C(PPh_2)(P(S)Ph_2)_2\}]$

Atoms	Distance
Rh(1)-I(1)	2.668(5)
Rh(1)-I(2)	2.749(6)
Rh(1)-S(1)	2.354(14)
Rh(1)-P(3)	2.345(15)
Rh(1)-C(38)	2.06(7)
Rh(1)-C(43)	1.89(7)
S(1)-P(1)	2.00(2)
S(2)-P(2)	1.97(2)
P(1)-C(1)	1.73(6)
P(1)-C(2)	1.85(3)
P(1)-C(8)	1.87(3)
P(2)-C(1)	1.79(6)
P(2)-C(14)	1.91(3)
P(2)-C(20)	1.82(3)
P(3)-C(1)	1.82(6)
P(3)-C(26)	1.90(4)
P(3)-C(32)	1.83(3)
N(1)-C(38)	1.16(7)
N(1)-C(39)	1.44(7)
N(2)-C(43)	1.23(7)
N(2)-C(44)	1.42(6)

C(x) and C(y) are the respective midpoints of the C(42)-C(43) and C(38)-C(39) double bonds. Estimated standard deviations are given in parentheses.

Table 4.8 Selected Bond Angles (°) for $[RhI_2(^tBuNC)_2\{C(PPh_2)(P(S)Ph_2)_2\}$

Atoms	Angle
I(1)-Rh(1)-I(2)	90.9(2)
I(1)-Rh(1)-P(3)	92.9(4)
I(1)-Rh(1)-C(38)	95(2)
I(1)-Rh(1)-C(43)	86(2)
I(2)-Rh(1)-S(1)	86.8(4)
I(2)-Rh(1)-C(38)	86(2)
I(2)-Rh(1)-C(43)	88(2)
S(1)-Rh(1)-P(3)	89.4(5)
S(1)-Rh(1)-C(38)	86(2)
S(1)-Rh(1)-C(43)	93(2)
P(3)-Rh(1)-C(38)	95(2)
P(3)-Rh(1)-C(43)	92(2)
Rh(1)-S(1)-P(1)	107.5(8)
S(1)-P(1)-C(1)	112(2)
Rh(1)-P(3)-C(1)	110(2)
C(38)-N(1)-C(39)	165(6)
C(43)-N(2)-C(44)	168(5)
P(1)-C(1)-P(2)	119(3)
P(1)-C(1)-P(3)	115(3)
P(2)-C(1)-P(3)	124(3)

C(*x*) and C(*y*) are the respective midpoints of the C(42)-C(43) and C(38)-C(39) double bonds. Estimated standard deviations are given in the parentheses.

4.5 Conclusion

The novel rhodium, iridium and platinum complexes of anionic ligand $[M(Cod)\{C(PPh_2)(P(S)Ph_2)_2\}]$ (M = Rh, Ir), $[PtCl(PEt_3)\{C(PPh_2)(P(S)Ph_2)_2\}]$ and $[Pt(MeoCod)\{C(PPh_2)(P(S)Ph_2)_2\}]$ have been synthesised. The study of coordination of Pt, Rh, and Ir complexes of the deprotonated $[C(PPh_2)(P(S)Ph_2)_2]^-$ have been carried out. The tripodal ligand $[C(PPh_2)(P(S)Ph_2)_2]^-$ acted as a bidentate ligand coordinating via one sulphur atom and one phosphorus atom in the formation of metal complexes by adopting an η^2 structures as follows (phenyl groups are omitted for clarity).

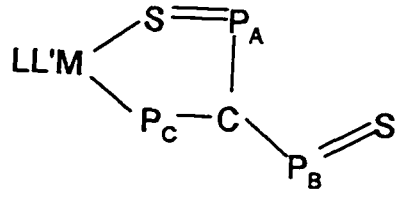

LL' represents other ligands such as *Cod*, Cl/PEt_3, MeoCod. A study of the reactivity of $[Rh(cod)\{C(PPh_2)(P(S)Ph_2)_2$-*P,S*$\}]$ was carried out. **Scheme 4.4** summarises the results of the study.

Reaction of $[Rh(cod)\{C(PPh_2)(P(S)Ph_2)_2$-*P,S*$\}]$ with t-BuNC results in a simple substitution of the cod ligand and the formation of $[Rh(^tBuNC)_2\{C(PPh_2)(P(S)Ph_2)_2$-*P,S*$\}]$. The oxidative addition of I_2 or benzyl bromide to the new complex gave isomeric mixtures of $[RhI_2(^tBuNC)_2\{C(PPh_2)(P(S)Ph_2)_2$-*P,S*$\}]$ and $[RhBr(Bz)(^tBuNC)_2\{C(PPh_2)(P(S)Ph_2)_2$-*P,S* $\}]$. The complexes were characterised primarily by ^{31}P nuclear magnetic resonance studies and by two crystal structure

determinations of $[Rh(cod)\{C(PPh_2)(P(S)Ph_2)_2\text{-}P,S\}]\cdot CH_2Cl_2$ and $[RhI_2(^tBuNC)_2\{C(PPh_2)(P(S)Ph_2)_2\text{-}P,S\}]$. **Scheme 4.5** illustrates the oxidative addition reactions mentioned above.

Scheme 4.5 Oxidative Addition Reactions of $[M(^tBuNC)_2\{C(PPh_2)(P(S)Ph_2)_2\text{-}P,S\}]$

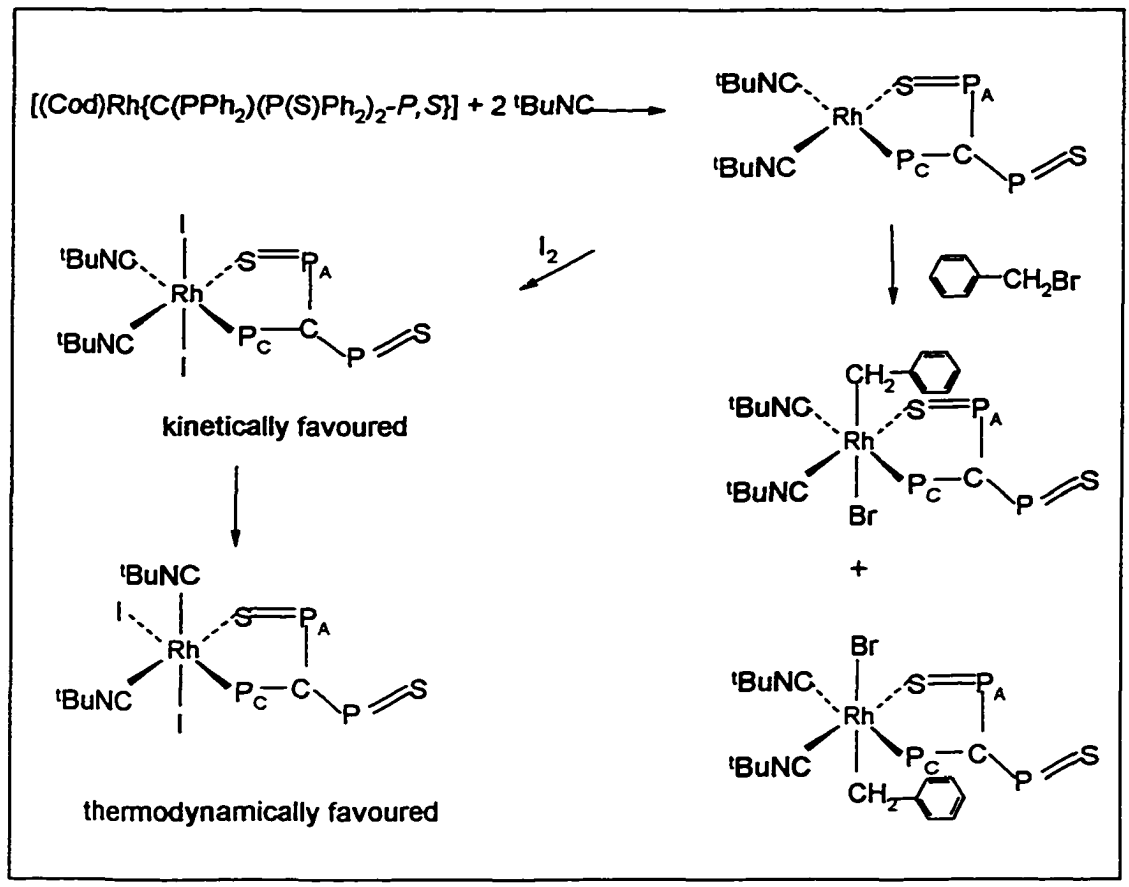

When iodine was added to [Rh(^{t}BuNC)$_2${C(PPh$_2$)(P(S)Ph$_2$)$_2$-*P,S*}] at -60 °C a kinetically preferred product was initially formed. Five minutes later the ^{31}P NMR showed at least three different isomers but overlap of their NMR signals prevented reliable assignments. Four hours later a stable mixture of two isomers was obtained.The other isomer, labelled as *isomer ii* in **Table 4.1**, is most likely a *cis*-isomer which has the structure of either isomer III or IV, since the ^1J(Rh-P$_c$) is very similar to the value in the above structure. This would not be expected with a change in the *trans* ligand fron iodide to ^{t}BuNC. From the analysis of ^{31}P NMR data and X-ray diffraction results obtained for one of the isomer, **Scheme 4.6** summarises the oxidative addition of iodine to [Rh(^{t}BuNC)$_2${C(PPh$_2$)(P(S)Ph$_2$)$_2$-*P,S*}]

However, asymmetrical oxidative addition of a reagent such as benzyl bromide to this complex is potentially far more complicated than for the symmetrical case. The addition of benzyl bromide to [Rh(^{t}-BuNC)$_2${C(PPh$_2$)(P(S)Ph$_2$)$_2$-*P,S*}] gave two isomers. The ^{31}P NMR parameters of these products are very similar to those obtained for the isomers observed for the I_2 addition. We can therefore be quite confident that these two products are analogous to the two thermodynamically preferred isomers for the I_2 addition i.e. the two *cis*-isomers shown in **Scheme 4.6**. However it is impossible to make definite structural assignments here. The possible isomers are outlined in **Scheme 4.7**.

In [Rh(cod){C(PPh$_2$)(P(S)Ph$_2$)$_2$-*P,S*}], approximate square coordination about rhodium is observed. In [RhI$_2$(^{t}BuNC)$_2$ {C(PPh$_2$)(P(S)Ph$_2$)$_2$-*P,S*}] the P,S ligand and two *cis* iodides comprise the equatorial plane of an octahedral centre which is completed by two ^{t}BuNC ligands.

Scheme 4.6 Oxidative Addition of Iodine to [Rh(^{t}BuNC)$_2${C(PPh$_2$)(P(S)Ph$_2$)$_2$-*P,S*}]

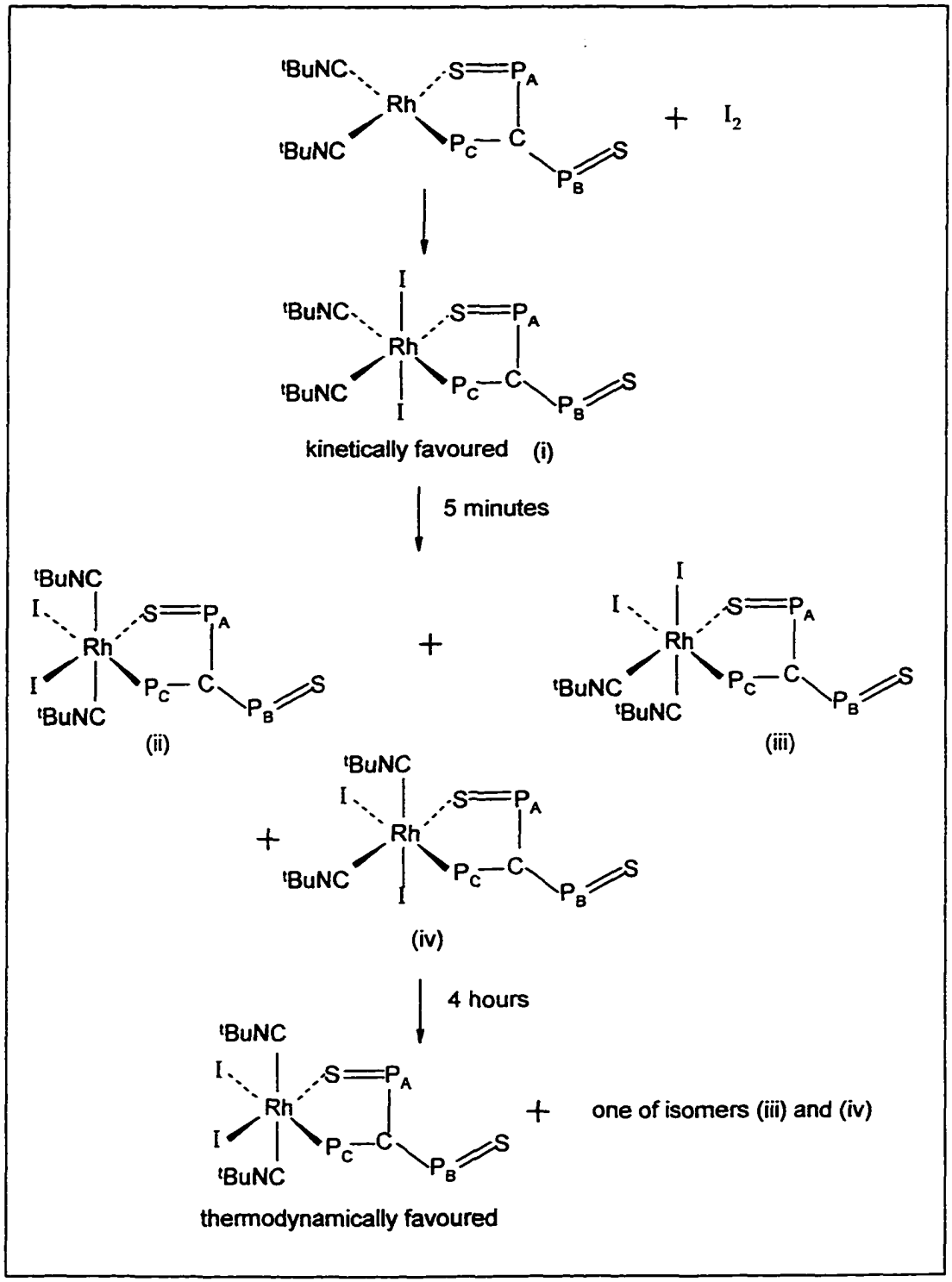

Scheme 4.7 Oxidative Addition of Benzyl Bromide to

[Rh(^{t}BuNC)$_2${C(PPh$_2$)(P(S)Ph$_2$)$_2$-*P,S*}]

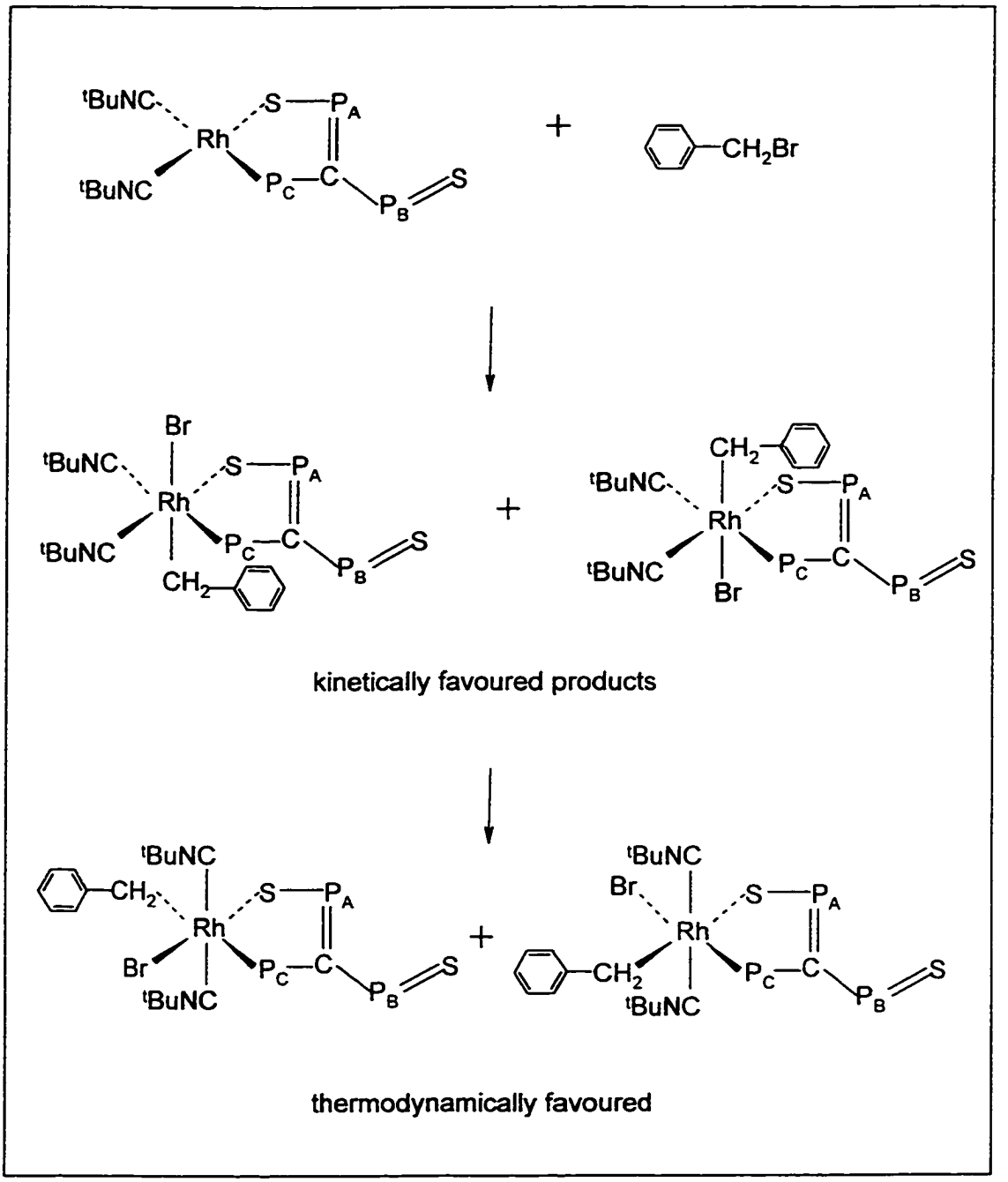

Chapter Five

Coordination Chemistry of $[CH(PPh_2)(P(S)Ph_2)_2]$; Platinum, Palladium, Rhodium, and Iridium Complexes

5.1 Synthesis and Characterization

Reactions of two molar equivalents of $[CH(PPh_2)(P(S)Ph_2)_2]$ with the chlorobridged complexes, $[M(Cod)(\mu\text{-}Cl)_2]$ (M = Rh or Ir), and $[M_2Cl_4(PEt_3)_2]$ (M = Pt or Pd), proceed smoothly under mild conditions (room temperature), resulting in the cleavage of the chloro bridges and formation of the complex cations, $[M(Cod)\{CH(PPh_2(P(S)Ph_2)_2\}]^+$ (M = Rh or Ir), and $[PtCl(PEt_3)\{CH(PPh_2)(P(S)Ph_2)_2\text{-}P,S\}]^+$ (M = Pt or Pd). Addition of $NaBF_4$ to the reaction mixtures enables isolation of the cations as fluoroborate salts in 70% and 77% yields respectively. With the exception of $[Rh(Cod)\{CH(PPh_2(P(S)Ph_2)_2\}]BF_4$, all the products were fully characterised by $^{31}P\{^1H\}$ NMR and microanalysis. In addition, a solid state structure, determined by X-ray diffraction, was obtained for $[Ir(Cod)\{CH(PPh_2(P(S)Ph_2)_2\}]BF_4$. The synthetic scheme is shown in **Scheme 5.1** and **5.2**.

In the case of reaction with $[Rh(Cod)(\mu\text{-}Cl)]_2$, partial deprotonation of the ligand occurred to give additional product, $[Rh(Cod)\{C(PPh_2)(P(S)Ph_2)_2\}]$, which made it impossible to obtain crystals of pure $[Rh(Cod)\{C(PPh_2)(P(S)Ph_2)_2\}]BF_4$ for microanalysis. As we have shown in Chapter Four, reactions of chlorobridged complexes with the ligand, $CH(PPh_2)(P(S)Ph_2)_2$, in the presence of a weak base ($NHEt_2$), results in deprotonated products for all the metals [65]. The fact that only partial deprotonation of the ligand occurred in the present rhodium complex indicates that the methine proton on the phosphine chalcogenide ligand is more acidic than that in the iridium analogue.

Scheme 5.1 Synthesis of [M(Cod){CH(PPh$_2$)(P(S)Ph$_2$)$_2$-*P,S,S*}]BF$_4$

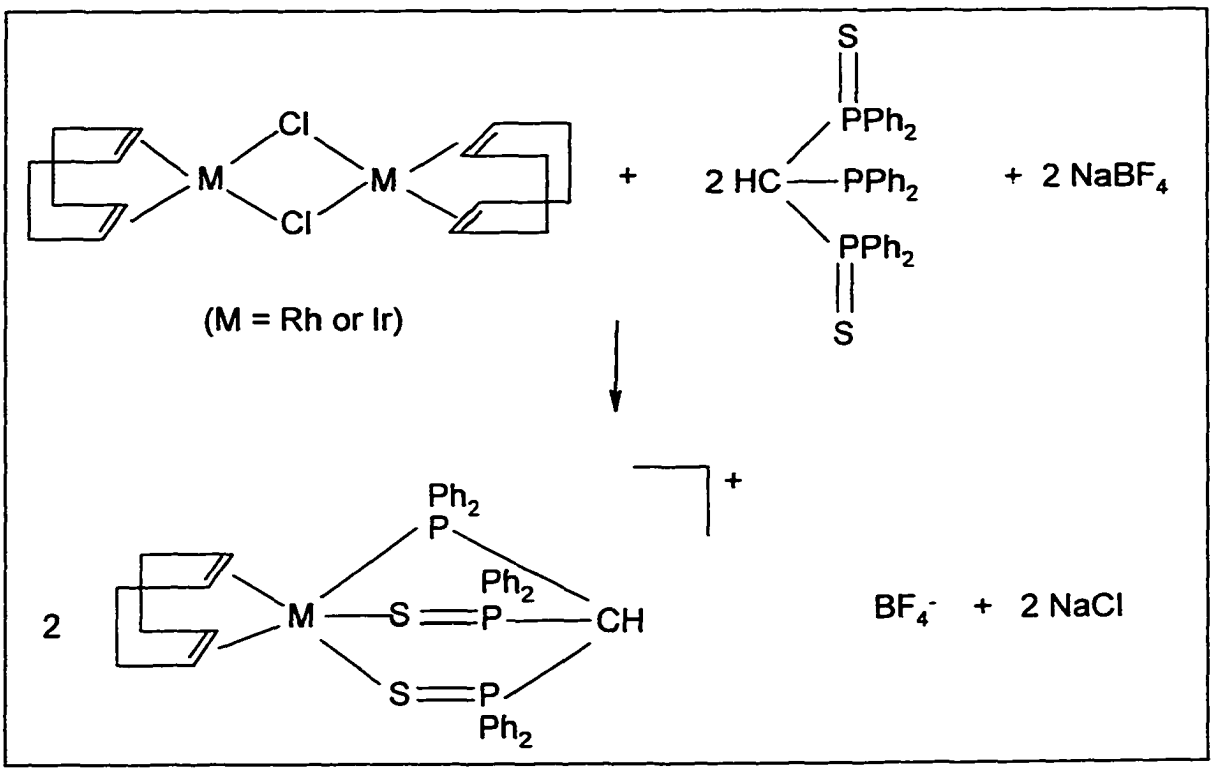

Scheme 5.2 Synthesis of [MCl(PEt$_3$){CH(PPh$_2$)(P(S)Ph$_2$)$_2$-*P,S*}]BF$_4$

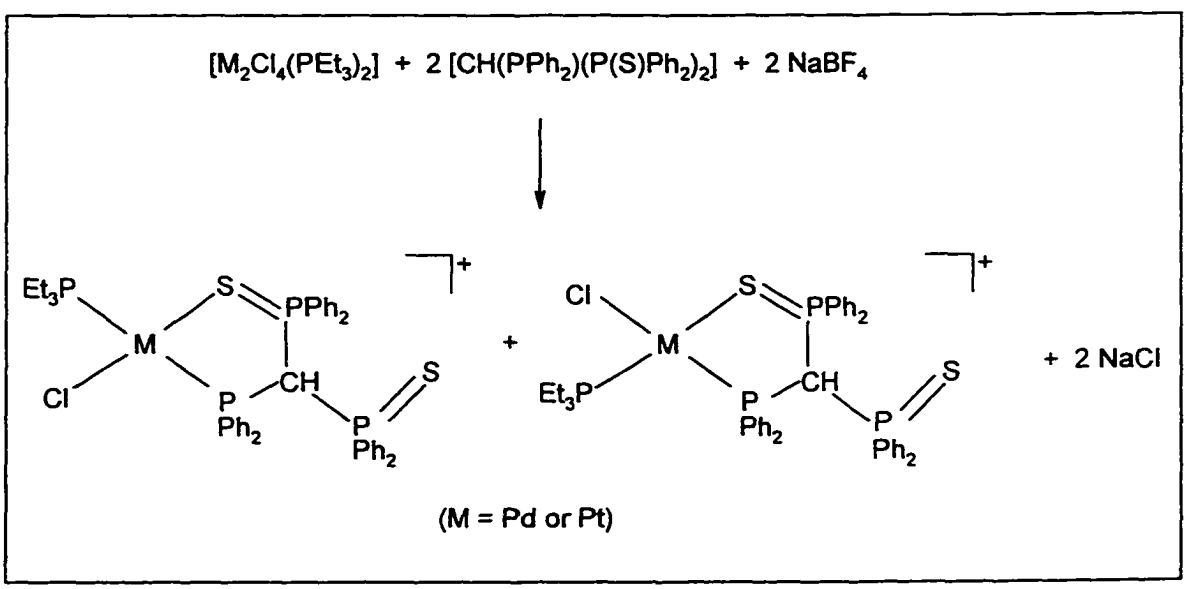

Deprotonation of $[Pt(PEt_3)(Cl)\{CH(PPh_2)(P(S)Ph_2)_2\}]BF_4$ by sodium hydride gave a product with an identical $^{31}P\{^1H\}$ NMR spectrum to that of $[Pt(PEt_3)(Cl)\{C(PPh_2)(P(S)Ph_2)_2\}]$, which was discussed in detail in Chapter Four [65]. Protonation of this product by aqueous tetrafluoroboric acid reformed $[Pt(PEt_3)(Cl)\{CH(PPh_2)(P(S)Ph_2)_2\}]BF_4$. The processes are summarised in **Scheme 5.3**.

Scheme 5.3 Deprotonation and protonation of $[Pt(PEt_3)(Cl)\{CH(PPh_2)(P(S)Ph_2)_2\}]BF_4$

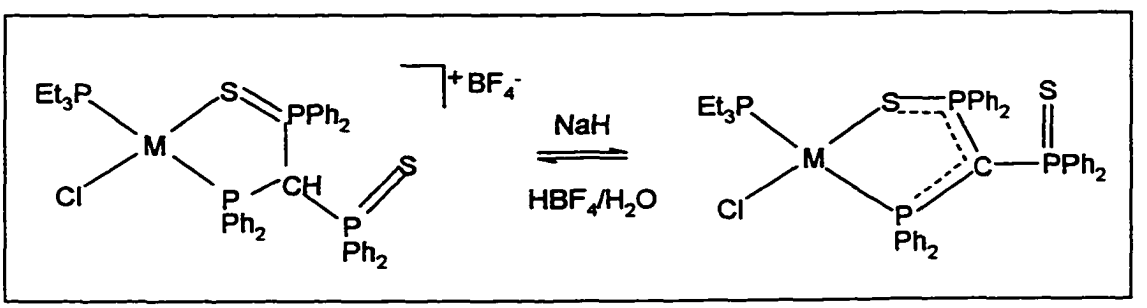

The atom labelling schemes for $[CH\{(PPh_2)(P(S)Ph_2)_2\}]$, $[M(Cod)\{CH(PPh_2)(P(S)Ph_2)_2\text{-}P,S,S\}]^+$ (M = Rh or Ir), and $[PtCl(PEt_3)\{CH(PPh_2)(P(S)Ph_2)_2\text{-}P,S\}]^+$ (M = Pt or Pd) are shown in **Scheme 5.4**. $[M(Cod)\{C(PPh_2)(P(S)Ph_2)_2\text{-}P,S]$ (M = Rh or Ir) is included for comparison. The $^{31}P\{^1H\}$ NMR spectrum of $[Ir(Cod)\{CH(PPh_2)(P(S)Ph_2)_2\}]^+$ exhibits two resonances; a triplet at 37.3 pm and a doublet at 52.8 ppm with a mutual coupling of 39 Hz. In

coparison to the deprotonated analogue, [Ir(Cod){C(PPh_2)($P(S)Ph_2$)$_2$}], in Chapter Four, which showed three resonances as expected for η^2-*P,S* coordination, the two resonances of [Ir(Cod){CH(PPh_2)($P(S)Ph_2$)$_2$}]$^+$ suggest either η^3-*P,S,S* coordination of the phosphine chalcogenide ligand or η^2-*P,S* coordination with a dynamic exchange between the two P=S groups. However, spectra recorded down to -90°C gave no indication of any slowing of such a dynamic process. Furthermore, the triplet shift of 37.3 ppm, assigned to P_C, is similar to that assigned to the directly coordinated phosphorus of [Ir(Cod){C(PPh_2)($P(S)Ph_2$)$_2$}], 36.3 ppm [65]. As well, the doublet shift of 52.8 ppm is intermediate between those of coordinated (65.6 ppm in [Ir(Cod){C(PPh_2)($P(S)Ph_2$)$_2$}]) and non-coordinated (41.7 ppm in [Ir(Cod){C(PPh_2)($P(S)Ph_2$)$_2$}]) Ph_2P=S groups. In addition, the coupling constant, $^2J(P_{A,B}$-$P_C)$ of 39 Hz in [Ir(Cod){CH(PPh_2)($P(S)Ph_2$)$_2$}]$^+$, is intermediate between the coupling constants of P_A-P_C of 112 Hz and P_B-P_C of 15 Hz in [Ir(Cod){C(PPh_2)($P(S)Ph_2$)$_2$}] [65] . All this evidence indicates an η^2-*P,S* coordination of the CH(PPh_2)($P(S)Ph_2$)$_2$ towards the metal centre with dynamic exchange of coordinated and non-coordinated Ph_2P=S groups in [Ir(Cod){CH(PPh_2)($P(S)Ph_2$)$_2$}]$^+$ in solution. Further study by X-ray diffraction of [Ir(Cod){CH(PPh_2)($P(S)Ph_2$)$_2$}]BF_4 however, indicates that the complex contains the ligand bonded in a tridentate η^3-*P,S,S* fashion, as suggested in the **Scheme 5.4**. The results of the X-ray diffraction study will be discussed in detail later in this Chapter. Analysis of the spectrum of the rhodium analogue, [Rh(Cod){CH(PPh_2)($P(S)Ph_2$)$_2$}]$^+$, is similar except for the existence of the Rh-P_C coupling of 134 Hz. All $^{31}P\{^1H\}$ NMR parameters for the complexes discussed above are collected in **Table 5.1** along with those for the ligand, [CH(PPh_2)($P(S)Ph_2$)$_2$].

Scheme 5.4 Structures and atom labelling schemes for compounds listed below. With the exception of the ligand itself, the two phenyl groups attached to each phosphorus have been omitted for clarity.

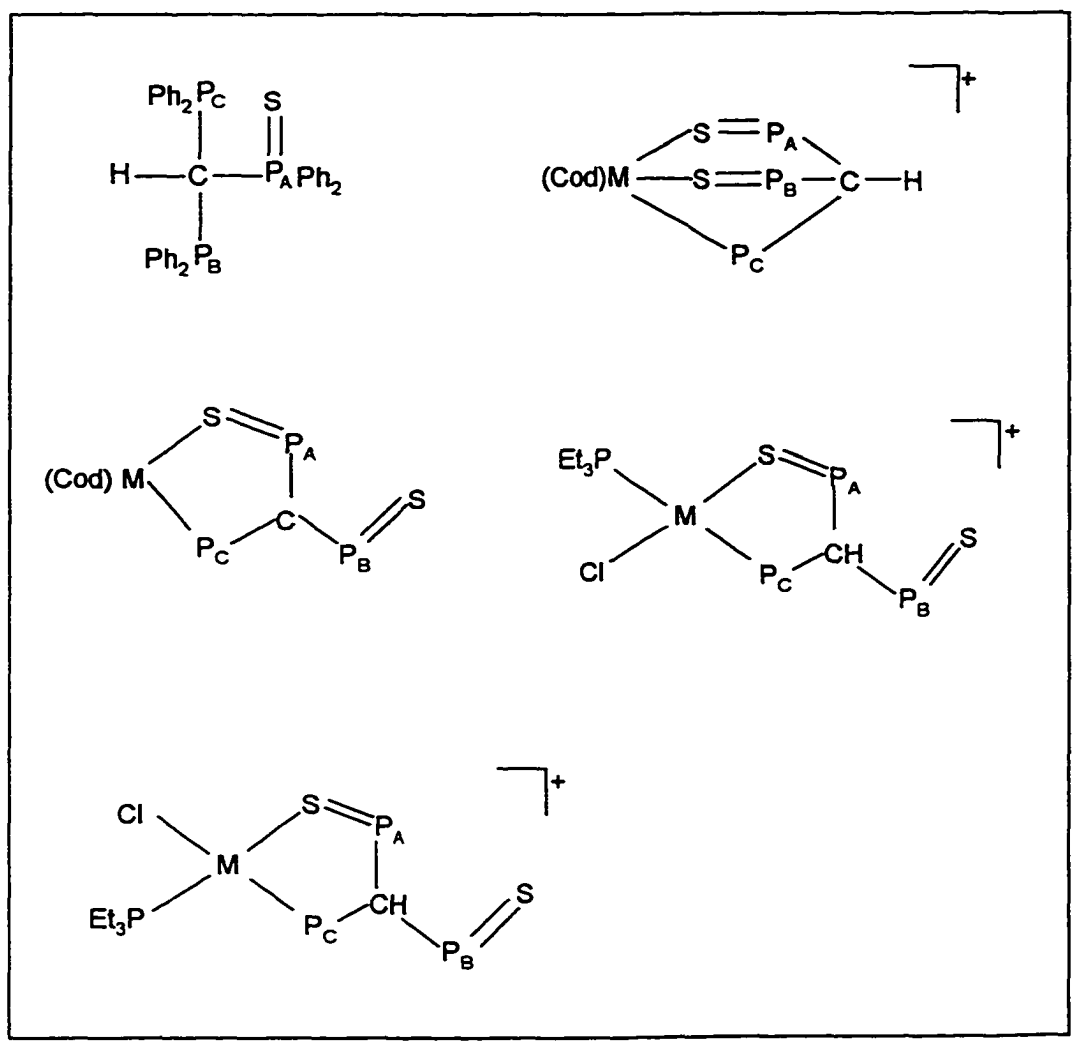

Figure 5.1 The ^{31}P $\{^1H\}$ NMR Spectra of A) $[PtCl(PEt_3)\{CH(PPh_2)(P(S)Ph_2)_2\text{-}P,S\}]^+$ and B) $[PtCl(PEt_3)\{C(PPh_2)(P(S)Ph_2)_2\text{-}P,S\}]$

A) $[PtCl(PEt_3)\{CH(PPh_2)(P(S)Ph_2)_2\text{-}P,S\}]^+$

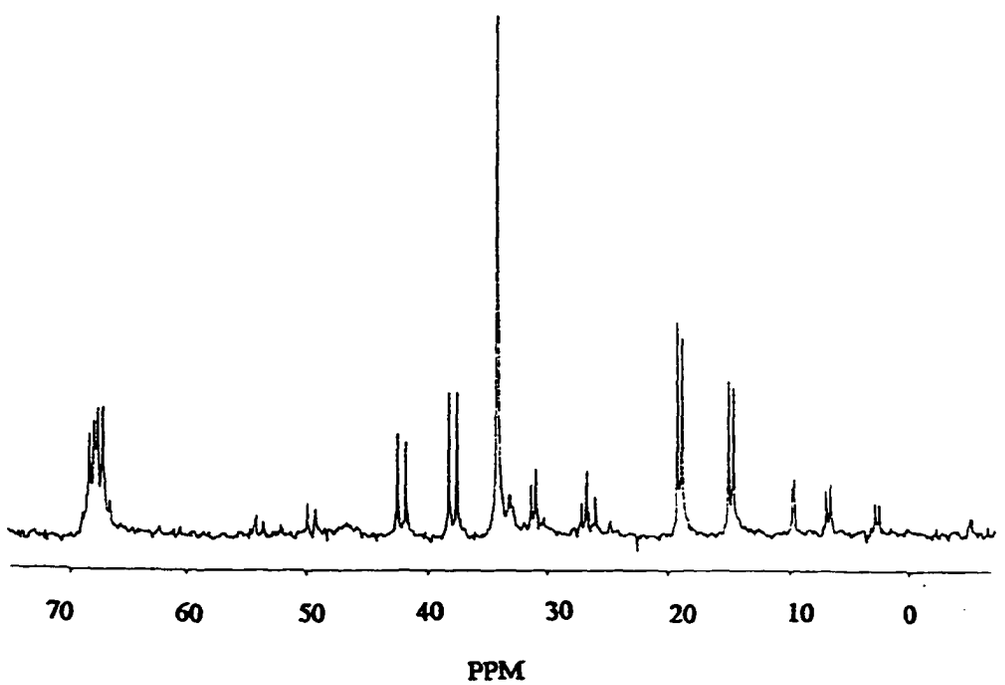

B) $[PtCl(PEt_3)\{C(PPh_2)(P(S)Ph_2)_2\text{-}P,S\}]$

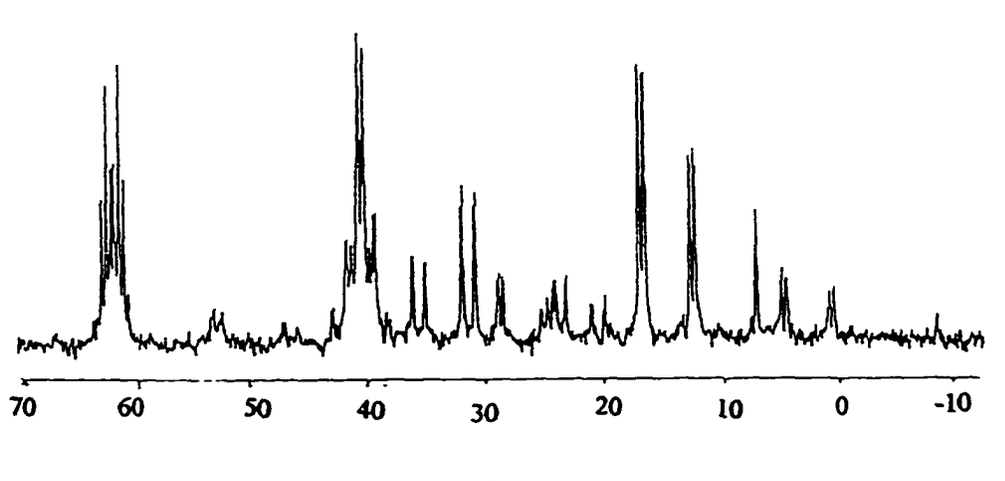

The ^{31}P $\{^1H\}$ NMR spectrum of $[PtCl(PEt_3)\{CH(PPh_2)(P(S)Ph_2)_2\text{-}P,S\}]^+$ shows three separate resonances, an indication of η^2 - *P,S* coordination of the ligand, $CH(PPh_2)(P(S)Ph_2)_2$. It closely resembles that of its deprotonated analogue, $[PtCl(PEt_3)\{C(PPh_2)(P(S)Ph_2)_2\text{-}P,S\}]$ discussed in Chapter Four [63]. There are two isomers present in the reaction mixtures with the majority being the *trans* isomer as indicated by its large two bond phosphorus coupling (430 Hz) of P_C to the phosphorus of the PEt_3, and relatively small ^1J(Pt-P) values of 2350Hz and 2457 Hz. The presence of traces of the *cis* isomer, however, cannot be reliably assigned due to the low intensities of the ^{31}P resonances in the spectrum. The ^{31}P $\{^1H\}$ NMR spectra of $[PtCl(PEt_3)\{CH(PPh_2)(P(S)Ph_2)_2\text{-}P,S\}]^+$ and its deprotonated analogue are shown in **Figure 5.1.** The comparison between the analysis of the $^{31}P\{^1H\}$ NMR of $[PtCl(PEt_3)\{CH(PPh_2)(P(S)Ph_2)_2\text{-}P,S\}]^+$ and its protonated analogue $[PtCl(PEt_3)\{C(PPh_2)(P(S)Ph_2)_2\text{-}P,S\}]$ shows different relative magnitudes of the two-bond and three-bond Pt-P coupling constants. In deprotonated complexes, $[PtCl(PEt_3)\{CH(PPh_2)(P(S)Ph_2)_2\text{-}P,S\}]^+$, ^3J(Pt-P) (197Hz) is larger than ^2J(Pt-P) (78 Hz) [64], which is slightly unusual. However, in the protonated complex, $[PtCl(PEt_3)\{CH(PPh_2)(P(S)Ph_2)_2\text{-}P,S\}]^+$, the two-bond coupling ^2J(Pt-P) is 117 Hz, and the three-bond coupling ^3J(Pt-P) is not resolved in the observed spectrum. Line width measurements suggest that the ^3J(Pt-P) cannot be larger than 40 Hz. The comparison of the difference in the relative magnitudes of ^2J(Pt-P) and ^3J(Pt-P) between these two complexes hence suggests that the hybridization of the methine carbon in the Pt-P-C-P chain has a larger influence on the three-bond coupling ^3J(Pt-P) than the two-bond

coupling ^2J(Pt-P), with a much smaller values for a sp^3 carbon (<40 Hz, in the case of $[PtCl(PEt_3)\{CH(PPh_2)(P(S)Ph_2)_2\text{-}P,S\}]^+$) and much larger values for a sp^2 carbon (197 Hz, in the case of $[PtCl(PEt_3)\{C(PPh_2)(P(S)Ph_2)_2\text{-}P,S\}]$ [65]) . In the cases of rhodium complexes $[Rh(Cod)\{CH(PPh_2)(P(S)Ph_2)_2\text{-}P,S,S\}]^+$ in this Chapter and $[Rh(Cod)\{C(PPh_2)(P(S)Ph_2)_2\text{-}P,S\}]$ in Chapter Four [65] similar observation with regards to metal (rhodium) - phosphorus bonds can be made, although different coordination modes of the phosphine chalcogenide ligand in the complexes have to be considered as well as the much smaller rhodium - phosphorus coupling.

The $^{31}P\{^1H\}$ NMR spectrum of the palladium complex, $[PdCl(PEt_3)\{CH(PPh_2)(P(S)Ph_2)_2\text{-}P,S\}]^+$, shows only two phosphorus resonances for the phosphine chalcogenide ligand. The chemical shift $\delta(P_A/P_B)$ of 52.8 ppm is intermediate between the coordinated P = S phosphorus shift of 62.8 ppm and the non-coordinated P = S phosphorus shift of 43.2 ppm in the platinum analog, $[PtCl(PEt_3)\{CH(PPh_2)(P(S)Ph_2)_2\text{-}P,S\}]^+$. The same comparisons also apply to the other parameters such as $J(P_A/P_B - P_C)$ and $J(P_A/P_B - P_D)$ where they are all close to the averages of the corresponding parameters in the platinum analog. Therefore, the structure assigned to the palladium complex, $[PdCl(PEt_3)\{CH(PPh_2)(P(S)Ph_2)_2\text{-}P,S\}]^+$ is most likely to be the following: a four-coordinate complex with a dynamic exchange between coordinated P_A and non-coordinated P_B as shown in **Scheme 5.5**

Scheme 5.5 Dynamic Exchange in $[PdCl(PEt_3)\{CH(PPh_2)(P(S)Ph_2)_2\text{-}P,S\}]^+$ (Phenyl groups attached to each phosphorus have been omitted for clarity).

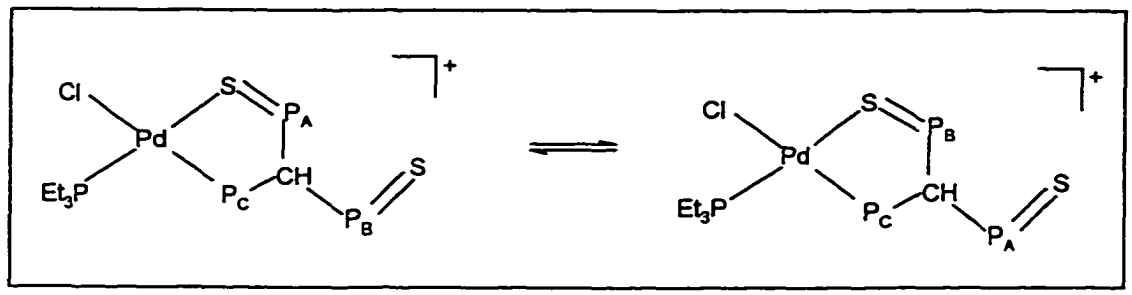

The generally more labile coordination sphere of palladium results in dynamic exchange between the coordinated and non-coordinated P = S groups. Further experiments with low temperature ^{31}P NMR studies of $[PdCl(PEt_3)\{CH(PPh_2)(P(S)Ph_2)_2\text{-}P,S\}]BF_4$ have indeed verified such exchange. As the temperature is reduced, the triplet at 52.8 ppm begins broadening at -10 °C and resolves into two multiplets at -80 °C, with shifts of 69 ppm (P_A) and 45 ppm (P_B) respectively. However, the multiplicity of the two resonances cannot be resolved thus precluding reliable measurements of kinetic parameters. The $^{31}P\{^1H\}$ NMR spectrum of the palladium complex also shows the existence of about 15 - 20 % of the *cis* isomer. As comparable to the platinum analogue, overlapping of resonances and low intensities make an accurate assignment of the *cis* isomer difficult. $^{31}P\{^1H\}$ NMR parameters for the Pt and Pd complexes discussed above are collected in **Table 5.2**. Both infrared and ^{19}F NMR demonstrate the presence of BF_4^-. For each complex the infrared shows a broad strong absorption around 1050 cm^{-1}, which is typical for BF_4^-. The ^{19}F NMR spectra of the complexes both show a doublet around -152 ppm, assignable to BF_4^-.

Table 5.1 $^{31}P\{^{1}H\}$ NMR parameters for (A) $[CH(PPh_2)(P(S)Ph_2)_2]$) and its complexes: (B) $[Ir(Cod)\{CH(PPh_2)(P(S)Ph_2)_2\}]^+$ and (C) $[Rh(Cod)\{CH(PPh_2)(P(S)Ph_2)_2\}]^+$

Compound	Notes	avg. $\delta(P_A)$ $\delta(P_B)$	$\delta(P_C)$	$J(P_A\text{-}P_B)$	avg.$J(P_A\text{-}P_C)$ $J(P_B\text{-}P_C)$	$J(M\text{-}P_A)$ $J(M\text{-}P_B)$	$J(M\text{-}P_C)$
(A)	a	---43.5---	-10.0	na	---49---		
(B)	b,c	---52.8---	37.3	na	---39---		
(C)	c,d	---51.4---	46.7	na	---37---	---nr---	134

Chemical shifts (δ) are quoted in parts per million relative to 85% H_3PO_4. Coupling constants (J) are in Hz. nr = not resolved. na = not available

Notes:

a. $CDCl_3$ solution. Data from ref [45]

b. Dichloromethane solution with an external C_6D_6 lock.

c. The P_A and P_B resonances are equivalent.

d. Tetrahydrofuran solution with an external C_6D_6 lock.

Table 5.2 ^{31}P NMR parameters for (A) $[Pt(PEt_3)(Cl)\{CH(PPh_2)(P(S)Ph_2)_2\}]$ and (B) $[Pd(PEt_3)(Cl)\{CH(PPh_2)(P(S)Ph_2)_2\}]$

Complex	Notes	$\delta(P_A)$	$\delta(P_B)$	$\delta(P_C)$	$\delta(P_D)$	$J(P_A\text{-}P_B)$	$J(P_A\text{-}P_C)$	$J(P_B\text{-}P_C)$	$J(P_A\text{-}P_D)$	$J(P_B\text{-}P_D)$	$J(P_C\text{-}P_D)$	$J(M\text{-}P_A)$	$J(M\text{-}P_B)$	$J(M\text{-}P_C)$	$J(M\text{-}P_D)$
(A)	a,b	68.8	35.1	40.8	18.1	46	115	20	nr	nr	430	117	nr[d]	2350	2457
(B)	c	52.8	52.8	42.5	30.7	na	39	39	22	22	484				

Chemical shifts (δ) are quoted in parts per million relative to 85% H_3PO_4. Coupling constants (J) are in Hz. nr = not resolved. na = not available

Notes:

a. Dichloromethane solution with an external C_6D_6 lock.

b. Isomer with Cl *trans* to the coordinated P=S group.

c. Acetone solution with an external C_6D_6 lock.

d. Less than 40 Hz.

5.2 Solid-state Structure of $CH(PPh_2)(P(S)Ph_2)_2$

$CH(PPh_2)(P(S)Ph_2)_2$ was prepared as described in the experimental section of Chapter Seven and crystals suitable for study by X - ray diffraction were grown by recrystallisation from dichloromethane and hexane. The crystallographic techniques employed have been described in detail in Chapter Seven and the Appendix. Selected crystallographic data are listed in **Table 5.3**. All phosphorus and sulphur atoms, and the methine carbon, C(1), were refined anisotropically. All other atoms were treated isotropically. The methine hydrogen, H(1), was located. The phenyl ring hydrogen positions were calculated and allowed to ride on their respective carbon atoms during the refinement. Each ring was treated separately but, within each ring, the hydrogens were refined using a common temperature factor. The final difference maps had significant residuals only close to the heavy atoms in $CH(PPh_2)(P(S)Ph_2)_2$ and gave no indication that any material had been overlooked.

The structure of a single molecule of $CH(PPh_2)(P(S)Ph_2)_2$ is shown as an ORTEP diagram in **Figure 5.2**, along with the atomic labelling scheme. Unit cell and other parameters related to the crystal structure determinations are in **Table 5.3**. Fractional atomic coordinates and isotropic temperature parameters are in **Appendix Table XIV** and anisotropic temperature parameters are in **Appendix Table XV**. Selected bond lengths and bond angles are presented in **Table 5.4**.

The structure shows a distorted tetrahedral configuration around the methine carbon with an average bond angles of 109.1°. This is comparable to its trisulfide

relative, $CH(P(S)Ph_2)_3$ [45]. Similar comparison can be made on most of the other parameters including other angles and lengths, which shows no significant differences. The only exception is a small difference in parameters related to the P^{III} group. For instance, the C-P lengths in $CH(P(S)Ph_2)_3$ [31] are 1.871, 1.881, and 1,896 Å, whereas $CH(PPh_2)(P(S)Ph_2)_2$ shows both shorter and longer distances with C-$P(S)Ph_2$ 1.863 and 1.868 Å, and C-PPh_2 1.898 Å.

Figure 5.2. ORTEP Plot for a Single Molecule of $CH(PPh_2)(P(S)Ph_2)_2$

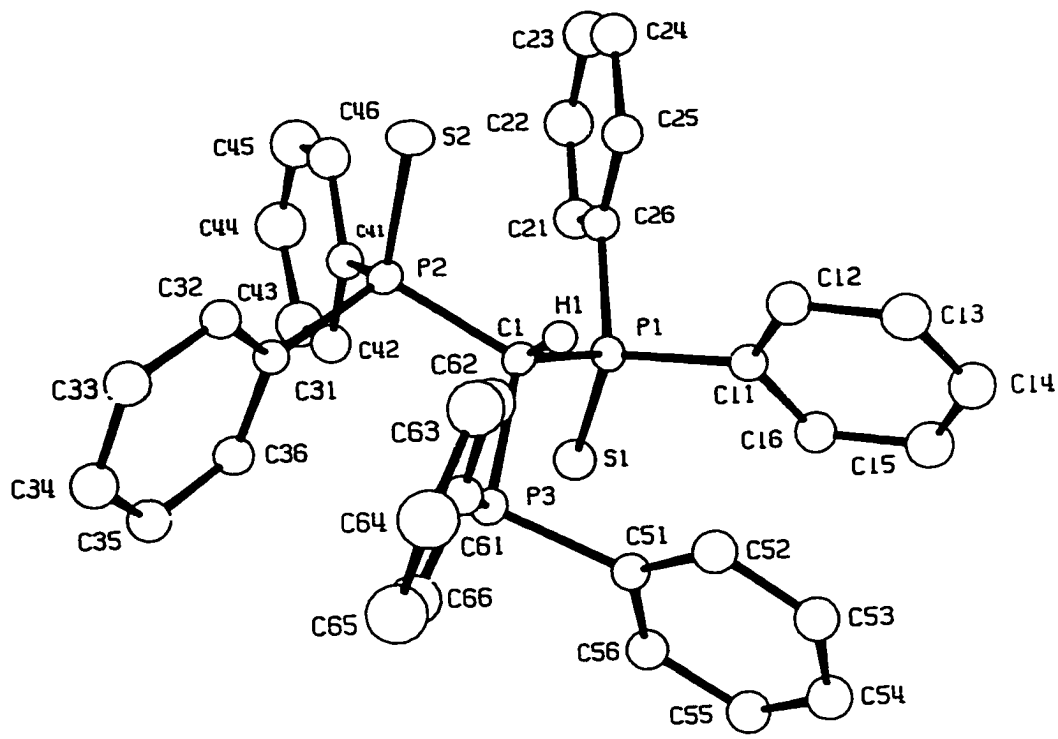

Table 5.3 Crystallographic data for (A) $CH(PPh_2)(P(S)Ph_2)_2$ and (B)[Ir(Cod){$CH(PPh_2)(P(S)Ph_2)_2$-*P,S,S*}].BF_4

Complex	(A)	(B)
Formula	$C_{51}H_{31}P_3S_2$	$C_{46}H_{45}BCl_2F_4P_3S_2Ir$
FW	632.7	1104.8
Space group	$P2_1/n$ (No. 14)	P 1 (No. 2)
a, Å	13.403(3)	16.375(1)
b, Å	12.625(2)	16.375(1)
c, Å	30.416(6)	16.371(1)
α, deg	90.0	101.312(6)
β, deg	117.52(1)	101.281(7)
γ, deg	90.0	101.312(6)
V, $Å^3$	4564	4094
Z	4	3
Diffractometer	Picker 4-circle	Nonius
Radiation (λ, Å)	Mo Kα(0.71069)	Cu Kα(1.542)
μ, cm^{-1}	6.79	1.542
Transform factor range	0.785-0.865	
Temperature, K	295	295
No. of obs. reflcns (I>3.06(I))	8605	3426
Parameters refined	481	364
R	0.0848	0.0779
R_w	0.1243	0.0975

$w = 1/(\sigma^2(F) + 0.001F^2)$; $\Delta = ||F_o|-|F_c||$. $R = (\Sigma\Delta/\Sigma F_o)$; $R_w = (\Sigma w\Delta^2/\Sigma wF_o^2)^{1/2}$

Table 5.4 Selected Interatomic distances (Å) and Bond Angles (°) for $CH(PPh_2)(P(S)Ph_2)_2$.

Atoms	Distance	Atoms	Angle
S(1) - P(1)	1.941(3)	S(1) - P(1) - C(1)	113.8(3)
S(2) - P(2)	1.958(3)	S(1) - P(1) - C(11)	112.8(2)
C(1) - H(1)	0.94(8)	S(1) - P(1) - C(21)	113.2(2)
P(1) - C(1)	1.863(7)	C(1) - P(1) - C(11)	103.8(3)
P(1) - C(11)	1.825(7)	C(1) - P(1) - C(21)	107.8(3)
P(1) - C(21)	1.822(7)	C(11) - P(1) - C(21)	104.6(3)
P(2) - C(1)	1.868(7)	S(2) - P(2) - C(1)	108.9(3)
P(2) - C(31)	1.831(7)	S(2) - P(2) - C(31)	110.8(2)
P(2) - C(41)	1.825(7)	S(2) - P(2) - C(41)	113.7(2)
P(3) - C(1)	1.898(7)	C(1) - P(2) - C(31)	107.6(3)
P(3) - C(51)	1.851(7)	C(1) - P(2) - C(41)	110.4(3)
P(3) - C(61)	1.851(7)	C(31) - P(2) - C(41)	105.4(3)
		C(1) - P(3) - C(51)	106.1(3)
		C(1) - P(3) - C(61)	101.3(3)
		C(51) - P(3) - C(61)	97.3(3)
		P(1) - C(1) - H(1)	107(5)
		P(2) - C(1) - H(1)	113(5)
		P(3) - C(1) - H(1)	94(5)
		P(1) - C(1) - P(2)	117.9(4)
		P(1) - C(1) - P(3)	110.8(3)
		P(2) - C(1) - P(3)	112.1(3)

Estimated standard deviations are given in parentheses.

5.3 Solid-state Structure of $[Ir(Cod)\{CH(PPh_2)(P(S)Ph_2)_2\text{-}P,S,S\}]BF_4 \cdot CH_2Cl_2$

$[Ir(Cod)\{CH(PPh_2)(P(S)Ph_2)_2\}]BF_4 \cdot CH_2Cl_2$ was prepared as described in the experimental section of Chapter Seven and crystals suitable for study by X - ray diffraction were grown by recrystallisation in dichloromethane and diethyl ether. The crystallographic techniques employed have been described in detail in Chapter Seven and Appendix. Selected crystallographic data are listed in **Table 5.3**. The iridium atom, and all phosphorus, sulfur, chlorine, boron and fluorine atoms were treated anisotropically, as were the methine carbon of the ligand, C(1), the carbon of the dichloromethane, and the carbons of the *Cod* ligand, C(71-78). All other atoms were treated isotropically. The methine hydrogen, H(1), was located . Other hydrogen atoms were not located and are not included in the refinement for the structure. The final difference maps had significant residuals only close to the heavy atoms such as the iridium and the BF_4 group in $[Ir(Cod)\{CH(PPh_2)(P(S)Ph_2)_2\}]BF_4 \cdot CH_2Cl_2$, and gave no indication that any material had been overlooked.

The structure of a single cation of $[Ir(Cod)\{CH(PPh_2)(P(S)Ph_2)_2\text{-}P,S,S\}]BF_4.CH_2Cl_2$ is shown as an ORTEP diagram in **Figure 5.3**. Unit cell and other parameters related to the crystal structure determinations are in **Table 5.3.** Fractional atomic coordinates and isotropic temperature parameters are in **Appendix Table XVI**, and anisotropic temperature parameters are in **Appendix Table XVII**. Selected bond lengths and bond angles are given in **Table 5.5**

Figure 5.3. ORTEP Plot for a Single Cation of [Ir(Cod){CH(PPh$_2$)(P(S)Ph$_2$)$_2$-*P,S,S*}]

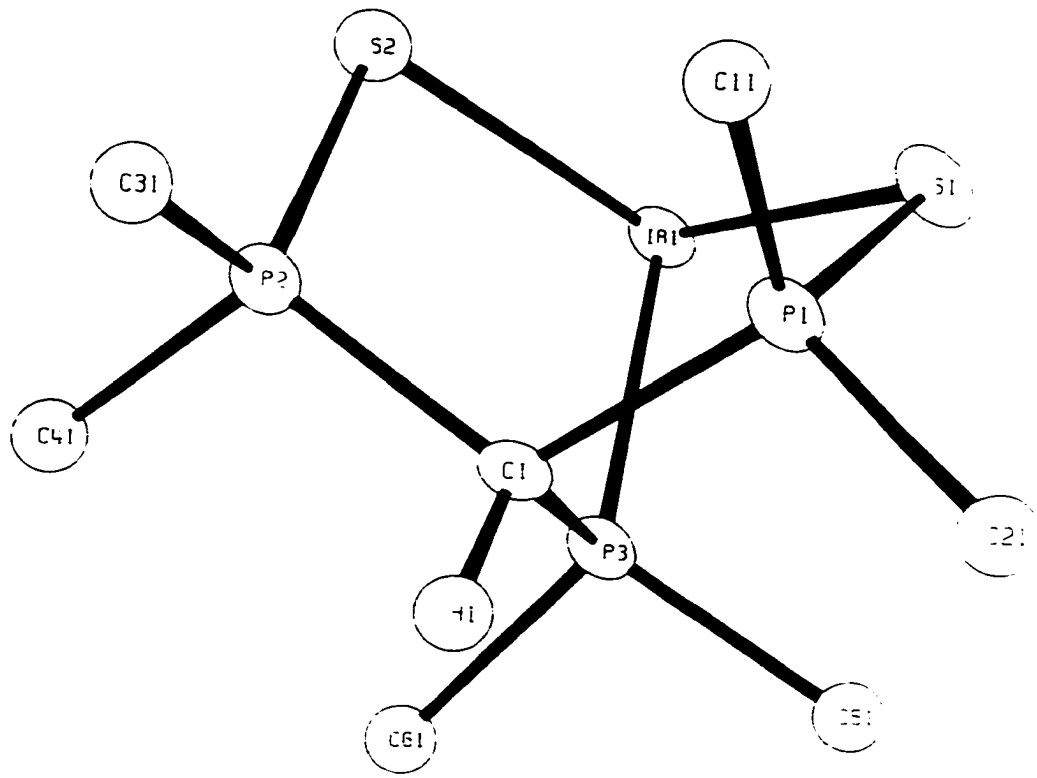

The structure shows irregular five-coordination geometry about the metal centre with the $CH(PPh_2)(P(S)Ph_2)_2$ ligand coordinated in an η^3-*P,S,S* tridentate fashion. The three S-Ir-S and S-Ir-P angles range from 81 to 92°, and are slightly smaller than the angles observed in the related palladium complex $[Pd(\eta^3\text{-}C_4H_7)\{CH(P(S)Ph_2)_3\}]BF_4$ discussed in Chapter Two [116], the angles in which range from 92 to 99°. The *Cod* ligand is coordinated via its two double bonds to the iridium atom. The bond distances between the iridium centre and the coordinated sulphur atoms are 2.44Å and 2.57Å, which are significantly longer than those found in the bidentate,η^2-*S,S* complexes, $[Ir(CO)\{CH(P(S)Ph_2)_3\text{-}S,S\}]$, av. 2.36Å in Chapter Three [68]. A similar observation can be made when the η^3-*S,S,S* bonded complex, $[Pd(\eta^3\text{-}C_4H_7)\{CH(P(S)Ph_2)_3\text{-}S,S,S\}]BF_4$ (av. Pd-S 2.52 Å) is compared to the bidentate $[Pd(\eta^3\text{-}C_4H_7)\{CH(PPh_2)(P(S)Ph_2)_2\text{-}P,S\}]BF_4.2H_2O$ (av. Pd-S 2.33Å), discussed in Chapter Two. [116]. These observations suggest that metal-sulphur bonding in a tridentate bonding mode with a tripodal ligand is weaker than in a bidentate bonding mode. This can be somehow explained as the steric effect caused by six phenyl groups is larger in a tridentate mode than that in a bidentate mode so that the longer metal to sulphur bonds are required to alleviate the crowding. The P-S bond distances range from 1.98Å to 2.00Å and are longer than in the free ligand, $CH(PPh_2)(P(S)Ph_2)_2$, 1.94Å to 1.96Å. This is consistent with the observation that the P-S bond lengthens upon coordination of the ligand to the metal centre [116] The other important structural observation involves the geometry at the central methine carbon, C(1), of the phosphine chalcogenide ligand and the location of H(1). In the free ligand, $CH(PPh_2)(P(S)Ph_2)_2$, the carbon, C(1) lies 0.48Å out of the plane define by P(1)-P(2)-P(3), and the average P-C-P

angles are 114°. This is consistent with a slightly distorted sp^3 geometry due to the bulky attachment of the phenyl rings. In $[Ir(Cod)\{CH(PPh_2)(P(S)Ph_2)_2\text{-}P,S,S\}]BF_4.CH_2Cl_2$, this displacement of C(1) from the P(1)-P(2)-P(3) plane is 0.73 Å and the average P-C-P angle is 107°, which is much closer to tetrahedral geometry than planar geometry. This is an important confirmation of the existence of the proton attached to the central methine carbon of the ligand. This also demonstrates that narrowing of the P-C-P angles is required to achieve tripodal coordination. Whether tripodal coordination is easier in the protonated or deprotonated ligands, one would think the narrowing of such angles in a basically sp^3 geometry, that is necessary in the protonated ligands, would be easier than the marked distortion of the planar sp^2 geometry which is often required in the deprotonated ligands. It is then not surprising to note that the only complexes in this thesis with the ligand bonded in three coordinate mode are those with the ligand in the protonated form. The bond distance between the iridium centre and the coordinated phosphorus atom is 2.31Å, which is significantly shorter than the sum of the covalent radii of iridium and phosphorus (2.46 Å [88]). This perhaps explains why, in the solution state, the complex very likely undergoes a facile exchange between coordinated and non-coordinated $Ph_2P{=}S$ groups. The stronger iridium-phosphorus bond can act as a pivot for the exchange of the weakeriridium-sulphur bonds. This was observed by a singlet at low temperature (-90°C) $^{31}P\{^1H\}$ NMR spectrum of this compound in solution.

Table 5.5 Selected Interatomic distances (Å) and Bond Angles (°) for [Ir(Cod){CH(PPh$_2$)(P(S)Ph$_2$)$_2$-*P,S,S*}]

Atoms	Distance	Atoms	Angle
Ir(1) - S(1)	2.438(3)	S(1) - Ir(1) - S(2)	87.8(1)
Ir(1) - S(2)	2.574(3)	S(1) - Ir(1) - P(3)	81.1(1)
Ir(1) - P(3)	2.314(2)	S(1) - Ir(1) - C_x	86.8
Ir(1) - C(71)	2.170(9)	S(1) - Ir(1) - C_y	161.2
Ir(1) - C(72)	2.177(10)	S(2) - Ir(1) - P(3)	91.5(1)
Ir(1) - C(75)	2.125(11)	S(2) - Ir(1) - C_x	106.4
Ir(1) - C(76)	2.125(10)	S(2) - Ir(1) - C_y	110.6
S(1) - P(1)	2.001(4)	P(3) - Ir(1) - C_x	159.1
S(2) - P(2)	1.977(4)	P(3) - Ir(1) - C_y	100.9
H(1) - C(1)	0.99(2)	C_x - Ir(1) - C_y	85.5
P(1) - C(1)	1.863(9)	Ir(1) - S(1) - P(1)	105.0(1)
P(1) - C(11)	1.798(10)	Ir(1) - S(2) - P(2)	100.2(1)
P(1) - C(21)	1.834(10)	S(1) - P(1) - C(1)	108.1(3)
P(2) - C(1)	1.852(9)	S(2) - P(2) - C(1)	108.2(3)
P(2) - C(31)	1.784(10)	Ir(1) - P(3) - C(1)	102.2(3)
P(2) - C(41)	1.817(10)	P(1) - C(1) - H(1)	117(3)
P(3) - C(1)	1.900(9)	P(2) - C(1) - H(1)	108(2)
P(3) - C(51)	1.834(10)	P(3) - C(1) - H(1)	110(2)
P(3) - C(61)	1.842(9)	P(1) - C(1) - P(2)	111.0(4)
		P(1) - C(1) - P(3)	104.0(4)
		P(2) - C(1) - P(3)	106.7(4)

Estimated standard deviations are given parentheses. C_x is the mid-point of the C(71) - C(72) bond and C_y is the mid-point of the C(75) - C(76) bond.

5.4 Conclusion

The new iridium, rhodium, palladium, and platinum complexes of $[M(Cod)\{CH(PPh_2)(P(S)Ph_2)_2]BF_4$ (M = Rh, Ir) and $[MCl(PEt_3)\{CH(PPh_2)(P(S)Ph_2)_2\}]BF_4$ (M = Pd and Pt) have been synthesised. The tripodal ligand, $[CH(PPh_2)(P(S)Ph_2)_2]$, has shown that it can act either as a bidentate 4-electron donor via one sulphur atom and one phosphorous atom, or a 6-electron donor, with one phosphorus and two sulphur atoms coordinated. These two possibilities are shown below:

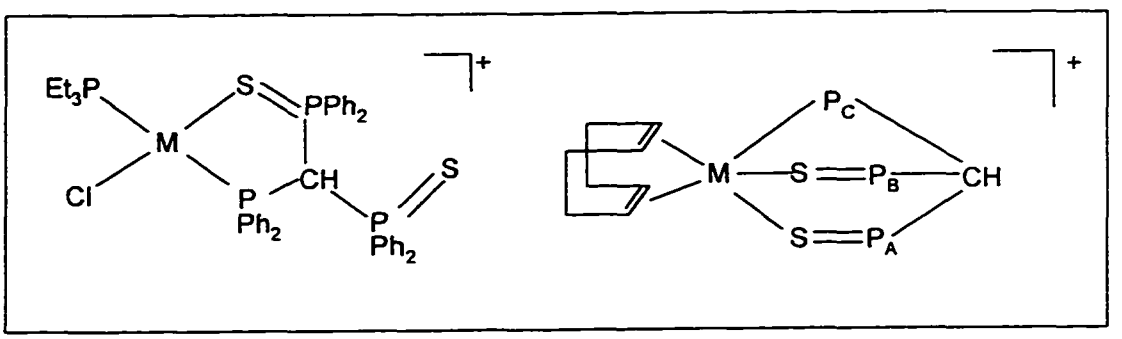

The bidentate mode was observed in the complexes of formula $[MCl(PEt_3)\{CH(PPh_2)(P(S)Ph_2)_2\}]BF_4$ (M = Pt, Pd). The more labile palladium complex exhibits a dynamic exchange at ambient temperature between coordinated and "dangling" $Ph_2P{=}S$ groups, which can be resolved at -80 °C. In contrast the platinum analogue shows a rigid η^2-*P,S* coordination of the ligand at ambient temperature.

The iridium complex, $[(Cod)Ir\{CH(PPh_2)(P(S)Ph_2)_2\}$-*P,S,S*$]BF_4$, shows the ligand

acting as a 6-electron donor with both sulphur atoms, as well as the phosphorus atom, coordinated. This η^3-*P,S,S* coordination mode was observed in the solid-state structure of the compound. However, in solution it is highly probable the ligand is coordinated in a bidentate fashion with a dynamic exchange between the coordinated and non-coordinated Ph_2P=S groups, even down to -90°C. The solid-state structure indicates a strong iridium- phosphorus bond and presumably, in solution, it would act as a very stable pivot around which the exchange of the coordinated and non-coordinated Ph_2P=S groups could occur. Analysis of the $^{31}P\{^1H\}$ NMR spectrum of $[Ir(Cod)\{CH(PPh_2)(P(S)Ph_2)_2\}]BF_4$ at ambient temperature suggests a fluxional process is occurring. The observation of rather strong iridium-sulphur bonds in the X-ray study supports this proposal.

The more labile rhodium analogue, $[Rh(Cod)\{CH(PPh_2)(P(S)Ph_2)_2\}]BF_4$, is also believed to undergo a similar dynamic exchange of coordinated and non-coordinated Ph_2P=S groups in solution at ambient temperature. However, isolation of the pure compound was difficult because the higher acidity of the methine proton always resulted in a mixture of protonated and deprotonated complexes.

Chapter 6

Summary and Prospects

The coordination chemistry of the phosphine chalcogenide ligands, $[CH(P(S)Ph_2)_3]$ / $[C(P(S)Ph_2)_3]^-$ and $[CH(PPh_2)(P(S)Ph_2)_2]$/ $[C(PPh_2)(P(S)Ph_2)_2]^-$ with the transition metals rhodium, iridium, platinum, and palladium was studied. Several new coordination compounds were synthesised. A general synthetic scheme for the synthesis of complexes with the protonated ligands is shown in **Scheme 6.1**.

Scheme 6.1 Synthetic Route for the Complexes of $[CH(PPh_2)(P(S)Ph_2)_2]$ and $[CH(P(S)Ph_2)_3]$

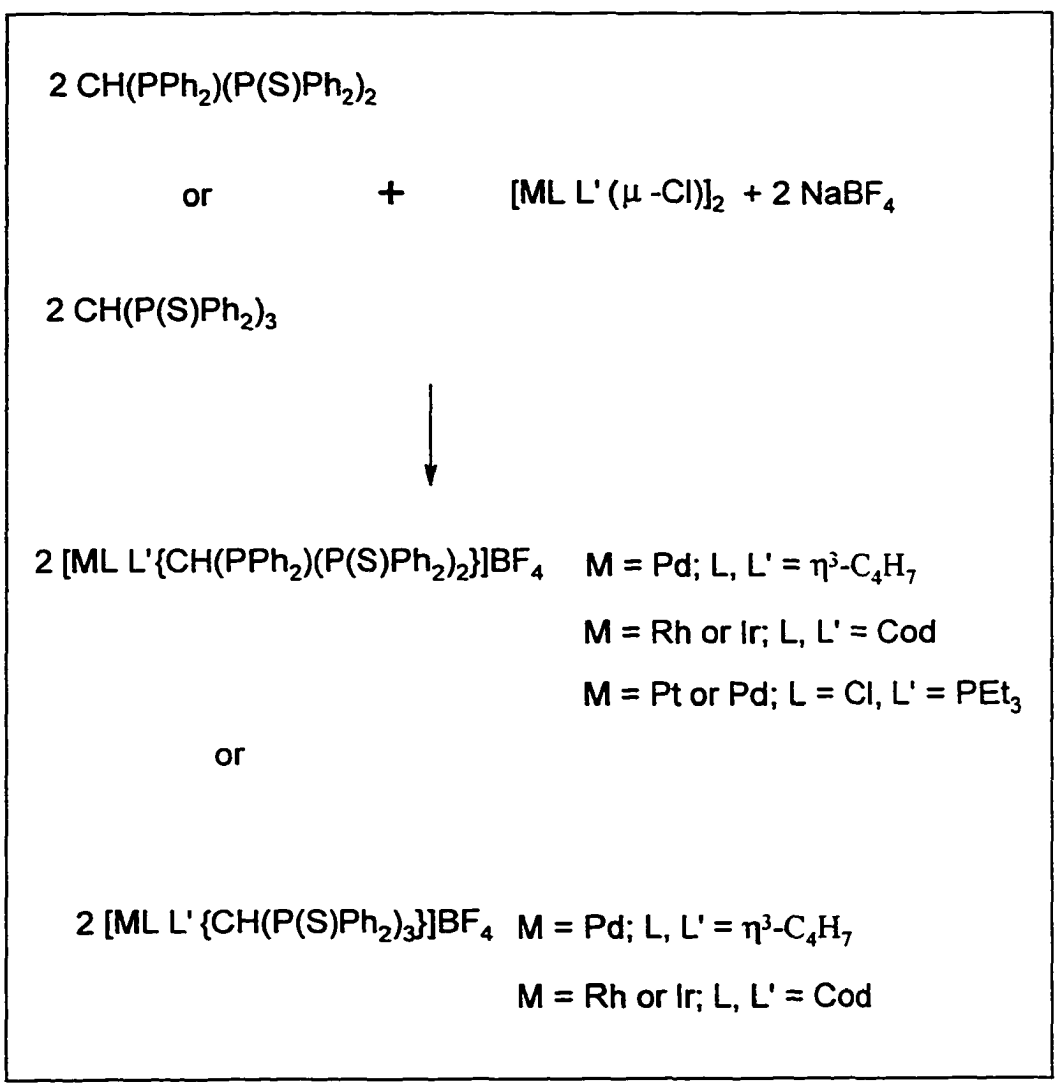

As can be seen in **Scheme 6.1** reactions of two mole equivalents of the protonated ligands, $[CH\{P(S)Ph_2\}_3]$ and $[CH(PPh_2)(P(S)Ph_2)_2]$, with the chlorobridged dimers, $[M(Cod)(\mu\text{-}Cl)]_2$ (M = Rh or Ir) or $[MCl(PEt_3)(\mu\text{-}Cl)]_2$ (M = Pt or Pd), proceed smoothly under mild conditions, in the presence of sodium tetrafluoroborate. The reactions result in the cleavage of the chloro bridges and the formation of the complex cations, $[M(Cod)\{CH(P(S)Ph_2)_3\}]^+$ (M = Rh or Ir) and $[Mcl(PEt_3)\{CH(PPh_2)(P(S)Ph_2)_2\}]^+$ (M = Pt or Pd), isolated as the tetrafluoroborate salts.

The synthesis scheme for the formation of complexes with the deprotonated ligands is shown in **Scheme 6.2**.

In the presence of a weak base, such as diethylamine, reactions of two molar equivalents of the free ligands, $[CH(P(S)Ph_2)_3]$ and $[CH(PPh_2)(P(S)Ph_2)_2]$, with the chlorobridged complexes, $[ML(\mu\text{-}Cl)]_2$ (M = Rh or Ir, L = Cod; M = Pt, L = MeoCod), $[PtCl(PEt_3)(\mu\text{-}Cl)]_2$, and $[Pd(\eta^3\text{-}C_4H_7)(\mu\text{-}Cl)]_2$, all result in the cleavage of the chlorobridges and loss of the ligand's methine proton to form the neutral complexes, $[ML\ L'\{C(P(S)Ph_2)_3\}]$ (M = Rh or Ir, L, L' = Cod; M = Pd, L, L' = η^3-C_4H_7) and $[ML\ L'\{C(P(S)Ph_2)_3\}]$ (M = Rh or Ir, L, L' = Cod; M = Pd, L, L' = η^3-C_4H_7; M = Pt, L, L' = MeoCod; M = Pt, L = Cl, L' = PEt_3).

Structural analyses of the complexes synthesised were mainly achieved by $^{31}P\{^1H\}$ NMR spectroscopy. Variable temperature $^{31}P\{^1H\}$ NMR was utilised to analyse complexes exhibiting dynamic intramolecular exchange processes in solution. The details of these analyses have been presented throughout this thesis. The solid-state structures of several complexes were determined by X-ray diffraction methods and the details of these

studies are presented in this thesis. The following is a summary of the studies, together with the current literature knowledge of the subject.

Scheme 6.2 Synthetic Route for the Complexes of $[CH(PPh_2)(P(S)Ph_2)_2]^-$ and $[C(P(S)Ph_2)_3]^-$

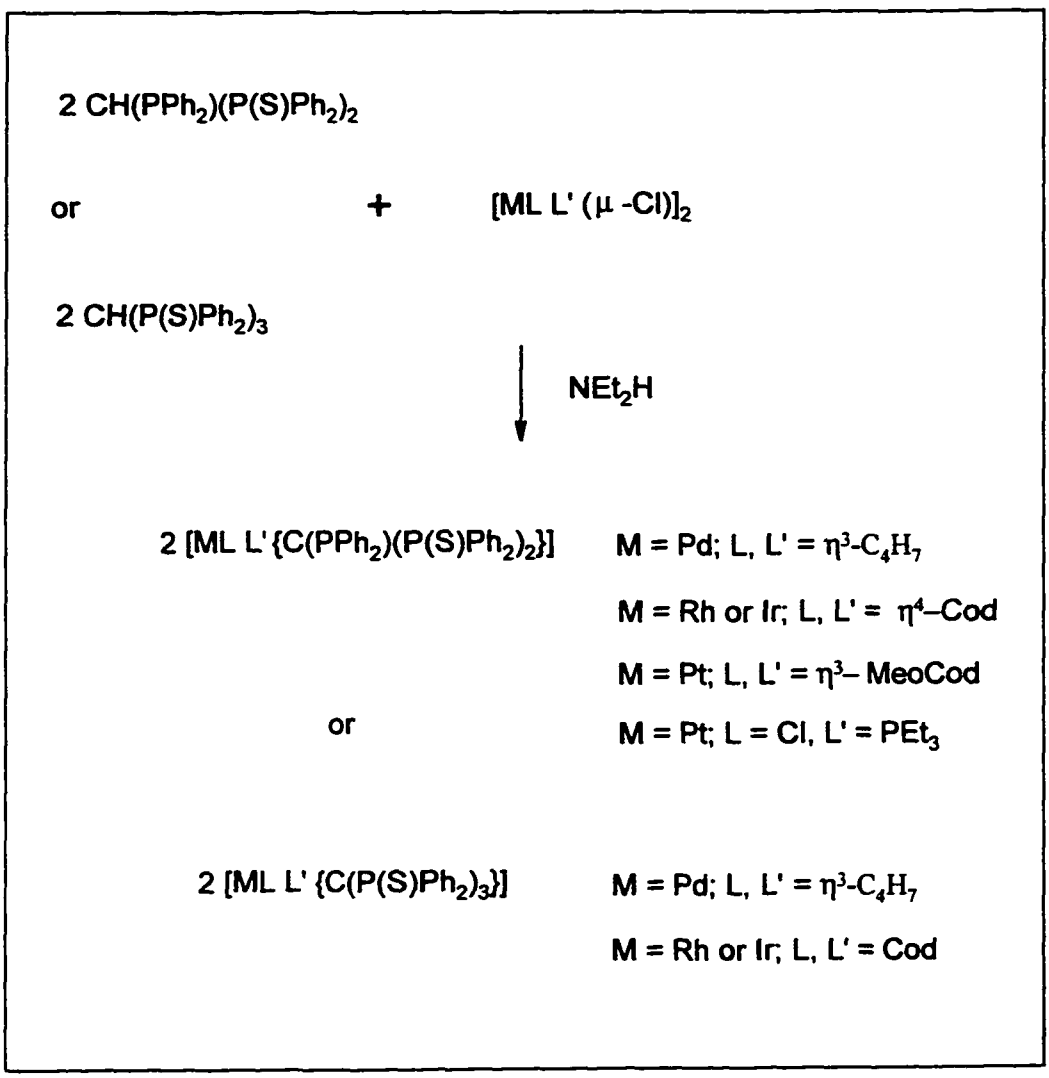

As was discussed earlier, in the Chapter one [51, 52, 53, and 54] $[C(P(S)Ph_2)_3]^-$ has been observed to coordinate to soft metal centres [48, 49], such as Hg^{2+}, Ag^+, Au^+ and Pt^{2+}, either in a bidentate fashion [49, 52, and 54], or a tridentate fashion [48, 51, and 53]. Our work has so far demonstrated η^2- *S,S* coordination via two P=S groups in complexes of palladium, platinum, rhodium, and iridium. This bidentate mode of bonding is not surprising considering the strong preference for four-coordinate, square planar geometry exhibited by Pd(II), Pt(II), Rh(I), and Ir(I) metal centres. It is interesting to note that only one complex with the related ligand, $[C(P(O)Ph_2)_3]^-$, has been reported in which it is bonded to the metal in a tridentate fashion [59]. However the proposed structure of $[\{(P(O)Ph_2)_3C\}IrH_2(SiR_3)_2]$ is based only on NMR data and an X-ray structure has not been determined [59]. It is believed that tridentate coordination is unfavourable because of the high steric crowding of the six phenyl rings caused by the small sizes of the coordinating oxygen atoms. Also the preference for planarity of the methine carbon would introduce considerable strain if tridentate coordination were to occurr. In contrast the larger size of the sulphur atom is believed to reduce the steric crowding in $[C(P(S)Ph_2)_3]^-$, thus making tridentate coordination more favourable and such a mode of coordination has been observed in complexes of Hg^{2+} [48] and Ag^+ [51].

We also reported the first X-ray structure determination of a complex containing the protonated ligand, $[CH(P(S)Ph_2)_3]$. In all previous reactions of this ligand [48-57] the complexes which were isolated contained the anionic ligand $[C(P(S)Ph_2)_3]^-$ because the methine hydrogen becomes more acidic upon coordination to the metal centre and is easily removed. The palladium complex, $[Pd(\eta^3\text{-}C_4H_7)\{CH(P(S)Ph_2)_3\}]BF_4$, has also been fully

analysed by NMR spectroscopy. The solid state structure of the compound shows the ligand to coordinate to the palladium centre via all three sulphur atoms. In solution, the $^{31}P\{^{1}H\}$ NMR gave only a singlet at room temperature suggestive of a dynamic exchange process between the coordinated sulphur atoms. Unfortunately, cooling the solution to -90 °C did not significantly change the spectrum. This observation suggests the complex is either five-coordinate, or four-coordinate with a facile dynamic exchange between the coordinated sulphur atoms and the non-coordinated sulphur atom. Similar observations of the $^{31}P\{^{1}H\}$ NMR were made for the complexes $[M(Cod)\{CH(P(S)Ph_2)_3\}]BF_4$ (M = Rh or Ir) discussed in detail in Chapter Three. Again the spectra could be interpreted in terms of the ligand being tridentate or bidentate with rapid exchange of the coordinated and uncoordinated sulphur atoms. The apparent preference for tridentate coordination by the protonated ligand can be at least partly explained by the geometry around the methine carbon. The tetrahedral geometry and sp^3 hybridisation of the carbon atom should result in significantly less strain on the chelate ligand as compared to the strain on the sp^2 hybridised methine carbon in the deprotonated ligand. This is best illustrated by the two palladium complexes, $[Pd(\eta^3\text{-}C_4H_7)\{C(P(S)Ph_2)_3\}]$ and $[Pd(\eta^3\text{-}C_4H_7)\{CH(P(S)Ph_2)_3\}]^+$, described in more detail in Chapter Two. In the former complex the ligand is bonded in an η^2-*S,S* fashion whereas in the latter the bonding is η^3-*S,S,S* , as shown in **Figure 6.1**.

Figure 6.1 Coordination Modes in $[Pd(\eta^3\text{-}C_4H_7)\{C(P(S)Ph_2)_3\}]$ and $[Pd(\eta^3\text{-}C_4H_7)\{CH(P(S)Ph_2)_3\}]^+$

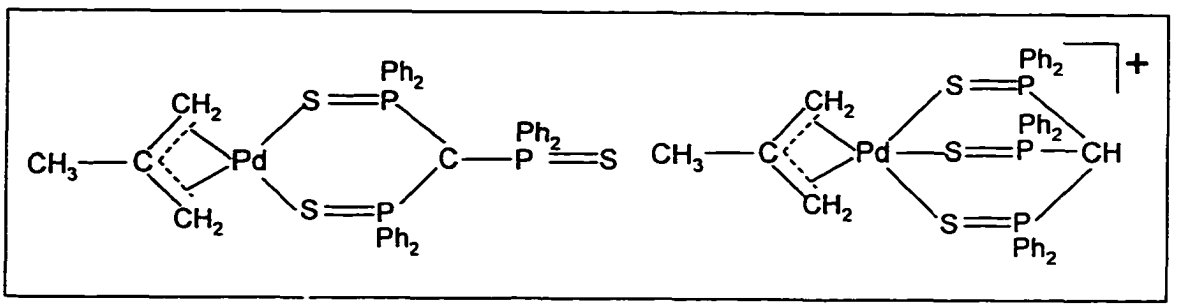

Quite similar structures have been observed in complexes containing the ligands, $[CH(PPh_2)(P(S)Ph_2)_2]$ and $[C(PPh_2)(P(S)Ph_2)_2]^-$ which were discussed in detail in Chapters Two, Four, and Five. All the complexes of palladium, platinum, rhodium, and iridium containing the deprotonated ligand, $[C(PPh_2)(P(S)Ph_2)_2]^-$, have shown a preference for η^2-P,*S* bidentate coordination (Chapters 2, 4, and 5). However, the protonated ligand, $[CH(PPh_2)(P(S)Ph_2)_2]$, can either coordinate in an η^2-*P,S* mode, as in $[Pd(\eta^3\text{-}C_4H_7)\{CH(PPh_2)(P(S)Ph_2)_2]BF_4$, or an η^3-*P,S,S* mode, as in the case of $[Ir(Cod)\{CH(PPh_2)(P(S)Ph_2)_2\}]BF_4$. These two different modes of coordination are illustrated in **Figure 6.2**.

Figure 6.2 Coordination Modes of $[CH(PPh_2)(P(S)Ph_2)_2]$ in Palladium and Iridium Complexes

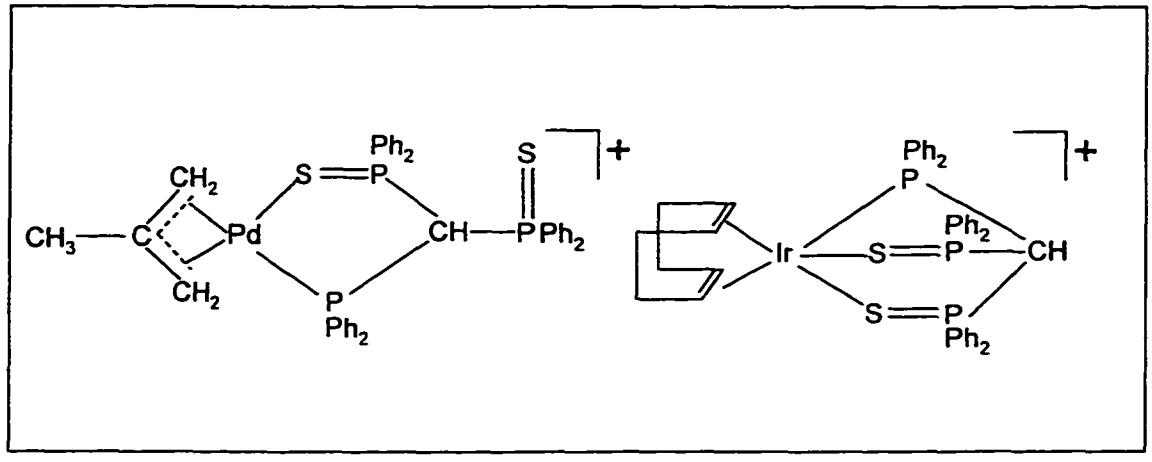

The apparent preference for tridentate coordination shown by $[CH(P(S)Ph_2)_3]$ as compared to $[CH(PPh_2)(P(S)Ph_2)_2]$ can probably be best explained by steric considerations. In the latter ligand the coordinated phosphorus has two phenyl groups which increase the steric crowding around the metal centre, thus discouraging coordination of a second sulphur atom. This crowding effect should be greater than in complexes of $[CH(P(S)Ph_2)_3]$ where only the sulphur atoms coordinate. Overall, in terms of preference of bidentate coordination to tridentate coordination of the ligands, the following sequence is suggested:

$[C(PPh_2)(P(S)Ph_2)_2]^- > [C(P(S)Ph_2)_3]^- > [CH(PPh_2)(P(S)Ph_2)_2] > [CH(P(S)Ph_2)_3]$

We have also examined the fluxional behaviours of $[Pd(\eta^3\text{-}C_4H_7)\{CH(PPh_2)(P(S)Ph_2)_2\text{-}P,S\}]BF_4$, $[Pd(\eta^3\text{-}C_4H_7)\{C(P(S)Ph_2)_3\text{-}S,S\}]$, $[Pt(MeoCod)\{C(P(S)Ph_2)_3\text{-}S,S\}]$, and $[Rh(Cod)\{C(P(S)Ph_2)_3\}]$ in detail. The thermodynamic parameters have been measured by NMR spectra band-shape analysis using the DNMR3 program [69]. The rate data were used to determine Eyring [70, 71] and Arrhenius [72] plots.

There is an increasing interest in understanding the solution structures and fluxional behaviours of palladium π-allyl compounds because they not only may be related to catalytic properties, such as precursors or intermediates in some catalytic reactions [118-121], but also they may be intermediates in synthetic processes leading to optically active derivatives [122-126]. There have been a number of mechanisms proposed to explain the exchange processes in transition metal allyl complexes [127 - 134, 73-85]. Some rotation of the allyl ligand in its plane about the axis containing the metal centre is often proposed to account for interchanges occurring in complexes of metals such as Mo, W, and Fe [127-133]. However, because of a high activation energy barrier encountered in square planar geometries, as estimated by orbital considerations [134], a simple rotation of the allyl ligand cannot be used to explain the fluxional behaviour in the square-planar palladium allyl complexes. A pentacoordinate activated intermediate was proposed as well [84,85]. Dissociative pathways have also been suggested to explain the fluxional behaviour. These include palladium allyl complexes with monodentate ligands [73-79] and

also N-donor chelate ligands [80,81].

Our studies on the fluxional behaviour of the palladium allyl complexes, $[Pd(\eta^3\text{-}C_4H_7)\{CH(PPh_2)(P(S)Ph_2)_2\text{-}P,S\}]BF_4$ and $[Pd(\eta^3\text{-}C_4H_7)\{C(P(S)Ph_2)_3\text{-}S,S\}]$ by $^{31}P\{^1H\}$ VT NMR support a tricoordinated palladium transition state being involved in $[Pd(\eta^3\text{-}C_4H_7)\{CH(PPh_2)(P(S)Ph_2)_2\text{-}P,S\}]BF_4$ and a pentacoordinated palladium transition state in $[Pd(\eta^3\text{-}C_4H_7)\{C(P(S)Ph_2)_3\text{-}S,S\}]$. The mechanisms proposed are those shown in **Schemes 2.4** and **2.6** in Chapter Two of this thesis. A similar mechanism involving a tricoordinate intermediate can also be used to explain the fluxionality of $[Pt(MeoCod)\{C(P(S)Ph_2)_3\text{-}S,S\}]$, which has a large positive ΔS^{o*} value of 98 J/K. However, a substantial negative ΔS^{o*} value (-27 J/K) was obtained with $[Rh(Cod)\{C(P(S)Ph_2)_3\}]$, for the process involving exchange between coordinated P=S and noncoordinated P=S groups, suggesting an associative pathway in which a pentacoordinate intermediate forms. In principle we could use the high resolution 360 MHz NMR instrument in the Department to design certain ^1H 2D-NOESY experiments at temperatures below and above the coalescence temperature to observe possible rupture of the Pd-S bond and thus confirm the tricoordinate palladium intermediate proposed, as was recently reported by Elguero et al [82]. Phase sensitive ^1H 2D-NOESY experiments examining NOEs of the *Cod* protons and phenyl protons, above and below the coalescence temperature could yield some definite evidence as to which pathway the exchange process takes place.

We can also conclude from the $^{31}P\{^1H\}$ VT NMR studies of various palladium allyl complexes of the ligands $[CH(P(S)Ph_2)_3]$, $[C(P(S)Ph_2)_3]^-$, $[CH(PPh_2)(P(S)Ph_2)_2]$, and

$[C(PPh_2)(P(S)Ph_2)_2]^-$, that the order of decreasing energy barrier around the P-C bond in these complexes (i.e. the exchange between the coordinated and the non-coordinated $Ph_2P{=}S$ groups) is:

$$[C(PPh_2)(P(S)Ph_2)_2]^- > [C(P(S)Ph_2)_3]^- > [CH(PPh_2)(P(S)Ph_2)_2] > [CH(P(S)Ph_2)_3]$$

This sequence is supported by the $\Delta G^{\circ *}$ values, calculated from Eyring [70,71] plots using rate data obtained from NMR simulation of the DNMR3 program[69] for $[Pd(\eta^3\text{-}C_4H_7)\{C(P(S)Ph_2)_3\}]$ (48 kJ/mol) and $[Pd(\eta^3\text{-}C_4H_7)\{C(PPh_2)(P(S)Ph_2)_2\}]$ (38 kJ/mol) and the fact that $[Pd(\eta^3\text{-}C_4H_7)\{C(PPh_2)(P(S)Ph_2)_2\text{-}P,S\}]$ is a rigid four-coordinate complex with the tripodal ligand bonding in bidentate mode indicating a large energy barrier, whereas a fast exchange makes all three phosphorus nuclei equivalent in $[Pd(\eta^3\text{-}C_4H_7)\{CH(PPh_2)(P(S)Ph_2)_2\text{-}P,S\}]BF_4$, even to -90 °C, indicating a rather small energy barrier for the C-P rotation. This sequence can also be extended to the other platinum group metals, such as iridium, rhodium, and platinum, with these ligands. This is mainly because a lower energy barrier would be required to allow rotation about the phosphorus to methine carbon bond (i.e. exchange between the coordinated and non-coordinated $Ph_2P{=}S$ groups) for the tetrahedral geometry in the protonated complexes than that for the trigonal planar geometry in the deprotonated complexes. Secondly, it is noted that the energy barrier for rotation around the P-C bond in the free ligand is 29 kJ/mol for $[CH(PPh_2)(P(S)Ph_2)_2]$, and 49 kJ/mol for $[CH(P(S)Ph_2)_3]$ [45].

This difference was explained by the increased steric repulsion of an additional sulphur atom on the phosphorus atom in the latter ligand compared to a lone pair in the former ligand [45]. However when the ligands are coordinated to the metals, the ease of rotation around the P-C bond is not only decided by the ligand itself, but also by the metal centre and the mode of coordination. In the palladium allyl cases, the 5-membered chelate rings in $[Pd(\eta^3\text{-}C_4H_7)\{C(PPh_2)(P(S)Ph_2)_2\}]$ are more strained than the six-membered chelate rings in $[Pd(\eta^3\text{-}C_4H_7)\{C(P(S)Ph_2)_3\}]$, as observed by the rigidity of the former complex and the fluxionality of the latter. Similar observations and comparisons can be made in the cases of $[Rh(Cod)\{C(PPh_2)(P(S)Ph_2)_2\}]$ and $[Rh(Cod)\{C(P(S)Ph_2)_3\}]$, where the former is rigid with η^2-P,S coordination and the later undergoes dynamic exchange between the coordinated $Ph_2P{=}S$ and non-coordinated $Ph_2P{=}S$ groups at ambient temperature.

In many ways the work presented in this thesis represents a beginning rather than an end. The research has mainly focussed on a thorough investigation of the coordinating properties of the various ligands as well as their fluxional behaviour in solution. This knowledge has built a strong base for doing further work on this ligand system. We have made a number of references to the effect of the steric bulk of the phenyl group in influencing the mode of coordination of the ligand, especially for complexes formed with $CH(PPh_2)(P(S)Ph_2)_2$ in which one of the phosphorus atoms bonds directly to the metal. How would the use of less sterically demanding groups on the coordinating phosphorus influence the coordination of the ligand? To this end $CH(PMe_2)(P(S)Ph_2)_2$ would be a good choice. Also the consequences of substituting the soft-donor sulphur atoms with hard-donor atoms, such as oxygen, should be probed. The coordination properties of

$CH(PPh_2)(P(O)Ph_2)_2$ should be investigated.

The catalytic potential of some of these complexes may also present some intriguing possibilities. There has been intense interest over the past thirty years in producing homogeneous catalysts that are regioselective, or stereoselective, or even enantioselective. Many of the effective hydrogenation catalysts which have been discovered to date are rhodium phosphine catalysts, as in the most notable example, Wilkinson's catalyst[1]. Cationic complexes of rhodium(I) have been used as enantioselective hydrogenation catalysts [135]. For example rhodium(I) complexes containing chiral diphosphines, P-P* have been used to prepare a number of amino acid derivatives and panthothenic acid [136]. In fact, a well known catalyst precursor is $[Rh(Cod)(P\text{-}P^*)]^+$, which is activated by treatment in solution with hydrogen to give the active $[Rh(P\text{-}P^*)(solv)_2]^+$, where solv = solvent molecule such as methanol or acetone [137]. It would certainly be of interest to explore the catalytic potential of one of our complexes such as $[(Cod)Rh\{CH(PPh_2)(P(S)Ph_2)_2\}]^+$. How would the fluxional nature of the $CH(PPh_2)(P(S)Ph_2)_2$ ligand influence the catalytic properties (if any) of the cation? Numerous other fluxional complexes have been found to be catalytically active although the underlying reasons are not well understood [138]. However, in our own complexes we would expect the ligand to be able to accommodate changes in coordination number and stereochemistry which inevitably occur during the course of a catalytic cycle. In the $CH(PPh_2)(P(S)Ph_2)_2$ ligand system the ligand should be able to switch between η^1-*P*, η^2-*P,S*, and η^3-*P,S,S*, as demanded by the coordination requirements of the particular intermediate in the cycle. Also, if required, chiral analogues of these ligands would not be

difficult to prepare.

In conclusion then the coordination chemistry of some ligands of the general type $[PPh_2(X)][PPh_2(Y)][PPh_2(Z)]CH$ (X, Y, and Z are various combinations of chalcogens and lone pairs) and their related anions has been explored and have showed interesting coordination behaviour and fluxionality.

Chapter Seven

Experimental

Unless otherwise stated, all the experiments described in this thesis were carried out under an atmosphere of dry nitrogen using standard Schlenk tube techniques at ambient temperature (although most of the compounds are generally stable in air). The solvents were dried by the appropriate methods and distilled under nitrogen prior to their use.

Infrared spectra were recorded in KBr disks from 4000 to 600 cm^{-1} on a Perkin-Elmer 1320 spectrophotometer calibrated against the 1601 cm^{-1} absorption of polystyrene film. Microanalyses were carried out by the Canadian Microanalytical Service, Vancouver, B.C., Canada.

^{1}H, ^{31}P, ^{13}C and ^{195}Pt NMR spectra were recorded at 250.1, 101.3, 62.9 and 53.5 MHz respectively, using a Bruker WM 250 Fourier transform spectrometer, except that the variable temperature ^{31}P spectra of $[Rh(Cod)\{C(PPh_2)(P(S)Ph_2)_2\}]$ were obtained at 145.9 MHz using a Bruker AMX 360 spectrometer. Solvents used were $CDCl_3$, CD_2Cl_2 or CH_2Cl_2 and for the last a lock signal was derived from the deuterium resonance of a capillary insert containing C_6D_6. For ^{31}P and ^{13}C spectra, protons were decoupled by broad band irradiation at appropriate frequencies. ^{1}H and ^{13}C chemical shifts were measured relative to external tetramethylsilane. ^{31}P chemical shifts were measured relative to external trimethylphosphite and are reported in parts per million relative to 85% phosphoric acid using a conversion factor of +141 ppm. ^{195}Pt chemical shifts are reported as absolute frequency values (MHz) with reference to the proton resonance of tetramethylsilane at exactly 100 MHz. Coupling constants are in Hertz (Hz). For all

nuclei, positive chemical shifts are downfield of the reference. Lineshapes for the dynamic ^{31}P NMR spectra were calculated using the DNMR3 program of Kleier and Binsch [69] .

Recrystallizations from solvent pairs were performed by dissolution of the complex in the first solvent (using about double the volume required for complete solution) followed by dropwise addition or layering of sufficient second solvent to cause turbidity at ambient temperature unless stated otherwise. The crystal structures were solved by Dr. J. Browning using either an Enraf-Nonius CAD4 or a Picker 4 circle diffractometer.

Most of the commonly used reagents, dppm, PPh_2Cl and $RhCl_3.3H_2O$ were purchased from Aldrich Chemical Ltd. K_2PtCl_4 and $(NH_4)_2IrCl_6$ were obtained by the recycling of laboratory residues by Dr. N.J. Meanwell. $PdCl_2$ and $PtCl_2$ were obtained from Johnson-Matthey Ltd. All reagents were used as supplied.

$CH(P(S)Ph_2)_3$ [45], $CH(PPh_2)(P(S)Ph_2)_2$ [45], $[Pd(\eta^3\text{-}C_4H_7)(\mu\text{-}Cl)]_2$ [94], $[Pd(PEt_3)(\mu\text{-}Cl)Cl]_2$ [138], $[Pt(PEt_3)(\mu\text{-}Cl)Cl]_2$ [139], $[Pt(MeoCod)(\mu\text{-}Cl)]_2$ [140], $[Rh(Cod)(\mu\text{-}Cl)]_2$ [141], and $[Ir(Cod)(\mu\text{-}Cl)]_2$ [142] were prepared as previously described.

$[Pd(\eta^3\text{-}C_4H_7)\{C(PPh_2)(P(S)Ph_2)_2\}]$

Dichloromethane (5 mL) was added, with stirring, to a mixture of

$CH(PPh_2)(P(S)Ph_2)_2$ (0.080 g, 0.13 mmol) and $[Pd(\eta^3\text{-}C_4H_7)(\mu\text{-}Cl)]_2$ (0.025 g, 0.063 mmol) to give a yellow solution. After 5 minutes a few drops of diethylamine (ca. 0.2 mL) were added, resulting in the formation of a white precipitate. The solvent was removed *in vacuo*. The residue was extracted with toluene (10 mL) and the extract filtered through a glass sinter with celite to give a clear yellow solution. The solvent was removed from the extract *in vacuo*, and the residue washed with hexanes (3 x 5 mL) and recrystallized from dichloromethane and hexanes to give $[Pd(\eta^3\text{-}C_4H_7)\{C(PPh_2)(P(S)Ph_2)_2\}]$ as bright yellow crystals (0.055 g, 0.069 mmol). Yield: 53%. Anal. Found: C, 61.2; H, 4.73. Calc. for $C_{41}H_{37}PdP_3S_2$: C, 62.1; H, 4.67%. $^{31}P\{^1H\}$ NMR data are presented in **Table 2.1**. The $^{31}P\{^1H\}$ NMR spectrum is shown in **Figure 2.2**.

$[Pd(\eta^3\text{-}C_4H_7)\{CH(PPh_2)(P(S)Ph_2)_2\}]BF_4$

Sodium tetrafluoroborate (0.016 g, 0.15 mmol), in a mixture of water and ethanol (2 mL) was added to a stirred solution of $[Pd(\eta^3\text{-}C_4H_7)(\mu\text{-}Cl)]_2$ (0.029 g, 0.073 mmol) and $CH(PPh_2)(P(S)Ph_2)_2$ (0.092 g, 0.15 mmol) in dichloromethane (10 mL). After 10 minutes the solvent was removed *in vacuo*. The residue was dissolved in dichloromethane (10 mL) and stirred with anhydrous magnesium sulphate and then filtered to give a clear yellow solution. Solvent was removed from the extract *in vacuo* and the residue crystallized from dichloromethane and hexanes to yield $[Pd(\eta^3\text{-}C_4H_7)\{CH(PPh_2)(P(S)Ph_2)_2\}]BF_4$ as yellow crystals (0.075 g, 0.086 mmol). Yield:

57%. Anal. Found: C, 55.5; H, 4.75. Calc. for $C_{41}H_{38}BF_4PdP_3S_2$: C, 55.9; H, 4.32%. Infrared: 1090(s), 1075(s), 1050(br) cm^{-1}. $^{31}P\{^1H\}$ NMR data are presented in **Table 2.1**. ^1H NMR dta are shown in **Table 2.1** and the spectrum is shown as **Figure 2.1(B)**. (δ, CD_2Cl_2), 2.3 (s, 3H, -CH_3), 3.6 (s, 2H, -CH_2), 4.3 (s, 2H, CH_2-), 6.1 (q, 1H, C(1)*H*), 7 - 8 (m, 30H, aromatic *H*). The X-ray structure is shown in **Figure 2.7** and related data are presented in **Tables 2.7, 2.8,** and **2.9** along with **Appendix Tables I, II,** and **III**.

$[Pd(\eta^3\text{-}C_4H_7)\{C(P(S)Ph_2)_3\}].CH_2Cl_2$

This preparation was similar to that described for $Pd(\eta^3\text{-}C_4H_7)\{C(PPh_2)(P(S)Ph_2)_2\}$ and gave $[Pd(\eta\text{-}C_4H_7)\{C(P(S)Ph_2)_3\}].CH_2Cl_2$ as orange crystals. Yield: 64%. Anal. Found: C, 55.8; H, 4.46. Calc. for $C_{42}H_{39}Cl_2PdP_3S_3$: C, 55.4; H, 4.29%. $^{31}P\{^1H\}$ NMR data are presented in **Table 2.2**.

$[Pd(\eta\text{-}C_4H_7)\{CH(P(S)Ph_2)_3\}]BF_4$

Sodium tetrafluoroborate (0.009 g, 0.08 mmol), in acetone (2 mL), was added to a stirred solution of $[Pd(\eta^3\text{-}C_4H_7)(\mu\text{-}Cl)]_2$ (0.017 g, 0.042 mmol) and $CH(P(S)Ph_2)_3$ (0.056 g, 0.084 mmol) in acetone (20 mL). After one hour the solvent was removed *in vacuo* and the residue was extracted with dichloromethane (10 mL) to remove precipitated sodium chloride. The solvent was removed from the extract *in vacuo*, and the

resulting residue crystallized from dichloromethane and hexanes to yield $[Pd(\eta^3\text{-}C_4H_7)\{CH(P(S)Ph_2)_3\}]BF_4$ as yellow crystals (0.050 g, 0.055 mmol). X-ray quality crystals were obtained by vapour diffusion of diethyl ether with a dichloromethane solution of the complex. Yield: 65%. Anal. Found: C, 53.4; H, 4.11. Calc. for $C_{41}H_{38}BF_4PdP_3S_3$: C, 54.0; H, 4.17%. $^{31}P\{^1H\}$ NMR data are presented in **Table 2.2**. ^1H NMR data are presented in **Table 2.2** and the actual spectrum is shown in **Figure 2.1(A)**. (δ, CD_2Cl_2), 2.1(s, 3H, -C*H*$_3$), 3.2 (s, 2H, =C*H*$_2$), 4.2 (s, 2H, =C*H*$_2$), 7-8 (m, 30H, aromatic). The X-ray structure is shown in **Figures 2.8** and **2.9** and related data are presented in **Tables 2.7, 2.11, 2.12, 2.13,** and in the **Appendix Tables IV** and **V**.

$[Rh(Cod)\{CH(P(S)Ph_2)_3\}]BF_4$

$CH\{P(S)Ph_2\}_3$ (0.26 g, 0.40 mmol), in acetone (20 mL), was added to a stirred solution of $[Rh(Cod)(\mu\text{-}Cl)]_2$ (0.10 g, 0.20 mmol) and sodium tetrafluoroborate (0.045 g, 0.41 mmol) in acetone (20 mL). The solution immediately became cloudy and changed in colour from yellow to orange. After one hour the solution was filtered to remove precipitated sodium chloride. Removal of the solvent from the filtrate *in vacuo* and crystallisation of the resulting residue from dichloromethane and hexanes yielded the product as orange crystals (0.28 g, 0.29 mmol). Yield: 72%. Anal. found: C, 55.4; H, 4.44. Calc. for $C_{45}H_{43}BF_4RhP_3S_3$: C, 56.2; H, 4.50%. $^{31}P\{^1H\}$ NMR data are presented in **Table 3.2**. ^1H NMR data are presented in **Table 3.2**. ^{13}C NMR data are presented in **Table 3.2**.

[Ir(Cod){CH(P(S)Ph$_2$)$_3$}]ClO$_4$

This preparation was very similar to that described above for the rhodium analogue except that NaClO$_4$·H$_2$O was used in place of NaBF$_4$. The product was isolated as yellow crystals in 78% yield. Anal. found: C, 51.0; H, 4.32. Calc. for $C_{45}H_{43}ClIrO_4P_3S_3$: C, 50.8; H, 4.07%. $^{31}P\{^1H\}$ NMR data are presented in **Table 3.2**. ^1H NMR data are presented in **Table 3.2**. ^{13}C NMR data are presented in **Table 3.2**.

[Rh(Cod){C(P(S)Ph$_2$)$_3$}]

Dichloromethane (10 mL) was added, with stirring, to a mixture of CH{P(S)Ph$_2$}$_3$ (0.13 g, 0.20 mmol) and [Rh(Cod)(μ-Cl)]$_2$ (0.048 g, 0.010 mmol) to give a yellow solution. After five minutes a few drops of diethylamine (ca. 0.2 mL) were added. The solvent was removed and the residue extracted into toluene (10 mL). Removal of the solvent and crystallisation of the resulting residue from dichloromethane and hexanes yielded the product as yellow crystals (0.12 g, 0.14 mmol). Yield: 70%. Anal. found: C, 61.5; H, 4.86. Calc. for $C_{45}H_{42}RhP_3S_3$: C, 61.8, H, 4.84%. $^{31}P\{^1H\}$ NMR data are presented in **Table 3.1**. The X-ray structure is shown in **Figure 3.6** and related data in **Tables 3.9, 3.10, 3.11**, and **Appendix Tables VI** and **VII**.

[Ir(Cod){C(P(S)Ph$_2$)$_3$}]

This preparation was similar to the rhodium analogue described above and gave the product as yellow crystals in 66% yield. Anal. found: C, 55.9; H, 4.55. Calc. for $C_{45}H_{42}IrP_3S_3$: C, 56.1; H, 4.39%. $^{31}P\{^1H\}$ NMR data are presented in **Table 3.1**.

[Ir(CO)$_2${C(P(S)Ph$_2$)$_3$}]

Carbon monoxide was bubbled through a solution of [Ir(Cod){C(P(S)Ph$_2$)$_3$}] (0.10 g, 0.10 mmol) in toluene (25 mL) for about one minute. During this time the solution turned a noticeably paler shade of yellow. The solvent was removed *in vacuo* and the residue washed with hexanes (3 x 5 mL) and then crystallised from dichloromethane and hexanes to give the product as pale yellow crystals (0.060 g, 0.066 mmol). Yield: 60%. Anal. found: C, 51.0; H, 3.33. Calc. for $C_{39}H_{30}IrO_2P_3S_3$: C, 51.4; H, 3.32%. Infra red (KBr): 2040(s), 1965(s,br) cm^{-1}. $^{31}P\{^1H\}$ NMR data are presented in **Table 3.1**. The X-ray structure is shown in **Figure 3.7** and related data is given in **Tables 3.9, 3.12, 3.13**, and **Appendix Tables VIII** and **IX**.

[Pt(MeoCod){C(P(S)Ph$_2$)$_3$}]

Acetone (15 mL) was added to [Pt(MeoCod)(μ-Cl)]$_2$ (0.100 g, 0.136 mmol) and

sodium tetrafluoroborate (0.032 g, 0.29 mmol). After stirring the mixture for 10 minutes, $[CH(P(S)Ph_2)_3]$ (0.179 g, 0.270 mmol) was added as a powder to the solution. Following one hour of stirring, the solvent was removed *in vacuo* and the pale yellow residue extracted into toluene (15 mL) and the solution filtered. The solvent was then removed under vacuum and the resulting yellow solid dissolved in tetrahydrofuran (1 mL). Addition of hexanes caused the precipitation of the product as a yellow powder in 94% yield (0.25 g). Attempted recrystallisation failed to produce a product suitable for elemental analysis. $^{31}P\{^1H\}$ NMR data are presented in **Table 3.3**

$[Ir(Cod)\{C(PPh_2)(P(S)Ph_2)_2$-*P,S*$\}]\cdot CH_2Cl_2$

$CH(PPh_2)(P(S)Ph_2)_2$ (0.19 g, 0.30 mmol) was added to a stirred solution of $[Ir_2Cl_2(Cod)_2]$ (0.10 g, 0.15 mmol) in dichloromethane (10 mL). Diethylamine (0.2 mL) was added. After 10 minutes the solvent was removed in vacuo and the residue extracted with toluene (20 mL). The solvent was removed from extract *in vacuo* and the resulting residue recrystallized from dichloromethane / hexanes to give $[Ir(Cod)\{C(PPh_2)(P(S)Ph_2)_2$-*P,S*$\}].CH_2Cl_2$ as orange crystals (0.18 g, 0.18 mmol). Anal. Calcd. for $C_{46}H_{44}Cl_2P_3S_2Ir$: C, 54.3; H, 4.36. Found: C, 54.1; H, 4.43%. $^{31}P\{^1H\}$ NMR data are presented in **Table 4.1**.

[Rh(Cod){C(PPh$_2$)(P(S)Ph$_2$)$_2$-*P,S*}].CH$_2$Cl$_2$

This complex was prepared by a procedure similar to that used above for the iridium analogue. [Rh(Cod){C(PPh$_2$)(P(S)Ph$_2$)$_2$-*P,S*}].CH$_2$Cl$_2$ was obtained as yellow crystals in 80% yield. Anal. Calcd. for $C_{46}H_{44}Cl_2P_3S_2Rh$: C, 59.6; H, 4.78. Found: C, 59.9; H, 5.55%. $^{31}P\{^1H\}$ NMR data are presented in **Table 4.1**. The X-ray structure is shown in **Figure 4.1** and related data are given in **Tables 4.4, 4.5, 4.6,** and **Appendix Tables X** and **XI.**

[Rh(^{t}BuNC)$_2${C(PPh$_2$)(P(S)Ph$_2$)$_2$-*P,S*}]. CH$_2$Cl$_2$

A solution of tertiarybutylisocyanide (0.2 g, 2.4 mmol) in dichloromethane (2 mL) was added dropwise to a stirred solution of [Rh(Cod){C(PPh$_2$)(P(S)Ph$_2$}] (1.0 g, 1.1 mmol) in dichloromethane (50 mL). After 5 minutes the solvent was removed *in vacuo* and the residue crystallized by layering a dichloromethane solution with hexanes to give [Rh(^{t}BuNC)$_2${C(PPh$_2$)(P(S)Ph$_2$)$_2$-*P,S*}]. CH$_2$Cl$_2$ as yellow crystals (0.76 g, 0.77 mmol). Anal. Calcd. for $C_{48}H_{50}Cl_2N_2P_3S_2Rh$: C, 58.5; H, 5.11. Found: C, 59.0; H, 5.18%. IR: υ(CN) 2140s, 2100s, 2070sh cm^{-1}. $^{31}P\{^1H\}$ NMR data are presented in **Table 4.1**.

[Ir(^{t}BuNC)$_2${C(PPh$_2$)(P(S)Ph$_2$)$_2$-*P,S*}]. *solvent*

This complex was prepared by a procedure similar to that used above for the

rhodium analogue, $[Rh(^tBuNC)_2\{C(PPh_2)(P(S)Ph_2)_2\text{-}P,S\}]$. CH_2Cl_2. $[Ir(^tBuNC)_2\{C(PPh_2)(P(S)Ph_2)_2\text{-}P,S\}]$. *solvent* was obtained as pale-yellow crystals in 55% yield. Anal. Calcd. for $C_{48}H_{50}Cl_2N_2P_3S_2Ir$ (CH_2Cl_2 as *solvent*): C, 53.6; H, 4.65. Found: C, 48.9; H, 4.80%. $^{31}P\{^1H\}$ NMR data are presented in **Table 4.1**.

$[RhI_2(^tBuNC)_2\{C(PPh_2)(P(S)Ph_2)_2\text{-}P,S\}]$

A solution of diiodine (0.060 g, 0.24 mmol) in toluene (5 mL) was added dropwise to a solution of $[Rh(^tBuNC)_2\{C(PPh_2)(P(S)Ph_2)_2\text{-}P,S\}]$ (0.212 g, 0.240 mmol) in toluene (10 mL) and dichloromethane (5 mL) at -60 °C. After 5 minutes the solution was warmed for a further 5 minutes to ambient temperature giving an initial mixture which contained at least three compounds (^{31}P NMR). After stirring for 4 hours, a stable mixture of two isomers was obtained. The solvent was removed *in vacuo*, and the residue recrystallized from dichloromethane / hexanes to give $[RhI_2(^tBuNC)_2\{C(PPh_2)(P(S)Ph_2)_2\text{-}P,S\}]$ (isomer(i)) as red crystals (0.080 g, 0.069 mmol). Anal. Calcd. for $C_{47}H_{48}I_2N_2P_3S_2Rh$: C, 48.9; H, 4.19. Found: C, 48.4; H, 4.17%. IR: υ(CN) 2157s cm^{-1}. A second isomer, isomer (ii), was present in the supernatant from the recrystallization. $^{31}P\{^1H\}$ NMR data are presented in **Table 4.1**. The X-ray structure is shown in **Figure 4.2** and related data are given in **Tables 4.7, 4.8**, and in **Appendix Tables XII** and **XII.**

[RhBr(CH_2Ph)(^tBuNC)$_2${C(PPh_2)(P(S)Ph_2)$_2$-*P,S*}]

A solution of benzyl bromide (0.012 mL, 0.10 mmol) in dichloromethane (1 mL) was added dropwise to a solution of [Rh(^{t}BuNC)$_2${C(PPh_2)(P(S)Ph_2)$_2$-*P,S*}] (0.087 g, 0.10 mmol) in dichloromethane (10 mL). A ^{31}P NMR spectrum recorded almost immediately showed the single isomer (isomer(i)). After 10 minutes a second isomer, isomer(ii), was found to be present. Removal of the solvent *in vacuo*, followed by recrystallization of the residue from dichloromethane / diethyl ether gave crystalline isomer(i), with isomer(ii) in the supernatant. Alternatively, addition of a few drops of methanol to the mixture gave complete conversion to isomer(ii) from isomer(i), but in neither case could crystals of sufficient quality for elemental analysis be isolated. $^{31}P\{^1H\}$ NMR data are presented in **Table 4.1**.

[PtCl(PEt_3){C(PPh_2)(P(S)Ph_2)$_2$-*P,S*}]

CH(PPh_2)(P(S)Ph_2)$_2$ (0.27 g, 0.42 mmol) was added to a stirred solution of [$Pt_2Cl_4(PEt_3)_2$] (0.16 g, 0.21 mmol) in dichloromethane (5 mL). Diethylamine (0.2 mL) was then added. After 5 minutes the solvent was removed *in vacuo* and the residue extracted with benzene (10 mL). The solvent was removed from the extract *in vacuo* and the resulting residue recrystallized from dichloromethane / diethyl ether to give [PtCl(PEt_3){C(PPh_2)(P(S)Ph_2)$_2$-*P,S*}] as yellow crystals. (0.33 g, 0.34 mmol). Anal. Calcd. for $C_{43}H_{45}ClP_4S_2Pt$: C, 52.7; H, 4.63. Found: C, 52.0; H, 4.48%. The product

contained both isomers (i) and (ii) in about a 10 : 1 ratio. $^{31}P\{^{1}H\}$ NMR data are presented in **Table 4.2**. The $^{31}P\{^{1}H\}$ NMR spectrum is shown in **Figure 5.1**. The ^{195}Pt NMR data are given in **Figure 5.1**.

[Pt(MeoCod){C(PPh$_2$)(P(S)Ph$_2$)$_2$-*P,S*}]

$CH(PPh_2)(P(S)Ph_2)_2$ (0.17 g, 0.27 mmol) was added to a stirred solution of $[Pt_2Cl_2(MeoCod)_2]$ (0.10 g, 0.14 mmol) in diethylamine (0.2 mL) was added. After 5 minutes the solvent was removed *in vacuo* and the residue extracted with toluene (5 mL). The solvent was removed from the extract *in vacuo* and the resulting residue recrystallized from dichloromethane / hexanes to give [Pt(MeoCod){C(PPh$_2$)(P(S)Ph$_2$)$_2$-*P,S*}] as colourless crystals (0.10 g, 0.10 mmol) characterized by ^{31}P and ^{195}Pt NMR spectroscopy. Isomer (i) and (ii) were present in about a 3 : 2 ratio. Attempts at recrystallization resulted in progressive decomposition so that we were unable to obtain good analytical data. ^{195}Pt NMR data are presented in **Table 4.3**.

[Ir(Cod){CH(PPh$_2$)(P(S)Ph$_2$)$_2$-*P,S,S*}]BF$_4$.CH$_2$Cl$_2$

A solution of $NaBF_4$ (0.033 g, 0.30 mmol) in 1 : 1 ethanol/water (2 mL) was added dropwise to a stirred solution of $CH(PPh_2)(P(S)Ph_2)_2$ (0.19 g, 0.30 mmol) and $[Ir(Cod)(\mu\text{-}Cl)]_2$ (0.10 g, 0.15 mmol) in dichloromethane (10 mL). After 10 minutes the

solvent was removed *in vacuo* and the residue extracted with dichloromethane (10 mL) and recrystallized from dichloromethane / hexanes to give $[Ir(Cod)\{CH(PPh_2)(P(S)Ph_2)_2\text{-}P,S,S\}]BF_4.CH_2Cl_2$ as orange crystals (0.25 g, 0.23 mmol). Anal. Found: C, 50.0; H, 4.23. Calc. for $C_{46}H_{45}BCl_2F_4P_3S_2Ir$: C, 50.0; H, 4.11%. $^{31}P\{^1H\}$ NMR data are presented in **Table 5.1**. The X-ray structure is shown in **Figure 5.3** and related data are presented in **Tables 5.3, 5.5,** and **Appendix Tables XVI** and **XVII**.

$[Rh(Cod)\{CH(PPh_2)(P(S)Ph_2)_2\text{-}P,S,S\}]BF_4$

Preparation of this complex was attempted by a procedure similar to that used above for the iridium analog. ^{31}P NMR spectra (see Results) indicated that the desired product was obtained but it was always contaminated by about 20% of the deprotonated complex, $[Rh(Cod)\{C(PPh_2)(P(S)Ph_2)_2\text{-}P,S]$, which was described in Chapter Four. Reaction of the deprotonated complex with acid (CF_3COOH) followed by base ($NHEt_2$) indicated that the complexes are readily interconverted, but we were unable to isolate pure samples of $[Rh(Cod)\{CH(PPh_2)(P(S)Ph_2)_2\text{-}P,S,S\}]BF_4$. $^{31}P\{^1H\}$ NMR data are presented in **Table 5.1**.

$[PdCl(PEt_3)\{CH(PPh_2)(P(S)Ph_2)_2\text{-}P,S\}]BF_4$

$CH(PPh_2)(P(S)Ph_2)_2$ (0.12 g, 0.19 mmol) was added to a stirred solution of $[Pd_2Cl_4(PEt_3)_2]$ (0.053 g, 0.09mmol) with $NaBF_4$ (0.022g, 0.20 mmol) in acetone (15 mL).

After 30 minutes the solvent was removed from the extract *in vacuo* and the resulting residue recrystallized from dichloromethane/hexanes to give $[PdCl(PEt_3)\{CH(PPh_2)(P(S)Ph_2)_2\text{-}P,S\}]BF_4$ as yellow crystals (0.14 g, 0.14 mmol). Anal. Found: C, 52.5; H, 4.49. Calc. for $C_{43}H_{46}BClF_4P_4S_2Pd$: C, 52.7; H, 4.73%. ^{31}P NMR spectra showed that the product was mainly the trans-isomer with about 15% of the *cis*-isomer. $^{31}P\{^1H\}$ NMR data are presented in **Table 5.2**.

$[PtCl(PEt_3)\{CH(PPh_2)(P(S)Ph_2)_2\text{-}P,S\}]BF_4$

This complex was prepared by a procedure similar to that used above for the palladium analog. $[PtCl(PEt_3)\{CH(PPh_2)(P(S)Ph_2)_2\text{-}P,S\}]BF_4$ was obtained as yellow crystals in 75% yield.. Anal. Found: C, 48.1; H, 4.24. Calc. for $C_{43}H_{46}BClF_4P_4S_2Pt$: C, 48.4 ; H, 4.34%. ^{31}P NMR spectra showed that the product was almost entirely the *trans*- isomer with only traces of the *cis* isomer. $^{31}P\{^1H\}$ NMR data are presented in **Table 5.2**. The $^{31}P\{^1H\}$ NMR spectrum is shown in **Figure 5.1**.

APPENDIX

CRYSTALLOGRAPHIC DATA

The crystal structures presented in this thesis were solved by Dr. J.Browning. In general, preliminary photographic work was carried out with Weisenberg and precession cameras using Cu-Kα radiation. After establishment of symmetry and approximate unit cells, the crystals were transfered to a Picker 4-circle diffractometer automated with a PDP11/10 computer and the unit cells refined by least squares methods employing pairs of centering measurements. Diffraction data were collected using a $\theta/2\theta$ step scan with 160 steps of 0.01° in 2θ, counting for 0.25 s per step. Background measurements were for 20 s at each end of the scan. Each batch of 50 reflections was preceded by the measurements of three standard reflections, and, after application of Lorentz and polarization factors, each batch was sealed to maintain the sum of the standard constants. Absorption corrections were applied by a numerical integration using a Gaussian grid and with the crystal shape defined by perpendicular distances to crystal faces from a central origin. There was no evidence of decomposition during the data collection. The structures were found and refined using the SHELX-76 program package [139], and illustrations were drawn using ORTEP [86]. The atomic scattering factors used were for neutral atoms with correction for anomalous dispersion. The structure was solved by direct methods, developed by standard Fourier synthesis procedures using difference maps, and refined by the method of least squares minimising $\Sigma W\Delta^2$ where $\Delta = |F_o| - |F_d|$. The weights were obtained from counting statistics using $W = 1/(\sigma^2(F) + 0.001F^2)$.

Table I Fractional Atomic Coordinates and Temperature Parameters for $[Pd(\eta^3\text{-}C_4H_7)\{CH(PPh_2)(P(S)Ph_2)_2\}]BF_4.2H_2O$

Atom	x/a	y/b	z/c	U_{eq}
Pd(1)	48172(9)	17885(10)	18687(4)	508(5)
S(1)	4668(3)	2454(4)	2552(1)	60(2)
S(2)	3185(3)	-241(4)	2447(2)	64(2)
P(1)	3034(3)	2824(3)	2223(1)	42(2)
P(2)	1836(3)	577(3)	2036(1)	44(2)
P(3)	2914(3)	1530(3)	1388(1)	42(2)
C(1)	2129(11)	1774(11)	1770(5)	41(6)
C(11)	2648(11)	3098(12)	2713(5)	53(7)
C(12)	3114(16)	2437(15)	3145(6)	79(10)
C(13)	2853(18)	2693(19)	3526(7)	93(12)
C(14)	2240(22)	3624(21)	3504(8)	105(15)
C(15)	1788(17)	4249(17)	3087(9)	88(12)
C(16)	1987(13)	4014(13)	2679(6)	63(8)
C(21)	2710(13)	4002(11)	1831(5)	48(7)
C(22)	3675(16)	4585(14)	1887(7)	80(11)
C(23)	3403(25)	5514(17)	1575(9)	122(17)
C(24)	2216(22)	5854(17)	1272(8)	102(13)
C(25)	1405(17)	5211(14)	1261(7)	81(10)
C(26)	1637(13)	4305(12)	1534(6)	56(8)
C(31)	1049(11)	975(12)	2357(5)	47(7)
C(32)	245(12)	1793(12)	2185(6)	58(7)
C(33)	-369(14)	2064(15)	2434(7)	79(10)

Atom	x/a	y/b	z/c	U_{eq}
C(34)	-161(16)	1469(17)	2864(8)	87(12)
C(35)	604(17)	680(18)	3034(7)	88(11)
C(36)	1248(14)	387(13)	2790(6)	68(9)
C(41)	806(11)	-134(11)	1507(5)	41(6)
C(42)	1005(13)	-1213(13)	1459(6)	57(8)
C(43)	183(17)	-1804(15)	1046(7)	78(11)
C(44)	-793(18)	-1271(16)	691(7)	79(11)
C(45)	-1008(13)	-182(16)	746(6)	67(8)
C(46)	-216(13)	393(13)	1170(6)	60(8)
C(51)	2616(11)	216(11)	1101(5)	42(7)
C(52)	1722(12)	29(12)	618(5)	48(7)
C(53)	1657(14)	-926(13)	400(6)	57(8)
C(54)	2458(17)	-1727(14)	634(7)	74(10)
C(55)	3347(14)	-1552(13)	1123(6)	65(9)
C(56)	3397(13)	-582(12)	1347(6)	55(8)
C(61)	2201(12)	2454(11)	874(5)	47(7)
C(62)	1032(14)	2552(14)	617(5)	62(8)
C(63)	495(16)	3303(14)	216(6)	72(9)
C(64)	1252(20)	3898(15)	84(7)	87(11)
C(65)	2369(21)	3785(16)	318(7)	92(12)
C(66)	2923(16)	3043(14)	738(7)	77(10)
C(71)	5437(15)	1053(18)	1388(8)	102(12)
C(72)	6679(13)	1787(15)	2232(7)	76(9)
C(73)	6230(15)	1874(18)	1696(9)	90(12)
C(74)	6392(20)	2776(23)	1442(9)	124(16)

Atom	x/a	y/b	z/c	U_{eq}
B(1)	-1607(14)	3476(17)	784(7)	148(19)
F(1)	-735(13)	3070(12)	1193(6)	204(13)
F(2)	-2505(14)	3618(21)	849(8)	289(20)
F(3)	-1832(18)	2804(23)	403(8)	438(26)
F(4)	-1268(16)	4430(16)	682(9)	279(22)
O(1)	5167(14)	870(14)	4244(6)	145(6)'
O(2)	4293(16)	1855(15)	4856(7)	164(7)'

Estimated standard deviations are given in parentheses.

Coordinates x 10^n where n = 5 for Pd and 4 otherwise.

Temperature parameters x 10^n where n = 4 for Pd and 3 otherwise.

U_{eq} = the equivalent isotropic temperature parameter = $1/3\ \Sigma_i\Sigma_j U_{ij}\ a_i^*\ a_j^*(a_i.a_j)$.

Primed values indicate that U_{iso} is given, where $T = \exp -(8\pi^2 U_{iso}\sin^2\theta/\lambda^2)$.

Table II Anisotropic Temperature Factors for
$[Pd(\eta^3\text{-}C_4H_7)\{CH(PPh_2)(P(S)Ph_2)_2\}]BF_4.2H_2O$

Atom	U_{11}	U_{22}	U_{33}	U_{23}	U_{13}	U_{23}
Pd(1)	386(6)	589(8)	578(8)	-135(7)	248(5)	-48(6)
S(1)	39(2)	90(3)	46(2)	-13(2)	15(2)	4(2)
S(2)	57(2)	68(3)	63(3)	21(2)	26(2)	18(2)
P(1)	37(2)	46(2)	41(2)	-2(2)	16(2)	0(2)
P(2)	44(2)	43(2)	47(2)	8(2)	24(2)	4(2)
P(3)	42(2)	46(2)	41(2)	-2(2)	21(2)	-4(2)
C(1)	44(8)	45(8)	32(7)	10(7)	16(6)	3(7)
C(11)	42(8)	63(11)	49(9)	-21(9)	18(7)	-11(8)
C(12)	101(5)	86(14)	47(11)	-4(10)	32(10)	-24(11)
C(13)	107(16)	121(18)	64(13)	-10(13)	50(12)	2(14)
C(14)	146(22)	117(20)	77(15)	-11(14)	73(16)	-1(16)
C(15)	85(14)	94(16)	110(17)	-34(14)	67(14)	-9(12)
C(16)	51(9)	62(11)	80(12)	-9(9)	32(9)	13(8)
C(21)	61(10)	38(9)	49(9)	-8(7)	28(8)	-12(8)
C(22)	104(14)	54(11)	94(14)	-20(11)	57(12)	-39(11)
C(23)	190(27)	73(16)	101(18)	-27(14)	66(19)	-89(17)
C(24)	133(20)	83(16)	72(15)	10(12)	32(15)	-16(15)
C(25)	110(16)	47(11)	71(13)	9(10)	29(12)	-15(11)
C(26)	61(11)	46(10)	47(10)	3(8)	14(8)	13(8)
C(31)	47(8)	53(9)	45(9)	-2(7)	24(7)	-10(8)
C(32)	44(8)	55(10)	81(11)	3(9)	35(8)	0(8)
C(33)	61(11)	93(15)	93(14)	-13(12)	45(11)	-13(10)
C(34)	71(13)	91(16)	116(17)	4(13)	58(13)	12(11)

Atom	U_{11}	U_{22}	U_{33}	U_{23}	U_{13}	U_{23}
C(35)	94(14)	115(18)	70(13)	-6(12)	51(12)	-29(13)
C(36)	86(12)	77(12)	59(11)	9(9)	49(10)	1(10)
C(41)	44(8)	40(9)	36(8)	4(7)	16(7)	1(7)
C(42)	66(10)	55(10)	61(10)	-6(8)	409 9)	-14(8)
C(43)	93(14)	72(13)	91(14)	-5(12)	61(12)	-20(12)
C(44)	102(16)	77(14)	86(14)	-27(11)	67(13)	-48(12)
C(45)	52(10)	101(15)	47(10)	4(10)	22(8)	-21(10)
C(46)	56(10)	63(10)	66(11)	6(9)	34(9)	-17(8)
C(51)	48(9)	38(8)	51(9)	2(7)	33(8)	0(7)
C(52)	55(9)	54(10)	36(9)	-11(7)	21(8)	-13(8)
C(53)	65(11)	50(10)	51(10)	4(9)	23(8)	-8(9)
C(54)	108(15)	55(11)	80(13)	-13(11)	62(12)	-34(12)
C(55)	76(12)	50(11)	73(12)	-7(9)	39(10)	-9(9)
C(56)	62(10)	45(10)	61(10)	2(8)	32(9)	3(8)
C(61)	54(9)	38(9)	52(9)	-2(7)	26(8)	-4(7)
C(62)	69(11)	72(12)	36(9)	3(8)	17(8)	5(9)
C(63)	98(14)	58(11)	48(10)	-1(9)	25(10)	-3(11)
C(64)	119(18)	63(13)	52(12)	-9(10)	15(13)	-11(13)
C(65)	129(19)	76(14)	61(13)	1(11)	36(13)	-30(14)
C(66)	106(15)	68(13)	85(13)	8(10)	68(12)	-13(11)
C(71)	64(12)	129(18)	143(19)	-79(16)	74(13)	-35(12)
C(72)	36(9)	97(14)	95(14)	-26(13)	32(9)	-4(9)
C(73)	53(11)	107(17)	132(19)	-24(16)	62(13)	-5(12)
C(74)	114(19)	160(24)	122(20)	-3(18)	74(17)	-33(17)
B(1)	63(16)	235(42)	84(19)	87(25)	-19(15)	-34(22)

Atom	U_{11}	U_{22}	U_{33}	U_{23}	U_{13}	U_{23}
F(1)	194(18)	143(15)	198(17)	45(12)	25(14)	-43(12)
F(2)	158(17)	518(42)	254(23)	133(26)	150(17)	80(22)
F(3)	199(24)	527(54)	324(33)	-275(37)	-105(23)	86(28)
F(4)	275(26)	280(27)	358(31)	212(25)	210(25)	98(20)

Estimated standard deviations are given in parentheses.

U values x 10^n where n = 4 for Pd and 3 otherwise.

$T = \exp -2\pi^2(U_{11}h^2a^{*2} + \ldots + 2U_{23}klb^*c^* + \ldots)$.

Table III. Hydrogen Atom Fractional Atomic Coordinates and Isotropic Temperature Parameters for $[Pd(\eta^3\text{-}C_4H_7)\{CH(PPh_2)(P(S)Ph_2)_2\}]BF_4.2H_2O$

Atom	x/a	y/b	z/c	U_{iso}
H(1)	1293(40)	2087(79)	1638(37)	36(32)

Estimated standard deviations are given in parentheses.

Coordinates x 10^4. Temperature parameters x 10^3. $T = \exp -(8\pi^2U_{iso}\sin^2\theta/\lambda^2)$

Table IV Fractional Atomic Coordinates and Temperature Parameters for $[Pd(\eta^3\text{-}C_4H_7)\{CH(P(S)Ph_2)_3\}]BF_4$

Atom	x/a	y/b	z/c	U_{eq}
Pd(2)	2300(0)	2300(0)	2300(0)	699(6)
Pd(1)	40523(16)	87360(16)	11484(16)	644(7)
S(1)	3903(4)	7426(4)	1605(4)	67(2)
S(2)	4955(4)	9753(4)	2505(4)	70(2)
S(3)	2509(4)	9082(4)	1515(4)	68(2)
S(10)	-1345(5)	289(4)	-589 4)	79(2)
P(1)	3291(4)	7518(3)	2531(4)	49(2)
P(2)	4650(4)	9226(4)	3430(4)	51(2)
P(3)	2715(4)	9240(4)	2756(3)	48(2)
P(10)	-2028(4)	-853(4)	-743(4)	56(2)
C(1)	3519(13)	8624(12)	3202(13)	52(4)
C(71)	4254(18)	9674(18)	405(15)	84(4)
C(72)	4260(21)	8847(21)	-94(19)	100(5)
C(73)	3389(31)	8181(32)	-184(17)	183(5)
C(74)	4866(34)	8572(24)	-532(28)	199(5)
C(11)	2143(13)	7069(13)	2127(13)	57(4)′
C(12)	1797(14)	6945(14)	1246(14)	61(5)′
C(13)	890(18)	6558(18)	938(19)	93(6)′
C(14)	423(19)	6278(19)	1459(20)	97(6)′
C(15)	752(18)	6402(18)	2351(18)	87(5)′
C(16)	1648(14)	6776(14)	2668(14)	60(5)′
C(21)	3655(12)	6936(12)	3307(13)	50(4)′
C(22)	3458(13)	7047(13)	4100(13)	54(4)′

Atom	x/a	y/b	z/c	U_{eq}
C(23)	3775(17)	6542(17)	4678(17)	82(5)'
C(24)	4224(18)	5941(17)	4375(18)	85(5)'
C(25)	4389(18)	5799(18)	3569(18)	87(5)'
C(26)	4096(14)	6299(14)	3040(14)	63(5)'
C(31)	4829(13)	10031(13)	4451(13)	53(4)'
C(32)	4423(14)	9829(14)	5083(14)	59(4)'
C(33)	4602(17)	10500(17)	5862(17)	81(5)'
C(34)	5198(19)	11267(18)	5955(18)	90(5)'
C(35)	5580(20)	11390(20)	5339(20)	102(6)'
C(36)	5398(16)	10784(16)	4539(16)	72(5)'
C(41)	5367(13)	8524(13)	3704(13)	55(4)'
C(42)	5846(14)	8257(14)	3138(14)	62(5)'
C(43)	6400(16)	7739(16)	3377(17)	78(5)'
C(44)	6474(16)	7556(16)	4167(17)	78(5)'
C(45)	6023(16)	7825(16)	4734(17)	77(5)'
C(46)	5435(16)	8325(16)	4540(15)	74(5)'
C(51)	1776(13)	8858(12)	3092(13)	51(4)'
C(52)	1829(15)	8745(15)	3944(15)	64(5)'
C(53)	1037(19)	8459(18)	4167(18)	91(5)'
C(54)	263(18)	8273(18)	3589(19)	89(5)'
C(55)	222(20)	8371(20)	2822(20)	101(6)'
C(56)	1005(16)	8679(15)	2530(15)	71(5)'
C(61)	3105(13)	10393(13)	3304(13)	50(4)'
C(62)	2920(14)	10704(14)	4091(14)	60(4)'
C(63)	3207(17)	11608(17)	4453(17)	80(5)'

Atom	x/a	y/b	z/c	U_{eq}
C(64)	3622(16)	12157(16)	4061(16)	75(5)'
C(65)	3758(17)	11837(18)	3313(17)	85(5)'
C(66)	3481(15)	10954(14)	2895(14)	62(5)'
C(75)	1203(15)	1203(15)	1203(15)	52(4)'

Estimated standard deviations are given in parentheses.

Coordinates x 10^n where n = 5, 4, 4, 4 for P, O, N, and C.

Temperature parameters x10^n where n = 4, 3, 3, 3 for P, O, N, and C.

U_{eq} = equivalnet isotropic temperature parameter.

$U_{eq} = 1/3\Sigma_i\Sigma_j U_{ij}\, a_i^*\, a_j^*(a_i.a_j)$

Primed values indicate that U_{iso} is given.

$T = \exp-(8\pi^2 U_{iso}\sin^2\theta/\lambda^2)$

Table V Anisotropic Temperature Factors for $[Pd(\eta^3\text{-}C_4H_7)\{CH(P(S)Ph_2)_3\}]BF_4$

Atom	U_{11}	U_{22}	U_{33}	U_{23}	U_{13}	U_{12}
Pd(2)	628(8)	628(8)	628(8)	-12(9)	-12(9)	-12(9)
Pd(1)	760(12)	701(12)	463(10)	149(8)	186(8)	113(9)
S(1)	82(4)	63(3)	60(3)	12(3)	22(3)	26(3)
S(2)	85(4)	57(3)	72(3)	26(3)	30(3)	8(3)
S(3)	86(4)	66(3)	51(3)	18(3)	11(3)	16(3)
S(10)	86(4)	57(3)	73(3)	-12(3)	10(3)	7(3)
P(1)	52(3)	66(3)	50(3)	13(2)	1(2)	11(2)
P(2)	51(3)	57(3)	56(3)	13(2)	12(2)	10(2)
P(3)	59(3)	40(3)	44(3)	16(2)	10(2)	12(2)
P(10)	64(3)	44(3)	45(3)	4(2)	13(2)	10(3)
C(1)	54(6)	43(3)	57(6)	9(6)	11(6)	15(6)
C(71)	110(7)	101(7)	47(6)	42(6)	36(6)	-1(7)
C(72)	109(7)	111(7)	83(7)	16(7)	46(6)	18(7)
C(73)	244(7)	299(7)	30(6)	9(7)	29(7)	160(7)
C(74)	322(7)	101(7)	183(7)	-13(7)	184(7)	-2(7)
C(75)	50(6)	50(6)	50(6)	8(6)	8(6)	8(6)
C(10)	45(5)	45(5)	45(5)	8(6)	8(6)	8(6)
C(76)	85(7)	173(7)	201(7)	43(7)	25(7)	63(7)

Estimated standard deviations are given in parentheses.

U values x 10^n where n = 4, 3, 3 for S, C, N.

$T = \exp -2\pi^2(U_{11}h^2a^{*2} + \ldots + 2U_{23}klb^*c^* + \ldots)$.

TableVI Fractional Atomic Coordinates and Temperature Parameters for [Rh(Cod){C(P(S)Ph$_2$)$_3$}].

Atoms	x/a	y/b	c/z	U_{eq}
Rh(1)	7777(4)	6349(5)	-32768(3)	318(3)
S(1)	1556(1)	466(2)	-2535(1)	34(1)
S(2)	-112(1)	490(2)	-2650(1)	41(1)
S(3)	502(2)	1447(2)	-237(1)	41(1)
P(1)	1447(1)	1348(2)	-1951(1)	29(1)
P(2)	186(1)	506(2)	-1809(1)	29(1)
P(3)	460(1)	1927(2)	-1011(1)	31(1)
C(1)	669(5)	1311(6)	-1605(4)	29(4)
C(2)	1587(5)	2293(6)	-2314(4)	32(3)'
C(3)	1112(6)	2530(7)	-2712(5)	48(3)'
C(4)	1202(7)	3256(9)	-3029(6)	70(4)'
C(5)	1776(8)	3703(9)	-2922(6)	75(5)'
C(6)	2234(7)	3472(8)	-2512(6)	67(4)'
C(7)	2151(6)	2748(7)	-2193(5)	46(3)'
C(8)	2165(5)	1195(6)	-1488(4)	32(3)'
C(9)	2779(5)	1187(6)	-1759(5)	35(3)'
C(10)	3339(5)	1096(7)	-1427(5)	39(3)'
C(11)	3294(6)	1025(7)	-820(5)	45(3)'
C(12)	2679(6)	1018(7)	-567(5)	45(3)'
C(13)	2109(5)	1081(6)	-897(4)	33(3)'
C(14)	-588(5)	508(6)	-1416(4)	32(3)'
C(15)	-629(5)	131(6)	-870(5)	37(3)'
C(16)	-1242(6)	121(7)	-577(5)	51(3)'
C(17)	-1792(6)	466(7)	-834(5)	49(3)'
C(18)	-1741(6)	841(7)	-1384(5)	45(3)'

Atom	x/a	y/b	z/c	U_{eq}
C(19)	-1142(5)	841(6)	-1673(5)	36(3)'
C(20)	556(5)	-430(6)	-1597(4)	29(3)'
C(21)	906(5)	-443(6)	-1077(5)	40(3)'
C(22)	1159(6)	-1180(7)	-868(5)	53(3)'
C(23)	1041(7)	-1878(8)	-1199(6)	67(4)'
C(24)	703(7)	-1840(8)	-1723(6)	71(4)'
C(25)	461(6)	-1110(7)	-1923(5)	52(3)'
C(26)	-365(5)	2339(6)	-1137(4)	34(3)'
C(27)	-785(6)	2395(7)	-665(5)	45(3)'
C(28)	-1420(7)	2704(7)	-742(5)	57(4)'
C(29)	-1614(7)	2955(8)	-1294(6)	68(4)'
C(30)	-1195(7)	2908(8)	-1760(6)	65(4)'
C(31)	-547(6)	2585(7)	-1693(5)	46(3)'
C(32)	1001(5)	2795(6)	-1046(5)	35(3)'
C(33)	1534(6)	2798(7)	-672(5)	44(3)'
C(34)	1992(6)	3461(8)	-715(5)	57(4)'
C(35)	1871(7)	4050(8)	-1104(6)	62(4)'
C(36)	1309(7)	4062(7)	-1447(5)	56(4)'
C(37)	869(6)	3428(7)	-1434(5)	46(3)'
C(38)	157(6)	220(8)	-3971(5)	42(5)
C(39)	161(6)	1048(8)	-3983(5)	45(5)
C(40)	526(7)	1532(8)	-4437(5)	59(5)
C(41)	1219(7)	1773(8)	-4222(5)	63(6)
C(42)	1513(6)	1187(8)	-3792(5)	61(5)
C(43)	1539(6)	358(8)	-3877(5)	52(5)
C(44)	1280(6)	-47(8)	-4423(5)	58(5)
C(45)	565(7)	-317(8)	-4339(5)	60(5)

Estimated standard deviations are given in parentheses.

Coordinates x 10^n where n = 5, 4, 4, 4 for P, O, N, and C.

Temperature parameters x10^n where n = 4, 3, 3, 3 for P, O, N, and C.

U_{eq} = equivalent isotropic temperature parameter.

$U_{eq} = 1/3 \Sigma_i \Sigma_j U_{ij} a_i^* a_j^* (a_i . a_j)$

Primed values indicate that U_{iso} is given.

$T = \exp-(8\pi^2 U_{iso} \sin^2\theta/\lambda^2)$

Table VII. Anisotropic Temperature Parameters (Å) for [Rh(Cod){C(P(S)Ph$_2$)$_3$}].

Atom	U_{11}	U_{22}	U_{33}	U_{23}	U_{13}	U_{12}
Rh(1)	271(5)	438(5)	245(5)	7(4)	4(4)	-21(5)
S(1)	30(2)	40(2)	32(2)	-6(1)	-3(1)	3(1)
S(2)	30(2)	67(2)	25(2)	-1(1)	-1(1)	-5(2)
S(3)	50(2)	45(2)	29(2)	3(1)	3(1)	6(2)
P(1)	26(2)	31(2)	30(2)	0(1)	0(1)	1(1)
P(2)	26(2)	35(2)	24(2)	-1(1)	2(1)	-1(1)
P(3)	32(2)	30(2)	30(2)	1(1)	3(1)	2(1)
C(1)	29(7)	24(6)	34(6)	3(5)	-7(5)	9(5)
C(38)	33(8)	64(9)	30(7)	-6(7)	-14(6)	-6(7)
C(39)	52(9)	56(9)	27(7)	8(6)	-17(6)	0(7)
C(40)	55(9)	75(10)	48(8)	25(7)	-4(7)	-11(8)
C(41)	77(11)	71(10)	42(8)	31(7)	-11(7)	-14(9)
C(42)	43(8)	63(9)	39(8)	-2(7)	18(6)	-6(7)
C(43)	41(8)	87(11)	27(7)	-18(7)	21(6)	-7(7)
C(44)	41(8)	84(11)	49(8)	-22(8)	8(7)	-1(8)
C(45)	58(9)	69(10)	52(8)	-15(7)	-12(7)	-5(8)

Estimated standard deviations are given in parentheses.

U values x 10^n where n = 4, 3, 3 for S, C, N.

$T = \exp -2\pi^2(U_{11}h^2a^{*2} + \ldots + 2U_{23}klb^*c^* + \ldots)$.

Table VIII. Fractional Atomic Coordinates and Temperature Parameters for $[Ir(CO)_2\{C(P(S)Ph_2)_3\}]$.

Atom	x/a	y/b	z/c	U_{eq}
Ir(1)	37404(6)	7316(5)	21581(7)	434(4)
S(1)	4456(4)	44(4)	2700(6)	58(3)
S(2)	3298(4)	27(3)	1158(5)	41(3)
S(3)	3509(4)	-2390(3)	3062(5)	57(3)
P(1)	4198(4)	-825(4)	2409(5)	35(3)
P(2)	2914(3)	-644(3)	1907(4)	35(3)
P(3)	3250(4)	-1577(3)	3402(5)	40(3)
O(1)	4424(12)	1666(12)	3202(17)	96(8)'
O(2)	2795(13)	1611(13)	1617(18)	104(9)'
C(1)	3437(15)	-1005(14)	2578(19)	54(13)
C(2)	3187(16)	1260(16)	1839(23)	74(11)'
C(3)	4156(15)	1300(15)	2775(23)	64(9)'
C(4)	4442(12)	-997(12)	1265(18)	40(8)'
C(5)	4878(12)	-636(13)	850(18)	43(8)'
C(6)	5079(13)	-807(14)	-33(20)	52(8)'
C(7)	4846(14)	-1308(15)	-477(21)	57(9)'
C(8)	4399(16)	-1645(16)	-33(24)	77(11)'
C(9)	4238(13)	-1513(13)	853(19)	48(8)'
C(10)	4711(14)	-1251(14)	3115(21)	60(10)'
C(11)	4886(15)	-1831(15)	2856(25)	69(10)'
C(12)	5250(15)	-2139(15)	3462(23)	70(10)'
C(13)	5490(19)	-1867(19)	4254(27)	93(13)'
C(14)	5317(20)	-1299(21)	4510(28)	101(14)'
C(15)	4918(14)	-983(14)	3957(21)	53(9)'
C(16)	2583(15)	-1107(15)	1008(21)	59(9)'

Atom	x/a	y/b	z/c	U_{eq}
C(17)	2683(12)	-1730(13)	975(19)	44(8)'
C(18)	2410(16)	-2062(15)	271(23)	71(10)'
C(19)	2040(15)	-1745(15)	-353(22)	63(10)'
C(20)	1927(16)	-1132(15)	-280(22)	65(10)'
C(21)	2206(13)	-827(13)	373(19)	47(8)'
C(22)	2262(12)	-339(12)	2500(16)	38(8)'
C(23)	2358(11)	124(11)	3117(16)	32(7)'
C(24)	1858(13)	386(12)	3532(18)	45(8)'
C(25)	1253(15)	196(12)	3368(19)	52(8)'
C(26)	1153(13)	-299(12)	2754(20)	50(8)'
C(27)	1697(12)	-552(11)	2334(17)	38(8)'
C(28)	2436(12)	-1597(11)	3557(17)	35(7)'
C(29)	2147(12)	-1248(12)	4262(17)	33(7)'
C(30)	1504(14)	-1333(14)	4404(21)	56(9)'
C(31)	1205(15)	-1704(13)	3866(20)	55(8)'
C(32)	1473(13)	-2017(13)	3173(19)	49(9)'
C(33)	2089(13)	-1977(12)	3053(18)	43(8)'
C(34)	3540(11)	-1347(11)	4499(17)	33(7)'
C(35)	3669(15)	-1791(13)	5121(21)	60(9)'
C(36)	3880(16)	-1604(16)	5985(24)	77(11)'
C(37)	3967(17)	-993(17)	6193(25)	84(12)'
C(38)	3801(17)	-559(15)	5578(23)	76(11)'
C(39)	3588(12)	-738(14)	4702(17)	47(8)'

Estimated standard deviations are given in parentheses.

Coordinates x 10^n where n = 5 for Ir, and 4 otherwise.

Temperature parameters x10^n where n = 4 for Ir, and 3 otherwise.

U_{eq} = equivalent isotropic temperature parameter.

$U_{eq} = 1/3\Sigma_i\Sigma_j U_{ij}\, a_i^*\, a_j^*(a_i.a_j)$

Primed values indicate that U_{iso} is given.

$T = \exp-(8\pi^2 U_{iso}\sin^2\theta/\lambda^2)$

Table IX. Anisotropic Temperature Parameters (Å) for $[Ir(CO)_2\{C(P(S)Ph_2)_3\}]$.

Atom	U_{11}	U_{22}	U_{33}	U_{23}	U_{13}	U_{12}
Ir(1)	606(7)	301(6)	396(7)	7(6)	56(8)	-25(8)
S(1)	53(5)	40(5)	81(6)	-14(5)	-11(5)	0(4)
S(2)	48(5)	40(5)	36(4)	4(4)	-4(4)	-49 4)
S(3)	72(6)	37(5)	62(6)	-5(4)	-3(5)	5(4)
P(1)	36(5)	31(5)	37(5)	0(4)	2(3)	1(4)
P(2)	46(5)	27(4)	33(4)	0(3)	2(3)	2(4)
P(3)	52(5)	29(4)	40(5)	7(4)	5(4)	1(4)
C(1)	52(21)	59(23)	51(22)	1(15)	8(16)	35(18)

Estimated standard deviations are given in parentheses.

U values x 10^n where n = 4for Ir, and 3 otherwise.

$T = \exp -2\pi^2(U_{11}h^2a^{*2} + \ldots + 2U_{23}klb^*c^* + \ldots)$.

Table X Fractional Atomic Coordinates and Temperature Parameters for [Rh(Cod){C(PPh$_2$)(P(S)Ph$_2$)-*P*,*S*}]·CH$_2$Cl$_2$

Atom	x	y	z	U_{eq}
Rh(1)	470819(10)	30511(9)	14635(6)	369(5)
S(1)	3972(3)	3204(3)	2465(2)	42(2)
S(2)	220(4)	4834(3)	1450(2)	47(2)
P(1)	2743(3)	39429(3)	2134(2)	34(2)
P(2)	625(3)	3647(3)	1455(2)	30(1)
P(3)	2938(3)	2869(3)	1062(2)	32(1)
C(1)	2035(11)	3457(9)	1520(7)	26(5)
C(2)	3369(13)	4919(10)	1941(8)	40(4)'
C(3)	4102(17)	5319(14)	2369(10)	72(6)'
C(4)	4632(18)	6055(15)	2199(11)	82(7)'
C(5)	4428(18)	6401(15)	1646(11)	85(7)'
C(6)	3690(18)	6074(14)	1203(11)	84(7)'
C(7)	3150(15)	5286(12)	1359(9)	60(5)'
C(8)	1948(13)	4176(11)	2811(8)	45(5)'
C(9)	1583(13)	49759(10)	2934(7)	40(4)'
C(10)	979(17)	5118(13)	3499(10)	71(6)'
C(11)	790(16)	4476(13)	3873(9)	67(6)'
C(12)	1120(15)	3662(12)	3774(9)	56(5)'
C(13)	1698(14)	3513(11)	3212(8)	45(5)'
C(14)	-49(12)	3084(10)	2091(7)	39(4)'
C(15)	341(13)	2295(10)	2266(8)	41(4)'
C(16)	-218(14)	1827(12)	2711(8)	55(5)'

Atom	x	y	z	U_{eq}
C(17)	-1100(15)	2179(12)	2992(9)	60(5)'
C(18)	-1471(14)	2957(12)	2843(8)	54(5)'
C(19)	-936(13)	3445(10)	2378(8)	43(5)'
C(20)	14(12)	3125(10)	759(7)	37(4)'
C(21)	-324(13)	3630(10)	255(8)	42(4)'
C(22)	-841(14)	3267(12)	-274(8)	56(5)'
C(23)	-997(16)	2404(13)	-298(9)	64(6)'
C(24)	-654(15)	1905(12)	210(9)	60(5)'
C(25)	-121(14)	2277(11)	752(8)	48(5)'
C(26)	2568(12)	1758(9)	1095(7)	33(4)'
C(27)	2759(15)	1393(12)	1680(9)	58(5)'
C(28)	2457(17)	549(14)	1780(10)	77(6)'
C(29)	2017(17)	99(13)	1283(10)	73(6)'
C(30)	1871(17)	435(14)	705(10)	75(6)'
C(31)	2103(15)	1299(12)	602(9)	58(5)'
C(32)	2727(12)	3150(10)	236(7)	33(4)'
C(33)	3194(13)	2630(11)	-226(8)	45(5)'
C(34)	3106(15)	2876(12)	-863(9)	58(5)'
C(35)	2542(15)	3613(12)	-1012(9)	59(5)'
C(36)	2086(15)	4087(12)	-576(9)	58(6)'
C(37)	2192(13)	3869(10)	74(8)	42(4)'
C(38)	6212(13)	3666(12)	1812(9)	54(8)
C(39)	6388(14)	2833(13)	1917(9)	57(8)
C(40)	7010(16)	2222(13)	1506(10)	75(9)
C(41)	6539(22)	2028(23)	919(14)	164(18)

Atom	x	y	z	U_{eq}
C(42)	5488(16)	2510(22)	672(11)	95(12)
C(43)	5412(20)	3326(20)	570(12)	90(11)
C(44)	6374(26)	3942(26)	668(11)	178(20)
C(45)	6698(26)	4168(14)	1287(8)	83(9)
C(46)	5329(25)	4458(27)	3989(19)	187(22)
Cl(1)	5960(8)	3533(6)	4185(5)	163(5)
Cl(2)	4056(9)	4500(7)	4244(5)	180(6)

Estimated standard deviations are given in parentheses. Coordinates x 10^n where n = 5 for rhodium and 4 otherwise. temperature parameters x 10^n where n = 4 for rhodium and 3 otherwise. U_{eq} = the equivalent isotropic temperature parameter = $1/3\Sigma_i\Sigma_j U_{ij} a_i^* a_j^* (\mathbf{a}_i \mathbf{a}_j)$. Primed values indicate that U_{iso} is given, where $T = \exp-(8\pi^2 U_{iso} \sin^2\theta/\lambda^2)$.

Table XI Anisotropic Temperature Parameters (Å^2) of [Rh(Cod){C(PPh$_2$)(P(S)Ph$_2$)-*P,S*}]·CH$_2$Cl$_2$

Atom	U_{11}	U_{22}	U_{33}	U_{23}	U_{13}	U_{12}
Rh(1)	278(8)	435(9)	394(8)	-28(7)	29(6)	15(7)
S(1)	36(3)	53(3)	36(2)	1(2)	-5(2)	9(2)
S(2)	54(3)	29(3)	58(3)	4(2)	-9(2)	14(2)
P(1)	31(3)	36(3)	33(3)	1(2)	0(2)	5(2)
P(2)	33(2)	26(3)	31(2)	-1(2)	-2(2)	1(2)
P(3)	27(2)	31(3)	37(3)	0(2)	2(2)	2(2)
C(1)	29(9)	21(9)	28(9)	-3(7)	1(7)	9(7)
C(38)	33(11)	60(14)	68(14)	11(11)	-7(10)	3(10)
C(39)	36(11)	74(16)	59(13)	0(11)	-26(9)	7(10)
C(40)	61(14)	82(16)	83(16)	-34(13)	-3(12)	37(12)
C(41)	98(21)	249(40)	141(26)	-141(29)	-57(19)	80(25)
C(42)	22(12)	205(31)	57(15)	-70(20)	0(10)	23(18)
C(43)	57(16)	144(25)	69(16)	-21(18)	21(12)	-41(18)
C(44)	174(30)	316(48)	42(16)	21(22)	-7(17)	-167(33)
C(45)	120(19)	101(18)	27(11)	-8(11)	9(12)	-76(16)
C(46)	87(23)	231(44)	241(44)	118(36)	2(25)	-22(26)
Cl(1)	160(8)	134(8)	195(10)	32(07)	3(7)	-37(7)
Cl(2)	154(9)	175(10)	212(11)	32(8)	5(8)	-21(8)

Estimated standard deviations are given in parentheses.

U values x 10^n where n = 4for Rh, and 3 otherwise.

$T = \exp -2\pi^2(U_{11}h^2a^{*2} + \ldots + 2U_{23}klb^*c^* + \ldots)$.

Table XII. Fractional Atomic Coordinates and Temperature Parameters for $[RhI_2(^tBuNC)_2\{C(PPh_2)(P(S)Ph_2)_2\}]$

Atom	x/a	y/b	z/c	U_{eq}
Rh(1)	2944(1)	4148(1)	2015(4)	33(2)
I(1)	3768(1)	4134(1)	2868(4)	57(2)
I(2)	3154(1)	3503(1)	393(4)	58(2)
S(1)	2228(4)	4147(5)	1183(16)	48(6)
S(2)	1415(5)	5422(5)	3946(17)	70(8)
P(1)	1906(4)	4672(5)	1828(15)	41(6)
P(2)	2023(5)	5493(5)	3336(16)	48(7)
P(3)	2718(5)	4702(4)	3336(13)	28(6)
N(1)	258(2)	332(2)	351(5)	8(2)'
N(2)	330(1)	480(1)	12(4)	3(1)'
C(1)	224(2)	499(2)	274(5)	5(2)'
C(2)	140(1)	441(1)	243(4)	7(1)'
C(3)	143(1)	416(1)	347(4)	7(1)'
C(4)	105(1)	397(1)	394(4)	7(1)'
C(5)	64(1)	402(1)	339(4)	7(1)'
C(6)	61(1)	427(1)	236(4)	7(1)'
C(7)	99(1)	447(1)	188(4)	7(1)'
C(8)	173(1)	503(1)	56(3)	5(1)'
C(9)	195(1)	498(1)	-52(3)	5(1)'
C(10)	183(1)	524(1)	-149(3)	5(1)'
C(11)	149(1)	555(1)	-138(3)	5(1)'
C(12)	127(1)	560(1)	-30(3)	5(1)'
C(13)	139(1)	534(1)	67(3)	5(1)'

Atom	x/a	y/b	z/c	U_{eq}
C(14)	237(1)	576(1)	456(3)	6(1)'
C(15)	228(1)	568(1)	574(3)	6(1)'
C(16)	252(1)	589(1)	662(3)	6(1)'
C(17)	286(1)	618(1)	632(3)	6(1)'
C(18)	296(1)	626(1)	513(3)	6(1)'
C(19)	271(1)	605(1)	425(3)	6(1)'
C(20)	204(1)	591(1)	217(3)	7(1)'
C(21)	234(1)	588(1)	124(3)	7(1)'
C(22)	235(1)	621(1)	38(3)	7(1)'
C(23)	206(1)	657(1)	44(3)	7(1)'
C(24)	176(1)	659(1)	137(3)	7(1)'
C(25)	175(1)	627(1)	223(3)	7(1)'
C(26)	258(1)	447(1)	485(3)	8(1)'
C(27)	290(2)	420(1)	536(3)	8(1)'
C(28)	283(2)	402(1)	648(3)	8(1)'
C(29)	244(2)	410(1)	708(3)	8(1)'
C(30)	211(2)	437(1)	657(3)	8(1)'
C(31)	219(2)	456(1)	546(3)	8(1)'
C(32)	316(1)	510(1)	364(3)	3(1)'
C(33)	330(1)	536(1)	268(3)	3(1)'
C(34)	366(1)	564(1)	280(3)	3(1)'
C(35)	389(1)	566(1)	387(3)	3(1)'
C(36)	375(1)	540(1)	483(3)	3(1)'
C(37)	339(1)	512(1)	471(3)	3(1)'
C(38)	273(2)	363(2)	306(6)	6(2)'

Atom	x/a	y/b	z/c	U_{eq}
C(39)	230(2)	300(2)	408(4)	3(1)'
C(40)	262(3)	280(3)	498(8)	11(3)'
C(41)	243(4)	257(4)	329(10)	20(5)'
C(42)	189(4)	315(4)	432(10)	19(4)'
C(43)	316(2)	457(2)	92(6)	7(2)'
C(44)	354(2)	503(2)	-77(5)	5(2)'
C(45)	393(3)	522(3)	-42(9)	15(4)'
C(46)	332(4)	541(4)	-96(10)	19(5)'
C(47)	374(4)	480(4)	-176(12)	21(5)'

Estimated standard deviations are given in parentheses. Coordinates x 10^n where n = 4 for Rh, I, S, P and 3 otherwise. Temperature parameters x 10^n where n = 3 for Rh, I, S, P and 2 otherwise. U_{eq} = the equivalent isotropic temperature parameter = $1/3\Sigma_i\Sigma_j U_{ij} a_i^* a_j^* (\mathbf{a}_i \cdot \mathbf{a}_j)$. Primed values indicate that U_{iso} is given, where T = exp-$(8\pi^2 U_{iso} \sin^2\theta/\lambda^2)$.

Table XIII Anisotropic Temperature Parameters ($Å^2$) of $[RhI_2(^tBuNC)_2\{C(PPh_2)(P(S)Ph_2)_2\}]$

Atoms	U_{11}	U_{22}	U_{33}	U_{23}	U_{13}	U_{12}
Rh(1)	30(3)	26(3)	44(3)	2(3)	1(3)	1(2)
I(1)	39(3)	58(3)	73(3)	-6(3)	-4(3)	15(2)
I(1)	48(3)	48(3)	80(3)	-22(3)	2(3)	6(2)
S(1)	21(9)	34(9)	88(13)	-12(10)	-8(9)	-11(8)
S(2)	45(11)	60(12)	104(15)	-18(12)	14(11)	2(9)
P(1)	11(8)	38(10)	76(14)	15(10)	-6(10)	-7(7)
P(2)	38(10)	26(10)	82(15)	-17(10)	15(10)	4(8)
P(3)	31(9)	17(9)	36(12)	12(8)	-9(9)	3(7)

Estimated standard deviations are given in parentheses.

U values x 10^n where n = 3 for Rh, I, S, P and 2 otherwise.

$T = \exp -2\pi^2(U_{11}h^2a^{*2} + \ldots + 2U_{23}klb^*c^* + \ldots)$.

Table XIV. Fractional Atomic Coordinates and Temperature Parameters for $CH(PPh_2)(P(S)Ph_2)_2$

Atom	x/a	y/b	z/c	U_{eq}
S(1)	1223(1)	4129(1)	3882(2)	54(1)
S(2)	861(1)	1681(1)	7683(2)	56(1)
P(1)	1521(1)	3592(1)	5757(2)	38(1)
P(2)	736(1)	2110(1)	5633(2)	37(1)
P(3)	1845(1)	2393(1)	3611(2)	44(1)
H(1)	192(4)	244(4)	609(9)	8(3)'
C(1)	1526(4)	2616(3)	5453(8)	37(2)
C(11)	2400(3)	3792(4)	6671(8)	43(2)'
C(12)	2763(4)	3387(4)	7866(9)	57(2)'
C(13)	3444(4)	3569(4)	8501(10)	67(2)'
C(14)	3735(4)	4139(4)	7952(10)	67(2)'
C(15)	3393(4)	4546(4)	6791(10)	66(2)'
C(16)	2714(4)	4375(4)	6138(9)	54(2)'
C(21)	1015(4)	3770(4)	7242(8)	44(2)'
C(22)	1141(4)	3438(4)	8653(8)	50(2)'
C(23)	738(4)	3587(4)	9737(10)	63(2)'
C(24)	217(5)	4069(5)	9416(11)	76(3)'
C(25)	98(4)	4414(5)	8030(10)	74(3)'
C(26)	497(4)	4272(4)	6917(9)	56(2)'
C(31)	614(3)	1429(3)	4134(8)	36(2)'
C(32)	686(3)	726(4)	4584(8)	44(2)'
C(33)	622(4)	195(4)	3472(9)	52(2)'

Atom	x/a	y/b	z/c	U_{eq}
C(34)	501(4)	366(4)	1939(9)	57(2)′
C(35)	429(4)	1056(4)	1468(9)	55(2)′
C(36)	475(3)	1588(4)	2572(8)	46(2)′
C(41)	-16(4)	2679(4)	5194(8)	43(2)′
C(42)	-180(4)	3055(4)	3827(9)	52(2)′
C(43)	-776(4)	3466(5)	3554(11)	75(3)′
C(44)	-1196(5)	3476(5)	4654(11)	84(3)′
C(45)	-1033(5)	3119(5)	6000(11)	77(3)′
C(46)	-438(4)	2711(4)	6282(9)	56(2)′
C(51)	2663(3)	2874(4)	3710(8)	41(2)′
C(52)	3259(4)	2701(4)	4715(9)	50(2)′
C(53)	3874(4)	3038(4)	4566(9)	56(2)′
C(54)	3871(4)	3552(4)	3460(9)	59(2)′
C(55)	3279(4)	3739(4)	2502(9)	54(2)′
C(56)	2671(4)	3389(4)	2618(9)	50(2)′
C(61)	2215(4)	1503(4)	4070(8)	45(2)′
C(62)	2385(4)	1188(4)	5486(10)	60(2)′
C(63)	2739(4)	527(5)	5664(12)	79(3)′
C(64)	2897(5)	217(5)	4394(12)	88(3)′
C(65)	2733(5)	512(5)	2984(13)	91(3)′
C(66)	2370(4)	1161(5)	2768(11)	72(3)′

Estimated standard deviations are given in parenthese. Coordinates x 10^n where n = 4 for S,P,C and 3 for H. Temperature parameters x 10^n where n = 3 for S,P,C and 2 for H. U_{eq} = the equivalent isotropic temperature parameter = $1/3\Sigma_i\Sigma_j U_{ij}\, a_i^* a_j^* (a_i . a_j)$.

Primed values indicatee that U_{iso} is given, where $T=\exp-(8\pi^2 U_{iso}\sin^2\theta/\lambda^2)$.

Table XV Anisotropic Temperature Parameters ($Å^2$) of $CH(PPh_2)(P(S)Ph_2)_2$

Atom	U_{11}	U_{22}	U_{33}	U_{23}	U_{13}	U_{12}
S(1)	54(1)	52(1)	50(1)	13(1)	0(1)	3(1)
S(2)	73(1)	56(1)	40(1)	8(1)	16(1)	-5(1)
P(1)	37(1)	36(1)	39(1)	1(1)	1(1)	0(1)
P(2)	36(1)	37(1)	39(1)	1(1)	10(1)	-2(1)
P(3)	39(1)	47(1)	45(1)	-3(1)	10(1)	-6(1)
C(1)	31(4)	37(4)	41(4)	1(4)	3(3)	0(3)

Estimated standard deviations are given in parentheses.

U values x 10^3.

$T = \exp -2\pi^2(U_{11}h^2a^{*2} + \ldots + 2U_{23}klb^*c^* + \ldots)$.

Table XVI. Fractional Atomic Coordinates and Temperature Parameters for [Ir(Cod){CH(PPh$_2$)(P(S)Ph$_2$)$_2$-*P,S,S*}]

Atom	x/a	y/b	z/c	U_{eq}
Ir(1)	68801(4)	30720(2)	15037(4)	349(2)
S(1)	6515(3)	1905(1)	1419(3)	45(1)
S(2)	5113(3)	2841(2)	2561(3)	48(1)
P(1)	4395(3)	1504(1)	461(3)	37(1)
P(2)	3278(3)	2548(1)	946(3)	37(1)
P(3)	5025(3)	2803)	-622(2)	34(1)
H(1)	2677(21)	2050(19)	-1118(21)	37(2)'
C(1)	3580(9)	2165(4)	-286(8)	31(1)
C(11)	3701(10)	1021(5)	1552(9)	41(2)'
C(12)	2344(11)	561(6)	1044(10)	57(2)'
C(13)	1860(13)	162(7)	1930(12)	76(2)'
C(14)	2843(12)	198(6)	3303(11)	71(2)'
C(15)	4169(12)	638(6)	3784(10)	62(2)'
C(16)	4651(11)	1062(5)	2937(10)	50(2)'
C(21)	3901(10)	936(5)	-923(9)	41(2)'
C(22)	2498(11)	729(6)	-1901(10)	53(2)'
C(23)	2193(12)	269(6)	-2939(11)	66(2)'
C(24)	3285(12)	53(6)	-2881(11)	69(2)'
C(25)	4626(12)	268(6)	-1970(11)	67(2)'
C(26)	4992(11)	739(5)	-916(10)	51(2)'
C(31)	1863(10)	2005(5)	1269(9)	44(2)'
C(32)	2076912)	1985(6)	2626(11)	66(2)'
C(33)	843914)	1589(7)	2888(12)	89(2)'

Atom	x/a	y/b	z/c	U_{eq}
C(34)	-409(14)	1299(8)	1867(13)	92(2)'
C(35)	-622(13)	1320(7)	519(12)	83(2)'
C(36)	529(12)	1676(6)	212(11)	63(2)'
C(41)	2571(10)	3211(5)	155(9)	43(2)'
C(42)	3119(11)	3798(6)	913(10)	56(2)'
C(43)	2515(11)	4303(6)	377(10)	60(2)'
C(44)	1389(12)	4216(6)	-868911)	69(2)'
C(45)	823(11)	3626(6)	-1624(10)	61(2)'
C(46)	1390(11)	3104(5)	-1115(10)	50(2)'
C(51)	5397(10)	2406(5)	-1765(9)	38(2)'
C(52)	4328(10)	2013(5)	-2913(9)	45(2)'
C(53)	4738(11)	1797(6)	-3779(10)	61(2)'
C(54)	6157(12)	1934(6)	-3529(11)	68(2)'
C(55)	7208(12)	2299(6)	-2369(11)	67(2)'
C(56)	6831(11)	2550(5)	-1495(10)	52(2)'
C(61)	4102(10)	3350(5)	-1762(9)	40(2)'
C(62)	4587(11)	3996(5)	-1433(10)	50(2)'
C(63)	3972(12)	4444(6)	-2342(11)	67(2)'
C(64)	2877(12)	4193(6)	-3586(11)	65(2)'
C(65)	2360(12)	3550(6)	-3913(11)	67(2)'
C(66)	2956(11)	3103(6)	-2978(10)	56(2)'
C(71)	8597(11)	3180(6)	3509(10)	59(2)
C(72)	9102(11)	3085(6)	2590(11)	58(2)
C(73)	10147(11)	3621(7)	2172(13)	83(2)
C(74)	9495(12)	4073(7)	1263(12)	79(2)

Atom	x/a	y/b	z/c	U_{eq}
C(75)	7951(10)	3958(5)	929(10)	50(2)
C(76)	7385(11)	40929 5)	1818(9)	46(2)
C(77)	8397(14)	4342(6)	3293(11)	93(2)
C(78)	8936(14)	3846(7)	4190(11)	86(2)
B(1)	547(14)	8461(8)	4028(13)	76(2)
F(1)	-111(12)	8500(6)	2755(9)	164(2)
F(2)	1816(11)	8674(8)	4649(12)	202(2)
F(3)	416(17)	7918(9)	4228(17)	445(2)
F(4)	-15(17)	8697(12)	4405914)	506(2)
C(80)	4066(15)	6238(8)	4124(13)	106(2)
Cl(1)	4925(8)	5790(3)	5387(5)	153(1)
Cl(2)	2437(7)	5728(4)	2962(7)	174(2)

Estimated standard are given in parentheses.

Coordinates x 10^n where n = 5 for Ir, and 4 otherwise.

Temperature parameters x 10^n where n = 4 for Ir, and 3 otherwise.

U_{eq} = equivalent isotropic temperature parameter = $1/3\Sigma_i\Sigma_j U_{ij}\, a_i^*\, a_j^*\, (a_i.aj)$.

Primed values indicate that U_{iso} is given, where $T = \exp -(8\pi^2 U_{iso}\sin^2\theta/\lambda^2)$.

Table XVII Anisotropic Temperature Parameters (Å²) of [Ir(Cod){CH(PPh$_2$)(P(S)Ph$_2$)$_2$-*P,S,S*}]

Atom	U_{11}	U_{22}	U_{33}	U_{23}	U_{11}	U_{12}
Ir(1)	272(2)	390(2)	324(2)	8(2)	25(2)	115(2)
S(1)	31(1)	46(1)	54(1)	5(1)	6(1)	19(1)
S(2)	41(1)	65(1)	38(1)	-5(1)	7(1)	20(1)
P(1)	33(1)	38(1)	39(1)	6(1)	10(1)	15(1)
P(2)	34(1)	39(1)	38(1)	3(1)	11(1)	15(1)
P(3)	27(1)	37(1)	34(1)	3(1)	6(1)	10(1)
C(1)	27(2)	32(2)	27(2)	2(2)	4(2)	9(2)
C(71)	37(2)	64(2)	53(2)	8(2)	-9(2)	14(2)
C(72)	40(2)	63(2)	60(2)	3(2)	8(2)	13(2)
C(73)	33(2)	73(2)	136(2)	32(2)	31(2)	12(2)
C(74)	41(2)	88(2)	101(2)	14(2)	28(2)	8(2)
C(75)	36(2)	49(2)	56(2)	10(2)	13(2)	5(2)
C(76)	50(2)	40(2)	39(2)	0(2)	6(2)	12(2)
C(77)	133(2)	52(2)	44(2)	-12(2)	-16(2)	15(2)
C(78)	100(2)	94(2)	47(2)	-20(2)	-20(2)	53(2)
B(1)	67(2)	64(2)	67(2)	9(2)	7(2)	-1(2)
F(1)	206(2)	229(2)	68(2)	-10(2)	1(2)	136(2)
F(2)	79(2)	297(2)	160(2)	-37(2)	-6(2)	9(2)
F(3)	356(2)	199(2)	356(2)	146(2)	-130(2)	-146(2)
F(4)	591(2)	1079(2)	206(2)	127(2)	200(2)	700(2)
C(80)	113(2)	95(2)	96(2)	32(2)	41(2)	16(2)
Cl(1)	225(2)	183(2)	97(2)	33(2)	73(2)	112(2)
Cl(2)	106(2)	196(2)	180(2)	-31(2)	29(2)	8(2)

Estimated standard deviations are given in parentheses.

U values x 10^n, where n = 4 for Ir, and 3 otherwise.

$T = \exp -2\pi^2(U_{11}h^2a^{*2} + ... + 2U_{23}klb^*c^* + ...)$.

References

1. Jardine, F.H.; Osborn, J.A.; Wilkinson, G.; Young, J.F., *J. Chem. Soc (A)*, **1966**, 1711.

2. Orchin, M.; Rupilius, W., *Catal. Rev.*, **1972**, *6*, 85.

3. Tsutsui, M.; Nakamura, A., *Principles and Applications of Homogeneous Catalysis*, Wiley Interscience, New York, **1980**, pages 9-13.

4. Sacconi, L.; Mani, F., *Transition Met. Chem.*, **1982**, *8*, 179.

5. Meek, D.W.; Mazanec, J., *Acc. Chem. Res.*, **1981**, *14*, 266.

6. Crumbliss, P.; Topping, R.J., *Phosphorus-31 NMR Spectroscopy in Stereochemical Analysis*, VCH, **1987**, 531.

7. O'Connor, J.M.; Casey, C.P., *Chem. Rev.*, **1987**, *87*, 308

8. Maitlis, P.M., *Tilden Lecture, Chem. Soc. Rev.*,**1981**, *10*, 1

9. Fernandez, M.J.;Maitlis, P.M. *J. Chem Soc.,Dalton Trans.*, **1984**, 2063

10. Tsutsui, M.; Nakamura, A., *Principles and Applications of Homogeneous Catalysis*, Wiley Interscience, New York, **1980**, pages 60-81

11. Sadimako, A.D.; Basson, S.S., *Coord. Chem. Rev.*, **1996**, *147*, 247

12. Trofimenko, S., *J. Am. Chem. Soc.*, **1970**, *92*, 5118

13. Trofimenko, S., *J. Am. Chem. Soc.*, **1966**, *88*, 1842

14. Trofimenko, S., *Acc. Chem. Res.*, **1971**, *4*, 17

15. Trofimenko, S., *Chem. Rev.*, **1972**, *72*, 497

16. Trofimenko, S., *Prog. Inorg. Chem.*, **1986**, *734*, 115

17. Trofimenko, S., *Chem. Rev.*, **1993**, *93*, 943

18. Jones, W.D.; Hessell, E.T., *Inorg. Chem.*, **1991**, *30*, 778

19. Ghosh, K.; Graham, W.A.G., *J. Am. Chem. Soc.*, **1989**, *111*, 375

20. Ghosh, C.K.; Rodgers, D.P.S.; Graham, W.A.G., *J. Chem. Soc., Chem.Commun.*, **1988**, 1511

21. Jalon, F.A.; Manzano, B.R.; Otero, A.; Rodriguez-Perez, M.C., *J. Organomet. Chem.*, **1995**, *494*, 179

22. Klăui, W.; Müller, A.; Eberspech, W.;Boese, R.; Goldberg, I., *J. Am. Chem. Soc.*, **1987**, *109*, 164

23. Klăui, W.; Müller, A.; Scotti, M., *J. Organomet. Chem.*, **1983**, *253*, 45

24. Müller, A., *Dissertation*, Technische Hochule Aachen **1985**.

25. Klăui, W.; Buchholz, E., *Angew. Chem.*, **1988**, *100*, 603

26. Klăui, W.; Buchholz, E., *Inorg. Chem.*, **1988**, *27*, 3500

27. Tanke, R.S.; Crabtree, R.H., *J. Am. Chem. Soc.*,**1990**, *112*, 7984

28. Domhover, B.; Hamers, H.; Klăui, W.; Pfeffer, M., *J. Organomet. Chem.*, **1996**, *522*, 197

29. Carmona, D.; Oro, L.A.; Lamata, M.P.; Elguero, J.; Apreda, M.C.; Foces-Foces, C.; Cano, F.H., *Angew. Chem., Int. Ed. Engl.*, **1986**, *25*, 1114

30. Carmona, D.; Lahoz, F.J.; Oro, L.A. *Organometallics*, **1991**, *10*. 3123

31. Carmona, D.; Lamata, M.P.; Ferrer, J.; Modrego, J.; Perales, M.; Lahoz, F.J.; Atencio, R.; Oro, L.A., *J.Chem.Soc., Chem.Commun.*,**1994**, 575

32. Carmona, D.; Ferrer, J.; Perales, M.; Lahoz, F.J.; Atencio, R.; Oro, L.A., *Organometallics*, **1996**, *14*. 2057

33. Carmona, D.; Lahoz, F.J.; Atencio, R.; Edwards, A.J.; Oro, L.A.; Lamata, M.P.; Esteban, M.; Trofimenko, S., *Inorg. Chem.*, **1996**, *35*, 2549

34. Issleib, K.; Abicht, H.P., *J. Prakt. Chem.*,**1970**, *312*, 456

35. Mague, J.T.; Dessens, S.E., *J. Organomet. Chem.*, **1984**, *262*, 347

36. van der Ploeg, A.F.M.J.; van Koten, G., *Inorg. Chim. Acta.*, **1981**, *51*, 225

37. Bahsoun, A.A.; Osborn, J.A.; Voelker, C.; Bonnet, J.J.; Lavigne, G., *Organometallics*, **1982**, *1*, 114

38. Harding, M.M.; Nicholls, B.S.; Smith, A.K., *J. Oganomet. Chem.*, **1982**, *226*, C17

39. Osborn, J.A.; Stanley, G.G., *Angew. Chem., Int. Ed. Eng.*, **1980**, *19* 1025

40. Harding, M.M.; Nicholls, B.S.; Smith, A.K., *J. Chem. Soc., Dalton Trans.*, **1983**, 1479

41. Selegue, J.; Goodrich, A., *Organometallics* **1985**, *4*. 795

42. El-Amouri, D.; Bahsoun, A.A.; Osborn, J.A., *Polyhedron*, **1988**, *7*, 2035

43. Bahsoun, A.A.; Osborn, J.A.; Bird, P.H.; Nucciarone, D.; Peters, A.Y., *J. Chem. Soc., Chem. Commun.*, **1984**, 74

44. Beckett, K.J.; Loeb, S.J., *Can. J. Chem.*, **1988**, *66*, 1073

45. Grim, S.O.; Sangokoya, S.A.; Colquhoun, I.J.; McFarlane, W.; Khanna, R.K., *Inorg. Chem.*, **1986**, *25*, 2699

46. Grim, S.O.; Sangokoya, S.A.; Colquhoun, I.J.; McFarlane, W., *J. Chem. Soc., Chem. Commun.*, **1980**, 1645

47. Grim, S.O.; Satek, L.C.; Walton, E.D.; Smith, P.H., unpublished results.from ref.45

48. Grim, S.O.; Smith, P.H.; Nittolo, S.; Ammon, H.L.; Satek, L.C.; Sangokoya, S.A.; Khanna, R.J.; Colquhoun, I.J.; McFarlane, W.; Holden, J.R., *Inorg. Chem.*, **1985**, *24*, 2889

49. Browning, J.; Berveridge, K.A.; Bushnell, G.W.; Dixon, K.R., *Inorg. Chem.*, **1986**, *25*, 1987

50. Grim, S.O.; Sangokoya, S.A.; Colquhoun, I.J.; McFarlane, W., *J. Chem. Soc., Chem. Commun.*, **1982**, 930

51. Grim, S.O.; Sangokoya, S.A.; Rheingold, A.L.; McFarlane, W.; Colquhoun, I.J.; Gilardi, R.D., *Inorg. Chem.*, **1991**, *24*, 2889

52. Staples, R.J.; Wang, S.; Fackler, J.P.; Grim, S.O.; de Laubenfels, E., *Acta Cryst.*, **1994**, *C50*, 1242

53. Gimeno, M.C.; Jones, P.G.; Laguna, A.; Villacampa, M.D., *Chem. Ber.*, **1996**, *129*, 585

54. Grim, S.O.; Kettler, P.B.; Merola, J.S.; *Inorganica Chimica Acta*, **1991**, *185*, 57

55. Browning, J.; Dixon, K.R.; Hitzs, R.; Meanwell, N.J.; Wang, F., *J. Oganomet. Chem.*, **1991**,.*410*, 389

56. Grim, S.O.; Sangokoya, S.A., unpublished results. from ref.54

57. Reger, D.L.; Knox, S.J.; Lebioda, L., *Inorganica Chimica Acta*, **1990**, *178*, 89

58 Gimeno, M.C.; Jones, P.G.; Laguna, A.; Villacampa, M.D., *Chem. Ber.*, **1996**, *129*, 585

59. Tanke, R.S.; Crabtree, R.H., *Organometallics*,**1991**, *10*, 415

60. Hilts, R.W.; *Ph.D. Dissertation*, University of Victoria, **1988**

61. Hilts, R.W.; *Ph.D. Dissertation*, University of Victoria, **1988**, Chapter Two,46

62. Hilts, R.W.; *Ph.D. Dissertation*, University of Victoria, **1988**, Chapter Three,110

63 Hilts, R.W.; *Ph.D. Dissertation*, University of Victoria, **1988**, Chapter Three, 97

64 Hilts, R.W.; *Ph.D. Dissertation*, University of Victoria, **1988**, Chapter Three, 132

65. Wang, S.F., this thesis, Chapter Four; Browning, J.; Dixon, K.R.; Meanwell, N.J.; Wang, S.F., *J. Oganomet. Chem.*, **1993**,.*460*, 117

66. Dixon, K.R., in *Multinuclear NMR*, **1987** Plenum, New York, 369-390

67. Wang, S.F., this thesis, Chapter Five. Browning, J.; Dixon, K.R.; Wang, S.F., *J. Organomet. Chem.*, **1994**, *474*, 199

68. Wang, S.F., this thesis, Chapter Three; Browning, J.; Dixon, K.R.; Hilts, R.W.; Meanwell, N.J.; Wang, F., *J. Oganomet. Chem.*, **1991**,.*410*, 389

69. Kleier, D.A.; Binsch, G., Quantum Chemistry Program Exchange, Program No. 165, University of Indiana, Bloomington, IN, 1969.

70. Eyring, H., *Chem. Revs.*, **1935**, *17*, 65

71. Laidler, K.J.; Eyring, H., in *The Theory of Rate Processes*, **1941**, McGaw-Hill, New York.

72. Arrhenius, S., *Z. Phys.Chem.*, **1889**, *4*, 226

73. Faller, J. W.; Incorvia, M. J. ; Tomsen, M. E.,*J. Am. Chem. Soc.*, **1969**, *91*, 2054.

74. Faller, J. W.; Incorvia, M. J. *J. Organomet. Chem.*, **1969**, *19*, 13.

75. Faller, J. W.; Mattina, M. J. *Inorg. Chem.*, **1972**, *11*, 1296.

76. Grassi, M.; Meille, S.V.; Musco, A.; Pontellini, R.; Sironi, A.*J. Chem. Soc., Dalton Trans.*, **1989**, 615.

77. Hunter, G; McAuley, A.; Withcombe, T. W., *Inorg. Chem.*, **1988**, *27*, 2634.

78. Liu, S.; Lucas, C. R.; Newlands, M. J.; Charland, J. P., *Inorg. Chem.*, **1990**, *29*, 4380.

79. Mabbott, D. J.; Mann, B. E.; Maitlis, P. M., *J. Chem. Soc., Dalton Trans.*, **1977**, 294.

80. Albinati, A.; Kunz, R. W.; Ammmann, C. J.; Pregosin, P. S., *Organometallics*, **1991**, *10*, 1800.

81. Gogoll, A.; Örnebro, J.; Bäckvall, J.E., *J. Am. Chem. Soc.*, **1994**, *116*, 3631.

82. Elguero, J.; Fruchier, A.; de la Hoz, A.; Jalón, F. A.; Manzano, B. R.; Otero, A.; Gómez-de la Torre, F., *Chem. Ber.* **1996**, *129*, 589.

83. Pregosin, P.S.; Salzmann, R.; Togni, A., *Organometallics*, **1995**, *4*, 842.

84. Crociani, B.; Bianca, D.; Giovemo, A.; Boschi, T., *Inorg. Chim. Acta.*, **1987**, *127*, 169.

85. Hansson, S.; Norrby, P.O.; Sjögren, M.P.T.; Åkermark, B.; Cucciolito, M.E.; Giorjuno, F.; Vitagliano, A., *Organometallics*, **1993**, *12*, 4949.

86. Johnson, C.K., ORTEP Report ORNL-3794, Oak Ridge National Laboratory, Oak Ridge. TN, USA **1965**

87. Colquhoun, I.J.; McFarlane, W.; Bassett, J.M.; Grim, S.O., *J. Chem. Soc., Dalton Trans.*,**1981**, 1645

88. The sum of Pd-P radii =1.37Å (Pd) + 1.10Å (P) = 2.47Å. Data from Shriver, D.F.; Atkins, P.; Lanford, C.H., in *Inorganic Chemistry*, 2nd. ed. **1994** Freeman, New York, 35 &58.

89. The sum of Pd-S(2) radii =1.37Å (Pd) + 0.95Å (P) = 2.32Å. Data from Shriver, D.F.; Atkins, P.; Lanford, C.H., in *Inorganic Chemistry*, 2nd. ed. **1994** Freeman, New York, 35 &58.

90. Mason, R.; Russell, D.R., *J. Chem. Soc., Chem. Commun.*, **1966**, 26

91. Nicholson, J.K.; Powell, J.; Shaw, B.L., *J. Chem. Soc., Chem. Commun.*, **1966**, 174

92 Powell, J.; Shaw, B.L., *J. Chem. Soc.* **1967**, *(A)*, 1839

93. Powell, J.; Robinson, S.D.; Shaw, B.L., *J. Chem. Soc., Chem. Commun.*,**1965**, 78

94. Dent, W.T.; Long, R.; Wilkinson, A.J., *J. Chem. Soc.*, **1964**, 1585

95. Oberhansli, W.E.; Dahl, L.F., *J. Organomet. Chem.*, **1965**, *3*, 43

96. Statton, G.L.; Ramey, K.C., *J. Am. Chem. Soc.*, **1965**, *88*, 1327

97. Vrieze, K.;Volger, H.C.; Pratt, A.P., *J. Organomet. Chem.*, **1968**, *15*, 447

98. van Leeuwen, P.W.N.M.; Vrieze, K.; Pratt, A.P., *J. Organomet. Chem.*,**1969**, *20*, 277

99. Heitner, H.I.; Lippard, S.J., *J. Am. Chem. Soc.*, **1970**, *92*, 3486

100. Heitner, H.I.; Lippard, S.J., *Inorg. Chem.*, **1972**, *11*, 1447

101. Browning, J.; Beveridge, K.A.; Bushnell, G.W.; Dixon, K.R., *Inorg. Chem.*, **1987**, *25*, 1986

102. Grim, S.O.; Kettler, P.B.; Thoden, J.B., *Organometallics*, **1991**, *10*, 2399

103. van Derveer, D.G. and Eisenberg, R., *J. Am. Chem. Soc.*, **1974**, *96*, 4994

104. Bart, J.C.J., *J. Chem. Soc. B*, **1969**, 350.

105. Schmidbaur, H., Deschler, V. and Nilewski-Mahla, B., *Chem. Ber.*, **1981**, *116*, 1393

106. Satek, L.C., Ammon, H.L. and Stewart, J.M., *Acta Cryst., Sect. B*, **1975**, *B31*, 592

107. Richardson, M.F., *Acta Cryst., Sect. C*, **1985**, *C41*, 27.

108. Tucker, P.A., Scutcher, W. and Russell, D.R., *Acta Cryst., Sect. B*, **1975**, *B31*, 592.

109. Leypoldt, J.G., Basson, S.S., Lamprecht, G.J., Bok, L.C.D. and Schlebusch, J.J.J., *Inorg. Chim. Acta*, **1980**, *40*, 43.

110. Hedberg, L. and Hedberg, K., Abstracts of Papers, National meeting of the American Crystallography Association, Bozeman, MT, July 1964, cited in reference 31.

111. Grim, S.O. and Kettler, P.B., *Inorg. Chim. Acta*, **1991**, *57*, 185.

112. Berry, D.E., Browning, J., Dixon, K.R. and Hilts, R.W., *Can. J. Chem.*, **1988**, *66*, 1272..

113. Browning, J., Bushnell, G.W., Dixon, K.R. and Hilts, R.W., *J. Organomet. Chem.*, **1993**, *452*, 205.

114. Browning, J., Dixon, K.R. and Hilts, R.W., *Organometallics*, **1989**, *8*, 552.

115. Grim, S.O. and Sangokoya, S.A., *J. Chem. Soc., Chem. Commun.*, **1984**, 1599.

116. Wang, S.F., Chapter Two of this thesis, pages 2-5 to 2-8.

117. Browning, J., Beveridge, K.A., Bushnell, G.W. and Dixon, K.R., *Inorg. Chem.*, **1986**, *25*, 1987.

118. Heck, F.F., *Acc. Chem. Res.*, **1979**, *12*, 147.

119. Trost, B.M., *Tetrahedron*, **1977**, *33*, 2615.

120. Bäckvall, J.E.; Granberg, P.G.; Gatti, A.R.; Gogoll, A., *J. Org. Chem.*, **1993**, *58*, 5445.

121. Tamaru, Y.; Bando, T.; Kawamura, Y.; Okamura, K.; Yoshida, Z.; Shiro, M., *J. Chem. Soc., Chem. Commun.*, **1992**, 1498.

122. Auburn, P.R.; Mackenzie, P.B.; Bosnich, B., *J. Am. Chem. Soc.*, **1985**, *107*, 2033.

123. Mackenzie, P.B.; Whelan, J.; Bosnich, B., *J. Am. Chem. Soc.*, **1985**, *107*, 2046.

124. Farrar, D.J.; Payne, N.C., *J. Am. Chem. Soc.*, **1985**, *107*, 2054.

125. Pregosin, P.S.; Ruegger, H.; Salzmann, R.; Albinati, A.; Lianza, F.; Kunz, R.W., *Organometallics*, **1994**, *13*, 83.

126. Cesarotti, E.; Grassi, M.; Prati, L.; Demartin, F., *J. Organomet. Chem.*, **1989**, *370*, 407.

127. Faller, J.W.; Incorvia, M.J., *Inorg. Chem.*, **1968**, *7*, 840.

128. Faller, J.W.; Haitu, D.A., *J. Organomet. Chem.*, **1978**, *7*, 840.

129. Faller, J.W.; Adams, M.A., *J. Organomet. Chem.*, **1979**, *170*, 71.

130. Benn, R.; Rutinska, A.; Schroth, G., *J. Organomet. Chem.*, **1981**, *217*, 91.

131. Baker, P.K.; Clamp, S.; Connelly, N.G.; Murray, M.; Sheridan, J.B., *J. Chem. Soc., Chem. Commun.*, **1986**, 459.

132. Horton, A.D.; Kemball, A.C.; Mays, M.J., *J. Chem. Soc., Chem. Commun.*, **1988**, 2953.

133. Vrieze, K.; in *Dynamic Nuclear Magnetic Resonance Spectroscopy*, L.M. Jackman and F. A. Cotton, Eds. Academic Press, New York, **1975**, pp 441-487.

134 Nakanura, A.; Tsutsui, M., in *Principles and Applications of Homogeneous Catalysis*, **1980**, Wiley, New York, 159-167.

135. Vinery, B.D; Knowles, W.S.; Sabacky, M.J.; Bachman, G.L.; Weinhauff, D.J., *J. Am. Chem. Soc.*,**1977**, *99*, 5946.

136. Halpern, J.; Ridley, D.P.; Chan, A.S.; Pluth, J.J., *J. Am. Chem. Soc.*,**1977**, *99*, 8055.

137. Nakanura, A.; Tsutsui, M., in *Principles and Applications of Homogeneous Catalysis*, **1980**, Wiley, New York, 88-92.

138. Chatt, J.; Venanzi, L.M., *J. Chem. Soc.*, **1957**, 2351

139. Chatt, J.; Venanzi, L.M., *J. Chem. Soc.*, **1955**, 287

140. Chatt, J.; Vallarino, L.M.; Venanzi, L.M., *J. Chem. Soc.*, **1957**, 2496.

141. Giordano, G.; Crabtree, R.H., *Inorg. Syn.*, **1979**, *19*, 218

142. Herole, J. L.; Lambert, J.C.; Senott, C.V., *Inorg. Syn.*, **1974**, *15*, 18

143. Sheldrick, G.M., SHELX-76. A Computer Program for Crystal Structure Determination, University of Cambridge, Cambridge, U.K. (1976).